Wind Farm Coordinated Control and Optimisation

Tanvir Ahmad

School of Engineering & Computing Sciences
Durham University

This dissertation is submitted for the degree of
Doctor of Philosophy

Monday 6th November, 2017

Abstract

This thesis develops and implements computationally efficient and accurate wind farm coordinated control strategies increasing energy per area by mitigating wake losses. Simulations with data from the Brazos, Le Sole de Moulin Vieux (SMV) and Lillgrund wind farms show an increase of up to 8% in farm production and up to 6% in efficiency. A live field implementation of coordinated control strategies show that curtailing upstream turbine by up to 17% in full or near-full wake conditions can increase downstream turbine's production by up to 11%. To the best knowledge of the author, this is the first practical implementation of Light Detection And Ranging (LiDAR) based coordinated control strategies in an operating wind farm.

With coordinated control, upstream turbines are curtailed using coefficient of power or yaw offsets in such a way that the decrease in upstream turbines' production is less than the increase in downstream turbines' production resulting in net gain. This optimum curtailment is achieved with on-line coordinated control which requires an accurate and fast processing wind deficit model and an optimiser which achieves the desired results with high processing speed using minimum overheads.

Performance evaluation of carefully selected optimisers was undertaken using an objective function developed for increasing farm production based on coordinated control. This evaluation concluded that Particle Swarm Optimisation (PSO) is the most suitable optimiser for on-line coordinated control due to its high processing speed, computational efficiency and solution quality.

The standard Jensen model was used as a starting point for developing a fast processing and accurate wind deficit model referred to as the Turbulence Intensity based Jensen Model (TI-JM), taking wake added turbulence intensity and deep array effect into consideration. The TI-JM uses free-stream and wake-added turbulence intensities for predicting effective values of wake decay coefficients deep inside the farm. This model is validated using WindPRO and data from three wind farms case studies as benchmarks.

A methodology for assessing the impact of wakes on farm production is developed. This methodology visualises wake effects (in 360°) by calculating power production using data from the wind farms (case-studies). The wake affected wind conditions are further analysed by calculating relative efficiency.

The innovative coordinated control strategies are evaluated using data from the wind farms case studies and WindPRO as benchmarks. A live field implementation of coordinated control strategies demonstrated that the production of downstream turbines can be increased by curtailing upstream turbines. This field setup consisted of two operating wind turbines equipped with modern LiDAR. Analyses of the high frequency real time data were performed comparing field results with simulations. It was found that simulations are in good agreement (within a range of 1.5%) with field results.

Declaration

The work in this thesis is based on research carried out by Tanvir Ahmad under the supervision of Dr. Peter Matthews and Dr. Behzad Kazemtabrizi within the School of Engineering and Computing Sciences at the University of Durham in the United Kingdom. No part of this thesis has been submitted elsewhere for any other degree or qualification. It all my own work unless referenced to the contrary in the text.

Tanvir Ahmad
Monday 6th November, 2017

Dedication

I would like to dedicate this thesis to my loving family; especially to my parents who taught me to dream big and to work hard for achieving those dreams.

Thank you all for encouraging and believing in me.

Acknowledgements

This thesis would not have been completed if it was not for the assistance of the many people, who have helped me throughout the three years since November, 2013. I would like to take this opportunity to thank them all. Specifically:

- My PhD supervisors; Dr. Peter Matthews and Dr. Behzad Kazemtabrizi, for their continuous support, guidance and positive words throughout the duration of this research.
- The Commonwealth Scholarship Commission (CSC) UK for funding this work. (Scholarship reference no. PKCS-2013-384).
- The International Office Durham University, for funding my field visit to Maïa Eolis (now Engie Green) France through the Erasmus + Staff Mobility Programme.
- The St Aidan's College Durham University, for the Clark Travel Award for supporting my work in Pakistan.
- Maïa Eolis (now Engie Green) France, for providing valuable data and providing an opportunity to work on the French National Project SMARTEOLE (ANR-14-CE05-0034).
- Dr. Nicolas Girard, Dr. Olivier Coupiac, Arthur Petit, Dr. Sophie Guignard (all from Maïa Eolis (now Engine Green)) for sharing their invaluable insights, perspectives and experiences.
- Pawel Gancarski, administrator Windbench: V&V Repositories for Wind Energy, for providing useful information about the Lillgrund wind farm.
- DNVGL: Garrad Hassan & Partners Limited, for their support and free license for the research version of WindFarmer software.

- Dr. Christopher Crabtree for his support and assistance over the period of this research.
- Christopher Smith for always giving me directions making this journey easy for me.
- Mrs Sharne Procter, the Director International Office Durham University, for her guidance, support and kind words making my stay in Durham very special.
- Hunza Zainab and Ifrah Idrees, the two interns from Lahore University of Management Sciences (LUMS) Pakistan, for their contribution towards this research and the International Office Durham University for funding this internship.
- The colleagues I have met around the world throughout my travels and throughout my time at Durham; for making the PhD tolerable.
- The people at Durham; Donatella Zappala, Jamie Godwin, Bindi Chen, Baseer Ullah, Adnan Cheema and the many others for their support and joys in the department.
- My family, for always believing in me. Without there support, this would not have been possible and I would not be where I am today.

List of publications

1. Tanvir Ahmad, Olivier Coupiac, Arthur Petit, Sophie Guignard, Nicolas Girard, Behzad Kazemtabrizi, and Peter C. Matthews. Field Implementation and Trial of Coordinated Control of Wind Farms. IEEE Transactions on Sustainable Energy, 2017 (Approved)

2. Tanvir Ahmad, Peter C. Matthews, Behzad Kazemtabrizi, and Olivier Coupiac. Intelligent and fast processing wind farm controller for production maximisation. Journal of Renewable Energy, 2017 (under review)

Conference Papers

1. Tanvir Ahmad, Nicolas Girard, Behzad Kazemtabrizi, and Peter Matthews. Analysis of two onshore wind farms with a dynamic farm controller. In European Wind Energy Association (EWEA) Annual Conference, Paris France, November, 2015

2. T. Ahmad, P. Matthews, B. Kazemtabrizi. PSO based wind farm controller. In The 11th edition of the International Conference on Evolutionary and Deterministic Methods for Design, Optimization and Control with Applications to Industrial and Societal Problems, EUROGEN-2015 Glasgow, UK, 560 2015, pp. 277 - 283

3. Tanvir Ahmad, Peter Matthews, Behzad Kazemtabrizi and Christopher J. Smith. Dynamic Wind Farm Controller. In The 11th European Association of Wind Energy (EAWE) PhD Seminar on Wind Energy in Europe, Stuttgart Germany, September 2015 **(Session Award Winner)**

4. Tanvir Ahmad, Peter Matthews, and Behzad Kazemtabrizi. Wake Flow Model for Wind Farm Control. In The 10th European Association of Wind Energy

(EAWE) PhD Seminar on Wind Energy in Europe, Orleans France, October, 2014, pp. 123-126

5. Tanvir Ahmad, Christopher J. Smith, Peter Matthews, and Behzad Kazemtabrizi. Determining the Wind Speed Distribution within a Wind Farm considering Site Wind Characteristics and Wake Effects. In The 10th European Association of Wind Energy (EAWE) PhD Seminar on Wind Energy in Europe, Orleans France, October, 2014, pp. 131-134

Poster Presentations

1. Intelligent wind farm controller - Durham Energy Institute (DEI) Annual Symposium, Durham UK, September 2016. **(Best poster award and Dong Energy cash prize)**

2. Fast processing wind farm controller for production maximisation - SUPERGEN Wind Assembly, Strathclyde Glasgow, UK May, 2016. **(Best poster award)**

3. Analysis of two onshore wind farms with a dynamic farm controller - European Wind Energy Association (EWEA) Annual Conference, Paris France, November, 2015 (Peer reviewed).

4. Intelligent control strategies for wind farms - School of Engineering & Computing Sciences Durham University, annual research day October, 2015. **(Second prize for best poster)**

5. Wake Flow Model for Wind Farm Control - 10th European Association of Wind Energy (EAWE) PhD Seminar on Wind Energy in Europe, Orleans France, October, 2014 (Peer reviewed).

6. Determining the Wind Speed Distribution within a Wind Farm considering Site Wind Characteristics and Wake Effects - 10th European Association of Wind Energy (EAWE) PhD Seminar on Wind Energy in Europe, Orleans France, October, 2014 (Peer reviewed).

Table of contents

List of figures

List of tables

Nomenclature

α	Yaw-offset
α_F	Wake decay constant in Frandsen model
α_i	Yaw-offset of the i^{th} turbine
a	Axial induction factor
a_c	Acceleration (Chapter 2)
A	Rotor swept area
A_s	Percentage turbine swept area affected by wake
A_w	Area of the wake
β	Blade pitch angle
B	Frandsen model wake expansion parameter (Chapter 2)
B_n	Number of blades
$c_1,\ c_2$	Constants in PSO
C_l	Mixing length
C_n	Constant in section 3.1.3 for objective function
C_P	Coefficient of power

$C_{P(max)}$	Maximum coefficient of power
C_T	Coefficient of thrust
D	Rotor diameter
$D_{initial}$	Wake diameter in the first regime
D_{wake}	Wake expansion at any position
ε	Turbulent dissipation
ε_c	Transport of turbulent dissipation by convection
ε_d	Transport of turbulent dissipation by diffusion
ε_{dsp}	Dissipation of turbulent dissipation
ε_{prod}	Production of turbulent dissipation
η	Efficiency of Brazos and SMV
η_{Lill}	Efficiency of Lillgrund wind farm
η_{Rel}	Relative Efficiency
$f(P_{max}, C_{P(max)}, \alpha_{max})$	Objective function
F_{grvt}	Force due to gravity
F_{prsr}	Force due to pressure
F_{visc}	Force due to viscosity
γ	Wake skew angle
I_0	Free stream turbulence intensity

I_+	Wake added turbulence intensity
I_u	Longitudinal turbulence intensity
I_{wake}	Effective turbulence intensity inside the wake
j	Set of turbines used for normalising Lillgrund efficiency
k	Turbulent kinetic energy
k_c	Transport of kinetic energy by convection
k_d	Transport of kinetic energy by diffusion
k_{dsp}	Dissipation of kinetic energy
k_{prod}	Production of kinetic energy
k_{Jensen}	Wake decay coefficient in the Jensen model
$k_{Frandsen}$	Wake decay coefficient in the Frandsen model
λ	Tip speed ratio
$L(m)$	Obukhov length
m	Mass
N_j	Number of turbines in set j
p_g	Global best of the swarm in PSO
p_i	Personal best of particle i
P_{Actual}	Actual production of the wind farm
P_{Farm_Wakes}	Wind Farm Production in presence of wakes

P_n	Normalised power production
P_{max}	Maximum possible wind farm production assuming no wakes
$P_{Turbine}$	Production of an individual wind turbine
ρ	Air density
r	Radius of the wake
r_0	Rotor diameter
r_x	Radius of the wake at distance x
$R_1,\ R_2,\ R_3$	Randomness generators
t	Time
u	Wind speed
u'	Turbulent velocity fluctuations
u_0	Free-stream wind speed
u_{ef}	Effective wind speed
u_T	Wind speed just behind the rotor
u_x	Wind speed at distance x
$u_{x(ef)}$	Effective wind speed at distance x
U	Average of the wind speeds (six data points)
v	velocity (Chapter 2)
V	Velocity

x	Distance
x_n	Length of the near wake
ζ	Inertia in PSO (Chapter 3)
z_0	Surface roughness length
z	Hub height
Matlab	Matlab®is a registered trademark of Mathworks. It will be referred to as Matlab in this thesis.

List of abbreviations

ABC	Artificial Bee Colony
AI	Artificial Intelligence
ANN	Artificial Neural Network
ARPS	Advanced Regional Prediction Systems
ACO	Ant Colony Optimisation
BFO	Bacterial Foraging Optimisation
BF	Brute Force
CFD	Computational Fluid Dynamics
CSA	Clonal Selection Algorithm
DE	Differential Evolution
DEL	Damage Equivalent Load
DNS	Direct Numerical Simulation
DWM	Dynamic Wake Meandering
EA	Evolutionary Algorithms
ECN	Energy Research Centre Netherlands
EWTW	ECN Wind Turbine Test Site Wieringermeer

FLaP	Farm Layout Program
FLORIS	FLOw Redirection and Induction in Steady-state
GA	Genetic Algorithm
GHG	Green House Gases
JIT	Just In Time
kWh	kilo Watt hour
LCoE	Levelised Cost of Energy
LES	Large Eddy Simulation
LiDAR	Light Detection And Ranging
MPPT	Maximum PowerPoint Tracking
MA	Memetic Algorithm
MOL	Monin Obukhov length
MPSO	Modified Particle Swarm Optimisation
MWh	Mega Watt hour
NREL	National Renewable Energy Limited
NS	Navier-Stokes
PC	Personal Computer
PDE	Partial Differential Equation
PSO	Particle Swarm Optimisation
RANS	Reynolds Averaged Navier-Stokes Equations
RQ	Research Question

SA	Simulated Annealing
SAM	Storpark Analytical Model
SCADA	Supervisory Control And Data Acquisition
SFL	Shuffled Frog Leaping
SMV	Le Sole de Moulin Vieux
SOWFA	Simulator for Offshore / Onshore Wind Farm Application
TS	Tabu Search
UN	United Nations
WAsP	Wind Atlas Analysis and Application Program

Chapter 1

Introduction

Interest in renewable energy systems is currently at the highest level for many reasons, such as unlimited availability, global warming and hazards associated with nuclear energy. Wind energy systems in particular have attained more attention in comparison to other renewable energy sources. Wind is a safe, green and clean source of energy. Cumulative capacity of wind energy systems has increased from 6.1GW to 432.4GW over the last two decades [1]. Effective use of the latest technology, the ever increasing size of wind turbines and the clustering of turbines in wind farms have made wind energy more attractive and affordable as compared to other renewable energy sources [1].

The large sized wind turbines and wind farms have helped in reducing cost of energy per area, by taking advantage of economies of scale. However there is a price to pay in terms of wake effects. The wake effects decrease farm production and increase fatigue loading on the turbines. Mitigating and controlling these wakes optimally, can increase overall farm production and reduce Operation & Maintenance (O&M) costs by decreasing fatigue loads. Developing control strategies for increasing production per area by optimally controlling wake effects is the main aim of this thesis which will be discussed in subsequent chapters.

This chapter briefly introduces the growing interest in renewable energy systems because of global warming and climate change in section 1.1. This is followed by a discussion about historical growth and future projection about growth of wind energy systems in section 1.2. Based on these objectives, a set of research questions is presented in section 1.3. Structure of the thesis is given in section 1.4. The chapter ends with a

presentation of original contributions in section 1.5. The structure of this chapter is presented in Figure 1.1.

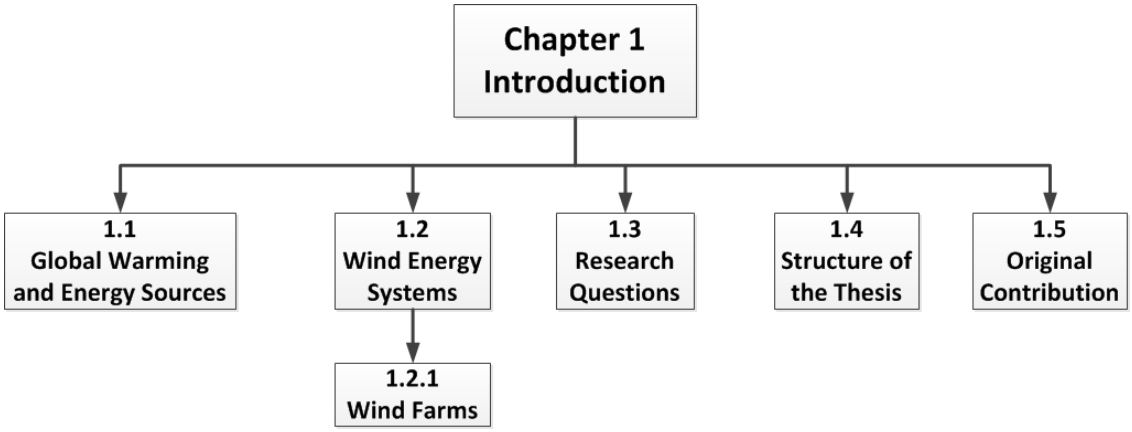

Figure 1.1 Structure of chapter 1

1.1 Global Warming and Energy Sources

The average global temperature has increased by 0.85°C from 1880 to 2012, oceans have warmed, large amounts of snow and ice have diminished, and the sea level has risen [2]. Global emissions of carbon dioxide (CO_2) have increased by almost 50% since 1990 [2]. Hydro-carbon based fuels are the primary sources of global warming and are responsible for more than 70% of greenhouse gas emissions [3]. This section presents a brief overview of the impact of different energy sources on the environment.

A comparison of impact of different energy sources on the environment is presented in Table 1.1 [4]. It is clearly visible that the impact of nuclear, solar and wind is low on climate change and air pollution, as compared to fossil fuels. Carbon reduction can be achieved by using sustainable and renewable energy sources efficiently [5]. Nuclear has lower emissions but at the same time higher impact on land, water and planning, and cost risks are associated with it. It is mentioned in [4] that the terms high, moderate and low are inevitably subjective, as different kinds of impacts are weighed against each other. A detailed description of these impacts and Table 1.1 is given in Appendix A.

This impact of energy or power sources on Green House Gases (GHG) emission is quantified in Figure 1.2. The emissions from manufacturing of the equipment used for

power generation and combustion of fuel are reported separately in Figure 1.2. It can be observed that the overall emissions from renewables are low as compared to the traditional sources of energy. Renewable energy sources can help reduce emission of greenhouse gases as they are green and sustainable. The United Nations (UN) report on climate action suggests that it is still possible, using technological measures, to limit the increase in global mean temperature to 2° C above pre-industrial levels [3].

Table 1.1 Comparing the environmental impact of energy sources [4]

	Biomass	**Coal**	**Nuclear**	**Natural Gas**	**Solar**	**Wind**
Planning and Cost Risk	Moderate	High	High	Moderate	Low	Low
Climate Change Impact	Moderate	High	Low	High	Low	Low
Air Pollution Impact	Moderate	High	Low	Moderate	Low	Low
Land Impact	Moderate	High	High	Moderate	Moderate	Moderate
Water Impact	Moderate	High	High	High	Low	Low
Noise and Visual Impacts	Moderate	Moderate	High	Moderate	Low	Moderate

The environment-friendly nature of renewable energy sources is one of the major reasons for the rapid growth of renewables as compared to traditional sources of energy [6]. It is projected that the trend will continue in the future [6] as shown in Figure 1.3. Wind is currently, and will remain, the fastest growing renewable energy source [6] as can be seen in Figure 1.4. The next section briefly discusses the history and innovations in wind energy systems.

1.2 Wind Energy Systems

Wind is one of the most environment-friendly sources of energy. It can be seen in Table 1.1 that the climate change, air pollution and water impact of wind is low. As more wind farms are built offshore, the land, noise and visual impacts are also reducing. Technological innovations have helped the wind industry grow by reducing

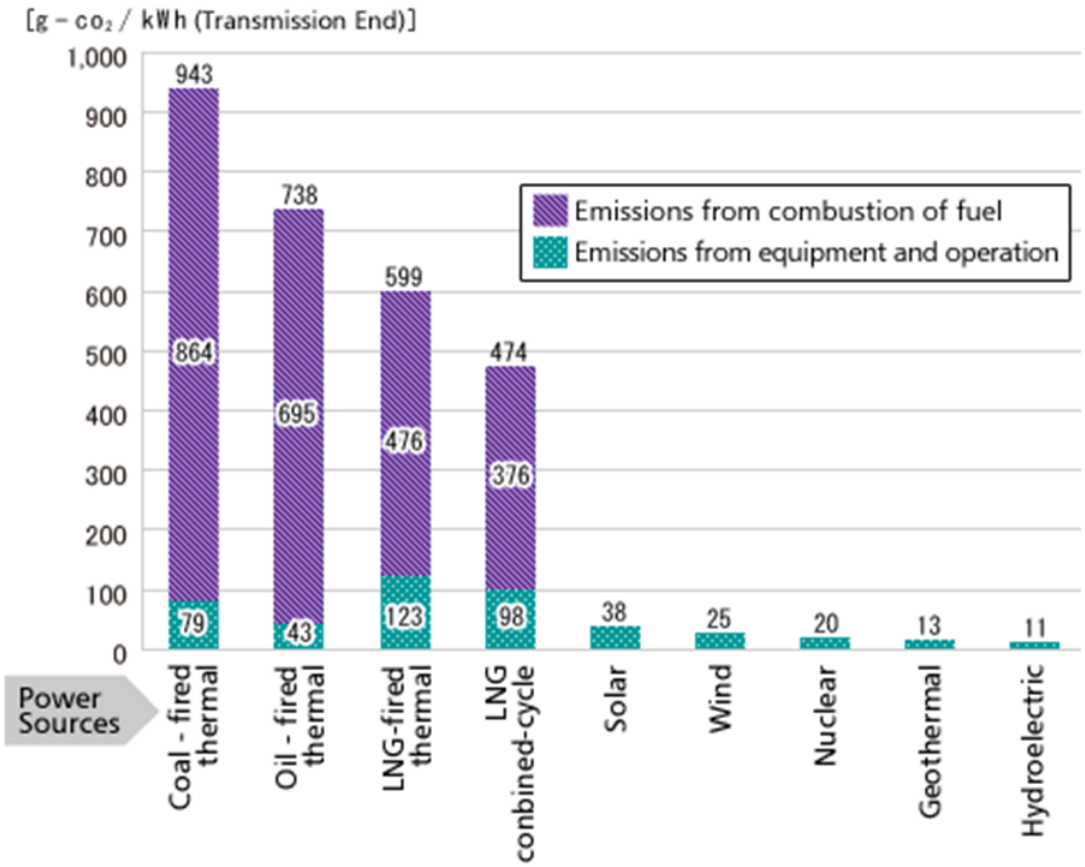

Figure 1.2 Greenhouse gases emission from different energy sources [5]

the Levelised Cost of Energy (LCoE), though it still requires further reduction [7]. The global wind power cumulative capacity for the past 20 years is shown in Figure 1.5. The cumulative capacity has increased by almost 71% in the last twenty years [1]. It is expected that LCoE of offshore wind energy will keep declining in the future [8] as shown in Figure 1.6.

The higher LCoE remains one of the major hindrances in the growth of wind energy. LCoE has to be reduced to less than £100/MWh in order to meet the EU renewable energy targets for 2020 and beyond [7]. Therefore every effort shall be made to reduce the LCoE. Clustering turbines together in wind farms is a good example of techniques used for reducing LCoE, taking advantage of economies of scale as detailed in the next section.

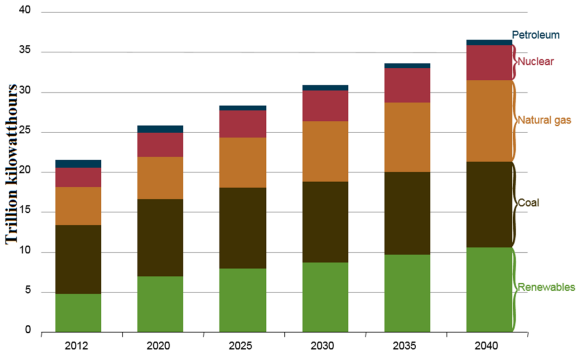

Figure 1.3 World net electricity generation by fuel (2012 - 2040) [6]

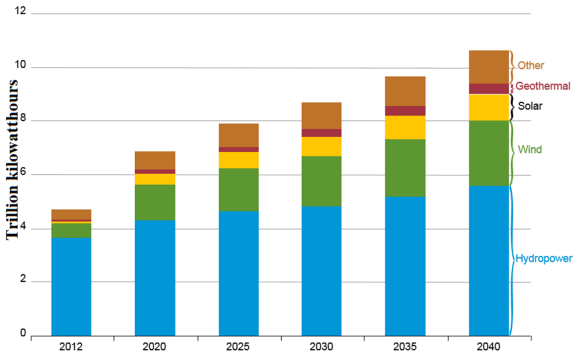

Figure 1.4 Projected world net electricity generation by renewable energy sources [6]

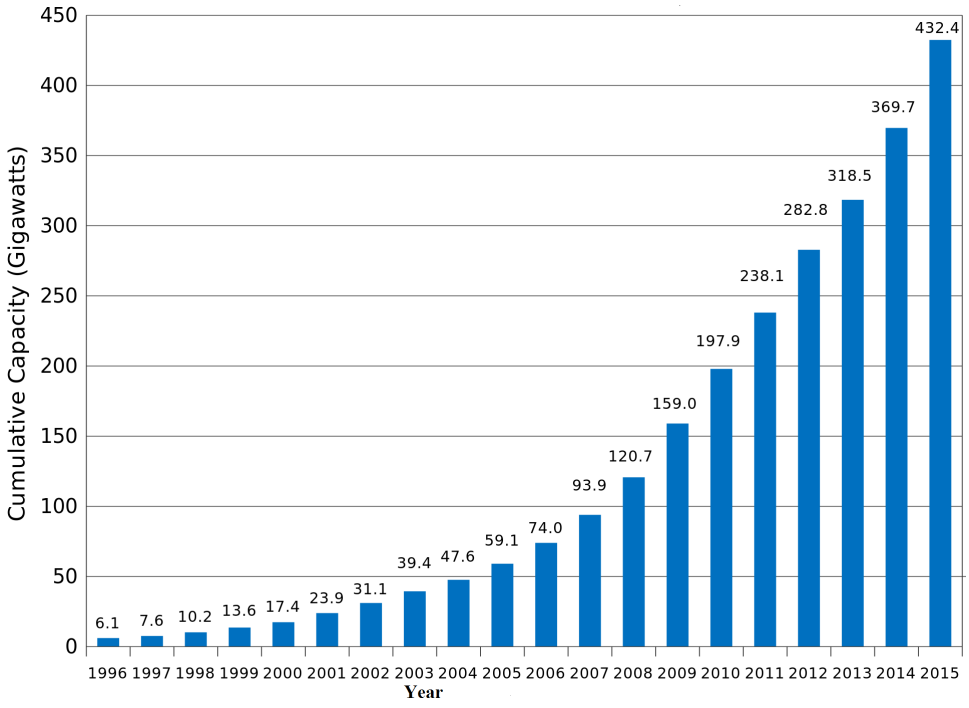

Figure 1.5 Global wind power cumulative capacity from 1996 to 2015 [1]

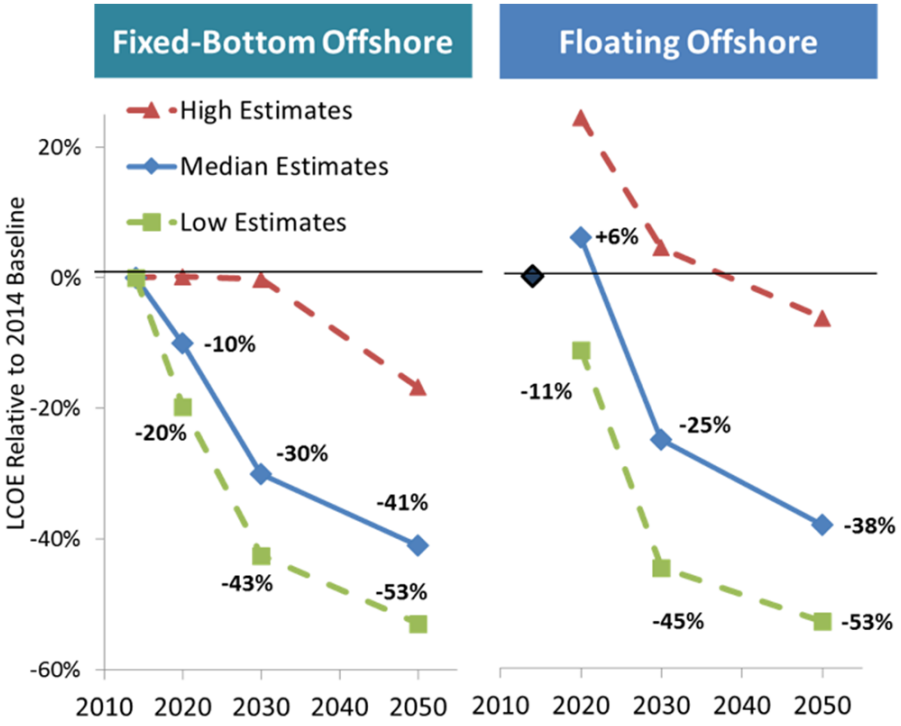

Figure 1.6 Historical and predicted reduction in LCoE of offshore wind energy [8]

1.2.1 Wind Farms

Wind farms mainly reduce civil engineering, grid connection and O&M costs by taking advantage of economies of scale. A wind farm may contain from two to hundreds of turbines. A wind farm layout may follow a pattern like a rectangular grid or turbines may be installed in any other shape. The layout of a wind farm depends upon many factors such as available area, number of turbines in the farm, wake effects, cable connection topology and sometimes navigational issues [9].

The aerodynamic interactions, namely wake effects, created by the upstream turbines in these farms can greatly decrease the total production compared to the same number of turbines under free flow conditions [10–12]. The wind flow is the main coupling between turbines in a farm [13] and wake is the main interaction [14].

Figure 1.7 shows wake effects in the Horn Rev wind farm. Wake effects reduce production per area, decreasing farm production by up to 60% in the worst case situation when turbines are under full wake effects [9]. It is always desired to reduce wake effects in a wind farm.

Figure 1.7 Wake effects at the Horn Rev wind farm [15]

A generic power curve of a wind turbine is shown in Figure 1.8. The region between cut-in wind speed and rated wind represents the below rated wind conditions. Wake effects are mainly noticeable in below rated wind conditions [9]. Cut-in wind speed represents the wind speed at which the turbine starts operating. The coefficient of power (C_P) increases from cut-in wind speed up to rated wind speed. At higher wind speeds (above rated wind speed), the C_P of a turbine decreases as it has more wind to produce with. Hence wake effects are also negligible as wind speed is high and the C_P is low [9]. The wake recovers quickly, diminishing the wind deficit created by an upstream turbine. The above-rated wind speed is around 12+m/s for modern wind turbines [16, 17]. The turbine controller is designed in such a way that it automatically (by default) chooses the optimum C_P for the given wind speed, according to the power curve of the turbine as shown in Figure 1.8. This is called Maximum Power Point Tracking (MPPT) [12]. With an MPPT approach, a turbine maximises its own production, ignoring the wake effects produced on downstream turbines. Wake effects will be discussed in detail in Chapter 2.

Operating wind farms with coordinated control can reduce wake effects and hence production losses as will be discussed in Chapter 2. Developing and implementing fast processing and accurate on-line operating strategies based on coordinated control is the main objective of this PhD work.

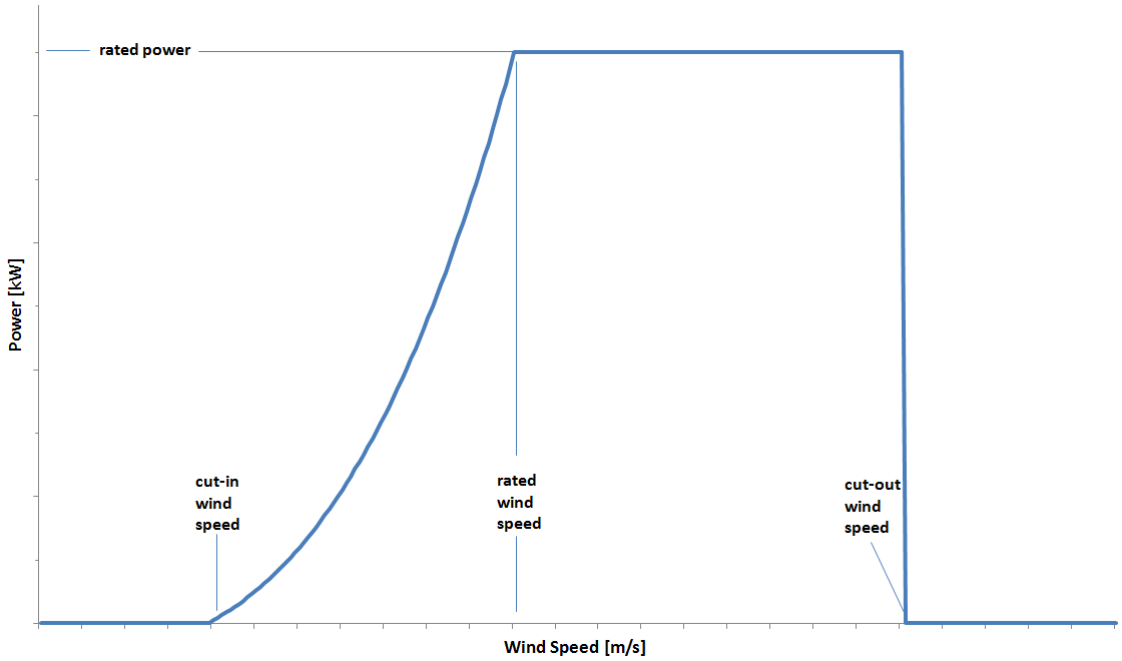

Figure 1.8 Generic power curve of a wind turbine

A set of research questions has been generated for achieving this objective. These research questions provide a step by step approach for achieving the aims of this work. Coordinated control is also called cooperative control and global optimisation of the wind farm in this thesis. Coordinated control of wind farms can be used for increasing farm production in below rated wind conditions. If the available power production (maximum a farm can produce for a given wind speed) is more than the production required by the grid, then coordinated control can be used for minimising fatigue loads on the turbines by distributing the required power production among the turbines optimally.

1.3 Research Questions

The main goal of this PhD work is to develop fast processing and accurate coordinated control strategies for wind farm production maximisation as discussed in section 1.2.1. This goal is achieved by answering the following research questions.

RQ-1: What is the state of the art in coordinated control of wind farms? What are the requirements for developing on-line coordinated control strategies?

RQ-2: What are the key properties of the optimisation technique that enables on-line coordinate control? Which optimisation technique is the most appropriate for optimising wind farm power production using on-line coordinated control?

RQ-3: What is the most appropriate wind deficit model for on-line coordinated control, which can achieve the required level of accuracy without compromising computational efficiency? How the accuracy of CFD models and computationally efficiency of engineering models can be combined for developing hybrid wind deficit models having positive characteristics of both the models?

RQ-4: What is the most appropriate methodology / strategy for assessing impacts of wakes on farm production and identifying wind conditions where coordinated control can be beneficial for increasing farm production? How can Supervisory Control And Data Acquisition (SCADA) data from wind farms be used effectively for visualising and analysing wake effects on production?

RQ-5: How different control strategies (Conventional greedy, C_P-based or yaw-based) behave in different wind conditions? Which strategy is better considering full, partial and no-wake conditions?

RQ-6: What is the best approach for practical implementation of coordinated control?

All these research questions are answered in detail in this thesis as explained in the following section.

1.4 Structure of the Thesis

This thesis is structured to reflect the approach, methodology and results of the research. As such, it is divided into chapters based on different areas of research.

This introduction, Chapter 1, has briefly discussed the basis for interest in wind power. The concepts of wind farms, wake effects and coordinated control of wind farms are briefly discussed. Based on this discussion six research questions are presented. This chapter also shows the original contribution of this PhD work.

Chapter 2 answers RQ-1 and part of RQ-2 and RQ-3. The concept of wake effects is discussed, detailing the adverse effects wakes can produce on wind farms by reviewing previous studies. Different wake modelling techniques and models are also presented, detailing their benefits and shortcomings. Previous studies regarding coordinated

control are reviewed for explaining the concept and benefits of coordinated control and identifying requirements of control strategies based on this concept.

Chapter 2 also defines the criteria for selecting an appropriate optimiser for on-line coordinated control, partially answering RQ-2 , by identifying key properties of such optimiser. The properties of a wind deficit model suitable for on-line coordinated control are also identified using previous studies answering first part of RQ-3.

Chapter 3 answers RQ-2 by choosing a suitable optimiser for solving the coordinated control problem. Previous studies are reviewed for selecting a set of heuristic optimisation techniques fulfilling the criteria set in Chapter 2. An objective function is developed using an artificial wind farm for evaluating performance of the selected optimisers. A coordinated control strategy based on coefficient of power (C_P) is used for evaluation. Yaw-based optimised control strategies are also explained. The evaluation criteria are based on processing speed, success rate, computational efficiency and accuracy.

Chapter 4 answers RQ-3 and RQ-4. First a fast processing and accurate wind deficit model is developed for predicting the mean wind deficit inside the farm. A wake assessment methodology is presented which is used for identifying wind conditions where wakes significantly affect farm production and where coordinated control can potentially bring improvement in farm production.

Chapter 5 contains results based on simulations using data from three wind farms case studies. The wind deficit model developed in Chapter 4 is validated using real time data from one of the wind farms case studies. The wake assessment methodology is applied using data from the wind farms case studies. The wind farm coordinated control strategies are simulated in different wind conditions and results are evaluated using data from the farms case studies and WindPRO, answering RQ-5.

Chapter 6 presents field implementation of wind farm coordinated control strategies answering the final RQ-6. This chapter is based on the collaborative work with the French wind farm operator Maïa Eolis (now Engie Green). The C_P-based and yaw-based coordinated control strategies are implemented with a setup of two wind turbines using state of the art LiDARs as part of the French Government SmartEOLE project. Results based on real time data are compared with simulations.

Finally, Chapter 7 draws conclusions from this research. It also proposes possibilities for further research based on experiences from this PhD project.

The appendices contain a detailed description of Table 1.1, a summary of the previous studies about wake effects, coordinated control and the performance evaluation and implementation of optimisation techniques, the wind turbines' characteristics installed in the wind farms case studies and the submitted journal publications resulting from this work.

1.5 Original Contribution

Coordinated control of wind farms has been an active area of research over the last few years as will be discussed in Chapter 2. Researchers have used both Computational Fluid Dynamics (CFD) and engineering models for understanding the aerodynamic interactions using coordinated control. All these previous studies are based on simulations or experiments based on scaled wind farms tested in wind tunnels. These studies provide understanding and in-depth analysis of the aerodynamics. However, the field implementation of coordinated control strategies is lacking. One major reason for this is the lack of fast processing and accurate wake modelling and optimisation techniques.

This PhD work addresses the coordinated control problem from a different angle, looking at both the aerodynamics and optimisation. Performance evaluation of carefully selected heuristic optimisation techniques is performed using coordinated control in Chapter 3.

A fast processing and accurate wind deficit model (TI-JM) is developed in Chapter 4. This model combines the accuracy of CFD models with computational efficiency of engineering models presenting a new methodology for developing wind deficit models.

An assessment methodology for analysing the impact of wakes on farm production is presented in Chapter 4. This methodology uses data from wind farms for visualising and analysing wake effects as detailed in Chapter 5. This methodology can be used for analysing wake effects in wind farm with any layout. These are significant contributions of this work.

The experimental setup presented in Chapter 6 is the first of its kind in the history of wind energy for analysing wind farm coordinated control strategies in an operating wind farm using modern Light Detection And Ranging (LiDAR). The C_P-based and yaw-based coordinated control strategies are implemented in the field given the operational limitations.

To summarise, fast processing, computationally efficient and accurate wind farm coordinated control strategies are developed for on-line field implementation. Implementation of the coordinated control strategies in an operating wind farm stands up as an important contribution to the renewable energy community.

Chapter 2

Literature Review

This chapter presents motivation for this research by conducting a detailed literature review of wake effects and mitigating these wakes using coordinated control in an operating wind farm.

One of the most important areas of research in wind energy is to reduce the LCoE. This can be achieved by increasing production per area and reducing Operations and Maintenance (O&M) costs. Therefore, wind turbines are clustered together in the shape of wind farms for efficiently utilising areas with sustainable wind resources using economies of scale. This reduces civil engineering, grid connection and maintenance costs. However, wind turbines extract kinetic energy from the wind leaving less energy for downstream turbines' production. This decreases the wind speed making the wind more turbulent because of momentum loss - this is called the wake effect [18]. The increase in turbulence intensity occurs due to wind shear (from the velocity reduction) inside the wake affected area and blade rotation.

Wake effects created by turbines in a wind farm can greatly decrease the total production compared to combined production of the same number of turbines under free flow conditions [10–12]. Wakes result in lower wind speed and increased turbulence intensity for the shadowed turbines. This results in lower production and increased fatigue loading [10, 11, 19, 20]. It is always desirable to reduce wake effects in a wind farm.

One possible way of reducing wake effects is to install the turbines as far as possible from one another with an optimised layout by ensuring the turbines are not aligned in the prevailing wind direction. Many researchers have worked on wind farm layout optimisation [21–24]. Due to space and economic constraints it is impossible to

completely diminish these interactions (even with an optimised layout) [25] as wakes can prevail for a distance of 5 - 20 km [11]. Other constraints such as navigational issues also result in close spacing between the turbines in a wind farm [9]. For example the proximity to the fairway for the ships through Öresund and proximity to the Danish border resulted in close spacing ($3.5D$ to $4.5D$) between the turbines in the Lillgrund wind farm [9].

Another way of reducing wake effects is to operate a wind farm with coordinated control, which is the main topic of this thesis. In this type of control, upstream turbines are curtailed for increasing production of the downstream turbines. This is achieved by reducing coefficient of power (C_P) of upstream turbines or using yaw offsets on upstream turbines. With the C_P control, it is the coefficient of thrust (C_T) which is driving the wake and the control of C_P is an indirect way of adjusting C_T. This will be further explained in section 3.1.3. The wind farm is operated in such a way that decrease in upstream turbines' production is less than increase in downstream turbines' production, hence increasing net production.

This chapter presents a detailed literature review of wake effects, wake modelling techniques and mitigating wakes in an operating wind farm. The concept of coordinated control is discussed answering RQ-1 by describing how coordinated control can be implemented and what the main requirements of this type of control are. RQ-2 and RQ-3 are also addressed by identifying characteristics of the optimiser and wind deficit model required for coordinated control.

The structure of this chapter is given in Figure 2.1. A description of wakes and impacts of wakes on the wind farm is given in section 2.1. This is followed by a literature review of different wake modelling techniques in section 2.2. Studies regarding wind farm coordinated control strategies are summarised in section 2.4. Conclusion of this chapter is presented in section 2.5.

2.1 Wake Effects

A turbine is in the wake of an upstream turbine when the wake produced intersects the swept area of the downstream turbine [18] as illustrated in Figure 2.2. Wake effects decrease with increasing downstream distance, completely diminishing after some distance behind the wake producing turbine. The distance at which the wake diminishes depends upon several factors such as turbine diameter, wind characteristics

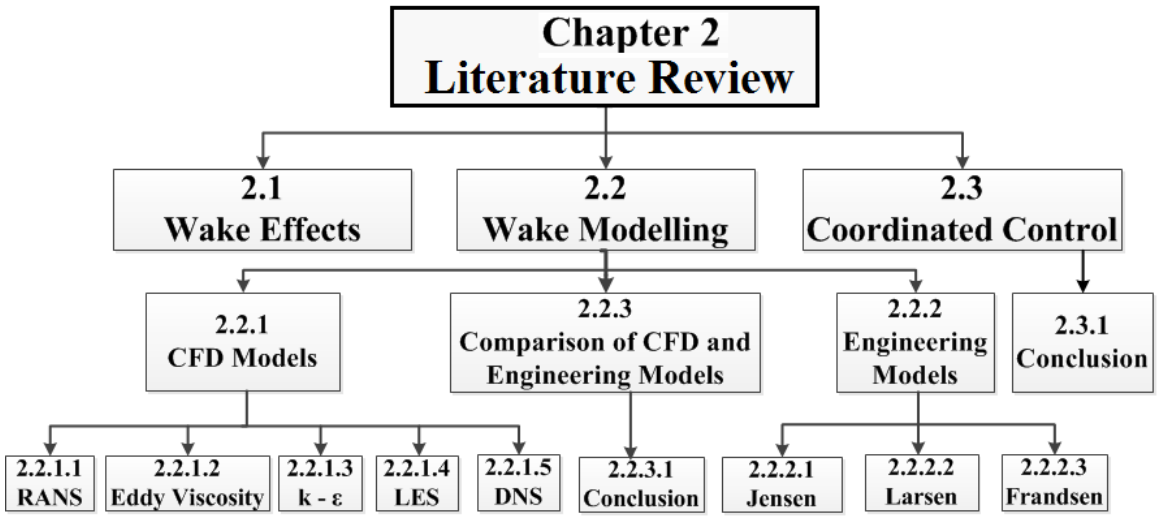

Figure 2.1 Structure of chapter 2

and the surface roughness. The distance at which a wake is diminishes is directly proportional to the distance from the wake producing turbine. Wakes recover quickly in above rated conditions as explained in section 1.2.1. Wakes recover relatively quickly in high turbulent wind conditions than in low turbulence conditions [26, 27]. Wake effects diminish quickly when surface roughness is high, such as onshore wakes recover relatively quickly as compared to offshore wakes [26, 28].

As a compromise, industry best practice tends to concentrate on prevailing wind directions by installing turbines with increased spacing between them in this direction, termed as downwind. For non-prevailing wind directions spacing between the turbines is low, termed as crosswind [11]. For example, the spacing between wind turbines in the Brazos wind farm in the prevailing wind direction is more than 7 rotor diameters ($7D$) but the spacing in non-prevailing wind direction is as low as $2D$ for some of the rows [29]. Lillgrund, an offshore wind farm, has spacing equivalent to $4.4D$ and $3.3D$ in downwind and crosswind directions respectively [30]. When wind flows in the crosswind direction, wake losses can reach a significant level and can be as high as 60% in the worst case situation [9] mainly at the centreline of the wake [31]. A wake will primarily disturb the wind flow inside a farm producing the following two main affects downstream.

1. Reduced wind speed resulting in decreased power production of downstream turbines as wind speed is decreased [10, 11, 28, 31–33]. Power produced is

proportional to the cube of the wind speed so this significantly affects economic performance of the farm [19, 34].

2. The loss in momentum increases turbulence intensity as wind from surroundings flows for making the loss in momentum [28, 35, 36]. Increased turbulence intensity added by wakes is one of the major causes of dynamic fatigue loading [20, 28, 31]. This reduces turbines' life considerably and also results in increased O&M costs [19, 20, 25, 28, 32, 34, 36]. The turbulence is primarily shear generated due to the reduction in wind speed within the wake, relative to the free-stream outside the wake.

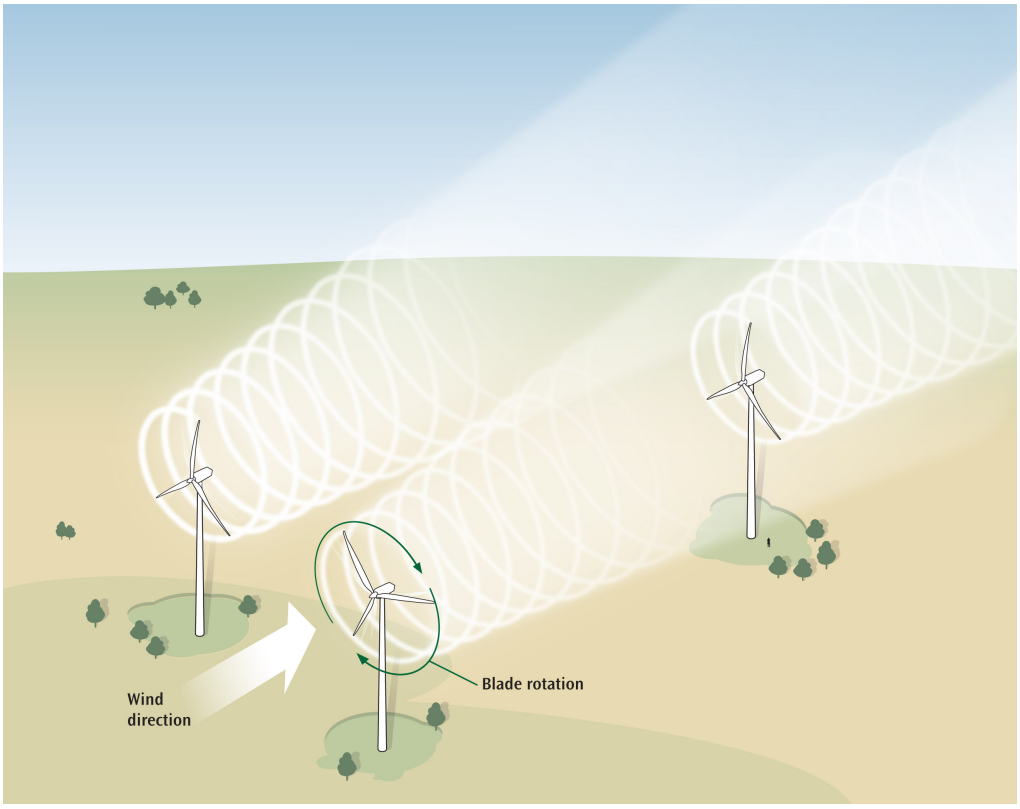

Figure 2.2 Illustration of wake effects [37]

Wake effects are more noticeable offshore than onshore. Sea surface has less roughness and therefore wind takes more time to recover [18, 28, 42]. Large offshore wind farms can produce long distance wakes [43]. Wind farms not only suffer from wakes inside the farm but also neighbouring farms, if present [44]. It can be seen in Table 2.1 that wake losses can be as high as 60%, depending upon the wind farm layout and wind characteristics.

Table 2.1 Wake Powers losses in wind farms with references

Ref	**Type of wind farm considered and conclusion**	**Estimated % Power Losses**
[9]	Maximum power losses in full wake conditions in Lillgrund wind farm (medium size farm)	50 - 60
	33% on average in below rated wind conditions and 23% in all wind conditions	23 - 33
[25]	Wake losses are significantly affected by wind conditions	20 - 45
[28]	Averaged over different directions in small wind farms	5 - 8
	Full wake conditions in small wind farms	30 - 40
[29]	Wake losses can severely affect economic performance of dense wind farms where turbines are closely spaced	20 - 50
[34]	Wake losses depend upon layout and wind conditions	5 - 10
[38]	Average power losses in large offshore wind farms	10 - 20
[39]	Losses with spacing of $8D \times 4D$	5 - 15
[40]	This study is conducted considering a large offshore wind farm	10 - 20
[41]	Results are based on original data from offshore wind farms	10 - 50

In the past decades, wake effects were not that significant because turbines were smaller, which is not the case now as turbines are getting larger [11] as can be seen in Figure 2.3. As turbine size has increased, it is often hit by turbulence which is smaller than rotor size; these smaller turbulence structures can cause extreme damage as compared to a one larger than the rotor [11]. The fatigue loading on the shadowed turbines can increase by up to 80%, shortening turbines' life time [25]. The small cracks in the structure created by fatigue loading increase in size with the passage of time leading to major failures. Wake affected turbines usually require regular maintenance preventing them from producing any useful power when switched off, increasing O&M costs [45].

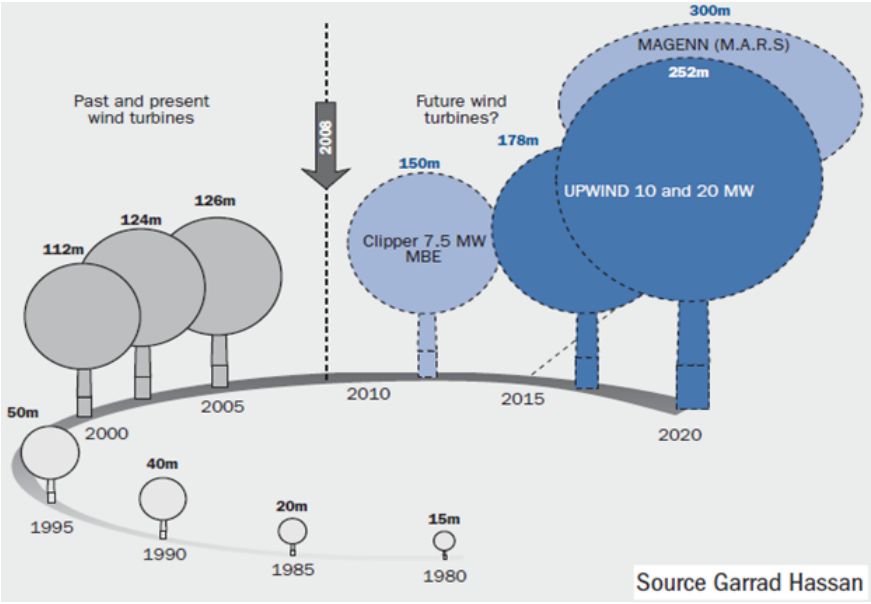

Figure 2.3 Growth in Size of Commercial Wind Turbines [46]

2.2 Wake Modelling

Accurate wake modelling is important for design, development and assessment of wind energy projects [28, 47, 48]. Accurate and fast wake models can also be used for wind farm coordinated control, as will be discussed in section 2.4.

By convention, wakes are divided into a near and far wake regions as shown in Figure 2.4. The near wake persists between $2D$ and $5D$ (normally) behind the rotor where the wind speed deficit is maximum [49, 50]. The pressure recovery is about $1D$ downstream. Far wake is just beyond the near wake where rotor characteristics become negligible and atmospheric flow effects are dominant [51]. There is a gradual transition from near to far wake. Modelling of the actual rotor is less important in far wakes because the main focus in this area is on wake interference, turbulence intensities and turbine influence on each other [41, 49, 52]. Far downstream, the wake effect vanishes because of turbulent diffusion [49]. Wake effects can be neglected if turbines are spaced apart by $10D$ or more [41].

Wind flow can be considered as the main coupling among the turbines in a wind farm while wake is the main interaction [13, 14]. Wind flow depends upon many variables such as turbulence intensity, wind shear and terrain characteristics. These parameters are not generally available with any degree of certainty because of the

stochastic nature of wind [53, 54]. This makes wind and wake modelling a complex task.

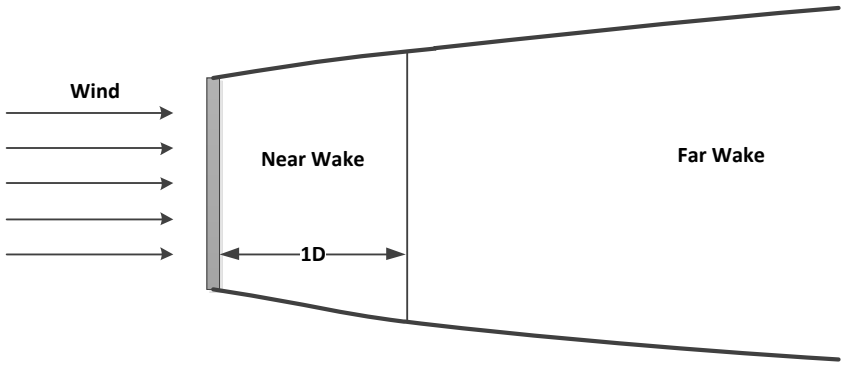

Figure 2.4 Near and far wake regions

Wake models can generally be divided into two categories: Complex Computational Fluid Dynamics (CFD) models and simplified engineering models [14, 28, 39, 40, 55–57]. Following is a detailed description of these models.

2.2.1 Computational Fluid Dynamics (CFD) Models

Wind is a complex fluid as a number of parameters affect the wind flow such as boundary layer conditions, wind shear, turbulence intensity and terrain characteristics [49]. Complex fluids can be considered homogeneous at the macroscopic (or bulk) scale, but are disordered at the "microscopic" scale, and possess structure at an intermediate scale [58]. CFD models and solves the fluid flow considering space (in three dimension) and time. The key elements of CFD modelling are the grid or mesh generation, algorithm development and turbulence modelling. The higher the resolution of the mesh, the higher will be the computational requirements. Mathematical theories exist for grid generation and algorithm development but turbulence modelling is a complex problem. Turbulence is three-dimensional and time dependent, a great deal of information (from friction to turbulence fluctuation) is required for accurately describing the whole flow mechanics. Generally CFD modelling requires the following steps [28, 59–63].

1. Wind flow is modelled mathematically with partial differential equation (PDEs).

2. It is ensured that laws of conservation of mass, momentum and energy stay valid throughout the volume of interest.

3. Forces which cause and influence the wind flow are identified and wind properties are modelled empirically.

4. Reasonable assumptions based on the first three steps are made to simplify the problem. These assumptions depend upon the CFD model used. For example in Large Eddie Simulation (LES), the eddies containing most of the energy are solved while eddies with lesser energy are modelled. This modelling of smaller eddies is based on solution of the larger eddies. A filter is applied to differentiate between smaller and larger eddies and reasonable assumptions has be made for deciding on the filtering criteria.

5. Initial and boundary conditions are provided.

6. The mesh grid is generated by dividing the volume of interest into cells by applying numerical techniques for discretisation.

7. General conservation equations of mass, momentum and energy are discretised into algebraic equations using techniques such as Finite-Difference method and Finite-Volume method.

8. Software tools are used for solving systems of equations.

9. The solution is post-processed for extracting quantities of interest.

The accuracy and computational efficiency of CFD models has an inverse relationship. Accuracy depends upon the grid resolution and problem setup and is reflected by the way in which turbulence is modelled. The PDEs are complex and difficult to solve [59]. Solving the whole flow field and turbulence requires high computational resources and efforts [28, 38, 56, 64].

CFD models can be divided into different types based on the way the turbulence and flow field is described and solved. It can range from simple empirical models where the magnitude of the flow and turbulence is modelled rather than explicitly resolved to models where the whole area of interest is mathematically solved. The kinematic models are also often based on CFD based models as discussed in [65, 66]. Complexity of CFD model depends upon the number of equations used [62]. This can range from simple algebraic zero-equation models to models with five PDEs [49, 62]. Details of

some of these CFD models are given in sections 2.2.1.1, 2.2.1.2, 2.2.1.3, 2.2.1.4 and 2.2.1.5.

2.2.1.1 Reynolds Averaged Navier-Stokes Equations (RANS)

The Navier-Stokes (NS) equation is based on Newton's second law of motion for fluids which is about conservation of momentum [61]. It is yet to be proved that a complete solution exists for these equations [59]. Velocity fluctuations in wind flow in all directions add to the complexity of NS.

The three general forces acting on wind flow are gravity (F_{grvt}), pressure (F_{prsr}) and viscosity (F_{visc}). The NS equation is the sum of these three forces equals to mass (m) times acceleration (a_c) as given in equation (2.1) [61]. Usually time (t) average is taken to reduce the complexity of NS and the resulting equation is called RANS as given in equation (2.2) [61]. Substantial time derivative is the rate of change for a moving fluid particle. Local time derivative is the rate of change at a fixed point. The three dimensions are represented by (x), (y) and (z) and (v) represents velocity of the fluid (wind).

$$F_{grvt} + F_{prsr} + F_{visc} = ma_c \tag{2.1}$$

$$\sum F = ma_c = \frac{D(mv)}{\partial t} = \frac{\partial mv}{\partial t} + \frac{\partial mv}{\partial x}\frac{\partial x}{\partial t} + \frac{\partial mv}{\partial y}\frac{\partial y}{\partial t} + \frac{\partial mv}{\partial z}\frac{\partial z}{\partial t} \tag{2.2}$$

The term ($\frac{D(mv)}{\partial t}$) represents substantial derivative. The local derivative is denoted by ($\frac{\partial mv}{\partial t}$) while convective derivative is represented by the term ($\frac{\partial mv}{\partial x}\frac{\partial x}{\partial t} + \frac{\partial mv}{\partial y}\frac{\partial y}{\partial t} + \frac{\partial mv}{\partial z}\frac{\partial z}{\partial t}$). When simply RANS are used in a CFD model, the equations are not completely solved for turbulence. Only the average motion is computed and the effect of fluctuation is modelled [63]. All the turbulence is modelled estimating their dynamics based on experiments. RANS gives a prediction of the mean velocity and the mean level of turbulent quantities [67]. RANS based CFD wind models are the most practical CFD tools because of the reasonable computational requirements [28, 63, 68]. The computational time can be in hours for a single wake case [59]. Fuga wake flow software uses RANS [67]. The actuator disk model in [56] is based on NS equations.

2.2.1.2 Eddy Viscosity Model

This model is based on the eddy-viscosity concept, which assumes that, in analogy to the viscous stresses, turbulent stresses are proportional to the mean velocity gradient [50].

Turbulent eddies are treated in a similar way that molecules are treated and analysed in kinetic theory. Here, eddies are the carrier of thermal energy and momentum, in place of molecules.

The Ainslie wake flow model [50] is a simple eddy viscosity model which is also a part of WindPRO (one of the industry standard software for wake modelling) [48]. WindFarmer (a widely used commercial software in wind energy projects and research) also uses the Eddy viscosity model for wake effects prediction [69]. The foundation of the wake deficit model used in the Dynamic Wake Meandering Model (DWM) is the eddy viscosity model [56].

2.2.1.3 $k-\varepsilon$ Model

This model uses two PDEs and therefore is a two equation model [59]. The $k-\varepsilon$ model focuses on the mechanisms that affect the turbulent kinetic energy (per unit mass). It is based on the solution of equations for the turbulent kinetic energy (k) and the turbulent dissipation (ε). Following are the general form for k and ε as given in equations (2.3) and (2.4) respectively [61, 70, 71].

$$\frac{\partial k}{\partial t} + k_c = k_d + \frac{\partial k_{prod}}{\partial t} - \frac{\partial k_{dsp}}{\partial t} \tag{2.3}$$

$$\frac{\partial \varepsilon}{\partial t} + \varepsilon_c = \varepsilon_d + \frac{\partial \varepsilon_{prod}}{\partial t} - \frac{\partial \varepsilon_{dsp}}{\partial t} \tag{2.4}$$

where transport of k by convection is denoted by (k_c), (k_d) represents transport of k by diffusion, rate of production of k is given by ($\frac{\partial k_{prod}}{\partial t}$) and rate of dissipation of k is denoted by ($\frac{\partial k_{dsp}}{\partial t}$). Transport of ε by convection is denoted by (ε_c), (ε_d) represents transport of ε by diffusion, rate of production of ε is given by ($\frac{\partial \varepsilon_{prod}}{\partial t}$) and rate of dissipation of ε is denoted by ($\frac{\partial \varepsilon_{dsp}}{\partial t}$). A CFD model based on $k-\varepsilon$ is presented in [70]. $k-\varepsilon$ is the industry standard CFD model and is widely used in wind energy research [36, 62].

2.2.1.4 Large Eddy Simulation (LES)

In LES models, turbulence is divided into large and small eddy turbulences. LES solves the large eddies and models the smaller ones, making it more accurate as

compared to RANS and $k-\varepsilon$ models but the computational requirements are much higher [47, 49, 59]. Solving the large eddies makes it relatively computationally less efficient; massive parallel computing is required. Large scale eddies contain most of the energy and are significantly affected by the flow configuration [68]. First a filter is applied to differentiate between the important eddies: energy-containing eddies and not so important eddies: containing lesser energy [59, 62]. Large eddies are explicitly calculated while smaller ones are parametrised and modelled based on the behaviour of the large scale eddies [59].

Complexity of the model is somewhere in the middle of RANS and a complete numerical solution as only part of the turbulence is solved [63, 64]. RANS models the whole flow field as was discussed in section 2.2.1.1 while numerical simulations solve the whole flow field mathematically. LES falls in the middle and the complexity of the model depends upon the filtering criteria. If most of the eddies are solved mathematically and less are modelled, complexity and computational requirements are high and vice versa. As compared to RANS the computational time of LES increases to days for a single wake case using the same computational resources [59]. Details of the computer used in [59] are not given. LES can require about 1000 times greater computational resources as compared to RANS [59]. Simulator for Offshore / Onshore Wind Farm Application (SOWFA) wake model is based on LES [72, 73].

2.2.1.5 Direct Numerical Simulation (DNS)

DNS presents the most complex, accurate and computationally demanding CFD models. The wake flow is not modelled empirically, as the whole flow is solved mathematically. Unlike LES, no filtering is applied to differentiate between large and small eddies [64]. Solving of the whole flow field mathematically requires large computational resources [59, 62, 63, 68]. Models using DNS provide detailed and valuable information for verifying and revising turbulence models [59]. Due to the large computational requirements it can be said that DNS is not a practical tool and is not feasible [59, 62, 63, 68].

2.2.2 Engineering Wind Deficit Models

These models use empirical or analytical expressions for predicting wind deficit in a wind farm. This makes them computationally efficient but relatively less accurate as compared to CFD models. These models contain simple models for turbulence and

surface roughness and can provide quick and accurate solution for mean wind flows [68]. Engineering models are useful for predicting mean wind deficit inside the wind farm and for estimating wind farm efficiency but they do not provide details of the wake flow process [50]. These models can be easily executed on a standard Personal Computer (PC). Despite their simplicity, engineering models can be highly effective for predicting power production if the parameters are tuned well [74] as will be discussed in detail in sections 2.3 and 4.2. As engineering models do not provide information about the whole flow-field, these are also referred to as wind deficit models. The flow-field is not the area of interest in this thesis, hence the two terms "wind deficit models" and "wake models" are used synonymously.

The Jensen model [75, 76], Larsen model [77] and Frandsen model [78] are examples of engineering wake flow models. A brief overview of these models is provided in the following sections 2.2.2.1, 2.2.2.2 and 2.2.2.3 respectively.

2.2.2.1 Jensen Model

The Jensen model is the simplest but sufficiently precise and reliable wake flow model and has widely been used for wind energy research because of its high computational speed [11, 18, 29, 36, 42, 56, 75, 76, 79–81]. This model is based on law of conservation of momentum [75]. Wind flow is considered to be ideal i.e. frictionless and incompressible [75] which means that deep array effect and wake added turbulence intensity are ignored. Deep inside the wind farm, the turbines act as roughness generators, increasing the turbulence intensity and resulting in quick wake recovery, this is called deep array effect [11, 80]. These assumptions and limited number of parameters required for wind deficit estimation (equation (2.5)) make it the simplest model.

The downstream decrease in wind speed (u_x) depends upon free-stream wind speed (u_0), rotor diameter (r_0), distance at which the wake is calculated (x), thrust coefficient (C_T) and wake decay coefficient (k_{Jensen}) as given in equation (2.5) [75, 76]. Wake decay coefficient shows how quickly the wake diffuses in the far wake region and depends upon hub height of the wake generating turbine (z) and the surface roughness length (z_0) as given in equation (2.6) [75, 76]. Surface roughness length depends upon terrain characteristics [75, 76]. Wake expands linearly (hat-shaped) behind the wake generating turbine, starting with a diameter equal to the rotor diameter and is proportional to x. Radius of the wake (r_x) can be found with equation (2.7) [75, 76].

The Jensen model is a part of many commercial wind modelling software such as WindPRO [48] and WindFarmer [69]. The model is also called Park, Park Jensen or Jensen Park at times. In case of multiple wakes, the total velocity deficit is achieved by taking the linear sum of deficits created by all upstream turbines [76].

$$u_x = u_0 \left[1 - \left(\frac{1 - \sqrt{1 - C_T}}{\left[1 + \frac{k_{Jensen} x}{r_0} \right]^2} \right) \right] \tag{2.5}$$

$$k_{Jensen} = 1/[2\ln(z/z_0)] \tag{2.6}$$

$$r_x = r_0 + k_{Jensen} x \tag{2.7}$$

2.2.2.2 Larsen Model

The Larsen model is a stationary semi-analytical model based on the Dynamic Wake Meandering (DWM) model [82]. The model is based on a two order system. The first order system is achieved using an approximate solution [83]. The second order system also provides an approximate solution by adding a term to the axial velocity field from the first order problem. The wake flow is assumed to be incompressible and axis-symmetric [84]. A detailed mathematical description of the model is given in [83]. Wind deficit u_x at any distance (x) can be found with the following equation (2.8) as given in [36, 84].

$$u_0 - u_x = -\frac{u_0}{9} (C_T A x^{-2})^{1/3} \left[r^{3/2} (3 c_l^2 C_T A x)^{-1/2} - (35/2\pi)^{3/10} (3 c_l^2)^{-1/5} \right]^2 \tag{2.8}$$

Rotor swept area is denoted by (A) and (c_l) is the non-dimensional mixing length. Radius of the wake (r) can be found with the following equation (2.9).

$$r = [35/2\pi]^{1/5} (3 c_l^2)^{1/5} (C_T A x)^{1/3} \tag{2.9}$$

As compared to the Jensen model, the Larsen model provides more details about the wake, such as turbulence intensity but this also makes it computationally less efficient as compared to the Jensen model. The Larsen model is also a part of WindPRO [84]. In case of multiple wakes, the total velocity deficit is achieved by taking the linear sum of deficits created by all upstream turbines [40].

2.2.2.3 Frandsen Model

This is also an analytical model first presented in [78] and is adopted in the Storpark Analytical Model (SAM) [41]. This model is valid for offshore wind farms with regular shape of straight rows with equidistant spacing between the turbines [36, 78].

The model works in three different regimes. First wake flow is presented ignoring interaction between neighbouring wakes. In the second regime the neighbouring wakes interact. Wake expansion is limited only in vertical direction. When the wake flow is in balance with planetary boundary layer, the third regime starts. Wind speed deficit inside wake is assumed to be hat-shaped, same as in the Jensen model [41].

The wake diameter in the first regime ($D_{initial}$) can be found as given in the following equation (2.10) [36, 41, 78, 85, 86]. The wake expansion parameter is denoted by (B) and can be found with equation (2.11) [41, 86] where turbine swept area is denoted by (A) while swept area affected by the wake is given by (A_w)..

$$D_{initial} = B \times A \tag{2.10}$$

$$B = \frac{1}{2}\frac{1+\sqrt{1-C_T}}{\sqrt{1-C_T}} \tag{2.11}$$

The wind speed deficit (u_x) at any position (x) in the wake can now be found with the following equation (2.12) [41, 86].

$$u_x = \frac{u_0}{2}\left[1 \pm \sqrt{1-2\frac{A}{A_w}C_T}\right] \tag{2.12}$$

The wake expansion (D_{wake}) at any position can now be found with the following equation (2.13) [41, 86].

$$D_{wake} = D_{initial}\max(Bk_{Frandsen}/2+\alpha_F x)^{1/k_{Frandsen}} \tag{2.13}$$

According to [41] the typical values of wake decay coefficient $k_{Frandsen}$ and wake decay constant (α_F) are 2 and 0.7 respectively and usually are set experimentally [86]. As discussed in [36, 78] the model provides detailed wake flow estimation but it has some major flaws as it is applicable only to offshore wind farms with regular (grid) shapes and equidistant turbines.

2.2.3 Conclusion

It is concluded from sections 2.2.1 and 2.2.2 that there is a trade-off between accuracy and computational efficiency of wake flow models. If detailed wind flow information is required with no computational and time constraints then the high level CFD models (LES and DNS) are the appropriate options. If there is a constraint on processing time and only limited information is required (such as the mean wind speed), then engineering models are a better option. Available parameters for modelling wake flow also have an impact on selection of the wake model as CFD models require many parameters.

It is also discussed in sections 2.2.1 and 2.2.2 that many commercial wake modelling software have both the engineering and CFD models available. A comparison of the engineering and CFD models can give a better idea of their performance in different environments and wind conditions. This performance comparison is presented in the next section by reviewing previous studies evaluating performance of CFD and engineering wake models in different conditions.

2.3 Performance Comparison of Engineering and CFD Wake Models

Researchers have reported different results when comparing performance of CFD and engineering models. There is no consensus if one is better than the other. Wake models such as SOWFA [72] calculates the complete wake flow behind the turbine. On the other hand simplified assumptions such as ideal and incompressible wind flow make engineering models computationally efficient but less accurate as discussed in section 2.2.2. A choice has to be made between accuracy and computational efficiency while choosing a wake model. This section presents a literature review of performance comparison of different wake models.

Coordinated control of wind farms requires a wind deficit model as will be discussed in section 2.4. Therefore, previous studies which have compared wind deficit models for farm control are also discussed in this section.

The Jensen Park model, variations of DWM model, Actuator Disk Model and SOWFA are evaluated for wind farm control in [56]. Simulations show that the Jensen model is the fastest wake model requiring minimum input parameters and is suitable

for wind farm feedback control systems. Implementing DWM for farm control is not feasible because of its complexity and slow processing speed. The actuator disk model can also be used in dynamic feedback control systems, however the parameters and processing time required for wake modelling is greater than the Jensen model making the DWM unsuitable for wind farm coordinated control [56]. SOWFA can be used for testing realistic wind farm control strategies but a large amount of computing resources is required. When the k_{Jensen} in the Jensen model was tuned, it produced almost the same results as SOWFA in the far wake region. Details of this tuning is not provided. However, it is mentioned that the standard value of k_{Jensen} must be varied according to the conditions for better wake estimation. These results are summarised in Table 2.2. The Park, DWM and Actuator Disk models were run on a desktop computer (details of this desktop computer are not given). SOWFA was run on 256 cores at the Minnesota Supercomputing Institute. The terms (low, medium, high) for computing resources required in Table 2.2 are relative to each other and no quantification is provided for differentiating among these terms [56]. The Jensen model requires the minimum resources among all the evaluated models, hence the term low is used. SOWFA, even on 256 cores took 30 hours to process a single wake for two turbines, hence computational resources required are high. The DWM model estimates the flow field for each turbine over its entire simulation time, hence the computational requirements are medium and it is harder to implement. The NS equations are used for implementing the Actuator Disk model in [56] as discussed in section 2.2.1.1, hence the complexity level is termed medium as is the case for model based on NS equations.

The work in [12] concludes that even the most sophisticated, computationally expensive models do not always accurately predict the wake effects in a wind farm. It is also concluded that for simple terrains, engineering models have the same accuracy and significantly high computational efficiency as compared to CFD models. It is discussed in [12] that the Park Jensen model can give sufficiently accurate results for velocity deficits in a wind farm and this model is a better option for feedback control systems.

Six different CFD and engineering models are compared using different experiments in [39]. It is concluded that engineering models perform as good as CFD models despite their simplicity. The Jensen model, an advanced version of the Larsen model (based on RANS) and Fuga CFD model are compared using data from two offshore wind farms in [40]. This study concludes that the three models provided accurate predictions within a 1.5% error margin for a 30° directional bin. It is also mentioned that the Jensen model over-predicted production with the current recommended settings for offshore wind farms i.e. ($k_{Jensen} = 0.04$).

Table 2.2 Summary of wake models used for coordinated control for 1000 seconds simulation [56]

Model	**Computation Time**	**Computing Resources Required**	**Feasibility for farm control**
Jensen Park	5 seconds	Low	Most suitable because of speed and accuracy
DWM	8 minutes	Medium	Not feasible because of complexity
Actuator Disk	25 seconds	Medium	Can be used in feedback control systems, computationally expensive
SOWFA	30 hours	High	Not feasible as the model is computationally very expensive

One engineering and three CFD models are compared using data from a large offshore wind farm in [27]. It is concluded that engineering models have a tendency to under-predict wake losses while CFD based models over-predict them. Engineering and CFD wake models are used in [87] for modelling the impact of wakes on power output of the Horns Rev and the Nysted wind farms. It is concluded in this study [87] that all the models predicted farm efficiencies accurately in most of the wind conditions.

The Jensen, Ainslie and Larsen wake models are compared for predicting the efficiency of two wind farms in [80]. This study [80] concludes that if the standard k_{Jensen} in the Jensen model is tuned according to the wind conditions (by increasing value of k_{Jensne} inside the wind farm) then despite simplicity of the model, it produces more precise and reliable results than Ainslie and Larsen models.

An overview of six commercial and research engineering and CFD wake models for large offshore wind farms (Horns Rev and Nysted) is presented in [67]. It is shown that the Park Jensen accurately predicted the wake within the first 2-3 turbines in a row but can significantly underestimates wake losses after that. A reason for this is the constant value of k_{Jensen}. As turbulence increases inside the wake, effective values of k_{Jensen} shall also increase creating a wider wake. CFD models performed relatively better in this study [67].

Performance of different engineering and CFD models is evaluated in [57] with data from offshore wind farms. None of the models predicted the wakes accurately. All the models overestimate wake losses in neutral atmospheric conditions. It is concluded in this study [57] that wake models needs further improvement for multiple wake situations. FLaP-Jensen (Farm Layout Program-Jensen), FLaP-Ainslie and the FarmFlow model are compared for power prediction in single and double wake situations using data from the wind farm Alpha Ventus in [44]. It is concluded in this study [44] that reliabilities (accuracy in different cases) of FLaP-Ainslie and FarmFlow (both CFD) are of equal order and higher than FLaP-Jensen (engineering).

Comparative analysis for evaluating performance of the Jensen, Larsen, Frandsen and eddy viscosity models using data from the Sungsan onshore wind farm are performed, considering single wake conditions in [36]. Results in this study [36] show that Jensen model is the best in predicting velocity deficit while eddy viscosity and Larsen model perform better in predicting the wake width and profile. It is concluded that a wake model, suitable for all wind conditions cannot be selected (among the evaluated models) [36].

A comparison of the DWM and LES with field data from the Egmond aan Zee offshore wind farm is presented in [47] for predicting power losses and fatigue loading caused by wakes. It is shown in this work [47] that both the models under-predict power production and over-predict fatigue loads.

Six different models are used for modelling and measuring wake flow in the Horns Rev wind farm in [38]. This study [38] confirms that engineering models require modification for reducing under-prediction of wake losses while CFD models generally over-predict wake losses. The work in [28, 88] concludes that CFD based model are more reliable and accurate while engineering models underestimate wake losses.

The Jensen and Frandsen models are assessed for different scenarios using LES and RANS in [89]. Simulations in different wake conditions show that no fixed value of expansion factors fit well in all conditions [89]. These values must be tuned according to the wind and wake conditions for increasing the wake expansion inside the wind farm. Details of the tuning process are not given.

A review of wind turbine wake models with recommendations is presented in [74]. It is concluded in this study [74] that deep array correction is required for parameters in engineering models as increased surface roughness is created by the wind turbines under wakes in a wind farm. These simple models can be highly effective if parameters

are tuned well [74]. It is also suggested that computationally expensive CFD models should be used for tuning parameters and reducing complexity of other models [74].

The experiments in [29, 35, 90] conclude that parameters in engineering models must be tuned according to wind conditions and terrain characteristic for accurately predicting wake effects. These studies [29, 35, 90] also suggest that CFD based models are accurate but computationally expensive. The studies discussed in this section are also summarised in Appendix B in Table B.1.

2.3.1 Conclusion

The literature review in section 2.3 confirms that there is no consensus on superiority of a specific wake flow model. However the following common points can be taken from the literature review in section 2.3.

1. CFD models are complex, relatively accurate but computationally demanding. In some cases, these models over-predict wake losses.
2. CFD models can provide detailed information about the wake flow.
3. CFD models require detailed input information such as boundary layer conditions and mesh density.
4. Ainslie, $(k-\varepsilon)$ and LES are the most widely used CFD models but processing for estimating a single wake flow can take from hours to days using the same computational resources [59]. However the computational resources used for these calculations are not mentioned as discussed in section 2.2.1.4.
5. If there are no time and computational constraints then CFD models are the appropriate option.
6. Engineering models are computationally efficient but have low accuracy relative to CFD models. Generally these models under-predict wake losses.
7. Engineering models can provide mean wind speed for production calculation in the farm but cannot provide detailed wake flow information.
8. Engineering models require limited number of parameters for wake flow modelling.

9. Engineering models can provide better results if the standard parameters (wake expansion factors and coefficients) are tuned using wind farm data, wind conditions or high fidelity CFD models.

10. The Frandsen model is valid only for regular (grid) shape offshore wind farms with equidistant turbines.

11. The Jensen model is the most widely used engineering model because of its simplicity, relatively accurate results and computational efficiency. The model is most suitable for feedback control systems.

It is concluded that the choice of a suitable model depends upon user requirements such as required accuracy of prediction, desired computational efficiency, available parameters and the problem under consideration.

It is also concluded that if detailed wake flow information is not required then it is better to combine the accuracy of CFD models with computational efficiency of engineering models [29, 35]. The parameters such as wake decay coefficients and wake expansion factors shall be tuned with reference to wind farm data or a higher order CFD model as suggested in [29, 35, 38–40, 48, 67, 69, 74, 80, 91–93]. This can be achieved by combining analytical expressions based on CFD models with engineering models. The Jensen model is most suitable for feedback control systems, due to its computational efficiency [11, 56].

Section 2.1 established the point that wake effects can significantly affect economic performance and efficiency of wind farms. Power losses due to wakes can be as high as 60% [9]. An operating wind farm will always lose some of its power due to wake effects [11]. Coordinated control cannot only reduce these power losses but also reduce fatigue damage to the turbines without incurring any major additional cost. This type of control has recently been an active area of research. A detailed literature review of optimised control strategies based on coordinated control is presented in the next section 2.4.

2.4 Coordinated Control of Wind Farms

This section reviews previous research about wind farm coordinated control. The concept of coordinated control is explained identifying basic requirements for such control answering RQ-1.

The current state of the art wind farm greedy control instructs every turbine to produce the maximum power it can produce, neglecting wake effects on the downstream turbines [11]. A turbine follows its MPPT curve, optimising its individual power [12]. This increases wind deficit for downstream turbines. Details of MPPT were provided in section 1.2.1.

What if the farm is operated in a cooperative way where turbines in a farm coordinate with each other for increasing net power production / farm output? In this type of control the whole wind farm production is optimised rather than individual turbine's production. The aim is to curtail upstream turbines, hence reducing the wake produced and leaving more wind for the downstream turbines. If this curtailment is optimised in such a way that decrease in upstream turbine' power production is less than increase in downstream turbines' power production then net production will increase.

The concept of coordinated control was first presented in [94] almost three decades ago. Simulation of an experimental wind farm in [94, 95] show that compensation of aerodynamic interactions between wind turbines in a wind farm is beneficial. Reducing these unfavourable interactions can maximise farm production and reduce fatigue loads on the shadowed turbines.

Work in [12] uses the ideal case of two turbines for explaining the concept of coordinated control as shown in Figure 2.5. The horizontal axis in Figure 2.5 represents the axial induction factor (a) which is a measure of the slowing of the wind speed between the free stream and the rotor plane. The upstream turbine produces maximum power at $a = 0.33$, which is the theoretical maximum at Betz' limit, capturing 59.3% of the kinetic energy in the wind [12, 91]. However, the total production is maximum at $a = 0.20$ where power production of upstream turbine is reduced from maximum. This increases production of the downstream turbine as wake effect of upstream turbine is reduced. The loss in upstream turbine's production is compensated by increase in downstream turbine's production, hence a net gain in production. This study [12] also suggests that the farm controller should be developed with intelligence or adaptive learning.

Wind tunnel experiments in [96] suggest that wind farm production can be increased by reducing axial induction factor of upstream turbines. The Heat & Flux and Active wake control (Controlling Wind) patents [34, 97–102] perform numerical optimisation using axial induction factor with WAKEFARM model or yaw misalignment achieving a gain of maximum 2% with simulations on real time data.

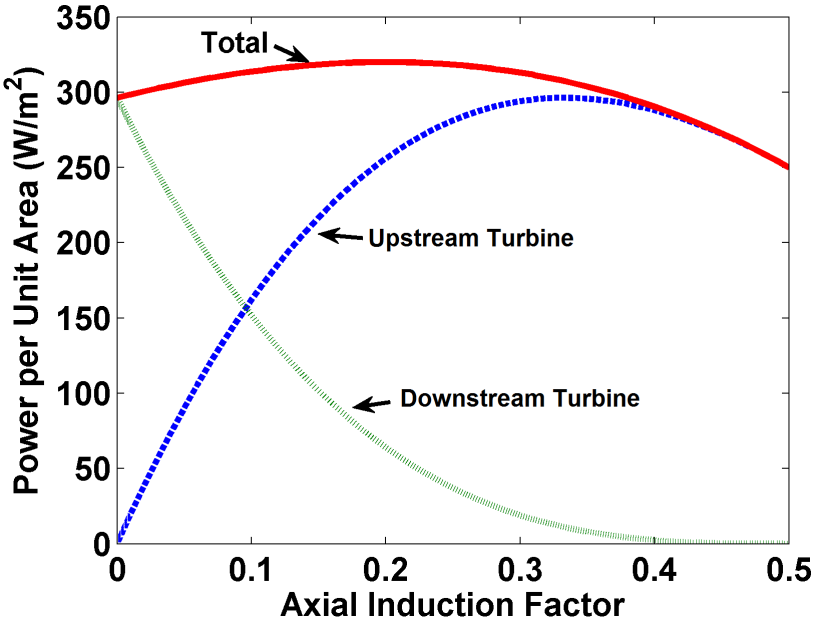

Figure 2.5 Coordinated control using an array of two ideal turbines in full wake conditions [12]

The work in [19] concludes that coordinated control can increase wind farm production and off-line lookup tables should be used for minimising computational efforts. However wind conditions and turbines' properties (such as switching off due to O&M) in a wind farm vary; therefore going completely off-line is not always desirable.

The work in [20] also confirms that coordinated control of a wind park is beneficial for reducing unavoidable disadvantages of operating wind turbines in a wind farm. This work [20] discusses different operating conditions of a wind farm and shows how coordinated control can be beneficial not only for the wind farm but also for the grid.

The farm controller in [103–105] uses CFD models and numerical optimisation for exploiting the benefits of coordinated control. These control strategies can optimise farm production and loads on the turbines but are computationally expensive making them unsuitable for real time on-line operations [103–105].

Simulations of artificial wind farms consisting of two and three wind turbines in [12] resulted in increased combined output with coordinated control. Numerical analyses in [10] are used to show increase in combined production of a three turbine wind farm.

The Jensen Park model is used in combination with numerical optimisation for increasing farm production in [106]. Simulations show a clear potential for improving the wind farm generation [106].

The farm control problem is distributed into sub-problems for analysing impact on structural load on the wind turbines in [107–109]. Simulations are performed using the SimWindFarm wind deficit model and numerical optimisation. This control approach concludes that structural load reduction is possible using coordinated control of wind turbines in a wind farm [107–109]. Simulations in [109] conclude that Damage Equivalent load (DEL) can be reduced by up to 8% on the downstream turbine in a two-turbine example array.

The work in [110] uses a modified version of the Park-Jensen model for increasing energy capture using the extremum seeking control. It is concluded that coordinated control can increase the energy captured in low turbulence intensity conditions, but not in high turbulence intensity conditions [110].

Game theory has been used in [111] for coordinated control of a simple three turbine wind farm. It is shown in this work [111] that coordinated control can increase the farm output by 25% as compared to the conventional greedy control. Another study in [112] uses game theoretic control with multi-agent systems for optimising farm production using the Jensen model for wind deficit calculation. This study [112] concludes that coordinated control can increase farm production by up to 10% in suitable wind conditions. The survey and review of studies about wind farm control in [112] emphasises fast processing of farm controllers for practical implementation of coordinated control strategies for production maximisation and fatigue load minimisation.

Cooperating static game approach using yaw offset angles is used for maximising efficiency of a wind farm with numerical simulations [113]. However, most of the assumptions about wind farm conditions are unrealistic. The unrealistic assumptions include maximum ideal axial induction factor (0.33) which corresponds to maximum ideal C_P of 0.593 [11], invariant wind conditions and ignoring wake added turbulence intensity inside the farm.

Studies in [35, 114–116] used a high-order wind farm model SOWFA and an engineering model FLOw Redirection and Induction in Steady-state (FLORIS) for coordinated control of an artificial wind farm. It is concluded that an adaptive optimisation strategy would be beneficial for coordinated control of the wind farms [35, 114–116]. The work in [114] simulates control strategies for a two turbine artificial

wind farm using SOWFA. This work [114] suggests that production of the downstream turbine can be increased significantly by properly curtailing or yawing the upstream turbine.

The Work in **[29, 79]** [1] uses a modified version of the Park-Jensen model and Particle Swarm Optimisation (PSO) for maximising farm production by up to 7%. It is concluded in these studies **[29, 79]** that it is possible to optimise the farm production on-line if the wind deficit model and the optimiser are accurate and fast enough. In on-line coordinated control, the farm controller must optimise the whole wind farm production, identifying power production or C_P of each turbine, before the wind reaches that specific turbine in the wind farm. This will be discussed in detail in section 2.4.2 and Chapter 3.

The work in [117] uses the Park model and a Genetic Algorithm (GA) for optimising farm production. Details of the optimisation process are not provided. It is recommended to use heuristic optimisation techniques for on-line coordinated control due to their ability to solve complex optimisation problems and for increasing computational efficiency. Heuristic algorithms are used (off-line) for maximising farm production using the AEOLUS SimWindFarm model in [118]. This work concludes that the possible energy gain depends upon the wake model used and can go up to 7%. Details of the heuristic optimisation techniques and process are not provided. This will be further discussed in Chapter 3.

The work in [119] presents a survey of wind farm control and optimisation studies. Some other studies about wind farm control are presented in [120, 121]. A complete list of studies of coordinated control with details is given in Appendix B in Table B.2.

Different optimisation techniques used in coordinated control studies are also discussed in the above literature review and summarised in Table B.2. Numerical optimisation [10, 94, 96, 103–109], game theoretic approach [112, 113, 116], hill climbing algorithm [120], PSO **[29, 79]** and GA [95, 117] have been used for wind farm control and optimisation. However, little or no information about the optimisation process are provided in these studies as will be discussed in section 3.1.

It is suggested in [12, 19] that iterative learning control algorithms can improve performance of the farm controller. Better and faster systems are required to help optimise the wind farm control [122]. The work in [122] summarises work done by different researchers and concludes that some of the open areas of research in

[1] Self-citations by the author are presented in bold

coordinated control are faster systems and tools for optimisation and wake modelling. If on-line coordinated control is required, the controller must optimise production of the whole wind farm accurately before the wind reaches the turbines [122]. A LiDAR can be used for measuring the free-stream wind speed and direction before it reaches the front-row turbines [11, 122]. The controller can then optimise production of the turbines in such a way that overall farm production is increased and instructs each turbine to produce accordingly. The optimisation process must be in the order of seconds as will be discussed in detail in section 2.4.2 and Chapters 3 and 5.

It is concluded from these studies [10, 94, 96, 103–109, 112, 113, 116, 120, 29, 79, 95, 117] that if properly implemented, coordinated control cannot only increase farm production but also reduce wake added turbulence intensity and hence fatigue loading on the shadowed turbines. The literature review conducted in this section used for identifying wind conditions and other factors which can impact the benefits of coordinated control as follows.

1. **Terrain characteristics** - Wakes can travel for longer distances in terrains with low roughness such as offshore wind farms.
2. **Wind conditions** - This includes turbulence intensity, wind direction and speed. In certain wind directions downstream turbines can be under full wakes, producing the highest impact on farm production.
3. **Layout of the wind farm** - Farms with lesser spacing between the turbines (denser farms) are affected more by wakes compared to farms with more spacing between the turbines.
4. Number of turbines in a wind farm which can benefit from curtailing upstream turbines.

Studies discussed in this section [10, 94, 96, 103–109, 112, 113, 116, 120, 29, 79, 95, 117] suggest that a controller based on coordinated control shall have two parts - a wind deficit model and an optimiser. A generic farm controller is presented in Figure 2.6. The optimiser generates different combinations of turbines' productions (trials) using the wind deficit model and selects the one which results in maximum farm production. As discussed in Section 2.2, a trade-off has to be made between accuracy and computational efficiency in the selection of a wind deficit model. The criteria for selecting a wind deficit model and optimiser for on-line coordinated control strategies

is defined in sections 2.4.1 and 2.4.2 respectively which are based on the discussion in this section.

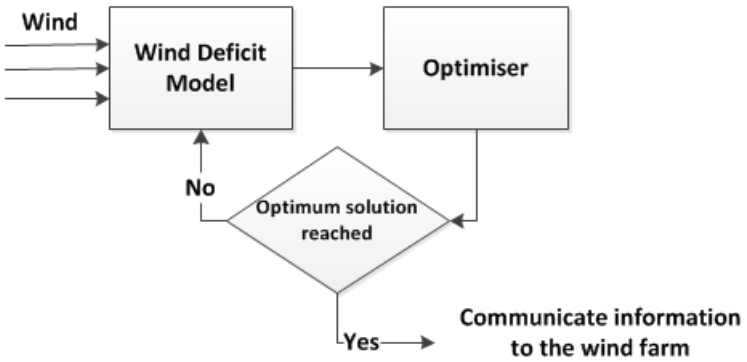

Figure 2.6 Generic model of a wind farm controller based on coordinated control

2.4.1 Selection Criteria for Wind Deficit Model for Coordinated Control

Researchers have used different wind deficit models for coordinated control as discussed in section 2.4 and summarised in Table B.2. The following criteria is defined for selection of wind deficit model for on-line coordinated control.

1. **Accuracy:** The wind deficit model should be accurate. The accuracy should be as high as possible; preferably within the range of ±0.5m/s [26, 87, 123].
2. **Processing speed:** The wind deficit model shall have high processing speed, in order of seconds [11, 110].
3. **Mean wind deficit:** Coordinated control does not require detailed wind flow information. Only mean wind deficit in the vicinity of each turbine is required for production estimation [11, 19, 112].

CFD models are relatively more accurate as compared to engineering wind deficit models as concluded in section 2.3.1. However, CFD models cannot be used for on-line coordinated control because of their low processing speed (as discussed in section 2.3.1). Engineering wind deficit models have high processing speed as discussed in section 2.3.1. It is concluded in [11, 56] that the Jensen model is most suitable for feedback coordinated control when compared with other models. It was concluded in

section 2.3.1 that accuracy of the Jensen model can be increased by tuning the k_{Jensen} according to the wind conditions. The Jensen model must be modified for developing a realistic farm controller to make the assumptions realistic, such as taking wake added turbulence intensity into account for tuning the value of k_{Jensen} inside the wind farm. This will be discussed in detail in chapter 4. The Jensen model can provide mean wind deficit in the vicinity of each turbine for production estimation. Hence if the k_{Jensen} is tuned according to the wind conditions, then it shall be used for developing on-line coordinated control strategies.

The Frandsen model is valid only for regular (grid) shape offshore wind farms with equidistant turbines installed in straight lines as discussed in sections 2.2.2.3 and 2.3.1. However, wind farms do not necessarily have a regular layout and turbines may have different spacing between them such as the Le Sole de Moulin Vieux (SMV) onshore wind farm **[29]**. The model cannot be used for onshore conditions where terrain is rough.

The Larsen model is based on the DWM model and is a semi-analytical model as discussed in section 2.2.2.2. The model can provide detailed information about the wind flow at the cost of processing speed. The Larsen model has low processing speed as compared to the Jensen model as discussed in section 2.2.2.2. Hence, it is concluded that the Jensen model shall be used for on-line coordinated control because of its high processing speed. The model must be tuned for increasing its accuracy. This will be further discussed in Chapter 4.

2.4.2 Selection Criteria for Optimisation Technique for Coordinated Control

Researchers have used different optimisation techniques for coordinated control of wind farms as discussed in section 2.4. Based on the discussion in section 2.4, the following selection criteria for is set for choosing a suitable optimiser for on-line coordinated control.

1. The optimisation process must be as fast as possible, in the order of seconds for on-line coordinated control [11, 19, 122]. The controller must optimise the wind farm production by estimating production or C_P of each turbine before the wind reaches the downstream turbines in the wind farm, allowing the turbine controller to act accordingly as per the instructions from the farm controller

when the wind reaches it. The time taken by the wind to move through the wind farm depends upon the wind speed and distance between the turbines.

2. The optimiser must provide a solution which is as close as possible to the global optimum [11, 110, 19, 122, 112]. The heuristic optimisation techniques do not guarantee to find the global maximum of the total farm production but the result must be an improvement (if possible) compared to the greedy control [118]. The solution quality shows the accuracy of the optimiser.

3. The optimiser must use minimum overheads [112]. These overhead are the trials made for achieving an optimum solution and the number of calls made to the wind deficit model for evaluating different combinations of wind turbines' power productions.

4. The optimiser must have high success rate and should avoid the local optimum achieving the desired results (acceptable solution) in different simulations (runs) [112]. Heuristic optimisation techniques do not always guarantee that the achieved optimal point is indeed the global optimum of the problem [121]. A high success rate means that the probability of achieving an acceptable solution should be as close to 100% as possible when multiple runs of the control (optimisation) process are executed.

It is recommended that the heuristic optimisation techniques shall be used for solving the coordinated control problem intelligently and iteratively [11, 19, 35, 117, 118, 122]. A suitable optimiser will avoid the local optimum for reaching or getting closer to the global optimum value. This will be further discussed in Chapter 3.

2.5 Conclusion

This chapter presented a detailed literature review of impact and modelling of wake effects in wind farms. Power losses due to wake effects can increase by up to 60% in the worst case situation [9]. Wakes can also increase fatigue loading on the shadowed turbines reducing their lifetime and increasing O&M costs. Accurate wake modelling is important for design, development and assessment of wind energy projects. These modelling techniques are broadly categorised as CFD and engineering models.

It was concluded that CFD-based wind models can give detailed information of the wake flow with relatively better accuracy. However, many parameters are required

for CFD models which are not easily available and these models are computationally expensive. LES and DNS can accurately predict wake flow but the processing time is in days. RANS and eddy viscosity models can predict wakes with less accuracy whereas the computational time is in hours.

Engineering models on the other hand are based on simple analytical expression and are highly computationally efficient. However, these models give little information about wake flow and are relatively less accurate. If only mean wind speed inside the farm is required with high processing speed then engineering models are a better option.

A literature review of performance comparison engineering and CFD wake models showed that researchers do not agree on the superiority of any specific model. It was concluded that the choice of a suitable wake model depends upon requirements of the problem under consideration such as desired accuracy, processing speed and time, available parameters and computational efficiency. Previous studies suggest tuning the parameters in engineering models, using wind conditions or CFD models. This way CFD and engineering models can be combined for developing computationally efficient and accurate wake flow models.

An operating wind farm always loses some power due to wakes (even with an optimised layout) because of wake effects in certain wind conditions. Coordinated control of wind farms can be used for increasing total wind farm production and reducing fatigue loading on downstream turbines. This reduces LCoE and O&M costs. In coordinated control, upstream turbines are curtailed optimally for reducing the wake produced on downstream turbines in such a way that combined production is increased.

A controller based on coordinated control requires a wind deficit model and an optimiser as two main components. It was concluded that the Jensen model is the most appropriate model for wind farm control. High processing speed, limited number of input parameters and sufficient accuracy makes the Jensen model most suitable for wind farm control; especially for on-line farm control. It was concluded that proper tuning of parameters in the Jensen model can increase its accuracy making it the first choice for wind farm coordinated control answering RQ-3.

For on-line control, the controller has to be fast (in order of seconds) and accurate as the algorithm must calculate power of each turbine before the wind reaches the downstream turbines. It was concluded that farm control algorithms shall be developed with intrinsic intelligence and iterative techniques for improved performance. Requirements

for appropriate optimisation techniques for farm control are fast processing speed, higher success rate and computational efficiency (using minimum trials (overheads)) producing accurate results - criteria for answering RQ-2.

Chapter 3

Selection of a Suitable Optimiser and Developing Control Strategies

This chapter evaluates performance of different optimisation techniques based on the criteria defined in section 2.4.2, answering RQ-2 which is selecting an appropriate optimiser for solving wind farm coordinated control problem.

It was concluded in Chapter 2 that coordinated control strategies shall be developed with iterative learning techniques having intrinsic intelligence. Heuristic optimisation techniques are intelligent iterative algorithms and have successfully been used for solving complex optimisation problems.

Wind farm coordinated control is a complex problem as each turbine's output affects output of downstream turbines (usually two - three) in a farm and the total farm production. As the number of turbines increases in the wind farm so does the complexity of coordinated control. Heuristic techniques are used and evaluated for solving coordinated control problem for maximising wind farm production in this chapter. These optimisers create different combinations of farm production, varying production of upstream turbines in the farm, moving towards the combination resulting in maximum farm production.

The methodology for selecting a suitable set of optimisers for solving the coordinated control problem is presented in section 3.1. Previous studies, evaluating the performance of different optimisation techniques by solving complex non-linear problems, are summarised in section 3.1.1 for selecting a suitable set of optimisation techniques for solving the coordinated control problem. An artificial wind farm of seven wind turbines presented in section 3.1.2 is used for evaluating the selected optimisers using

the objective function developed in section 3.1.3 based on C_P-based control. Yaw-based coordinated control strategies are explained in section 3.1.4. Details of the problem formulation for performance evaluation of selected optimisers are given in section 3.2. The Brute Force (BF) technique is used as a benchmark for finding global optimum value as detailed in section 3.3.

A brief description of the selected optimisers (GA, Simulated Annealing (SA), Ant Colony Optimisation (ACO) and PSO) is given in sections 3.4, 3.5, 3.6 and 3.7 respectively. Comparative analysis in section 3.8 concludes that PSO is the most suitable optimiser for wind farm coordinated control. Detailed description of PSO is provided in section 3.9. A comparison of PSO neighbourhood topologies (global best or fully connected and circle or ring topology) is presented in section 3.9.10 which concludes in section 3.10 that PSO with global-best topology is the most suitable technique for optimising farm production answering RQ-2. Figure 3.1 depicts the structure of this chapter.

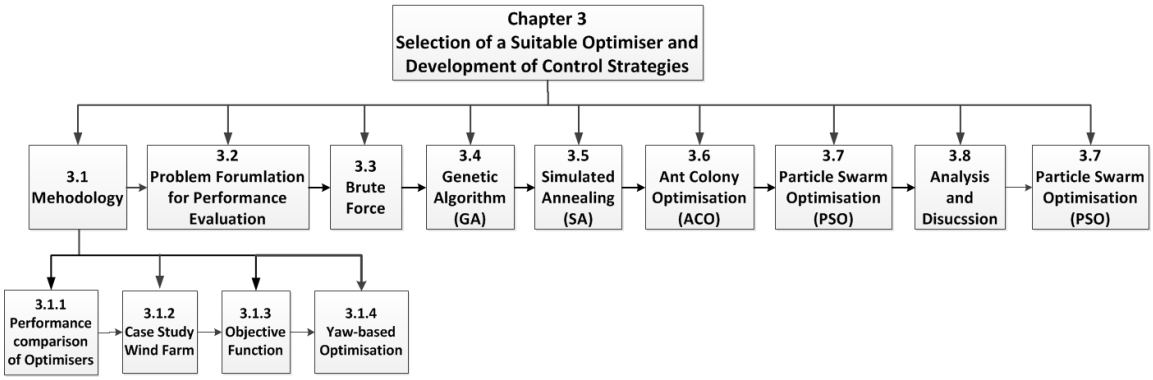

Figure 3.1 Structure of chapter 3

3.1 Methodology

Previous research on wind farm coordinated control emphasises more on the aerodynamics of the problem, providing little or no information of the optimisation process as discussed in section 2.4. Wind farm coordinated control is a complex optimisation problem as each individual turbine's production is a dimension of the farm production [**79**] [1]. The greater the number of turbines in a wind farm, the greater the complexity of the coordinate control problem will be, as the number of dimensions has increased.

[1]Self-citations by the author are presented in bold

Numerical optimisation [10, 94, 96, 103–109], game theoretic approach [112, 113, 116], hill climbing algorithm [120] and GA [95, 117] are some of the techniques used for solving coordinated control problem as discussed in chapter 2 and summarised in Table B.2. However, none of these previous studies evaluated performance of optimisation techniques using coordinated control. The works in [117–121] mention the optimisers used with the aim to improve computational efficiency. However no specific details such as the optimisation time, overheads used, solution quality and success rate are provided. Following is a detailed description of these [117–121] studies.

The work in [117] used GA for optimising (maximising) wind farm production. However no information about the optimisation process (processing speed, overhead and success rate) is provided. It is suggested in [117] that heuristic optimisation techniques must be used for minimising computational efforts. No rationale is provided for using GA for farm production maximisation in [117].

It is mentioned in [118] that the BF technique shall not be used for farm production maximisation as this technique (BF) is computationally exhaustive. To address this issue, the use of heuristic algorithm is proposed. It is mentioned that an iterative heuristic algorithm is used for farm production optimisation [118], however name of the optimisation technique is not mentioned. It is concluded in [118] that the optimiser showed good performance and improved the farm production as compared to the greedy control, however no quantification is provided about the performance of this optimiser, optimisation process and increase in farm production.

The survey in [119] summarises previous studies about wind farm coordinated control and makes some recommendations for practical implementation of this type of control. The farm control problem is solved numerically in this study [119]. However it is mentioned that computationally efficient and accurate intelligent optimisation techniques (no specific names given) must be used for practical (on-line) implementation of coordinate control [119].

The work in [120] uses the gradient-based (hill climbing) optimisation technique to find the control settings that yield a maximum total power production of the wind farm. The optimisation technique is a local optimisation technique and may converge to a local maximum instead of a global maximum of the total production [120]. This technique is used in order to improve the computational efficiency of the optimisation [120]. No further information about the optimisation process is provided. Optimisation time, overheads used and success rate are not mentioned.

The work in [121] uses the sequential quadratic programming algorithm, implemented in Matlab global optimisation toolbox [124]. An improvement of 2.85% is achieved in farm production with simulations of coordinated control relative to the normal operations with greedy control. It is mentioned that the optimisation problem is non-convex, both in the objective function and constraints [121]. There is no readily available solver that can handle such optimisation problems and guarantee that the achieved optimal point is indeed the global optimum of the problem [121]. It is mentioned in [121] that a global search is implemented in order to increase the probability of finding the global optimum and several iterations (number of iterations is not mentioned) are used to find the best solution. No further details about the optimisation process are provided.

Performance evaluation of different optimisation techniques for coordinated control has not been performed in these previous studies [10, 94–96, 103–109, 117, 120] as discussed earlier. However, researchers have evaluated and compared performance of different optimisers for solving complex discrete and continuous problems. These studies are reviewed in section 3.1.1 for selecting a suitable set of optimisers for performance evaluation, using the coordinated control problem. The aim is to select computationally efficient and accurate optimisers with high success rate as discussed in section 2.4.2. As heuristic optimisation techniques does not always guarantee to achieve the global optimum point [121], the aim is to achieve an acceptable solution in multiple runs of the control process, termed as success rate here.

An artificial wind farm of seven wind turbines is detailed in section 3.1.2, for evaluating performance of the selected optimisers. An objective function (based on C_P, yaw-offsets or both) for maximising overall farm production is developed in section 3.1.3. This objective function is used for comparing performance of the selected optimisers based on the evaluation criteria described in section 2.4.2.

3.1.1 Performance Comparison of Optimisers

Different Artificial Intelligence (AI) and Evolutionary Algorithms (EAs) have been used for solving complex optimisation problems, for which traditional mathematical techniques may fail [79, 125–131]. EAs are stochastic search methods that mimic natural biological evolution and/or the social behaviour of species for solving non-linear problems [125, 132]. Generally EAs solve complex problems iteratively and intelligently by evaluating a fitness value for reaching an optimum value.

Five evolutionary techniques, GA, Memetic Algorithms (MA), PSO, ACO, and Shuffled Frog Leaping (SFL) are compared for optimising discrete and continuous test problems in [125]. This study [125] concludes that PSO outperforms other algorithms in terms of solutions quality and success rate for continuous problems. ACO is ranked as the fastest algorithm but the success rate is low. SFL solution quality is as good as PSO and ACO, better than GA but the processing speed is the least amongst all the techniques. The behaviour of all optimisers is the same for all discrete problems.

GA, PSO, Artificial Bee Colony (ABC), Clonal Selection Algorithm (CSA), Bacterial Foraging Optimisation Algorithm (BFO), Firefly Algorithm and ACO are compared for optimal power flow and economic dispatch problem in [126]. Economic dispatch is the short-term determination of the optimal output of a number of electricity generation facilities, to meet the system load, at the lowest possible cost, subject to transmission and operational constraints. It is concluded that PSO and BFO are the two fastest and best techniques for finding optimum solutions for complex problems such as optimal power flow and economic dispatch [126]. ACO has the same processing speed as PSO but the success rate is lower [126].

GA, Tabu Search (TS) method, a Modified PSO (MPSO), numerical methods, Artificial Neural Network (ANN) and different evolutionary programming approaches are evaluated for solving the economic dispatch problem in [127]. MPSO produces much better results than other techniques used for 3-generator and 40-generator systems, satisfying all the given constraints [127]. MPSO success rate and processing speed is the highest amongst all the techniques used in this work.

GA, PSO and differential evolution (DE) are evaluated for solving discrete and continuous problems in [128]. These problems include job shop, flexible job shop, vehicle routing, location-allocation and multi-mode resource constrained project scheduling. It is found that GAs are more suitable for solving complex discrete problems while PSO and DE can effectively solve continuous optimisation problems [128].

PSO and SA are used for real-time condition monitoring of induction motors in [129]. This work [129] concludes that PSO is suitable for real-time complex optimisation problems because of high success rate and processing speed. The success rate of PSO is reported to be 99% while for SA it is about 60%.

A comparison of the performance of GA, SA, Artificial Neural Network (ANN) and TS for optimising the number of kanbans for Just in Time (JIT) systems is presented in [130]. A kanban is a printed card describing the job information in JIT system. The number of kanbans allocated to each job is an important decision problem as it can

greatly affect the desired goals of JIT [130]. It is always desired to keep number of kanbans at an optimum level. All the techniques produced same quality solution. In terms of processing speed TS is the fastest, followed by SA, GA and ANN respectively [130].

Performance of a modified PSO (MPSO) is compared with several kinds of GA for solving binary problems with specified characteristics in [131]. PSO outperforms GA in solving complex problems [131]. Success rate of PSO is 100% and processing speed is better than GA.

ACO, GA, SA, PSO and TS are evaluated for solving the path planning in robotics in [133]. The robotic path planning is defined as the determination of a path of robot from a starting point to the destination point while avoiding any collision from obstacles in between [133]. One of the major difficulty in solving the path planning problem is computational efficiency, which means that it should take optimal time for finding a path avoiding collisions with obstacles [133]. SA and ACO outperformed other techniques in terms of processing speed in this study [133].

An elaborative comparative analysis of ACO and TS is provided in [134]. It is mentioned in this study [134] that if parameters are tuned according to the problem under consideration then TS is a better option for local search while ACO is a better option for global search. It is also mentioned that the processing speed, success rate and solution quality differs for solving different problems [134].

3.1.1.1 Conclusion

It is concluded that the choice of a suitable optimisation technique is problem dependent. Researchers have reported different results when comparing performances of different optimisation techniques as discussed in section 3.1.1. Despite widespread success of heuristics, there will always be questions related to the usefulness of a particular heuristic technique for solving a wide rage of problems [135]. The optimisers discussed in the studies reviewed in section 3.1.1 are evaluated as per the criteria given in section 2.4.2 in Table 3.1. The aim is to select five different optimisers for performance evaluation using coordinated control.

It can be concluded form the studies in section 3.1.1 that GA is one of the most widely used optimisation technique for solving complex non-linear problems [125–128, 130, 131, 133]. GAs are one of the most efficient heuristic techniques for solving complex problems in control systems engineering [136]. Hence, GA is one of the

optimisers selected for evaluation for solving coordinated control problem of wind farms.

ACO and PSO are relatively new techniques but are faster with high success rate for the problem under consideration in [125, 126, 128, 131, 133–135]. It can be observed in Table 3.1 that the studies in [125–129, 131] have chosen PSO as the fastest optimiser for the corresponding problem under consideration (as detailed in section 3.1.1). These studies [125, 128, 129, 131] conclude that the solution provided by PSO is of the highest quality. PSO has the highest success rate for the optimisation problems reported in [125–129, 131]. Based on the performance of PSO, reported in the studies summarised in section 3.1.1 and Table 3.1.1.1, PSO is the second optimiser chosen for evaluation for solving coordinated control problem of wind farms.

The BF technique is selected as the third optimiser. This technique will be used as the benchmark for finding the global optimum i.e. maximum achievable farm production. The work in [133] also uses BF as the benchmark for evaluating performance of the selected heuristic optimisers.

The studies in [126, 133, 134] selects ACO as the optimiser with the highest processing speed for the particular problems under consideration. It is concluded in [130, 134] that TS optimises the problems under consideration with high processing speed (processing time is not given). SA is chosen as the optimiser with high processing speed in [130, 133]. The work in [126] concludes that BFO is among the optimisers with fastest processing speed and success rate. It is mentioned in [134, 135] that ACO is more suitable for global optimisation while TS is suitable for local search. The aim in this thesis is to find the global optimum (maximum achievable) farm production with coordinated control using a suitable optimiser. Hence ACO is preferred over TS for solving the coordinated control problem.

A review of previous studies regarding the problem-solving abilities of SA and TS in [133, 135] prefers SA over TS for solving problems with many local minima. SA can optimise problems with many local minima with high processing speed as compared to TS [133]. The problem of coordinated control of wind farms has many local minima as will be discussed in section 3.3. Hence, SA is preferred over TS. GA, SA and ACO are all population based techniques. The selection of SA diversifies the optimisers set as SA is a non-population based technique. Performance evaluation of other optimisation techniques such as SA, BFO and ABC using coordinated control are left for the future work as will be discussed in section 7.2.4. The full set of optimisers for performance evaluation now includes BF, GA, SA, ACO and PSO.

Table 3.1 Evaluation of the optimisers discussed in the studies in section 3.1.1, showing the selected optimiser(s) as per the criteria established in section 2.4.2

Ref	Optimisers compared	Processing Speed	Solution Quality	Success Rate
[125]	GA, PSO, ACO, MA, SFL	PSO	PSO, SFL	PSO
[126]	GA, PSO, ABC, CSA, BFO, ACO, Firefly	PSO, BFO, ACO	Not given	PSO, BFO
[127]	GA, TS, MPSO, ANN, Evolutionary Programming, Numerical methods	MPSO	MPSO	MPSO
[128]	GA, PSO, DE	GA for discrete problems. PSO and DE for continuous problems	GA for discrete problems. PSO and DE for continuous problems	Not given
[129]	PSO, SA	PSO	PSO	PSO
[130]	GA, SA, ANN, TS	TS, SA	All are same	Not given
[131]	GA, MPSO	MPSO	MPSO	MPSO
[133]	GA, ACO, SA, PSO, TS	ACO, SA	SA	Not given
[134]	ACO, TS	TS for local optimisation while ACO for global optimisation	TS for local optimisation while ACO for global optimisation	Not given

3.1.2 Wind Farm Case Study

An artificial wind farm of seven NREL 5MW turbines [137], shown in Figure 3.2 is assumed for evaluating performance of the selected optimisers. It is assumed that turbines are installed in a straight line with $3D$ spacing between them as many farms have turbines installed in straight rows (grid like shape) [9, 29, 98]. The minimum spacing of $3D$ represents the industry standards accurately as many wind farms have such spacing between the turbines, for examples the Brazos, SMV and Lillgrund wind farms [9, 29, 138]. The Energy Research Centre Netherlands (ECN) Wind Turbine Test Site Wieringermeer (EWTW) also has the same layout of turbines [98]. This site

is widely used for wind energy research, protocol verification and certification [98, 101]. These are the bases for the layout of the assumed wind farm.

It is assumed that wind flow is parallel to the turbine array and that wind speed is 10m/s. The assumed wind conditions for the wind farm case study represent the worst case situation where the wake effects in the farm are maximum. The assumption that turbines are installed in a straight line and that wind flow is parallel to the turbine array is to consider maximum wake interaction representing the worst case situation which is most difficult to optimise. The optimiser has to evaluate a large number of combinations of power productions for achieving the global maximum as will be further discussed in sections 3.3 and 3.8. These assumptions do not influence the choice of optimisation technique. If an optimiser can achieve the desired results in the worst case scenario, then it will achieve the desired results in other cases as well. With more spacing ($\geq 3D$) between the turbines, wake effects will reduce and the optimiser has to evaluate lesser number of turbines' power productions as the search or solution space is reduced. The wind speed does not have any effect on the performance of selected optimisers and any other wind speed other than 10m/s can be used for evaluation.

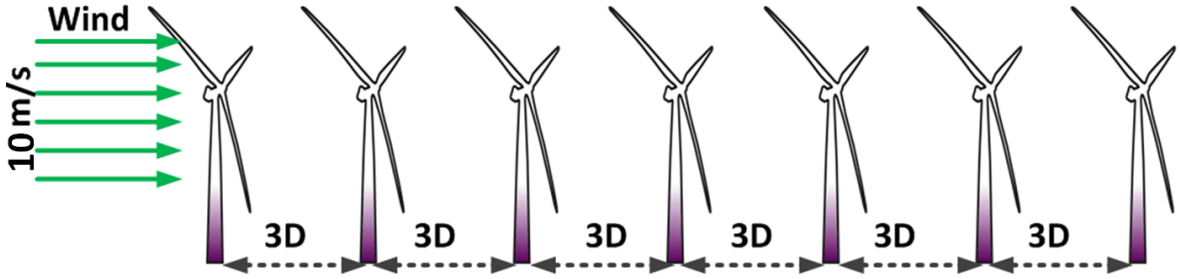

Figure 3.2 Case Study wind farm for performance comparison of selected optimisers

3.1.3 Objective Function

This section formulates the objective function for production maximisation of wind farms using coordinated control. It was discussed in Chapter 2 that the controller based on coordinated control generates different combinations of turbines' powers using a wind deficit model through a suitable optimiser, selecting the combination resulting in maximum farm power output as shown in Figure 2.6. This is achieved with an objective function aimed at maximising overall farm production.

The standard Jensen model [75] is used for wind deficit calculation while developing the objective function. The aim is to evaluate performance of the optimisers, hence the standard Jensen model [75] is used because of its simplicity of implementation. The Jensen model can be replaced by any other wind deficit model.

The total wind farm production is the sum of individual wind turbine's production. The power output of a single wind turbine is given by equation (3.1) [11].

$$P_{Turbine} = \frac{1}{2}\rho A u^3 C_P \cos^2\alpha \tag{3.1}$$

where ($P_{Turbine}$) is the output of an individual turbine, (ρ) is the air density, (A) is turbine swept area, (u) is the wind speed and (C_P) is the coefficient of power of the turbine. C_P determines how much energy a turbine extracts from the wind [11]. Yaw offset angle in degrees is denoted by (α). In normal operations and conventional greedy control, C_P is kept at maximum while α equals to 0°. The term $\cos^2\alpha$ represents the effect of yaw-offset on turbine's power production. Researchers have used different powers for the term $\cos\alpha$ (in equation (3.1)) [119]. The power of $\cos\alpha$ in equation (3.1) can range from 1 to 5 depending on the C_T or tip speed ratio and the farm under consideration (study) [119, 11]. Different powers of $\cos\alpha$ were evaluated in this thesis. It was found that the power of "2" models the actual wind conditions and power production more accurately as also discussed in [11, 118, 139, 140], hence the power of "2" is used in this thesis. This will be further discussed in section 6.5.

A turbine controller following MPPT (greedy control) is intelligent and can vary C_P according to the wind conditions (following its standard power curve) or as directed by the wind farm operator [141], as was discussed in section 1.2.1. C_P is a function of blade pitch angle (β) and Tip Speed Ratio (λ) [140]. C_P can be found with the following equation (3.2) using axial induction factor (a) [140]. Axial induction factor is defined as the loss in momentum or measure of the slowing of wind speed between free stream and the rotor plane [12, 96].

$$C_P(\beta, \lambda) = 4a(1-a)^2 \tag{3.2}$$

Varying β or λ changes a. C_P is related to coefficient of thrust (C_T) through a. C_T characterises thrust on a wind turbine and can be found using equation (3.3) [140].

$$C_T = 4a(1-a) \tag{3.3}$$

The Jensen model uses C_T for wind speed deficit prediction while power production is calculated using C_P. These two variables are correlated using a as given in equations 3.2 and 3.3.

Total wind farm power production is the sum of the power produced by all the turbines in the wind farm as given in equation (3.4) where total number of turbines in the wind farm is given by (N). Wind speed experienced by a particular turbine (i) in the wind farm is given by $u(i)$.

$$P_{Farm\_Wakes} = \sum_{i=1}^{N} P_{Turbine(i)} = \sum_{i=1}^{N} \frac{1}{2}\rho A u(i)^3 C_P(i) \cos^2 \alpha_i \tag{3.4}$$

Usually all the turbines in a wind farm have the same configuration and characteristics i.e. hub height, blade length, power curve and hence maximum C_P given by $(C_{P(max)})$. If it is assumed that ρ remains constant inside the wind farm then the term $(\frac{1}{2}\rho A)$ is constant in equation (3.4), denoted by C_n. Equation (3.4) can be rewritten as equation (3.5).

$$P_{Farm\_Wakes} = \frac{1}{2}\rho A \sum_{i=1}^{N} u(i)^3 C_P(i) \cos^2 \alpha_i = C_n \sum_{i=1}^{N} u(i)^3 C_P(i) \cos^2 \alpha_i \tag{3.5}$$

If C_n in equation (3.5) is ignored then the control problem or objective function is to maximise the expression $\sum_{i=1}^{N} u(i)^3 C_P(i) \cos^2 \alpha_i$ in equation (3.5).

Now if it is assumed that all the turbines are under no wake effects then all of them will experience the same wind speed which is the free stream wind speed (u_0) and α becomes $0°$ (ideally). As the aim is to maximise the overall farm production, all the turbines operate with their $C_{P(max)}$. In this case the maximum achievable farm output is given by equation (3.6).

$$P_{Farm\_Free\_Flow} = \frac{1}{2}\rho A \sum_{i=1}^{N} u_0^3 C_{P(max)} = C_n \sum_{i=1}^{N} u_0^3 C_{P(max)} \tag{3.6}$$

The control objective now is to minimise the difference between equation (3.6) and equation (3.5).

$$\begin{aligned} &min\,(P_{Farm\_Free\_Flow} - P_{Farm\_Wakes}) \\ &= min\left(C_n \sum_{i=1}^{N} u_0^3 C_{P(max)} - C_n \sum_{i=1}^{N} u(i)^3 C_P(i) \cos^2 \alpha_i\right) \end{aligned} \tag{3.7}$$

Ignoring C_n in equation (3.7), the objective function ($f(P_{max}, C_{P(max)}, \alpha_{max})$) or control problem for wind farm production maximisation can be formulated as equation (3.8).

$$f(P_{max}, C_{P(max)}, \alpha_{max}) = min\left(\sum_{i=1}^{N} u_0^3 C_{P(max)} - \sum_{i=1}^{N} u(i)^3 C_P(i) \cos^2 \alpha_i\right) \tag{3.8}$$

The controller is aimed at minimising $f(P_{max}, C_{P(max)}, \alpha_{max})$ in equation (3.8) using C_P or α or both. It can be seen that if there are no wakes and $\alpha = 0°$, farm production is maximum, making $f(P_{max}, C_{P(max)}, \alpha_{max})$ equals to zero. The range of C_T and C_P for the objective function are defined in section 3.4. The objective function is under no constraints. The objective function has no units as C_n is ignored in equation (3.8), if C_n is included in the objective function then the unit is Watt (same as power production).

3.1.4 Yaw-based Optimisation

Coordinated control strategies for wind farm production maximisation are aimed at optimally curtailing upstream turbines. This optimal curtailment can be achieved using C_P or yaw-offsets or both. This section explains coordinated control strategy based on yaw-optimisation.

Yaw offset is denoted by α and the term $\cos^2 \alpha$ in equation (3.1) gives the impact of yaw-offset on a turbine's production. With the conventional greedy control, ideally a turbine faces the wind with $\alpha = 0°$. Yawing a turbine not only changes its production but also the direction of the wake produced [100, 101]. This change in direction of the wake is called skewing and the angle at which the wake is directed away from the normal course is called skewing angle denoted by (γ).

The principle behind yaw-optimisation is that γ is greater than α, as given in equation (3.9) [100]. A smaller α can skew the wake away from the downstream

shadowed turbines. This reduces production of the upstream turbine but increases productions of the downstream turbines. Hence optimal settings of yaw-offsets can be used for increasing net power production of the wind farm.

The analytical relationship between α and γ given in [100] is used in this study as shown in the following equation (3.9). This expression is developed using a series of experiments in a scaled wind farm [100]. The expression clearly shows that for a yaw offset of 1°, the wake is skewed by 1.2°. Equation (3.9) is developed using different wind tunnel experiments and validated using real-time field data from wind farms with different layouts in [98, 101, 140]. Equation (3.9) is also used and validated through simulations in [113] using field data. The aim of this thesis is to develop and implement fast processing and accurate real time on-line coordinated control strategies. Using the analytical expression given in equation (3.9) provides a faster approach for estimating γ as compared to solving the whole flow field and then estimating γ. Hence equation (3.9) is used in this work for estimating γ.

$$\gamma = 1.20 * \alpha \tag{3.9}$$

3.2 Problem Formulation for Performance Evaluation

This section is mainly based on the work in **[79]**. Performance of the selected optimisers, for production maximisation with coordinated control, is evaluated using the case study wind farm detailed in section 3.1.2 with the objective function given in equation 3.8. Evaluation criteria are based upon solution quality, processing speed, number of overheads used and success rate for achieving an acceptable solution as described in section 2.4.2.

The standard Jensen model [75] is used for wind deficit calculation because of its simplicity, limited number of parameters required and simple implementation as discussed in section 3.1.3. The selected optimisers use the Jensen model for generating different combinations of turbines' productions.

The decision variable can be either C_P, α or both in the optimisation process. Varying C_P of an upstream turbine varies its power production and hence the wake produced. It shall be noted that varying C_P indirectly changes C_T, which is the main parameter affecting the strength of the wake. If optimal yaw offsets are applied on

upstream turbines using α, wakes can be deflected away from downstream turbines, increasing net production. The most appropriate optimiser will vary C_P or α intelligently achieving an optimum value with high processing speed using minimum overheads i.e. number of trials made. The processing speed should be in the order of seconds as was detailed in section 2.4.2. The overheads or trials show the different combinations of power production evaluated by the optimiser for achieving an optimum solution. The wind deficit model (the Jensen model) is used for creating these combinations of productions. Using lower number of trials significantly increases the processing speed, hence the optimiser should achieve the optimum solution with minimum number of trials. This was detailed in section 2.4.2.

The decision variable for optimisation is assumed to be C_P for evaluating the performance of selected optimisers. It is assumed that the turbines are perfectly aligned with the wind direction resulting in $\alpha = 0°$. The wind speed bin is maintained at 1m/s as suggested in [38, 87, 123]. With this bin size, it is assumed that the wake effects remain the same over $\pm$0.5m/s. This bin size is also used in most of the standard power curves provided by manufacturers use a bin size of $\pm$0.5m/s [16, 142–144]. Decreasing the bin size increases complexity of the optimisation problem as more combinations of power productions can be generated.

It shall also be noted that the last turbine in the array should be operated greedily. The wake produced by this turbine does not impact the farm production. Hence, it shall always produce the maximum it can. This also reduces one dimension of the problem as the number of turbines' productions to be optimised now is $(N-1)$, which makes it six for the example wind farm. The aim is to use the selected optimiser for on-line real time farm control. Reducing a dimension reduces complexity of the optimisation process, resulting in higher processing speed and reduced number of overheads used.

When the wind turbines operate greedily, $f(P_{max}, C_{P(max)}, \alpha_{max})$ in equation (3.8) become 6830. Any decrease in this value (6830) will bring an increase in farm production as the objective is to minimise the difference between farm production in no-wake conditions and the actual farm production. An explanation of how the selected optimisers perform coordinated control of the example wind farm is given in the following sections 3.3, 3.4, 3.5, 3.6 and 3.7.

3.3 Brute Force (BF)

The BF technique evaluates the whole solution space for finding global optimum value. That's why this technique is also called the exhaustive search or generate and test technique [**79**]. All combinations of turbines' power productions are generated and evaluated according to equation (3.8). When a combination of productions is generated, it is compared with the previous best value. This makes sure that the global optimum value is achieved.

3.3.1 Results

A farm production array is generated which contains all combinations of power productions that can be produced in the example wind farm in the given wind conditions. This array is presented in Figure 3.3 with reference to the first two upstream turbines (total dimensions are six). Figure 3.3 clearly exhibits the complexity of the coordinated control problem. An optimiser has to avoid many local optima in order to reach closer to the global optimum. The global optimum value for $f(P_{max}, C_{P(max)}, \alpha_{max})$ is 6532 corresponding to an increase of 4.5% in farm production relative to the greedy control as the value of $f(P_{max}, C_{P(max)}, \alpha_{max})$ for greedy control is 6830 as discussed in section 3.2.

3.4 Genetic Algorithms (GAs)

GAs have proved to be useful at tackling problems that cannot be solved using conventional methods [136, 145]. GA starts with a population of random chromosomes which are potential solutions of the problem under consideration [146]. Selection, crossover and mutation are used for generating better solutions from the existing population in every iteration, if possible [136, 145, 146].

Crossover combines two individuals (parents), to form a new individual (child) for the next generation [124, 146]. The new offspring created are put into the next generation of the population. As population size is static, some of the weak individuals (with low fitness values) will die. Mutation introduces some random modification (random walk through solution space) to the new generation [136]. A portion of the new individuals will have some of their bits flipped (mutated) to maintain diversity and inhibit premature convergence. Mutation enables GA to search a broader space

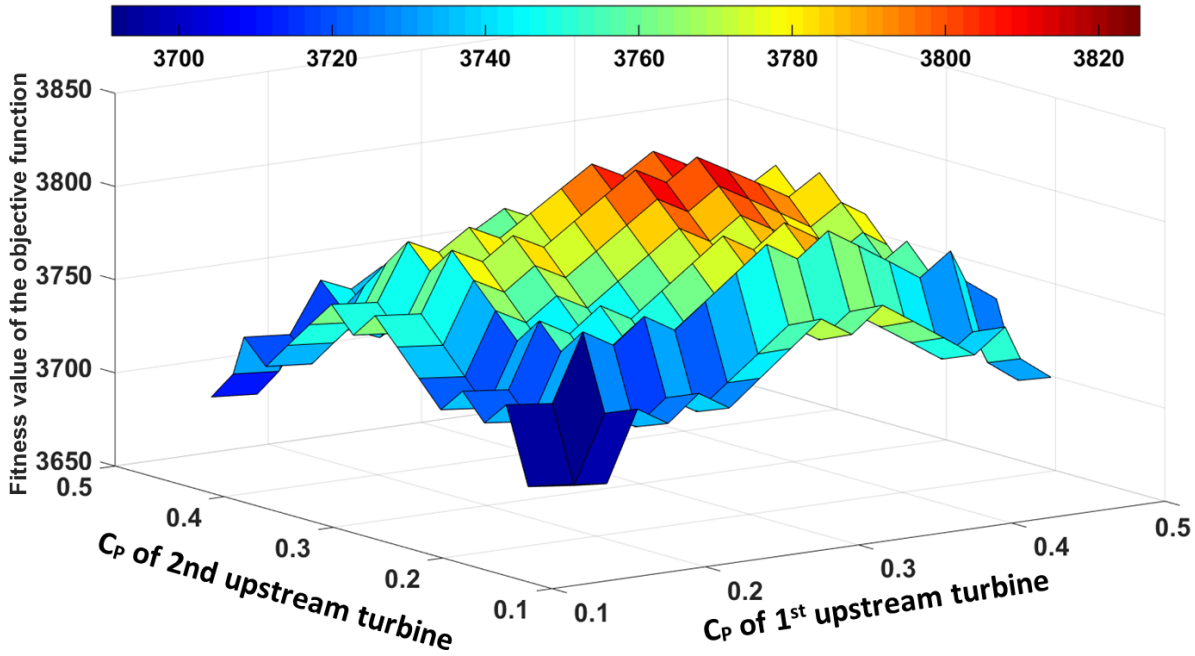

Figure 3.3 Power array with reference to first two upstream turbines

providing a chance to avoid local optima [124, 145]. The algorithm terminates when a satisfactory solution is reached or when the loop terminates.

The objective function in equation 3.8 is optimised using GAs with the Matlab global optimisation toolbox [124, 147]. The Matlab global optimisation toolbox has widely been used for solving complex optimisation problems [124, 147]. The major strength of Matlab global optimisation toolbox is that different functions are available for defining the population size, selection, reproduction, mutation and crossover [124]. These different options were used and evaluated for solving the coordinated control problem by tuning parameters for achieving accurate results with high processing speed as detailed in Appendix C in section C.1.

3.4.1 Results

The flow chart in Figure 3.4 represents optimisation of the control process using GA. Figure 3.5 shows how GA achieves the fitness value. The value achieved for $f(P_{max}, C_{P(max)}, \alpha_{max})$ is 6632 which shows an improvement over the greedy control ($f(P_{max}, C_{P(max)}, \alpha_{max}) = 6830$). However, the global optimum value ($f(P_{max}, C_{P(max)}, \alpha_{max})$

= 6532) is not achieved. This will be further discussed in section 3.8. Further information about GAs can be found in [124, 136, 145–148].

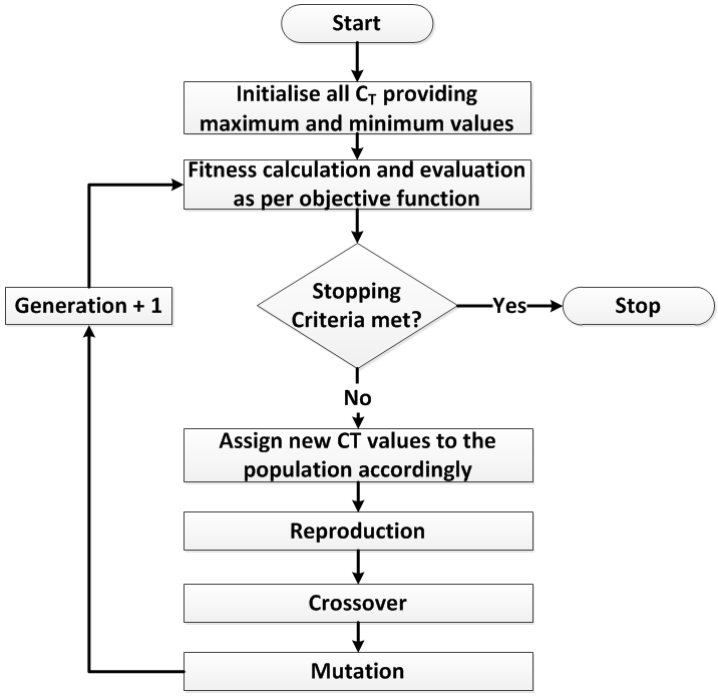

Figure 3.4 GA flow chart for coordinated control problem

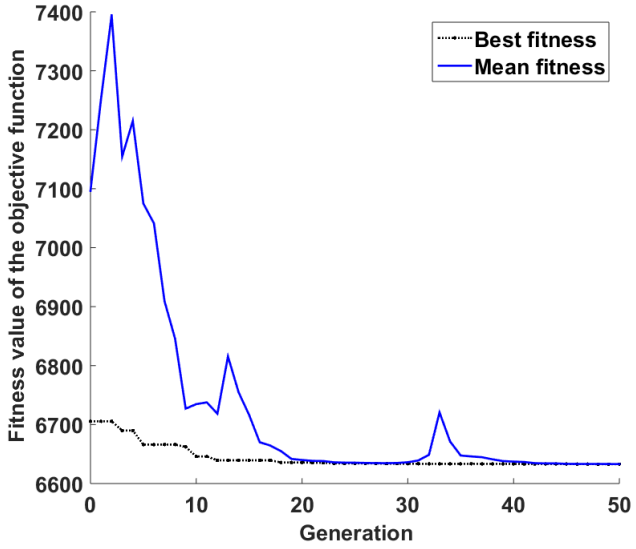

Figure 3.5 GA movement towards the optimum solution

3.5 Simulated Annealing (SA)

SA is motivated by an analogy to annealing in solids [149, 150]. It provides a means to escape local optima by worsening the value in objective function hoping that global optimum may be reached [151]. Each iteration, the algorithm generates two values i.e. the current solution and a newly selected solution. A comparison is made between the solutions; improved (superior) solutions are accepted while some of the non-improving (inferior) solutions are also accepted. These inferior solutions are used for escaping a local optima [150]. The probability of accepting inferior solutions depends upon the temperature [151]. The temperature parameter is defined initially and changes as the algorithm runs through iterations. This approach (escape from local optima) gives a better chance of not trapping in a local optima as more area of the solution space can be searched [151].

The wind farm production optimisation problem is complex with many local optimum as can be seen in Figure 3.3. SA is used in effort to escape those local optimum for reaching the global optima. SA from the Matlab global optimisation toolbox [124, 147] is used. The Matlab global optimisation toolbox has different functions and parameters for SA, which were tuned for maximising farm production. Details of evaluating and tuning of the parameters are given in section C.2.

3.5.1 Results

The flow chart in Figure 3.6 shows the complete process of SA solving coordinated control problem. Same bounds of C_T are used as with GA. Movement towards the optimum solution is shown in Figure 3.7. The value achieved for $f(P_{max}, C_{P(max)}, \alpha_{max})$ is 6632 which shows an improvement over the greedy control ($f(P_{max}, C_{P(max)}, \alpha_{max})$ = 6830). However, the global optimum value ($f(P_{max}, C_{P(max)}, \alpha_{max}) = 6532$) is not achieved. This will be further discussed in section 3.8. The algorithm terminates after the specified number of iterations are executed. Further details of SA optimisation process can be found in [124, 149–151].

3.6 Ant Colony Optimisation (ACO)

ACO is inspired by the food-seeking behaviour of real ants [152–155]. Ants move from nest to food sources following different paths stochastically, leaving pheromone behind

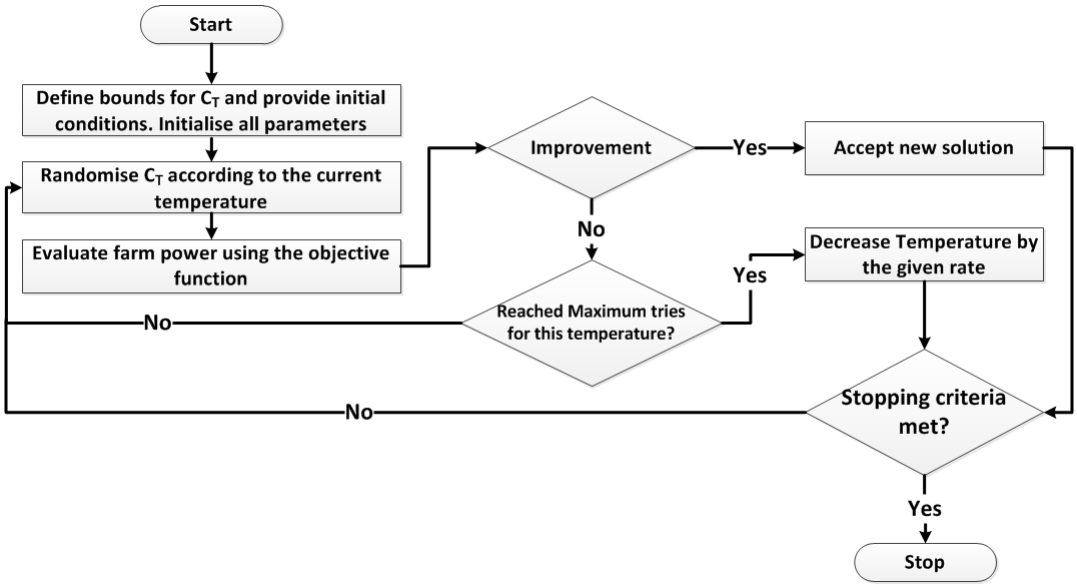

Figure 3.6 SA flow chart for coordinated control problem

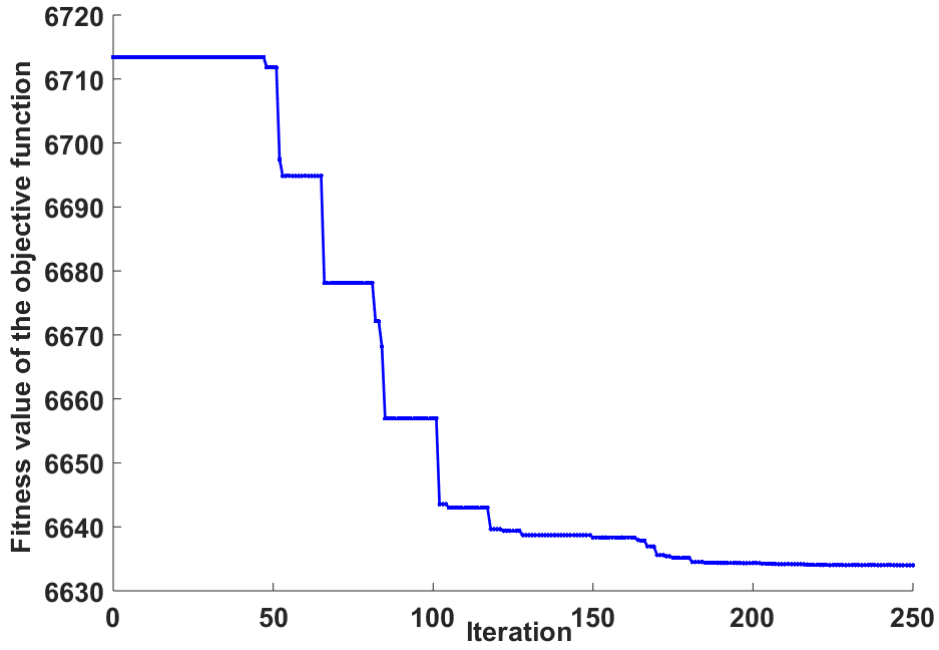

Figure 3.7 SA movement towards the optimum solution

them. Other ants can detect these pheromones. With the passages of time, more ants follow the shortest path making the pheromones trail stronger. In the meanwhile, no ants follow the longer paths hence the pheromone evaporates and vanishes there.

This way, ants use their combined knowledge to follow the shortest path to the most abundant food source.

Figure 3.8 [156] represents different steps of ants travelling from nest towards food source choosing the shortest path. It can be seen that there are different paths leading to the food source. Initially ants travel through these paths leaving pheromones behind. Ants travelling through the shortest path returns first, hence more ants follow that path making the pheromone trail stronger. As the number of ants travelling through the longer path decreases, the pheromone evaporates making that path less attractive for other ants.

ACO uses ants as agents and food source as the potential solution for solving complex problems [152]. In the coordinated control problem different ants represent C_T of turbines, while the optimised production (maximum farm production) is the best food source. A prerequisite for designing an ACO algorithm is to have a constructive method which can be used by an ant to create different solutions through a sequence of decisions [157]. Every decision extends a partial solution by adding a new solution component until a complete solution is derived. These different solutions are paths on a graph. This graph is called construction graph [152, 154–157]. Construction graph is used for generating artificial pheromones and partial solutions. That is why ACO is mostly used for scheduling problems such as travelling salesman and scheduling activities problems [133, 158].

Partial solutions were created using combination of C_T and fitting them to the objective function given in equation (3.8). Providing the scheduling information in the construction graph for coordinated control problem makes it complex to implement ACO for such problems as there are many different combinations of powers (paths for ACO) and many local optima as shown in Figure 3.3. The algorithm terminates when an acceptable (optimum) solution is achieved or when the number of loops is terminated. Details of ACO implementation in Matlab are given in section C.3.

3.6.1 Results

Movement of ACO towards the optimum value of $f(P_{max}, C_{P(max)}, \alpha_{max})$ is shown in Figure 3.9. ACO also achieved almost the same optimum value as GA and SA for $f(P_{max}, C_{P(max)}, \alpha_{max})$, which is 6637. This shows an improvement over the greedy control ($f(P_{max}, C_{P(max)}, \alpha_{max}) = 6830$). However, the global optimum value

$(f(P_{max}, C_{P(max)}, \alpha_{max}) = 6532)$ is not achieved. This will be further discussed in section 3.8.

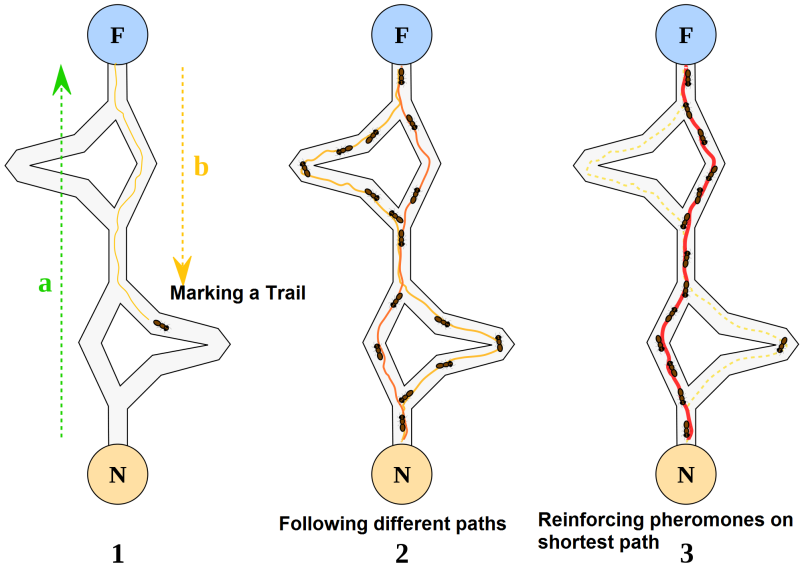

Figure 3.8 Ants moving towards food-source choosing shortest path using pheromones [156]

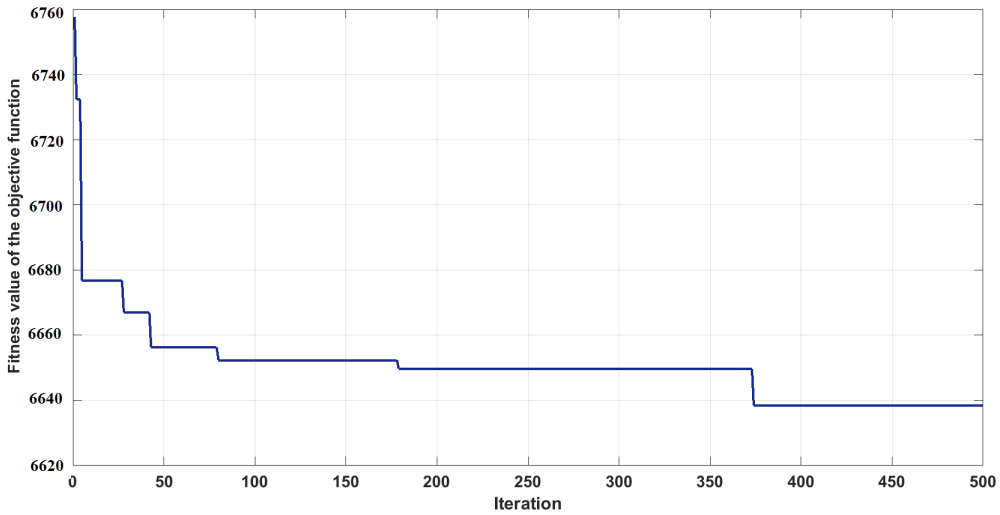

Figure 3.9 ACO movement towards optimum solution

3.7 Particle Swarm Optimisation (PSO)

PSO consists of particles which are artificial agents but with no individual intelligence [159]. These particles move through the solution space by creating collective intelligence solving complex optimisation problems. Each particle is a potential solution in the given solution space.

The algorithm keeps a record of each particle's best fitness value achieved in different iterations - called the local best of the particle. The best solution or best fitness value among all the particles is also recorded - called the swarm's global best. The particles use their current position in the solution space, local best and global best to generate a velocity for moving towards the best possible solution [159, 160]. The process is iterative. Each iteration, the swarm builds up an organised movement and direction towards the optimum value using a set of equations [79, 159, 160]. The algorithm terminates when the required (acceptable) solution is reached or when the number of iterations is completed.

PSO was implemented in Matlab as PSO is not a part of Matlab global optimisation toolbox .In coordinated control, each swarm represents C_T of an individual turbine. The C_T upper and lower bounds are same as for other optimisers. Detailed description of tuning other variable is given in section 3.9 and summarised in Table 3.2.

3.7.1 Results

The control process using PSO is presented in Figure 3.10. Figure 3.11 shows the movement of PSO finding the optimum value of $f(P_{max}, C_{P(max)}, \alpha_{max})$. PSO also achieved the same optimum value as GA and SA for $f(P_{max}, C_{P(max)}, \alpha_{max})$, which is 6632. This shows an improvement over the greedy control ($f(P_{max}, C_{P(max)}, \alpha_{max})$ = 6830). However, the global optimum value ($f(P_{max}, C_{P(max)}, \alpha_{max})$ = 6532) is not achieved. This will be further discussed in section 3.8.

3.8 Analysis and Discussion

This section discusses performance of different optimisers by analysing the results given in Table 3.3 and is based on the discussion in sections 3.3, 3.4, 3.5, 3.6 and 3.7. Performances of GA, SA, ACO and PSO are shown in Table 3.3 and evaluated in this

Table 3.2 Evaluating the parameters in PSO as per the criteria in section 2.4.2

Parameter	**Values / Functions evaluated**	**Selected value / function**	**Reason for selection**
Population	20 to 100 in a step of 10	30	Achieves optimum solution with higher computational efficiency
Distribution of randomness generators	Gaussian, Uniform, Poisson, Normal	Normal	All the distributions have the same processing speed and solution quality. The default Normal is used
Constants	Different positive values of the two variables with a sum equal to 4	2 and 2	Relatively better solution quality
Inertia (global search)	0.90	Supports global search	Relatively better solution quality
Inertia (local search)	0.20	Supports local search	Relatively better solution quality
Inertia decrease rate	0.02 to 0.10 in a step of 0.01	0.03	Relatively better solution quality
Neighbourhood topology	Global best, ring best	Global best	Relatively high processing speed
Number of particles in a ring	3 to 9 with a step of	5	Reaches optimum solution with high processing speed

section as per the criteria describe in section 2.4.2. Evaluation criteria is based upon number of iterations used for achieving the optimum (acceptable) solution, processing time, number of overheads used, success rate and closeness to the global optimum farm production, as describe in section 2.4.2. A total of 100 runs are used for getting these results.

All the optimisers curtail the first four upstream turbines by reducing their C_P. The last three turbines are operated at their maximum capacity. It was discussed in

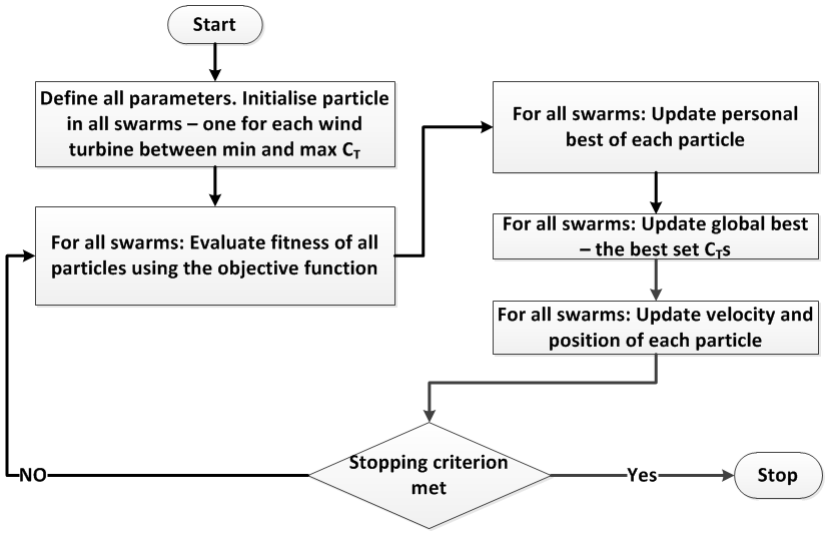

Figure 3.10 PSO flowchart for solving coordinated control problem

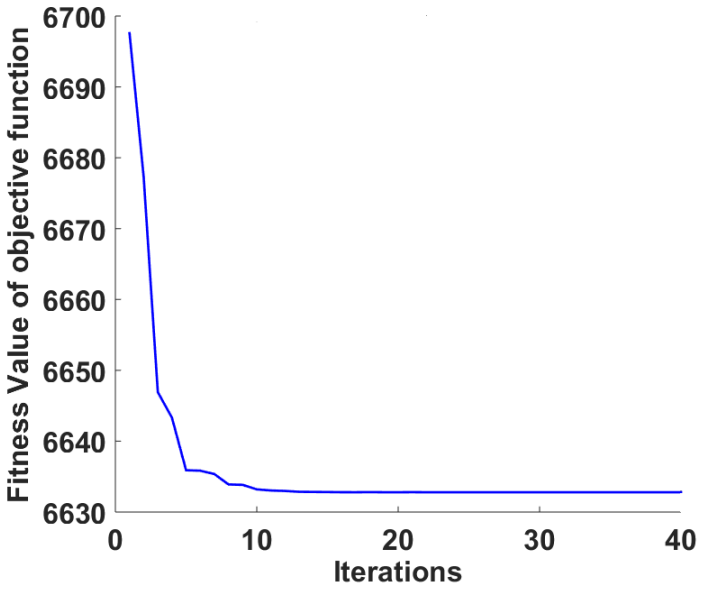

Figure 3.11 PSO movement towards the optimum solution

section 3.2 that the last turbine in the array is operated greedily and is not considered for optimisation.

The number of iterations, processing time and overheads used by BF techniques shows the complexity associated with this technique. That is why it is used only as a benchmark for finding the global optimum value i.e. maximum possible production of the case-study wind farm. Hence, closeness to the global optimum ($f(P_{max}, C_{P(max)}, \alpha_{max})$

Table 3.3 Performance comparison of selected optimisers for wind farm coordinated control. Value of the objective function for greedy control is 6830.

Variables	**Brute Force**	**GA**	**SA**	**ACO**	**PSO**
C_P1	0.29	0.29	0.29	0.29	0.29
C_P2	0.33	0.33	0.33	0.33	0.33
C_P3	0.33	0.37	0.37	0.37	0.37
C_P4	0.41	0.43	0.43	0.43	0.43
C_P5	0.44	0.44	0.44	0.44	0.44
C_P6	0.44	0.44	0.44	0.44	0.44
Population size	NA	50	NA	50	30
Success rate after 100 trials	NA	100%	100%	100%	100%
Value of the objective function	6532	6632	6632	6637	6632
Closeness to global optimum	100%	98.5%	98.5%	98.5%	98.5%
Improvement over greedy control	4.5%	3.0%	3.0%	3.0%	3.0%
Iterations	1.5625×10^{10}	51	250	400	40
Processing time in seconds	8400	0.51	2	3	0.33
Overheads (calls to the wake model)	7.8×10^{11}	85200	7854	26600	6654

= 6532) is 100%. BF shows that a maximum of 4.5% increase is possible in production of the case study wind farm, in the given wind conditions, as compared to state of the art greedy control as discussed in section 3.3.

The population sizes of GA, ACO and PSO were evaluated within a range of 20 to 100 according to the criteria given is section 2.4.2. It was found that a population size of 50 (for GA and ACO) provided better results as compared to other population sizes. When GA and ACO population size was reduced to 30, the processing time increased because of extra iterations used and more overheads (trials) used for reaching the optimum solution. The optimum population size for PSO for solving the coordinated control problem was found to be 30. PSO was able to achieve the optimum solution

with high processing speed using a population size of 30. These population sizes were determined by simulating equation 3.8 in Matlab in 100 different runs.

GA, SA, ACO and PSO produced a solution of almost the same quality having the same success rate. These optimisers are trapped in a local optimum ($f(P_{max}, C_{P(max)}, \alpha_{max})$ = 6632) at a distance of 1.5% from the global optimum ($f(P_{max}, C_{P(max)}, \alpha_{max})$ = 6532). The difference in solution quality of BF and other optimisers is because of the C_P of Turbine3 and Turbine4. BF curtails them more as compared to other optimisers. In the case of GA, SA, ACO and PSO, the last three downstream turbines have less wind to produce with. This still results in an increase of 3% in farm production as compared to the conventional control ($f(P_{max}, C_{P(max)}, \alpha_{max})$ = 6830) which is acceptable.

Success rate of GA, SA, ACO and PSO for achieving the optimum (acceptable) solution of the same quality is 100%. This means that all these optimisers obtained the optimum (acceptable) solution ($f(P_{max}, C_{P(max)}, \alpha_{max})$ = 6632) in all the 100 runs. Parameters in these optimisers were tuned to test if the local optima can be avoided as discussed in section 3.7.1 and appendix C. With the optimum values for all the corresponding variables in the optimisation techniques, the optimisers result in the same solution quality during the 100 runs, being trapped in the same local optimum. As this solution quality is acceptable, the success rate is 100%.

PSO uses the minimum number of iterations (40) for achieving the optimum result. GA requires 51 iterations for achieving the same solution as PSO. While SA and ACO require 250 and 400 iterations respectively for achieving the optimum result. The number of iterations has an impact on processing speed and processing time. Processing speed decreases and processing time increases with the increase in number of iterations. Hence PSO has the highest processing speed, with GA second, SA at the third and ACO at fourth place. PSO and GA complete the optimisation in less than one second while SA takes two seconds and ACO takes three seconds for completing the optimisation process.

PSO outperformed GA, SA and ACO in terms of number of calls (trials) made to the wake model which represents the number of overheads used. SA is rated second in terms of number of overheads used with GA at third and ACO at fourth place. GA used almost 13 times more overheads than PSO and 11 times more than SA. The number of overheads used along with processing speed shows computational efficiency of the optimisers. The processing speed of both GA and PSO is under one second, however PSO has lower overheads which increases its computational efficiency. The

number of overheads becomes significant if the wind deficit model takes more time for processing. Lower number of overheads means lower number of calls made to the wind deficit model and evaluating fewer combinations of turbines' productions for reaching an optimum solution.

3.8.1 Conclusion

These analyses show that GA, SA, ACO and PSO produce the same solution quality and have the same success rate for achieving this solution. All these optimisers produce an improvement of 3.0% ($f(P_{max}, C_{P(max)}, \alpha_{max}) = 6632$ with coordinated control as compared to $f(P_{max}, C_{P(max)}, \alpha_{max}) = 6830$ with greedy control) in farm power production relative to conventional greedy control as detailed in section 3.4, 3.5, 3.6 and 3.7. PSO is computationally more efficient than GA and SA as processing speed is higher and the number of overheads used is lower. Hence PSO is more suitable for coordinated control of wind farms. Detailed explanation of PSO is given in the next section 3.9.

3.9 Particle Swarm Optimisation (PSO)

PSO is a population based Swarm Intelligence optimisation technique. Particles in a swarm mimic birds in a swarm or fish in a school [159]. Birds fly in swarms with no specific leader but they communicate with each other, creating a collective intelligence moving towards a food source. Each bird searches individually for a food source and at the same time communicate with other birds about the food sources already discovered by them. All the birds in the swarm move towards the bird that discovers the richest food source and at the same time keep an eye on the food source it has discovered on its own. This way an individual bird benefits from both the food sources. This process continues until all the given or specified area is searched for potential food sources. In the end all the birds reach the richest available food source.

This birds' swarm analogy is applied to particles in a swarm for solving complex optimisation problems. Particles in a swarm represent the birds. The richest food source represents the global optimum solution available. Other richer food sources are represented by local optima. The particles fly through the solution space searching for the best available solution.

This optimisation process is iterative. Each iteration, the particles create a direction moving towards the global optimum with a velocity (V_i). This V_i of a given particle (i) is determined using equation (3.10) [159, 161]. The position (x_i) of the particle i at time $(t+1)$ is simply the sum of particle i current position at time (t) and the velocity for moving towards the next positions as given in equation (3.11) [159, 161].

$$V_i(t+1) = R_1 V_i(t) * \zeta + c_1 R_2 * (p_i(t) - x_i(t)) - c_2 R_3 * (p_g(t) - x_i(t)) \tag{3.10}$$

$$x_i(t+1) = x_i(t) + V_i(t+1) \tag{3.11}$$

(R_1, R_2 and R_3) are randomness generators, inertia is denoted by (ζ) which controls velocity of the particles, (c_1, c_2) are constants used for controlling movement towards local and global best respectively, (p_i) is personal best of the i^{th} particle in all previous t iterations, (p_g) is the global best of the swarm and (x_i) is current position of the i^{th} particle in the solution space. The values of these variables depend upon the specific problem under observation. Detailed description of these variables is given in the following sections.

3.9.1 Velocity (V_i)

Velocity is the rate of change of movement or jump that a particle has while moving towards the optimum solution [131, 159, 162, 163]. Velocity is determined and updated each iteration using equation (3.10) [159, 164]. Velocity is always kept at a nominal rate according to the problem under consideration, depending upon values of other variables, given in equation (3.10) and varies in each iteration accordingly. If it is too high the particles may miss the optimum solution. Lower velocity may result in trapping of a particle in a local optima. Some researchers have termed velocity as habit or momentum [165, 166]. Movement of some random particles (PSO-global best) towards the optimum C_Ps is shown in Figure 3.12 considering the artificial wind farm detailed in section 3.1.2. The C_P values of each turbine in Figure 3.12 corresponds to the C_P values (for PSO) given in Table 3.3. The optimum C_P value for turbine1 to turbine6 (upstream to downstream) is 0.29, 0.33, 0.37, 0.43, 0.44 and 0.44 respectively as can be observed in Figure 3.12 and Table 3.3.

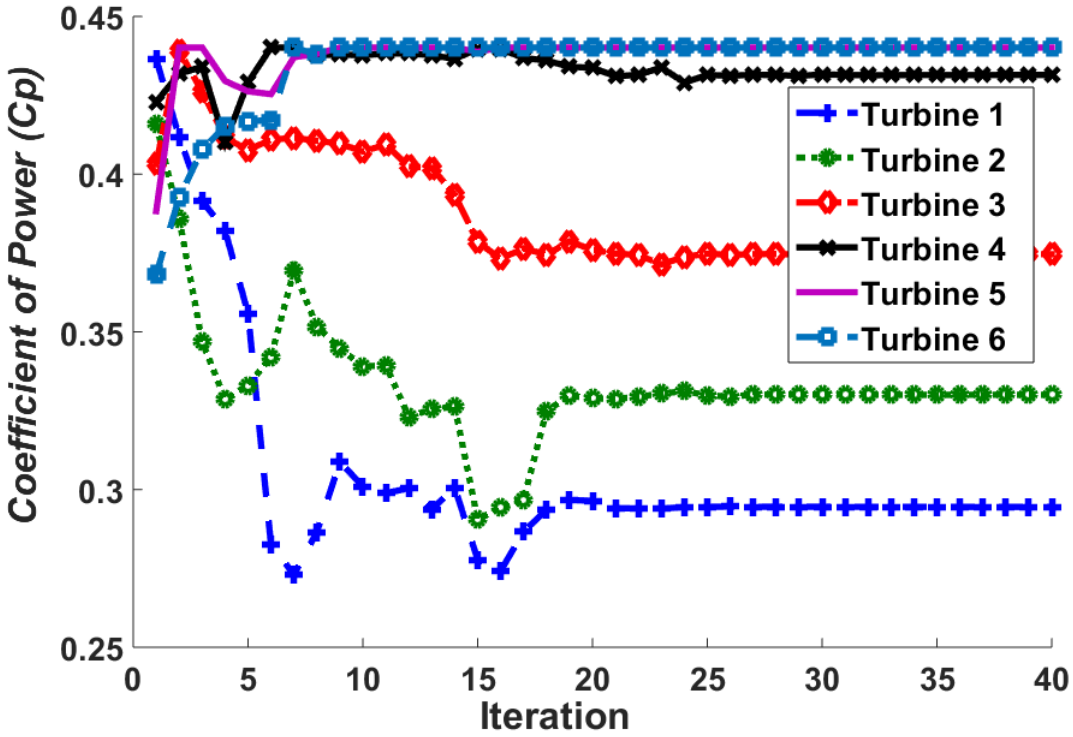

Figure 3.12 Movement of some random particles towards Optimum C_P

3.9.2 Position (x_i)

This shows the current position (fitness) of a given particle in the given solution space. In the start of the algorithm all the particles are initialised randomly within the given limits [159, 160]. Position of a particle represents a potential solution of the given problem. Position of each and every particle is determined each iteration using equation (3.11). If the position determined at time $t+1$ is better than position at time t (fitness of this solution outperforms the previous one) then the position of that particular particle is updated according to equation 3.11.

3.9.3 Random Variables (R_1, R_2, R_3)

Randomness in the search is introduced by (R_1, R_2, R_3). The randomness controls V_i and hence x_i of a given particle i [159, 160, 164]. The randomness or stochastic behaviour improves the chances of avoiding a local optima. Previous studies do not suggest any particular distribution for randomness generators. Different data distributions namely Gaussian, uniform, Poisson and normal distributions were used

and evaluated for solving equation (3.8) and no impact was found on the results. The default "Normal distribution" available in Matlab [124] is used in this work.

3.9.4 Constants (c_1, c_2)

The constants (c_1,c_2) in equation 3.10 are termed as acceleration constants [159]. Randomness generator control the velocity, constants accelerate the particles' velocities for achieving an optimum solution. Higher values of c_1 and c_2 mean more acceleration, this is good for exploring new areas of the solution space but particles may diverge [160–164, 166, 167]. Lower values of c_1 and c_2 limit the acceleration which may lead to refined search around the optimum solution [160–162, 164, 166]. Previous research suggests that a value of $c_1 + c_2 = 4$ shall be used for giving the particles a better chance for exploring all the solution space [160, 162]. Equal weight is given to c_1 and c_2 in this work, keeping their values equal to 2 as given in Table 3.4.

3.9.5 Inertia (ζ)

Inertia weight (ζ) is used for avoiding high velocity of the swarm [165, 167]. If velocity is too high for the problem under consideration, the particles may miss the global optimum moving towards a local optimum value. The particular high and low limits of velocity depends upon the problem under consideration (objective function) and other variables as was discussed in section 3.9.1. A large value of ζ (up to 0.90) is good for a global search while small values (up to 0.20) facilitate local search [162, 164, 168]. Researchers recommend a higher ζ up to 0.90 initially and then reducing it up to 0.20 [160, 162]. This allows a global search initially and once the solution space is confined, a local search is performed. This gives the swarm a better chance to find an optimum solution.

It is suggested in [160, 162, 164] that this rate of reduction should be linear for achieving better results. This recommendation is adopted in this work for solving the coordinated control problem. Each iteration the value of ζ was reduced by 0.03, starting from 0.90 to a minimum of 0.20, after that ($\zeta = 0.20$), ζ is kept constant at 0.20 as recommended by [160, 162, 164]. Other values, for reducing ζ, were also evaluated in the range of 0.02 to 0.10 (in a step of 0.01) and it was found that success rate is better when ζ is reduced by 0.03 each iteration. When ζ was kept constant or when other values for ζ reduction (other than 0.03) were used, success rate decreased as sometime

PSO was trapped in worst local optima (worst than the $f(P_{max}, C_{P(max)}, \alpha_{max}) = 6632$). When the rate of decrease of ζ was kept at 0.03, the success rate for achieving the optimum value (6632) of $f(P_{max}, C_{P(max)}, \alpha_{max})$ is 100% in 100 runs. This means that this optimum value ($f(P_{max}, C_{P(max)}, \alpha_{max}) = 6632$) was achieved in each run.

3.9.6 Personal Best (p_i)

Personal best (p_i) records particle i's best fitness value achieved up to current time t [159]. Each particle in the swarm has its own personal best which is evaluated and updated (if required) each iteration accordingly.

The term $(p_i(t) - x_i(t))$ in equation (3.10) represents the individual intelligence of the particle achieved with help from the swarm [159]. From the perspective of Newton's first law of motion, this term is the action of a particle [160]. This term has been referred to as self-knowledge, self-learning, local memory, remembrance and nostalgia of an individual particle [159, 160, 162, 165–167, 169]. This term mimics behaviour of an individual bird searching for a food source and p_i is the richest food source found by the bird i up to time t.

3.9.7 Global Best (p_g)

Global best (p_g) is the best solution achieved by the whole swarm up to time t [159]. In other words, it is the best p_i among all the particles in the swarm. Each particle's p_i is compared to p_g each iteration and updated if a p_i is better than p_g. This means that the whole swarm has a single p_g. The aim is to converge all the particles to p_g when the algorithm terminates - which is the highest quality solution achieved.

The term $(p_g(t) - x_i(t))$ in equation (3.10) represents the cooperation in the swarm. From the perspective of Newton's first law of motion, this term is the reaction of the term $(p_i(t) - x_i(t))$ [160]. If action and reaction are equal, there is no force, hence the particle is static and does not change its position (in absence of other variables, such as (ζ) and randomness generators). This is true for the particle i whose p_i is equal to p_g. As the solution achieved by this particle i is the best solution achieved by the swarm, there is no need to change its position and the velocity of this particle remains zero. The particular particle i is called leader of the swarm at time t [167]. Researchers have referred to the term $(p_g(t) - x_i(t))$ as social intelligence, experience sharing, group

learning, cooperation, social knowledge, group knowledge and information sharing in the swarm [159–162, 164–167, 169].

3.9.8 Population Size

PSO is a population based algorithm as discussed in section 3.1.1.1. The number of particles in a swarm represents the population size. For a multi-dimensional problem each dimension is represented by a separate swarm. Hence the number of swarms is equal to the number of dimensions to be optimised.

The algorithm optimises all these dimensions using the fitness value (objective function). Relatively larger population sizes are recommended for higher-dimensional complex problems but this increases processing time [159, 160]. There is no specific size of population as it depends upon the problem under consideration [170]. Different population sizes within a range of 20 to 100 with a step size of 10 were evaluated. It is found that a population size of 30 particles is suitable for wind farm coordinated control as was given in Table 3.4.

3.9.9 Iterations

The number of iterations determines how many chances a particle has to update its position [159]. Usually termination criterion of the algorithm is represented by the number of iterations [160, 170]. There is no fixed criterion for determining the number of iterations [161, 162, 164]. Higher number of iterations increases chances of achieving a better solution but this also increases the processing time. The number of iterations depends upon complexity of the problem, desired accuracy and processing time required. It is found with (around 100) simulations that PSO can successfully find the optimum solution for wind farm coordinated control in a maximum of 40 iterations as given in Table 3.4 and shown in Figure 3.12.

3.9.10 Neighbourhood Topologies

The way particles communicate with each other for finding the optimum value depends upon neighbourhood topology in the swarm. The neighbourhood topology represents how particles are connected. In the original (global-best) version of PSO [159], a

particle communicates with every other particle in the swarm (fully connected) as shown in Figure 3.13a.

Researchers [160, 162, 164, 169, 171] have used other neighbourhood topologies for reducing chances of getting trapped in local optimum such as the fully connected swarm, ring or circle neighbourhood, star or wheel neighbourhood, pyramid neighbourhood and Von-Neumann neighbourhood as shown in Figure 3.13. Detailed description of these topologies is provided in [169, 171]. Performances of these neighbourhood topologies are evaluated using complex optimisation functions in [161, 169, 171]. It is concluded in these studies [161, 169, 171] that the algorithm converges faster with the fully connected swarm (Figure 3.13a) and ring or circle neighbourhood topology (Figure 3.13b) as compared to the other neighbourhood topologies, with relatively better success rate and better solution quality. It is also recommended in [161, 169, 171] that if faster optimisation is required then fully connected or ring topology must be used as the other topologies reduces computational efficiency of the algorithm. As processing speed is one of the main criteria for solving the coordinated control problem, these two neighbourhood topologies (fully connected and ring) are evaluated in this work for maximising farm production.

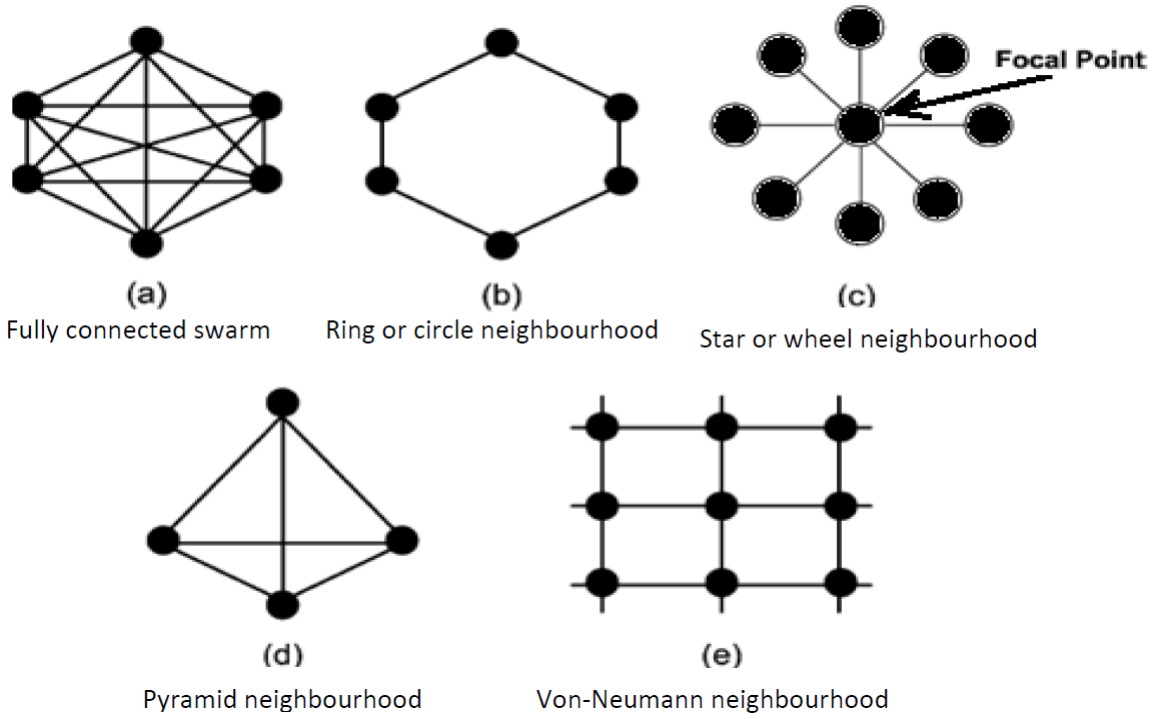

Figure 3.13 Different neighbourhood topologies in PSO [169, 171, 172]

Table 3.4 Performance comparison of fully connected and ring topology PSO

Variables	**Global-best**	**Ring-best**
Population size	30	30
Iterations	40	1000
c_1 and c_2	2	2
Processing time in seconds	0.25	6
Overheads (calls to the wake model)	6654	6654
Success rate after 100 trials	100%	100%
Closeness to global optimum	98.5%	98.5%

The ring topology is implemented and evaluated using the artificial wind farm detailed in section 3.1.2. Different number of particles in a ring (3 to 9) neighbourhood were evaluated in [79] for coordinated control of wind farms and it was found that a neighbourhood (ring) of five particles achieves the optimum solution with highest processing speed. This means that every five neighbouring particles exchange information with each other for finding their ring best value. Every particle exchanges information with its two immediate neighbours on both sides, keeping the particle under consideration in the middle.

The fully connected PSO was chosen as the most suitable optimiser for wind farm coordinated control in section 3.8. Performances of PSO with global best and ring topologies are evaluated and results are presented in Table 3.4. This shows the impact of the two neighbourhood topologies on performance of PSO for solving the coordinated control problem.

The neighbourhood topologies do not change behaviour of the swarm and only change the way in which particles exchange information with each other. Both the neighbourhood topologies produce the same quality solution and with the same success rate. However, fully connected PSO outperforms the ring topology based PSO in terms of processing speed. With higher processing speed and 25 times fewer iterations, fully connected PSO is the first choice for optimising wind farm coordinated control.

3.10 Conclusion

This chapter selected a suitable optimiser for solving coordinated control problem answering RQ-2 which is about selection of an appropriate optimiser for coordinated control problem and defining its characteristics. It was discussed in Chapter 2 that previous coordinated control studies emphasise more on the aerodynamics of the problem than the optimisation. This chapter filled this gap by evaluating performances of a set of carefully selected optimisers using coordinated control.

Previous studies suggest that the a suitable optimiser for coordinated control of wind farms shall reach an acceptable solution with high processing speed using minimum overheads. Heuristic techniques have been used by researchers for solving complex non-linear problems. These techniques are iterative with intrinsic intelligence, fulfilling the criteria established in section 2.4.2 for choosing a suitable optimiser for coordinated control. The literature review in section 3.1.1 concluded that BF, GA, SA, ACO and PSO make a suitable set of optimisation techniques for evaluation, solving wind farm coordinated control problem.

Performances of the selected optimisers were evaluated using an artificial wind farm of seven NREL 5MW wind turbines, installed in one-dimensional array. The Jensen model was used for predicting wind deficit in the farm because of its simplicity and ease of use.

Optimised control strategy based on yaw-offset was explained. The wake skew angle is greater than yaw-offset, hence this principle can be used for maximising wind farm power production for farm production maximisation. The analytical relationship between α and γ obtained from literature [100] was explained.

An objective function was formulated for maximising farm production, using C_P or α or both as the decision variable(s), using coordinated control. The objective is to minimise the difference between farm production assuming no-wake conditions and the actual farm production in the given wind conditions.

Comparative analysis of performances of GA, SA, ACO and PSO concluded that PSO is the most suitable optimiser for coordinated control. PSO is fast and computationally efficient relative to GA, SA and ACO. This makes PSO suitable for on-line real time coordinated control of wind farms.

In-depth analyses of PSO were presented. Performances of two neighbourhood topologies of PSO: the ring or circle topology and global best topology were compared

and evaluated. Comparative analysis concluded that the global best (full-connected) PSO has higher processing speed requiring lower overheads and is more suitable for wind farm coordinated control.

Chapter 4

Development of TI-JM and Wake Assessment Methodology

This chapter details the methodology adopted for developing a fast processing and accurate wind deficit model (TI-JM) answering RQ-3. The approach for developing this wind deficit model presents a novel methodology for combining accuracy of CFD-based wind deficit models with computational efficiency of engineering wind deficit models. An assessment methodology, for analysing impact of wake on farm production, is also developed, answering RQ-4, by identifying wind conditions where coordinated control can be beneficial for increasing overall farm production.

The farm controller has a wind deficit model and an optimiser as two integral parts as discussed in in Chapter 2. It was concluded in Chapter 2 that the Jensen model [75] is best suited for coordinated control of wind farms because of its computational efficiency and simplicity of implementation. However, it was also noted that simple assumptions of the standard Jensen model [75] make it relatively less accurate. Parameters in the model must be tuned for accurate wind deficit prediction in the wind farm as concluded in Chapter 2.

This chapter first details strengths and weaknesses of the Jensen model in section 4.1. This is followed by a literature review summarising methodologies for modifying parameters in the Jensen model for overcoming its shortcomings in section 4.2. The Turbulence Intensity based Jensen Model (TI-JM) is developed in section 4.3 considering realistic wind flow rather than the ideal wind flow as in the standard Jensen model. The TI-JM uses free-stream and wake added turbulence intensities (based on analytical expression from CFD models) for predicting mean wind speed deficit inside the farm

using the Jensen model, producing accurate results with high computational efficiency. An assessment methodology for analysing impact of wakes on power production is developed in section 4.4. The conclusion of this chapter is presented in section 4.5. The structure of this chapter is presented in Figure 4.1.

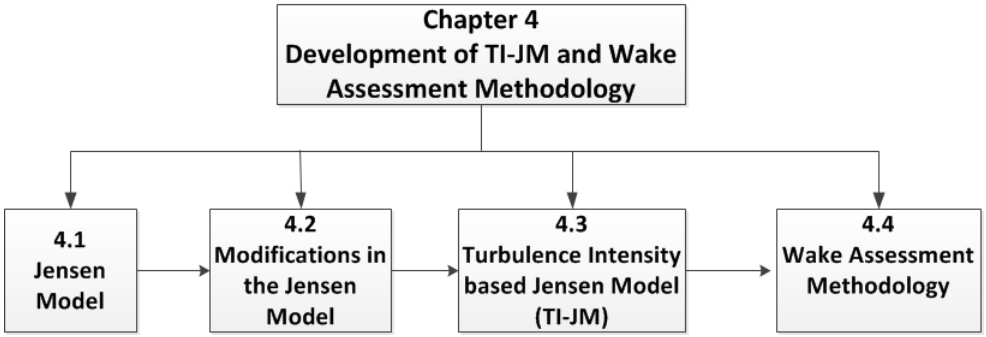

Figure 4.1 Structure of chapter 4

4.1 Jensen Model

The Jensen model is an analytical wake flow model, first presented in [75]. A short description of the Jensen model was presented in Chapter 2. It was noted in Chapter 2 that the Jensen model has been widely used for developing feedback control systems. This section discusses the Jensen model detailing its strengths and weaknesses.

The Jensen model is based on law of conservation of momentum which states that the overall momentum remains constant at any point in the flow field [75] as discussed in section 2.2.2.1. The Left Hand Side (LHS) of equation (4.1) is a combination of two terms. The first term represents the momentum just behind (downstream) the rotor while the second one gives momentum added by the wake spread. The Right Hand Side (RHS) of equation (4.1) gives the momentum at distance (x) where the wind speed is equal to (u_x). Free-stream wind speed is denoted by (u_0), wind speed just behind the rotor is given by (u_T), rotor radius is (r_0) and radius of the wake spread is denoted by (r_x). Wake flow with the Jensen model is shown in Figure 4.2.

$$\pi r_0^2 u_T + \pi(r^2 - r_0^2)u_0 = \pi r_x^2 u_x \tag{4.1}$$

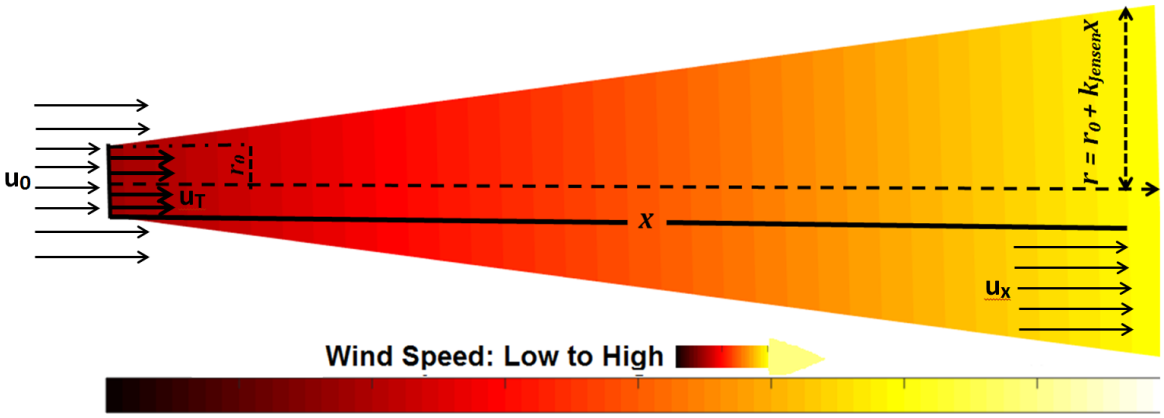

Figure 4.2 Wind deficit modelling with the Jensen model

Following are the basic assumptions and characteristics of the Jensen model [42, 75, 76].

1. Input parameters required - Wake decay coefficient (k_{Jensen}), C_T, r_0, u_0 and x.
2. The model is based on the law of conservation of momentum.
3. Ideal wind flow - It is assumed that the wind is frictionless and incompressible ignoring deep array effect and wake added turbulence intensity.
4. Constant k_{Jensen} - As wind flow is ideal, k_{Jensen} is assumed to be constant. Standard values of k_{Jensen} for different terrains along with surface roughness length and ambient turbulence intensity are given in Table 4.1 [91, 173].
5. Linear wake expansion - Wind expands linearly (in a hat shape) behind the rotor, starting with a diameter equal to rotor diameter as shown in Figure 4.2.
6. Wake spread - Wake spread at any point depends upon k_{Jensen}, x and r_0 as given in equation (2.7).
7. The model does not provide detailed wake flow information, only mean wind speed at the vicinity of each turbine in the farm is predicted.
8. The model is not valid for near wake prediction. Near wake is almost $1D$ behind the rotor of the wake producing turbine [49, 52].

The limited number of parameters required for wake modelling and simplicity of implementation with sufficient accuracy makes the Jensen model suitable for wind

Table 4.1 Standard values of k_{Jensen} and ambient turbulence intensities for different surfaces [91, 173]

Terrain	**Surface Roughness Length**	k_{Jensen}	**Ambient Turbulence Intensity**	**Description**
Offshore (Water areas)	0.0002	0.040	0.06	Oceans and large water areas.
Mixed water and land	0.0024	0.052	0.07	Can also be applied to very smooth terrains.
Very open farmland	0.0300	0.063	0.10	No crossing hedges. Scattered buildings. Smooth hills.
Open farmland	0.0550	0.075	0.11	Some buildings. Crossing hedges 8m high with distance 1250m apart.
Mixed farmland	0.1000	.083	0.12	Some building. Crossing hedges 8m high with distance 800m apart.
Trees and farmland	0.2000	0.092	0.13	Dense vegetation. 8m hedges 250m apart.
Forests and villages	0.4000	0.1000	0.15	Villages, small towns and much closed farmland. Many high hedges. Forests.
Large towns and cities	0.8000	0.108	0.17	Cities with extended buildings
Large build up cities	1.6000	0.117	0.21	Large cities with build-up areas and high buildings

farm coordinated control [11]. Linear expansion of the wake behind the rotor can be justified as it covers most of the wake affected area. This may affect the accuracy to some extent, but as concluded in Chapter 2, a compromise has to be made between accuracy and computational efficiency while selecting a wake model. The Jensen model is a practical tool as long as the aim is to predict wind deficit inside the wind farm, for estimating mean production [76]. Industry best practice is to install turbines in far

wake region of the upstream turbines, as intensity of wakes reduces in far wake region [11]. Hence with these assumptions and characteristics, the Jensen model is a suitable tool for on-line coordinated control.

However assumptions such as ideal wind flow and constant k_{Jensen} make the model relatively less accurate [35, 74]. Turbines under wake effects experience more turbulent wind because of the wake added turbulence intensity and the deep array effect [35, 74]. This affects atmospheric stability and k_{Jensen} inside the wind farm. The farm acts as a roughness generator itself [48]. Atmospheric stability is defined in terms of the tendency of air to move upward or downward after it has been displaced vertically, stable atmospheres tend to suppress vertical updrafts and reduce turbulence intensity [174]. Atmospheric stability has a profound effect on the wind profile and on turbulence intensity [175]. This affects wind conditions inside the wakes and brings abrupt changes in the wind direction and speed. Wake effects diffuse quickly in unstable wind conditions [174, 176]. The wake added turbulence intensity and extra roughness generated by the wind farm disturbs the free-stream wind flow and make the wind more turbulent, termed as deep array effect as was discussed in section 2.2.2.1. This increased turbulence intensity must be taken into account while estimating wind speed deficit inside a wind farm.

It can be seen in Table 4.1 that k_{Jensen} increases, as surface roughness and/or turbulence intensity increases. Sea surface (offshore) k_{Jensen} is lower than k_{Jensen} for grass or surfaces with vegetation. Water has lower roughness, hence wake takes longer to recover and can travel for longer distances as compared to wakes onshore. The increased value of k_{Jensen} also means increased wake expansion as per equation (2.7), affecting more downstream turbines. Assuming ideal wake flow means ignoring the extra roughness and wake-added turbulence intensity which results in lower values of k_{Jensen} producing inaccurate wind deficit prediction inside the farm.

Researchers have addressed this issue adopting different approaches for adjusting k_{Jensen} to match the actual wind speed deficit inside the wind farm. These approaches are summarised in the following section 4.2.

4.2 Modifications in the Jensen Model

It was concluded in chapter 2 that parameters in engineering models must be tuned according to the wind conditions for improving accuracy of these models. If the value

of k_{Jensen} is tuned according to the wind conditions, accuracy of the Jensen model can be increased [74]. Researchers have used SCADA data, CFD models and analytical expressions for tuning k_{Jensen} considering deep array effect for achieving better results. A review of these previous studies is presented as follows.

The work in [91] uses two different values of k_{Jensen}, one for free-stream conditions and the other one for wake affected conditions. The first value of k_{Jensen} for free-stream conditions is the standard value based on the terrain as given in Table 4.1. The second value is a predetermined value of k_{Jensen} for the wake affected conditions and remains constant second downstream turbine onwards. The wake affected k_{Jensen} is greater than free-stream value because of the deep array effect [91].

The GH WindFarmer uses a correction factor for considering deep array effect inside the wind farm [69]. This correction factor is applied to k_{Jensen} for taking deep array effect into account [69].

The modified version of the Jensen model in WindPRO combines different turbulence models with the Jensen model [41]. The turbulence models are used for estimating a new (modified) value of k_{Jensen} for the wake affected wind turbines. It is recommended in [48] to increase the k_{Jensen} inside the wind farm as the farm itself changes the roughness, hence the free-stream wind may not follow assumptions of the standard Jensen model.

Linear regression is used for estimating the actual value of k_{Jensen} using SOWFA as a benchmark in [35]. SOWFA is a high fidelity CFD wake modelling software, which gives detailed information about the flow field as discussed in Chapter 2. This study [35] concludes that k_{Jensen} shall be modified (increased inside the farm) according to the wind conditions for improving accuracy of the Jensen model.

Discrete bins of turbulence intensity are used in **[177]** [1] for determining the wake-affected value of k_{Jensen}, using WindPRO as benchmark. First the increased turbulence intensity inside the wake is estimated. This turbulence intensity is divided into discrete bins. Each bin is then associated with a pre-determined value of k_{Jensen}. Wind speed deficit is estimated with this modified k_{Jensen} and results are compared with WindPRO. It is concluded in **[177]** that k_{Jensen} shall be modified inside the wind farm using a continuous function.

The work in **[92]** evaluates k_{Jensen} using real time SCADA data under different wind conditions in the onshore Brazos wind farm. This work **[92]** concludes that k_{Jensen}

[1] Self-citations by the author are presented in bold

must be increased inside the wind farm for predicting the wind deficit accurately. The standard values of k_{Jensen} shall only be applied to free-stream conditions [**92**]. Analysis based on SCADA data confirms the additional roughness and turbulence intensity inside the farm.

These studies confirm that if k_{Jensen} is properly tuned, then the accuracy of the Jensen model can be increased. It was concluded in Chapter 2 that a better option is to tune the k_{Jensen} using analytical expressions obtained from CFD models. This can increase accuracy of the Jensen model without compromising its processing speed and computational efficiency.

The wind deficit model developed in this work (TI-JM) uses this approach. An analytical expression for estimating wake-affected turbulence intensity [178] is combined with the Jensen model [75, 76] for predicting mean wind speed deficit inside a wind farm. This model is presented in the next section.

4.3 Turbulence Intensity based Jensen Model (TI-JM)

This section explains the step by step approach for developing a computationally efficient and accurate wind deficit model. The model developed in this work is a modified version of the Jensen model. The value of k_{Jensen} is modified based on the wake-affected turbulence intensity inside the farm, hence the name Turbulence Intensity based Jensen Model (TI-JM).

An artificial wind farm of 16 equidistant wind turbines with $3D$ spacing between them, is assumed for this explanation. Wake effects reduce by increasing distance between the turbines, that is why a spacing of $3D$ is used and it also presents industry standard more accurately [138, 143]. However, any other spacing such as $2D$, $4D$, $5D$ or any other can also be used for developing the wind deficit model. The wind farm has a 4×4 layout and the wind direction is assumed to be 225° (south-west) as shown in Figure 4.3. The 4×4 layout is assumed just to consider a two-dimensional wind farm, any other two-dimensional layout such as 3×3, 4×3 or 5×5 can also be used for developing the wind deficit model. The aim here is to develop the model with a two-dimensional layout to enable the model to be used for wind deficit estimation in wind farm with any layout. The following steps explain development and assumptions of this model.

1. The input parameters required - (easting, northing) coordinates of the turbines, number or rows, number of turbines in each row (columns), free-steam wind speed and turbulence intensity, wind direction and an initial value of k_{Jensen} for free-steam conditions obtained from Table 4.1 according to the terrain characteristics.

2. It is assumed that wakes can affect downstream turbines up to $10D$ as suggested in [41, 179].

3. It is assumed that the wake expansion remains linear behind the rotor (hat shape), same as in the standard Jensen model [75].

4. First the wake centre-line is calculated up to $10D$ in the given wind direction. Wake expansion is calculated using free-stream (initial) value of k_{Jensen} in equation (2.7) as shown in Figure 4.3a.

5. A rectangle (box) is drawn with the wake centre-line as the diameter of this rectangle as shown in Figure 4.3b. This box is used for finding the turbines which can be affected by the wake produced when it is extended up to $10D$.

6. Turbines, actually affected by the wake are identified using geometry. It is assumed that the turbine hub is perpendicular to the centre-line of the wake. If the wake lines intersects rotor of any turbine, it is affected partially by the wake. if a rotor lies between the two wake lines, it is under full wake effects. If none of these conditions is present then the wake does not have any impact on the turbines.

7. If a shadowed turbine is under partial wake effects, the percentage (weight) of rotor swept area affected by the wakes (A_s) is determined.

8. Once the wake affected turbines are identified then wind speed deficits on these turbines, as a result of the wake under consideration, is calculated using the Jensen model in equation 2.5 as shown in Figure 4.3c.

9. In case of partial wakes, effective wind speed $u_{x(ef)}$ is the weighted sum of wind speed predicted in step 8 (u_x) multiplied by A_s and the free-stream wind speed (u_0) multiplied by rotor swept area not affected by wakes as given in the following equation (4.2).

$$u_{x(ef)} = \frac{u_x \times A_s + u_0 \times (1 - A_s)}{100} \tag{4.2}$$

10. The above steps are performed for all the turbines facing the free-stream wind according to the given wind direction.

11. The wake increases the turbulence intensity in the farm. This wake added turbulence intensity (I_+) can be estimated with the analytical expression given in equation (4.3) [178].

    The work in [178] presented different analytical expressions for estimating I_+ and concluded that the expression given in equation (4.3) is most suitable accurate for estimating I_+. The free-stream turbulence intensity is denoted by (I_0) and length of near wake is given by (x_n). It is mentioned in [178] that equation (4.3) can be used for estimating I_+ in a wind farm with any given layout, hence it is applicable to this work as well.

    There is some uncertainty about how equation (4.3) is to be interpreted. A cup anemometer is mostly sensitive to the longitudinal component of turbulence intensity. Therefore, equation (4.3) may only represent the longitudinal component of turbulence intensity, but there is some leeway to suggest it may be total turbulence intensity in the absence of explicit information about its use. It is assumed in this work that equation (4.3) represents the total turbulence intensity. The analysis with equation (4.3) being equal to the longitudinal component is left for future work as given in section 7.2.

$$I_+ = 5.7 \times C_T^{0.7} \times I_0^{0.68} \times (x/x_n)^{-0.96} \tag{4.3}$$

12. If I_0 is given then the only unknown is x_n which can be calculated using equation (4.4) as given in [178].

$$x_n = \frac{nR}{\frac{dr}{dx}} \tag{4.4}$$

    where

$$R = r_0\sqrt{\frac{m+1}{2}} \tag{4.5}$$

$$m = \frac{1}{\sqrt{1-C_T}} \tag{4.6}$$

$$n = \frac{\sqrt{0.214+0.144m}(1-\sqrt{0.314+0.124m})}{(1-\sqrt{0.214+0.144m})\sqrt{0.134+0.124m}} \tag{4.7}$$

and $\frac{dr}{dx}$ is the wake growth rate and can be found using the following equation (4.8) [178]:

$$\frac{dr}{dx} = \sqrt{\left(\frac{dr}{dx}\right)_{\alpha}^{2} + \left(\frac{dr}{dx}\right)_{m}^{2} + \left(\frac{dr}{dx}\right)_{\lambda}^{2}} \tag{4.8}$$

where

$$\left(\frac{dr}{dx}\right)_{\alpha} = 2.5I_0 + 0.0005 \tag{4.9}$$

is the growth rate contribution due to ambient turbulence,

$$\left(\frac{dr}{dx}\right)_{m} = \frac{(1-m)\sqrt{1.49+m}}{(1+m)9.76} \tag{4.10}$$

is the contribution due to shear-generated turbulence, and

$$\left(\frac{dr}{dx}\right)_{\lambda} = 0.0012B_n\lambda \tag{4.11}$$

is the contribution due to mechanical turbulence, where (B_n) is the number of blades and (λ) is the TSR.

13. The effective turbulence intensity inside wakes (I_{wake}) is estimated using equation (4.12) [178].

$$I_{wake} = \sqrt{I_{+}^{2} + I_{0}^{2}} \tag{4.12}$$

14. Turbulence intensity has three components: lateral, vertical and longitudinal. According to [178], the longitudinal component of turbulence intensity (I_u) can be specified by equation (4.13).

$$I_u = \frac{1}{\ln(z/z_0)} = 2k_{Jensen} \tag{4.13}$$

15. If isotropic conditions are assumed then the three components of turbulence intensity are equal. Therefore I_u is one third of I_{wake} as given in equation (4.14). It should be noted that if I_0 is measured by a cup anemometer then the value measured is actually I_u as a cup anemometer is mostly sensitive to I_u, except at very low wind speeds, this is left as future work as given in section 7.2.

$$I_u = \frac{I_{wake}}{3} \tag{4.14}$$

16. Equation (4.13) can now be replaced in Equation (2.6) to find the effective value of k_{Jensen} as given in the following equation (4.15).

$$k_{Jensen} = \frac{I_u}{2} \tag{4.15}$$

17. The upper limit on I_{wake} is 20% as suggested by [98]. The lower limit is I_0.

18. If a turbine is affected by multiple wakes then these are superimposed assuming that the wind deficit in the wake is same as the linear sum of the wind deficits of all wakes at the downstream turbine, as suggested in [42, 76]. This is shown in Figure 4.3d.

19. This process is repeated for all the turbines in the wind farm.

20. This model can be used for any number of turbines, with any given layout.

The TI-JM takes deep-array effect into account for estimating wind speed deficit inside the wind farm. The upper limit on turbulence intensity means that once this limit is reached, the turbulence is kept constant for all the downstream turbines, otherwise the turbulence intensity will rise to an impractical value. The higher turbulence intensity inside the wind farm means that the wake diffuses quickly which results in little or no wind speed deficit on downstream turbines deep inside the wind farm. The TI-JM will be used by the optimiser for creating different combinations of turbines' power productions. The TI-JM will be validated using real time data from the wind farms case studies in Chapter 5.

4.4 Wake Assessment Methodology

It was discussed in Chapter 2 that wakes can severely affect wind farm power production in certain wind conditions. An assessment methodology is developed in this section for identifying impact of wakes on power production in the wind farm, using SCADA data, answering RQ-4. Usually SCADA data is collected from each wind turbine and met-mast after every 10 minutes. This data contains useful information about the health and operational status of the turbines and wind conditions on site. SCADA data can be used for identifying potential wind conditions where coordinated control may improve wind farm power production. This wake assessment methodology can also be used for performance comparison of different wind farms with similar layouts.

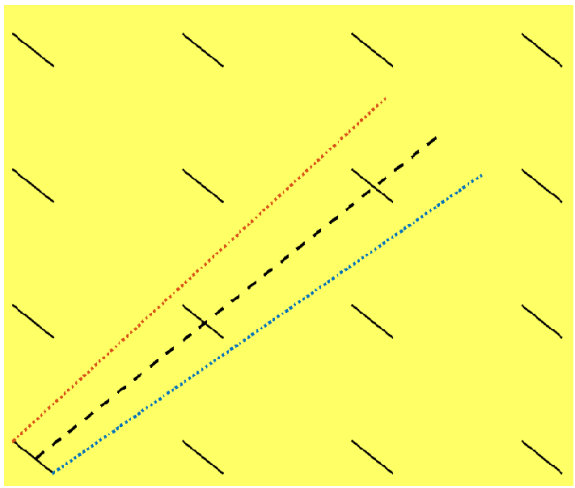

(a) Wake expansion up to $10D$

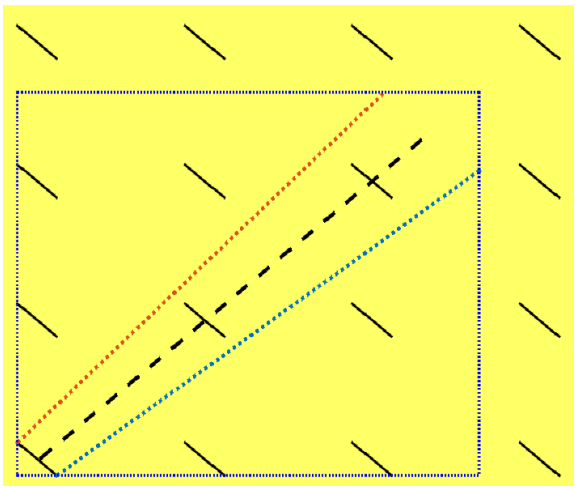

(b) Identifying wake-affected turbines

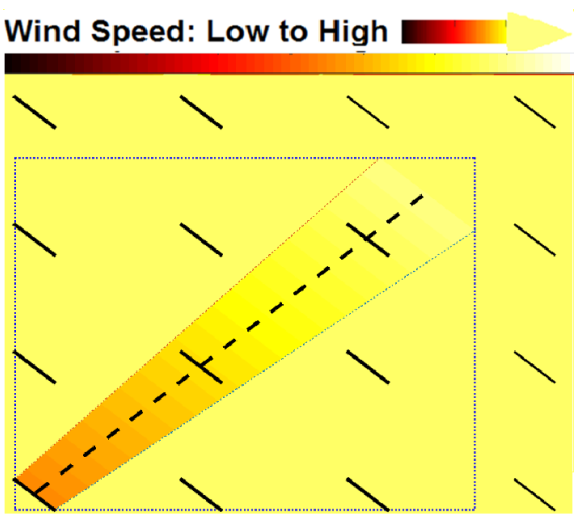

(c) Wind speed deficit on the wake-affected turbines using the Jensen model [75]

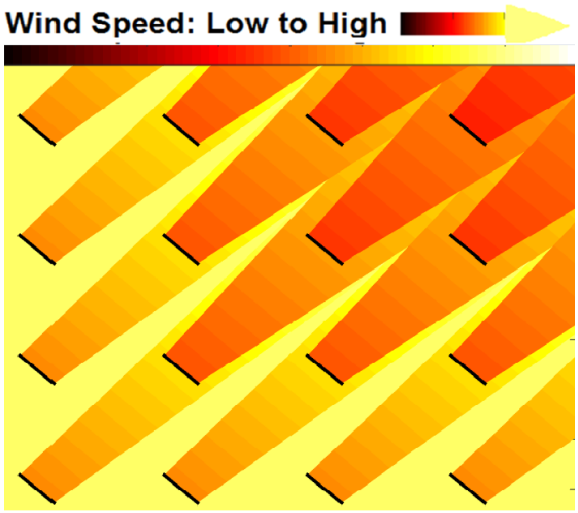

(d) Combining multiple wakes. Wake expansion and the k_{Jensen} increases inside the wind farm [42, 76]

Figure 4.3 Steps for predicting wind speed deficit with the TI-JM with a 4×4 wind farm assuming wind flows at 225° i.e. wind from south-west

Firstly, the power production along with wind speed and direction signals from the SCADA data are used. Data is filtered to use only those records where wind turbine operates at its maximum capacity (normal operations), no curtailment is applied and there are no O&M issues. For all the turbines, average of power production is taken in all wind speeds with a direction resolution of 1°. This visualises power production of

the turbines in 360° showing impact of wakes. This can also be used for identifying appropriate wind direction and speed bins for further analysis.

If the comparison is between farms with different capacities then power production is normalised (P_n) between 0 and 1 using equation (4.16), where i is the turbine under consideration and N is the total number of turbines and ($P(i)$) is power production of the i_{th} turbine.

$$P_n = \frac{P(i) - a}{b - a} \tag{4.16}$$

$a = \min(P(1), P(2), ..., (P(N))$
$b = \max(P(1), P(2), ..., (P(N))$

The denominator in equation (4.16) amplifies turbines' productions. Turbine producing maximum (among all) at a particular instance of time has $P_n = 1$ while turbine with minimum power production (among all) at that instance has $P_n = 0$. Comparing power production in 360° identifies wind conditions where impact of wakes is significant. In some wind directions, there are no or minimal wake effects while in other directions impact of wakes on farm production is significant. This wake impact depends upon different variables such as wind direction, layout of the farm, spacing between the turbines and surface roughness. This will be further discussed in section 5.3.

Secondly, relative efficiency (η_{Rel}) with respect to turbine producing the maximum power (b) is calculated as given in equation (4.17). It can be observed in equation (4.17) that for each record, the turbine producing maximum power has efficiency of 1 or 100%. This means that any data errors or unidentified O&M problems are ignored and only the impact of wakes on power production is considered. This step magnifies the impact of wakes in the chosen speed and directional bin.

$$\eta_{Rel} = \frac{P(i)}{b} \tag{4.17}$$

This assessment methodology can show performance of wind farms in different wind conditions. Coordinated control can be applied in identified wind conditions where power production is significantly affected by wakes. This assessment methodology answers RQ-4 which is about developing a strategy for assessing wake effects on farm production, identifying potential wind conditions where coordinated control can prove beneficial for mitigating these wakes and increasing farm production.

4.5 Conclusion

This chapter presented the wind deficit model developed in this work. First detailed description of the Jensen model was provided identifying its strength and weaknesses. Previous studies proposing methodologies for modifications in the Jensen model were summarised. A wind deficit model (TI-JM) was developed which combines the Jensen model with a CFD-based analytical expression of turbulence intensity.

The TI-JM requires limited parameters and overcomes limitations of the Jensen model by considering the deep array effect for wind speed deficit prediction inside the wind farm. The value of k_{Jensen} varies turbine by turbine basis depending upon the free-stream and wake-added turbulence intensities and distance between the turbines. This model can be used for any layout of the farm in any wind conditions.

An assessment methodology, for identifying wind condition where wakes can severely affect farm production, was presented. The assessment methodology uses SCADA data for calculating power production in 360°. Efficiency relative to the turbine producing maximum power (among all) was calculated for avoiding any data errors or unidentified O&M problems. This methodology will be used for assessing performance of the wind farms case studies in Chapter 5.

Chapter 5

Experimental Results based on Simulations

This chapter presents the experimental results obtained through simulations. A part of the work in this chapter is also presented in [29, 180][1]. This chapter answers RQ-5 by simulating different control strategies (greedy, C_P-based and yaw-based) in different wind conditions for maximising farm production. It is concluded that generally C_P-based control is beneficial in full-wake conditions while yaw-based optimisation is a better option in partial wake conditions. Greedy control is the best in no-wake conditions.

Data from three operating wind farms case studies (Brazos, Le Sole de Moulin Vieux (SMV) and Lillgrund) are used in the simulations. Detailed description of these wind farms is given in section 5.1 explaining the available data, layout, terrain and wind characteristics on site. This is followed by validation of the TI-JM using data from the SMV wind farm in section 5.2.

The assessment methodology developed in Chapter 4 is used for evaluating impact of wakes on turbines production in the SMV wind farm, identifying wind conditions where wake effects are severe, in section 5.3. Once the wake impacted wind conditions are identified, farm efficiencies are used for evaluating greedy, C_P-based and yaw-based control strategies in section 5.4. Efficiencies obtained from SCADA data and WindPRO are used as benchmarks. A brief description of WindPRO is provided in section 5.4.1. Some key results and analysis are presented in section 5.5.

[1]Self-citations by the author are presented in bold

It is concluded in section 5.6 that farm power production can be increased by up to 8% with the control strategies developed in this work. The control process is completed in less than 15 seconds for Brazos and SMV while it takes less than 50 seconds for Lillgrund wind farm. If the wind flows at 12m/s (maximum below rated) in parallel to the wind farms case studies , it will require at least 85 seconds for reaching the last turbine in Brazos case study row of seven turbines, 142 seconds for reaching the last turbine in SMV wind farm, 266 seconds for reaching the last turbine in the eight turbines row in Lillgrund. This shows that the controller has sufficient time to calculate and communicate the new power settings to the corresponding turbines. The structure of this chapter is presented in Figure 5.1.

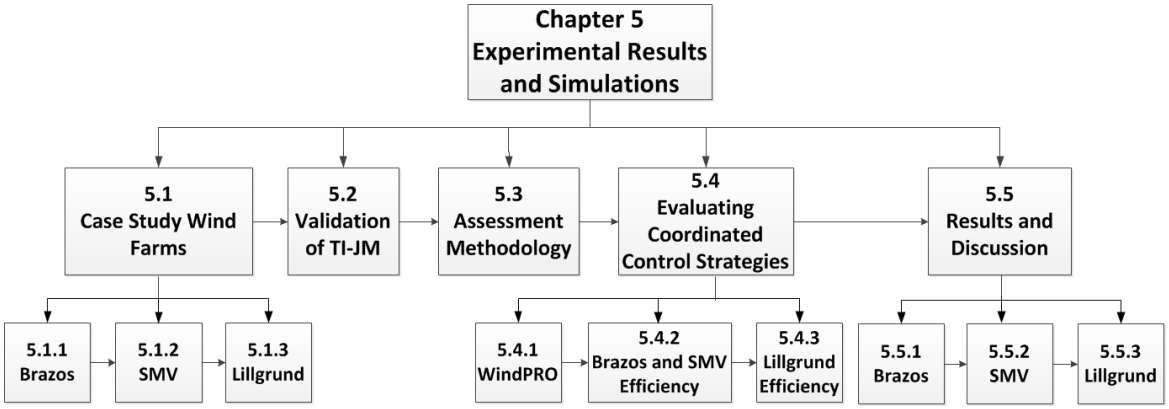

Figure 5.1 Structure of chapter 5

5.1 Wind Farms Case Studies

Two onshore wind farms, Brazos and SMV, and one offshore wind farm, Lillgrund, are used as case studies. Brazos is a medium size wind farm where turbines are placed in a non-grid pattern. SMV is a small wind farm with seven wind turbines installed approximately as a one-dimensional array. Lillgrund is a medium sized wind farm with a grid-like layout. A brief overview of Brazos, SMV and Lillgrund is presented in the following sections.

5.1.1 Brazos

The Brazos wind farm is located in Texas, USA and is owned by Shell Wind Energy/Mitsui. The farm can be divided into two sister wind farms, Brazos-A and Brazos-B. The downwind spacing in some of the rows is as high as $8D$ while the crosswind spacing can be as low as $2D$ for some rows. A wind farm with a non-grid shape and high downwind spacing such as Brazos can be considered made of several smaller sub-farms (each row or a group of turbines is a sub-farm) as shown in Figure 5.2a. This makes the control process fast and efficient as each sub-farm is optimised individually.

The case study in this work is based on the encircled row-2 from Brazos-A, shown in Figure 5.2a. The selected row-2 is made of seven Mitsubishi MWT-1000 turbines [142] with $3D$ spacing between them. Characteristics of Mitsubishi MWT-1000 turbines are given in Table D.1 in Appendix D. The $3D$ spacing represents industry standards more accurately as compared to the $2D$ spacing between turbines in some other rows.

When the wind flows from east, the wind speed is free-stream wind speed as no turbines are installed on east of the case study row. The nearest turbine to the west is installed at a distance of more than $20D$, hence it can be assumed that the wind speed is free-stream wind speed. The row in the north-west of the case study row can affect wind characteristics when wind flows from north-west. The terrain is flat and open with low grass [**92**]. The wind-rose in Figure 5.2b shows the prevailing wind direction and frequency of wind speeds. The wind flows almost 79% of the time from south and north in the downwind direction while it flows crosswind for rest of the time as can be seen in Figure 5.2b.

SCADA data from 2004 - 2006 is used in this study. This data is available on the ReliaWind server in Durham University, UK [143].

5.1.2 Le Sole de Moulin Vieux (SMV)

SMV is an onshore one-dimensional wind farm located in the northern France and is owned by Maïa Eolis (now Engie Green). The farm consists of seven Senvion MM82 2050 kW wind turbines [16]. Characteristics of Senvion MM82 2050 kW turbines are given in Table D.2 in Appendix D. Spacing between the turbines varies from $3.3D$ - $4.3D$.

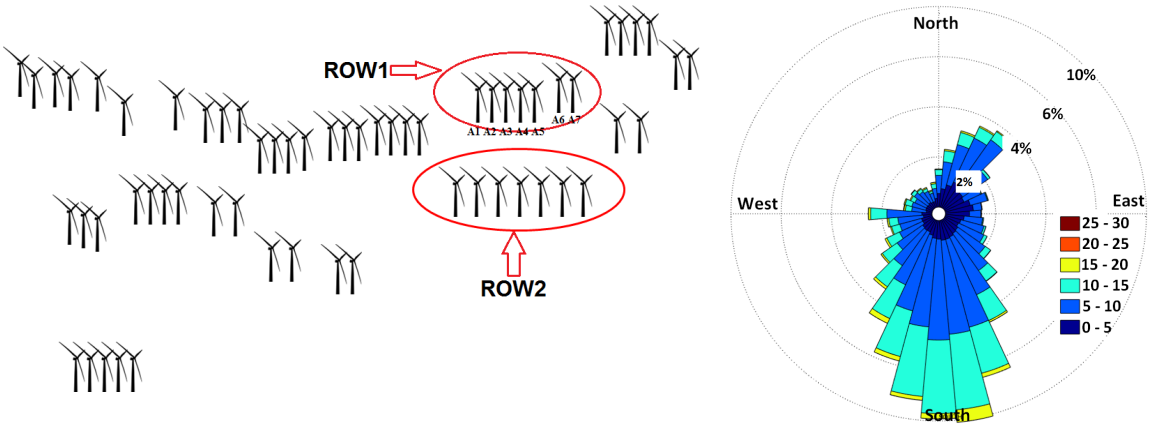

(a) Brazos A layout with selected rows (ROW-1 and ROW-2) encircled

(b) WindRose

Figure 5.2 Brazos A layout (rows under consideration encircled) and wind-rose obtained from SCADA data from 2004 - 2006

The farm initially consisted of five wind turbines (SMV1 - SMV5). Two turbines (SMV6 and SMV7) were added later to the farm. The farm layout is almost like a one-dimensional array as shown in Figure 5.3a. The first five turbines SMV1 - SMV5 are installed almost in a straight line. The last two turbines are not completely in-line with the other five turbines. These two turbines can be considered a different row, but with very close spacing. Spacing between the turbines is almost 3.7D to 4.3D. A 80 meters high lattice met mast with ultrasonic anemometers at 80, 60, 40 and 20m height, located 1km east of SMV2 and 1.6km north-east of SMV6, provides the free-stream wind characteristics.

The terrain is rough with fresh grass or vegetation. There are woods to the south at a distance of almost 100m (less than $1.5D$) from the wind farm affecting atmospheric stability in the farm [138, 175, 181]. The trees are about 15m high. This influences atmospheric stability and result in high turbulence intensity in the wind farm. The farm also suffers from diurnal and seasonal variations in wind conditions [138, 175].

WindPRO suggests free-stream turbulence intensity of 15% for this wind farm clearly exhibiting the roughness on site [48]. This high surface roughness and turbulence intensity results in quick wake recovery. Wind from surroundings flows quickly to make for the momentum loss created by wakes, resulting in increased turbulence intensity. This wake added turbulence intensity also means that wind speed and direction can change abruptly in the farm. The prevailing wind direction is from south and south-

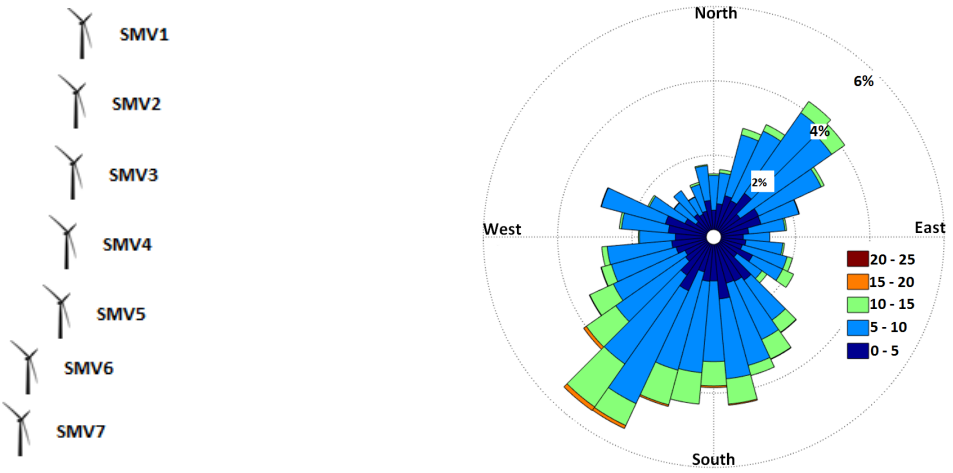

(a) SMV layout **(b)** WindRose

Figure 5.3 SMV layout and wind-rose obtained from SCADA data from 2011 - 2014

west as can be seen in the wind-rose in Figure 5.3b. SCADA data from 2011 - 2016 and details about the wind farm were provided by Maïa Eolis (now Engie Green).

5.1.3 Lillgrund

Third wind farm case study is a two-dimensional offshore wind farm; Lillgrund which is located between Sweden and Denmark in Öresund and is owned by Vattenfall. The farm consists of 48 Siemens SWT-2.3-93 wind turbines [17] installed in 8 rows and 8 columns. Characteristics of Siemens SWT-2.3-93 turbines are given in Table D.3 in Appendix D. Spacing between the turbines in rows is $4.5D$ and between rows it is $3.5D$ [17, 182]. Main reason for this close spacing between the turbines in the wind farm is the navigational issues [182].

The farm has a grid-like layout as can be seen in Figure 5.4a. The prevailing wind direction is from south and south-west and the mean wind speed is 8.5m/s [182] as shown in Figure 5.4b. Wind data from 2000 - 2015 at 50m height accessed from [183] was used to create the wind-rose in Figure 5.4b. Turbines inside the farm are almost always under wake effects as the layout is a very dense.

SCADA data for the wind farm could not be accessed. However, important information such as turbine characteristics, 360° farm efficiency and farm layout is given in [9, 182, 144, 184]. Access to details of the surface roughness length, turbulence intensity in all directions and average efficiency was given by [144].

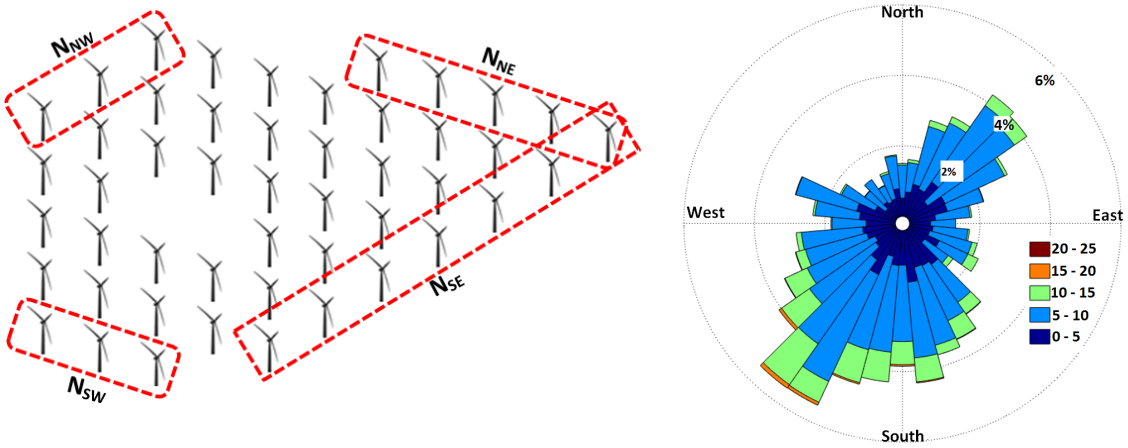

(a) Layout and highlighted rows (turbines) used for normalisation

(b) Lillgrund WindRose

Figure 5.4 Lillgrund layout and wind characteristics on the site

Details and data from these wind farms are used for validating and evaluating the TI-JM and optimised coordinated control strategies.

5.2 Validation of TI-JM

A wind deficit model (TI-JM) was presented in section 4.3. This section validates the TI-JM using SCADA data from the SMV wind farm.

5.2.1 Data Selection Criteria

Three days wind data at 10 minutes interval (almost 400 valid data points) was chosen for validating the wind deficit model. During this period the wind predominantly blew from north to south, parallel to the turbine array, producing full or near full wake effects in the wind farm. Data from the SMV wind farm is used because suitable wind data from the Brazos wind farm was not available for model validation and SCADA data for Lillgrund could not be accessed. The downwind distance is up to $8D$ in the Brazos wind farm and wind flow is predominantly in this direction as was discussed in section 5.1.1. The three days SCADA data from the SMV wind farm provides a suitable data set for validating the TI-JM. Other than this, the field implementation detailed in Chapter 6 is performed in the SMV wind farm, hence validating the TI-JM with SMV data is a better and reasonable option. SMV1 faced the free-stream wind

while all other turbines were under wake effects of corresponding upstream turbines. SMV6 and SMV7 were not operational during this period, hence these two turbines are not considered for validation. The five turbines (SMV1 - SMV5) are used for validation.

5.2.2 Validation

Figure 5.5 shows the comparison between the actual wind speed and predicted wind speed by the TI-JM. The actual wind speed was determined using each turbine's power production from the SCADA data using Turbine's power curve (given in Appendix D) in below rated wind conditions, as discrepancies were found in the wind speed reported by nacelle anemometers. The operation status signal from the SCADA data was used to make sure that only those records are considered where turbines operated without any curtailment and O&M issues.

An initial value of k_{Jensen} of 0.07 is used with TI-JM, as recommended in Table 4.1 for the type of terrain SMV has. This fits well for predicting the wind speed on SMV2 as can be seen in Figure 5.5a. The free-stream turbulence intensity was calculated from the SCADA data using equation (5.1). The free-stream wind speed is determined using power production of the wind turbine facing free-stream wind. The turbulent velocity fluctuations for every six data points (wind speed) is denoted by (u') while average of the same six data points (wind speed) is denoted by (U). It should be noted that any other number of data points (other than six) may be used for estimating free-stream turbulence intensity, however six data points are used in this work as suggested in [28, 58–63].

$$I_0 = \frac{u'}{U} \tag{5.1}$$

As the wind flows through the wind farm, TI-JM makes sure that effective value of k_{Jensen} increases as per the wind conditions inside the farm. It can be seen in Figure 5.5 that the model accurately predicts the wake affected wind speed on downstream turbines in most of the cases.

It shall be noted that the model is acceptable for developing control strategies as long as it is under-predicting the wind speed on shadowed turbines in a given limit. However, if it over-predicts the wake affected wind speed then the farm controller will result in false increase in power production. This can result in lower farm production in real time operations as compared to the conventional greedy control. It can be observed

in Figure 5.5 with the (Actual - Predicted) wind speed, that the model over-predicts the wind speed in very few cases (less than 3% of total data points).

The TI-JM took approximately 10 seconds for completing the wind deficit calculation using almost 70 hours data for five wind turbines with a 10 minutes interval, using a computer with 5 cores, 3.50GHz processor and 16GB RAM). This high processing speed and accuracy make the TI-JM very suitable for on-line coordinated control.

5.3 Wake Assessment Methodology

This section applies the wake assessment methodology developed in section 4.4 on the SMV wind farm. This assessment visualises the impact of wakes on turbines in the farm identifying suitable conditions for implementation of coordinated control. Turbine power, operational status and wind direction signal from the SCADA data were used. The assessment methodology was applied on the Brazos wind farm in [**29**]. SCADA data for Lillgrund could not be accessed, hence the assessment methodology was not applied on Lillgrund.

Normalised average powers were calculated comparing performance of Brazos row-1 and SMV in [**29**]. The selected Brazos row-1 and SMV have almost similar layout but the turbines' capacities and characteristics are different as can be seen in Tables D.1 and D.2 in Appendix D, hence normalising the power production makes the performance comparison easier. Further assessment steps were also applied for performance comparison in [**29**]. Figures 5.6 and 5.7 are reproduced from [**29**] to show the normalised power production of Brazos row-1 and the SMV wind farm. As stated, performance of the two wind farms in terms of power production can now be compared using these figures. It should be noted that wind direction in the Brazos wind farm is rotated by 90° in this case for the purpose of comparison with SMV wind farm. These details are also used for identifying wind conditions where wakes significantly affects power productions of the wind turbines and hence farms' productions as will be detailed in section 5.5.

Average production of the turbines at 8m/s±0.5m/s with a directional resolution of 1° is presented in Figure 5.8. For presentation purposes, productions of SMV1 - SMV4 are visualised in Figure 5.8a while productions of SMV5 - SMV7 are visualised in Figure 5.8b. It can be observed with this visualisation that the turbines' production is significantly affected when the wind flows from north or south. The wind direction

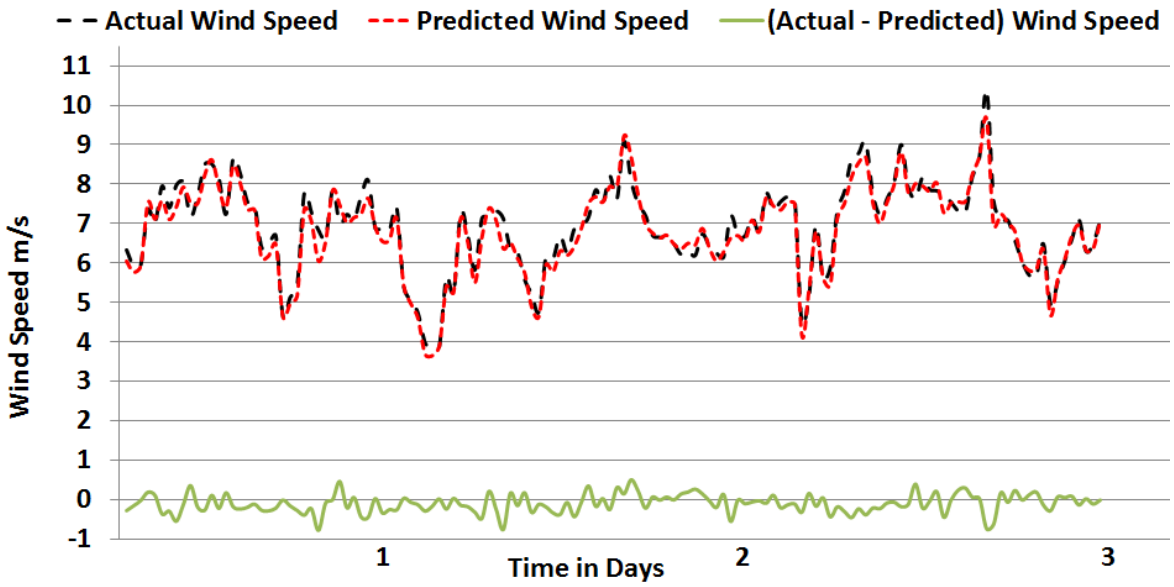

(a) Wind prediction of SMV2 $k_{Jensen} = 0.07$

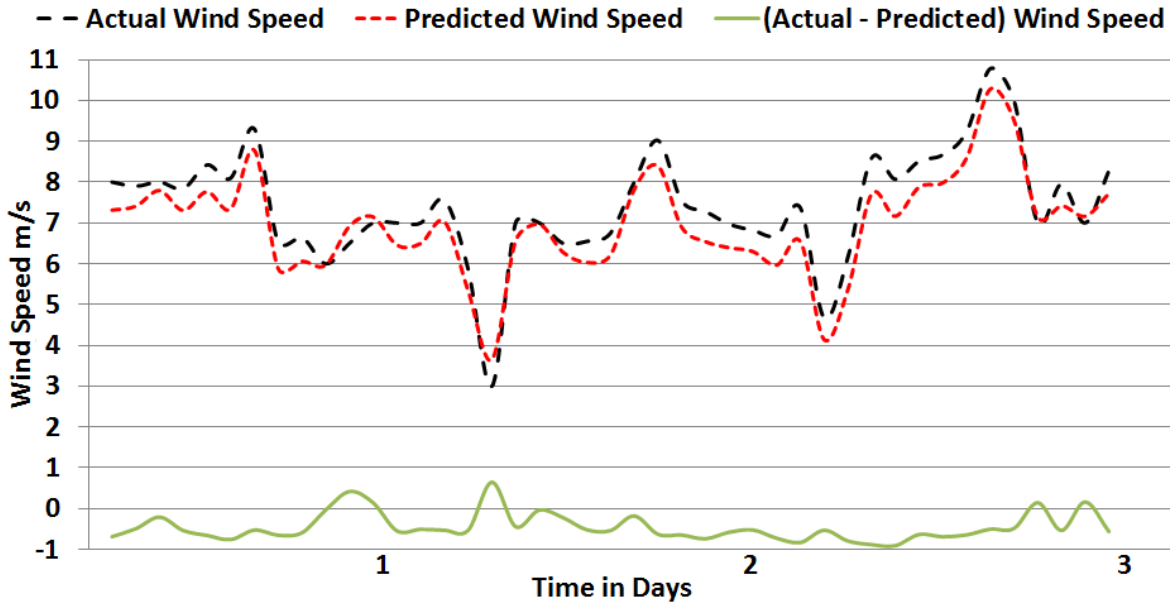

(b) Wind prediction on SMV3 using TI-JM

sectors $0° \pm 40°$ and $180° \pm 40°$ are significantly affected by wakes. The same pattern was observed for all other wind speed bins.

During the analysis it was noted that a wind speed bin of ± 0.5m/s is suitable for the SMV wind farm. For directional bin, analyses were performed starting with a bin of $\pm 20°$ refining the resolution to $\pm 1°$. It was observed that a bin size of $\pm 5°$ captures

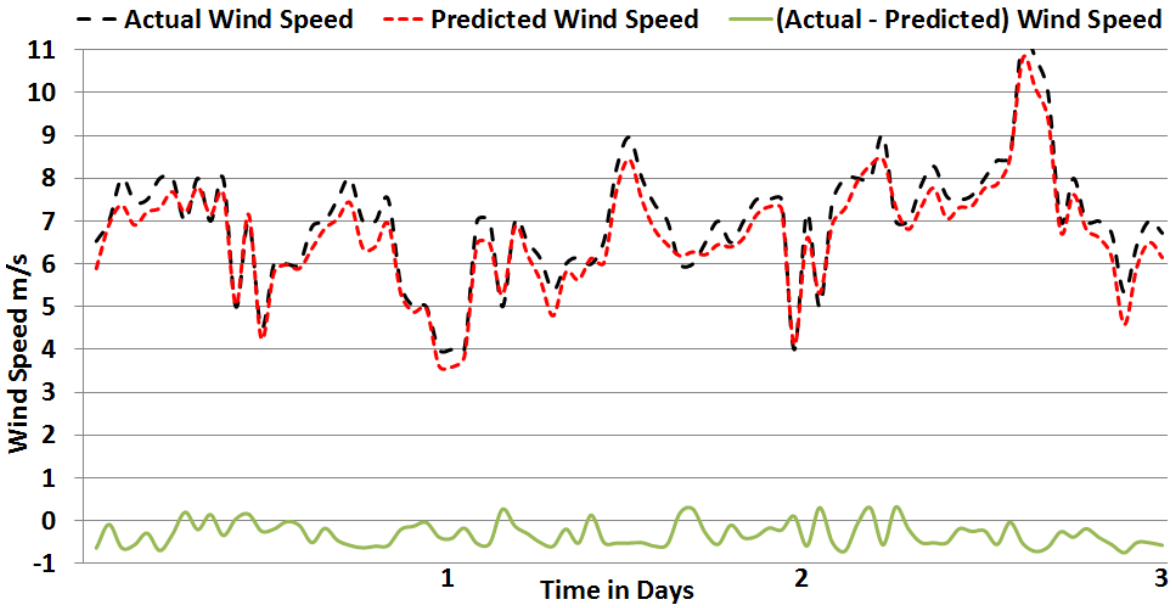

(c) Wind prediction on SMV4 using TI-JM

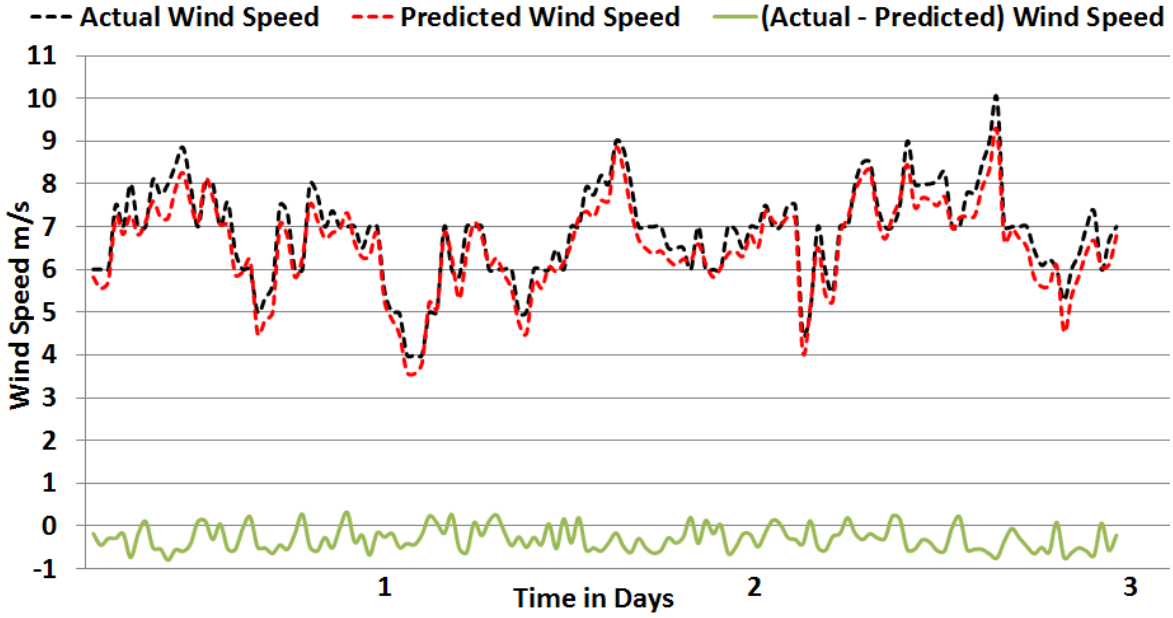

(d) Wind prediction on SMV5 using TI-JM

Figure 5.5 Validation of the TI-JM using SCADA data from the SMV wind farm when the wind flows predominantly from north to south parallel to the turbine array for almost three days

most of the wake affected area. Studies in [87] suggest a direction bin size of $\pm 10°$ using data from two offshore wind farms. However, surface roughness is high onshore

which results in quick wake recovery. Hence a bin size of $\pm 5^\circ$ shall be used for onshore wind farms.

Relative efficiency is calculated as per equation (4.17) in the wake affected wind sectors ($0^\circ \pm 40^\circ$ and $180 \pm 40^\circ$) in a 10° bin in the wind speed bin of 8m/s$\pm$0.5m/s and results are presented in Figure 5.9. It can be seen that downstream turbines are severely affected by wake effects. For example, relative efficiency of SMV5 can be as low as 40% when the wind flows in the $200^\circ - 210^\circ$ bin. This is when SMV5 is under full wake effects of SMV6. Relative efficiency of SMV6 is only 40% in the $170^\circ - 180^\circ$ bin when it is under full wake effects of SMV7. Impact of wakes on other turbines' productions can also be observed as shown in Figure 5.9.

The first step of the assessment methodology visualises the impact of wakes on turbines' productions in the farm. This identifies wind conditions where coordinated control can bring improvement in net production. This is also used for deciding suitable wind direction and speed bin size for wake effects calculation. The second step magnifies the wake affected directional sectors by analysing directional bins using relative efficiency.

The wind deficit model (TI-JM) has been validated and the assessment methodology has been applied on the SMV wind farm. The next step is to show the improvement coordinated control strategies can bring in the net power production of wind farms. This is explained in the next section 5.4.

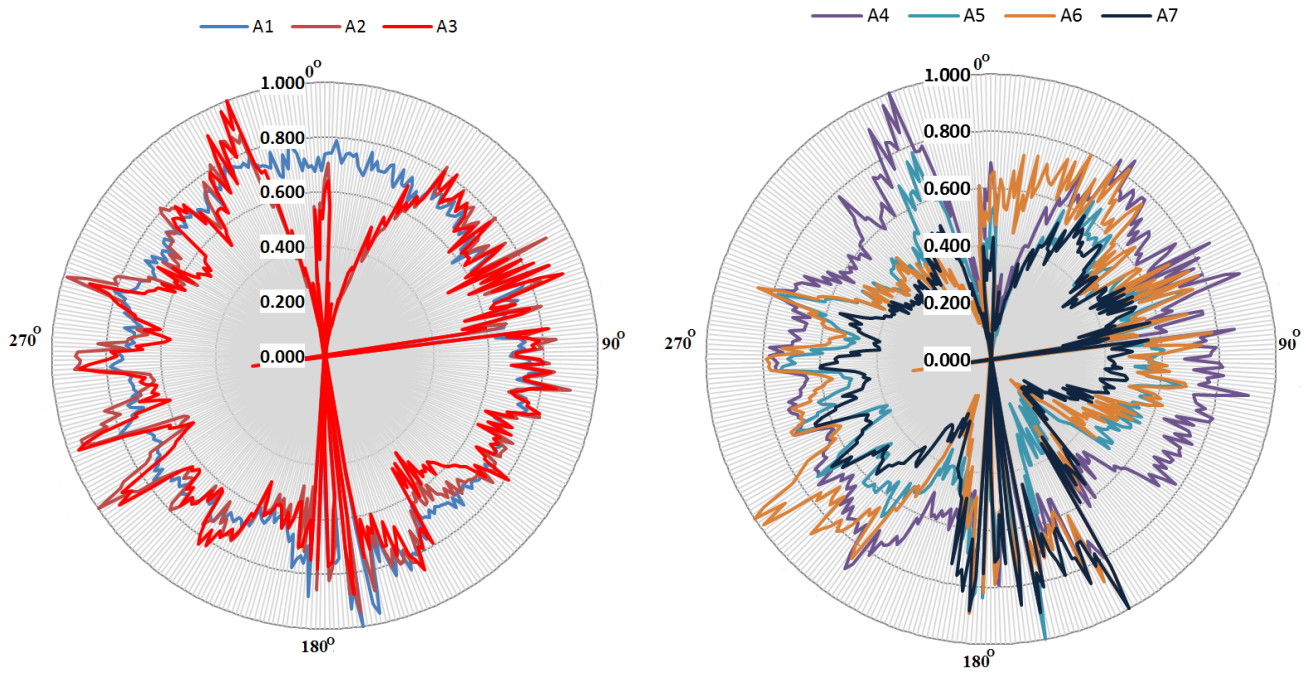

(a) Normalised average power of Brazos Row1 turbine A1 - A3

(b) Normalised average power of Brazos Row turbine A4 - A7

Figure 5.6 Normalised average power of Brazos Row1 (Wind direction rotated by 90° for comparison with SMV wind farm) [29]

5.4 Evaluating Coordinated Control Strategies

This section describes the methodology adopted for evaluating wind farm coordinated control strategies. Efficiencies obtained from SCADA data and WindPRO are used as benchmarks for evaluating the TI-JM. Only below rated wind speeds are considered in these simulations as there are no or minimal wake effects in above rated conditions [9]. The below rated wind conditions for turbines in each wind farm are presented in Appendix D. From this point onwards, average efficiency explicitly means average efficiency in below rated wind conditions unless otherwise described.

Standard values of k_{Jensen} (for onshore and offshore wind farms) given in Table 4.1 are used with WindPRO in a 10° direction bin (highest possible resolution). The initial value of k_{Jensen} in the TI-JM is tuned using the SCADA data (Brazos and SMV), for matching the efficiency based on SCADA data using the greedy control as discussed in [**92**].

The C_P-based and yaw based optimised control strategies are simulated for the three wind farms case studies using TI-JM. Efficiencies based on the optimised strategies

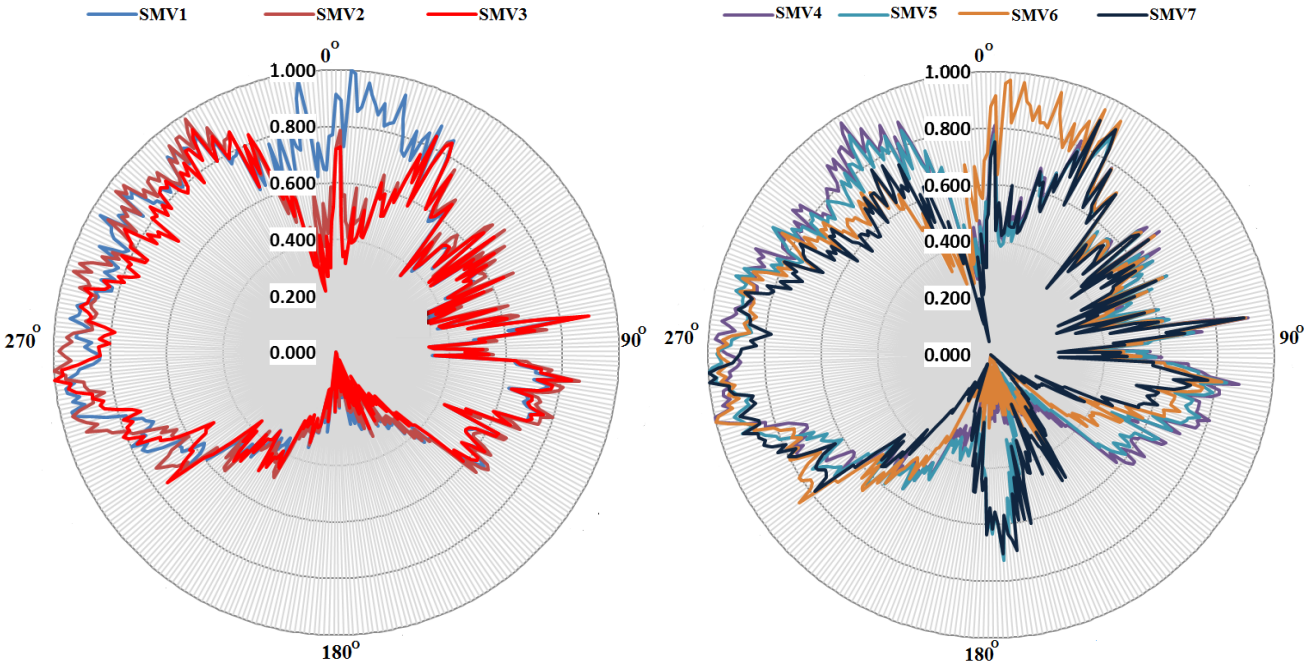

(a) Normalised average power of SMV1 - SMV3 **(b)** Normalised average power of SMV4- SMV7

Figure 5.7 Normalised Average power of wind turbines in SMV wind farm [29]

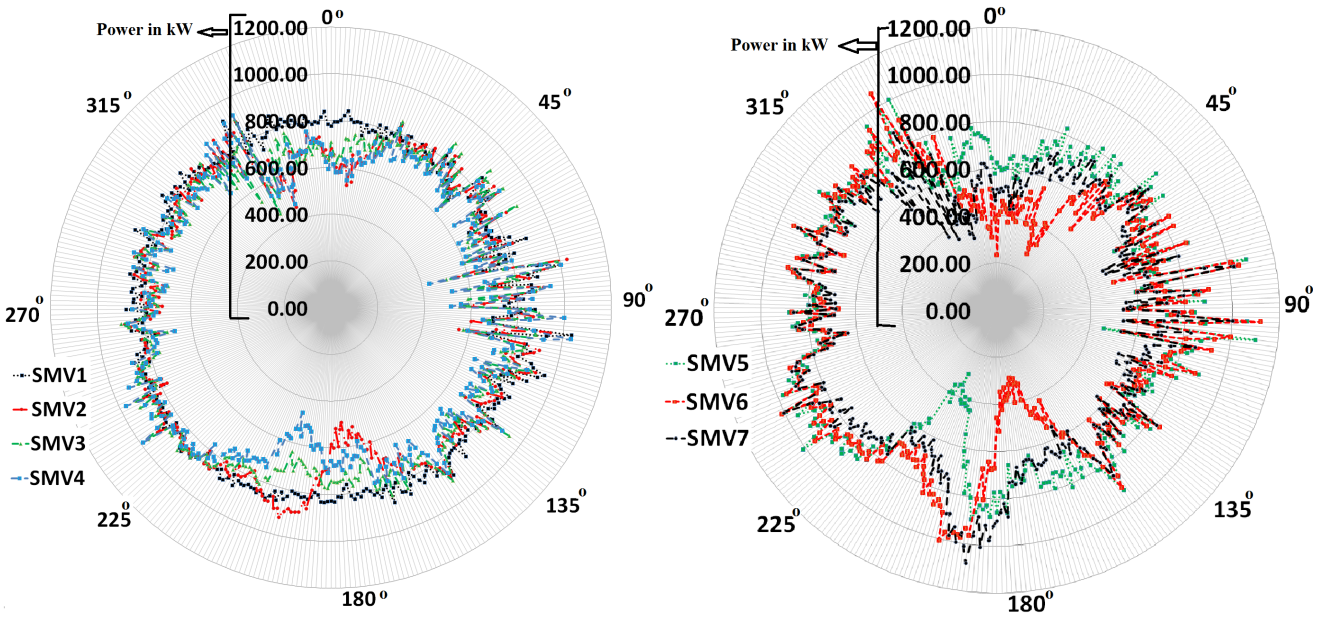

(a) Average power of SMV1 - SMV4 **(b)** Average power of SMV5- SMV7

Figure 5.8 Average power of wind turbine in SMV wind farm at 8m/s±0.5m/s

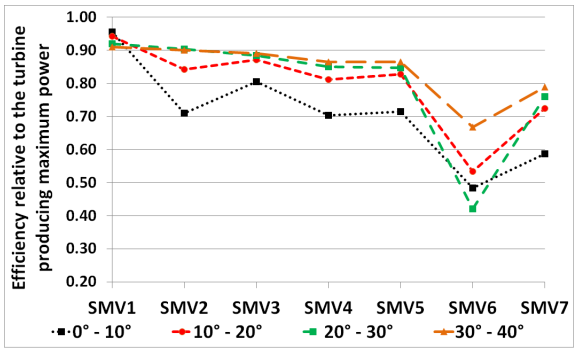

(a) Relative Efficiency $0° - 40°$ in $10°$ bin

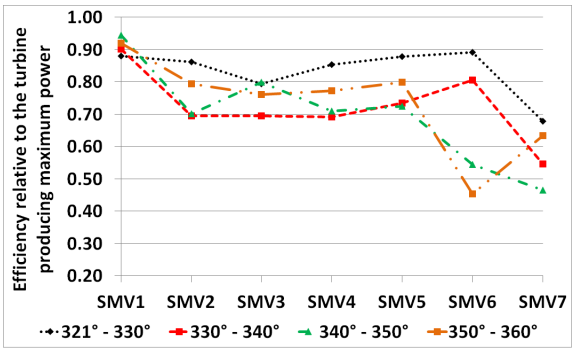

(b) Relative Efficiency $320° - 360°$ in $10°$ bin

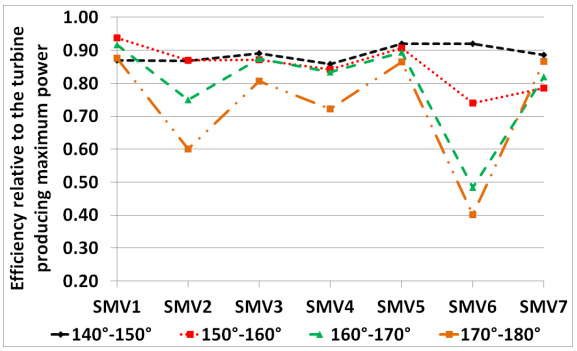

(c) Relative Efficiency $140° - 180°$ in $10°$ bin

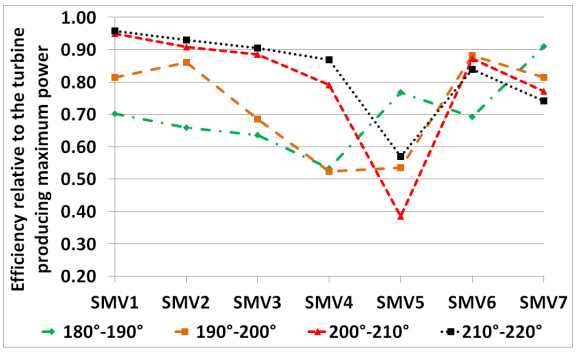

(d) Relative Efficiency $180° - 220°$ in $10°$ bin

Figure 5.9 Efficiency relative to the turbine producing maximum for wind direction sectors $0° \pm 40°$ and $180° \pm 40°$ in $10°$ bin

are compared with the standard greedy control. The direction resolution is kept at $1°$ for efficiencies obtained with SCADA data and TI-JM. PSO is used for optimisation as it is the most suitable optimiser for coordinated control as concluded in Chapter 3. A brief description of WindPRO is given in the section 5.4.1. This is followed by the methodology for determining efficiencies of the wind farms case studies.

5.4.1 WindPRO

This section is mainly based on the details provided in [48]. WindPRO is one of the most widely used and industry standard software for design, development and assessment of wind energy projects. The software has a number of modules and the user is free to use a single or combination of modules as required.

All calculations in this study, based on WindPRO, are performed using the Wind Atlas Program (WAsP) module. WAsP uses wind statistics and terrain assessment of the area within 20-km radius around the site. WAsP uses site specific topographical

data to generalize the regional wind climatology and then uses the inverse calculation to acquire the projected wind climatology at a specific location. The World Geological Survey (WGS) [48, 185, 186] has 10 meter spatial scale digital elevation models of the wind farm area. This information was exported to WAsP as elevation contour lines at 3m intervals recommended by WAsP [48]. WAsP solves the linearised NS equations by assuming a steady state flow in stable atmosphere, linear advection and first order turbulence closure [91]. This information is then combined with power curve of the wind turbine for production estimation. The project preparation for estimating production of the SMV wind farm using WindPRO (WAsP) is presented in Figure 5.10. The following information is required for production estimation using WAsP.

1. Wind Statistics - Wind data from MERRA [183] database at 50m height (maximum available) with a time resolution of one hour (highest possible resolution with the available data) is used.
2. Terrain assessment - The roughness, local obstacles and orography are analysed with Google Earth [187] and field surveys.
3. Power curve of the wind turbine under observation - WindPRO has built-in power curves for wind turbines with different capacities and characteristics made by different companies. A user can also develop a power curve according to the given requirements.

The standard Jensen model [75] (with a constant k_{Jensen}) available in WindPRO is used for estimating wake power losses using WAsP. The standard value of $k_{Jensen} = 0.07$ for Brazos and SMV and $k_{Jensen} = 0.04$ for Lillgrund is used as given in Table 4.1. The wind turbines are placed on the map according to the layout of the wind farm as shown in Figure 5.10.

5.4.2 Brazos and SMV Efficiency

Efficiencies of the Brazos and SMV (η) wind farms are estimated using equation (5.2) [11]. The actual power production of the wind farm is denoted by (P_{Actual}) while the maximum possible power assuming no-wake effects is given by (P_{max}). Full or near-full wake conditions are assumed in the simulations. Details of data filtering are the same for both these wind farms as discussed in section 5.3.

$$\eta = \frac{P_{Actual}}{P_{max}} \tag{5.2}$$

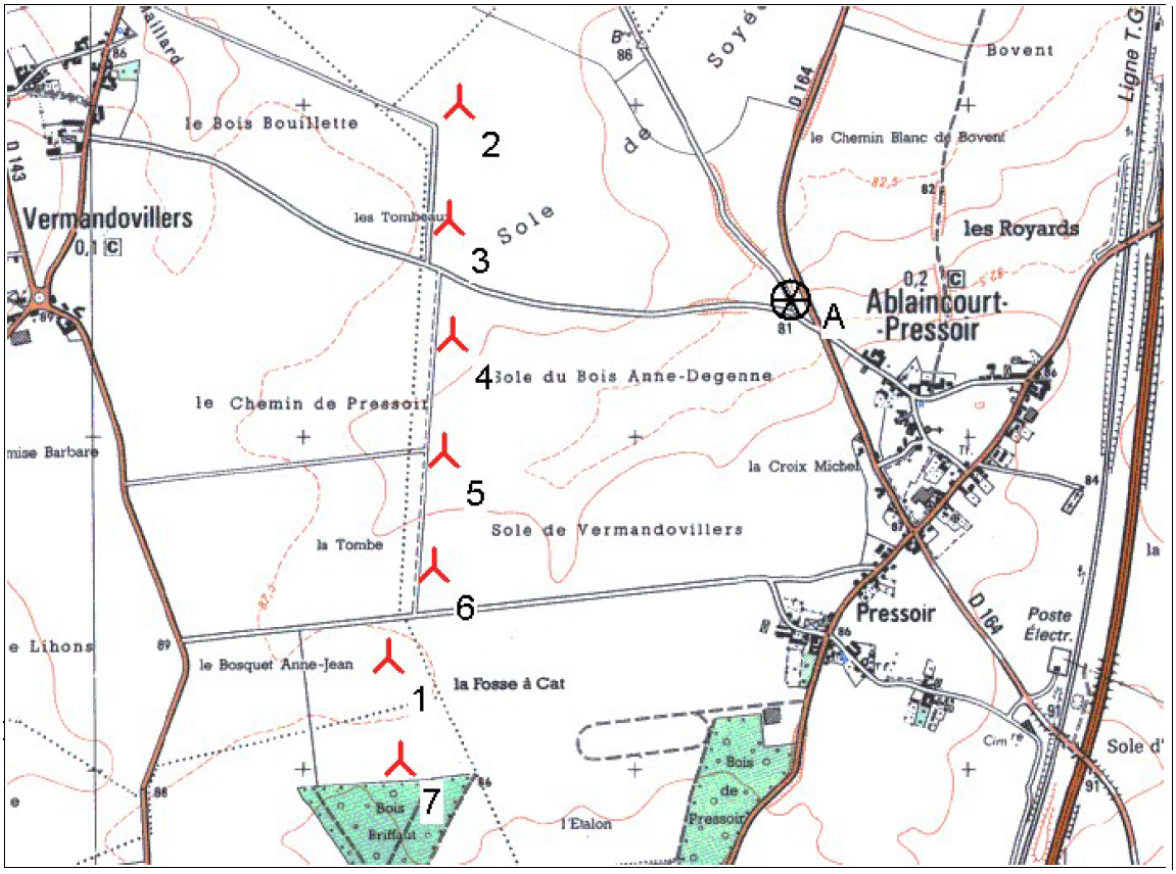

Figure 5.10 Preparing project for SMV wind farm using WindPRO

Efficiency based on SCADA data is maximum of 82% and 86% for Brazos and SMV respectively even in no-wake conditions. This can be due to errors in SCADA data or other unknown operational issues, as the efficiency should be almost 100% in no-wake conditions when turbines operate at their maximum capacity.

WindPRO and TI-JM only take the wake effects into account while estimating farm production. Therefore, the maximum efficiency is shifted to 1 i.e. 100% by adding the difference $(1 - \max(\text{Eff}(0-360)))$ to the whole efficiency curve. This does not change the shape of the efficiency curve but makes it possible to compare it with WindPRO and TI-JM by ignoring all other issues with the farm and data except wake effects. This also shows the importance of the second step of the assessment methodology as discussed in sections 4.4 and 5.3.

5.4.3 Lillgrund Efficiency

SCADA data for the wind farm could not be accessed. However, important information such as turbine characteristics, 360° farm efficiency and farm layout are given in [9, 17, 182, 184]. Access to details of the surface roughness length, turbulence intensity and average efficiency was provided by [17]. Average 360° efficiency based on SCADA data for below-rated wind conditions is reproduced from [9, 17] digitising data with [188]. Equation (5.3) [17] is used for calculating efficiency (η_{Lill}) of this wind farm.

$$\eta_{Lill} = \frac{N_j}{48} \frac{\sum_{i=1}^{48} P_i}{\sum_{j} P_j} \tag{5.3}$$

where (i) is the the turbine under consideration, (P_i) is the average power of a turbine, (j) denotes number of turbines and is a set containing only the turbines used for normalisation as given in Table 5.1 and shown in Figure 5.4a. The set j depends upon free stream wind direction and contains wind turbines facing the free-stream wind. Number of turbines in set j is denoted by (N_j) as given in Table 5.1.

According to [17], the average free-stream turbulence intensity in Lillgrund is 0.06, and that k_{Jensen} can be tuned as per the wind deficit model.

Table 5.1 Turbines used for normalisation for estimating Lillgrund efficiency [17]

Wind Direction	Figure 5.4a	N_j	j
North-east	N_{NE}	5	Turbine 1 of row 1 to row 5
South-east	N_{SE}	7	Seven turbines of row 1
South-west	N_{SW}	3	Turbine 8 of row 2 to row 4
North-west	N_{NW}	3	Three turbines of row 8

5.5 Results and Analysis

Analysis of efficiencies obtained through different sources and methods for Brazos, SMV and Lillgrund are presented in this section. Below rated wind conditions are used

in these analysis as suggested in [9]. This was discussed in detail in sections 1.2.1 and 5.4.

5.5.1 Brazos

Turbines in the case study row-2 are installed in a straight line as can be seen in Figure 5.2a. Hence the same wake effects are produced when the wind flows from east or west. Average efficiency for $90° \pm 30°$ is shown in Figure 5.11. The wind sector of $90° \pm 10°$ represents the full or near-full wake conditions. Partial wakes are observed in the sector of $70° \pm 10°$ and $110° \pm 10°$. It can be seen in Figure 5.11 that shifted efficiency can be as low as 58% showing how adversely wakes can impact the farm production. WindPRO predicts that the efficiency can be as low as 30% in the worst cases (full wakes) with such layout.

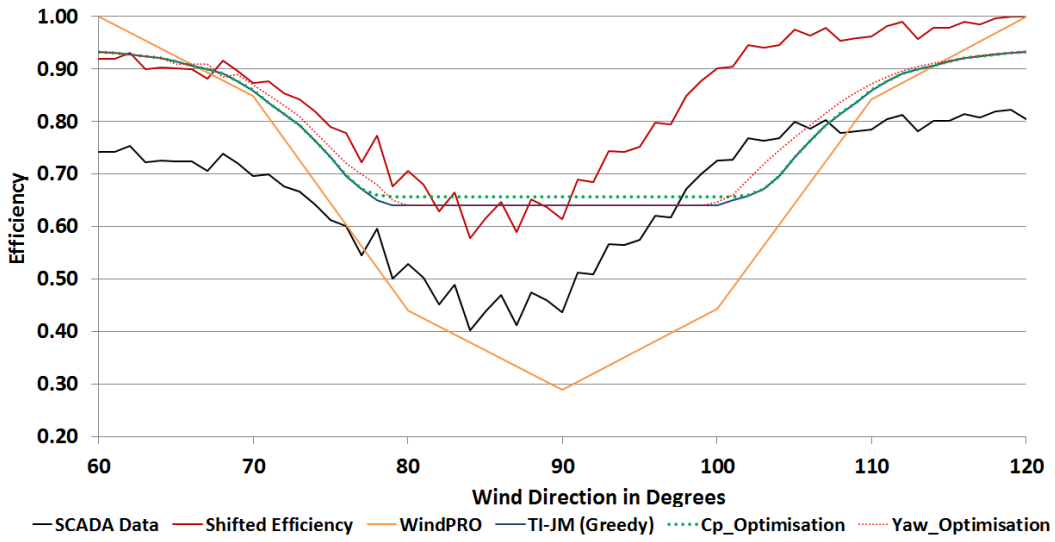

Figure 5.11 Brazos Efficiency in Full and near-full wake conditions

TI-JM predicts a minimum average efficiency of 62% in full wake conditions. The methodology for obtaining efficiency of this wind farm was explained in section 5.4.2. Higher values of wake decay coefficient (up to $k_{Jensen} = 0.25$) are used, as estimated by TI-JM for calculating speed deficits deep inside the farm as shown in Figure 5.13. This shows that the standard value of $k_{Jensen} = 0.07$ for onshore wind farms must be tuned according to the wind conditions (inside the farm). The data driven initial value of k_{Jensen} keeps the efficiency constant and closer to the efficiency based on SCADA data in the $80° - 100°$ sector, as can be observed in Figure 5.11. This (data driven)

higher initial value of k_{Jensen} increases the wake spread, which is further increased inside the farm because of the wake-added turbulence intensity as discussed in section 4.3. With a constant k_{Jensen}, efficiency based on the TI-JM follows efficiency obtained with WindPRO, as WindPRO also uses the constant standard value of k_{Jensen}. Other factors affecting the difference between efficiencies obtained with TI-JM and WindPRO are the different ambient turbulence intensities used for these two models and the fact that WindPRO includes the WAsP terrain model while TI-JM does not take account of terrain. These are the sources of uncertainty in model prediction accuracy.

The average efficiency predicted by TI-JM follows the shifted efficiency much closer as compared to WindPRO, especially from $60° - 90°$. WindPRO and TI-JM produce symmetrical results around 90° as it is a straight line one-dimensional array of turbines. However the shifted efficiency based on SCADA data is not symmetrical. Unknown operational issues, errors in the SCADA data or wakes produced by the Brazos-B wind farm can be a reason for this loss in production. WindPRO and TI-JM ignore the impact of nearby turbines assuming free-stream conditions.

It can also be seen in Figures 5.11 and 5.12 that C_P-based and yaw-based control strategies can improve the average efficiency by up to 2%. C_P-based control can perform better in full or near-full wakes ($90° \pm 10°$) while yaw-based control can perform better in partial wake conditions ($70° \pm 10°$ and $110° \pm 10°$). In full wake situation, a larger yaw-offset (can be more than 30°) is required for skewing the wake away from the downstream turbine [113, 189, 190]. This significantly reduces production of the upstream turbine (on which the yaw-offset is applied) as discussed in section 3.1.4. Even a yaw-offset of up to 30° does not fully skew the wake away from the downstream turbine, rather a full-wake is converted to partial wake [113, 189, 190]. In partial wake conditions, the yaw-offset applied is smaller (yaw-offset value depends upon wake, usually within a range of ±15°), which does not have significant impact on production of the upstream turbine and this also converts a partial wake into no-wake condition, which significantly increases production of downstream turbine.

The contour plots in Figure 5.13 compare the wind flow using conventional, C_P-based and yaw-based control. It can be seen that upstream turbines produce lower wind speed deficit with C_P-based control as compared to conventional control as their production has been curtailed. Yaw-based control on the other hand skews the wake away from the downstream turbines by yawing the upstream turbine. It was observed while estimating the efficiency that C_P-based optimisation strategy can increase the farm production by up to 5% while yaw-based optimised control can

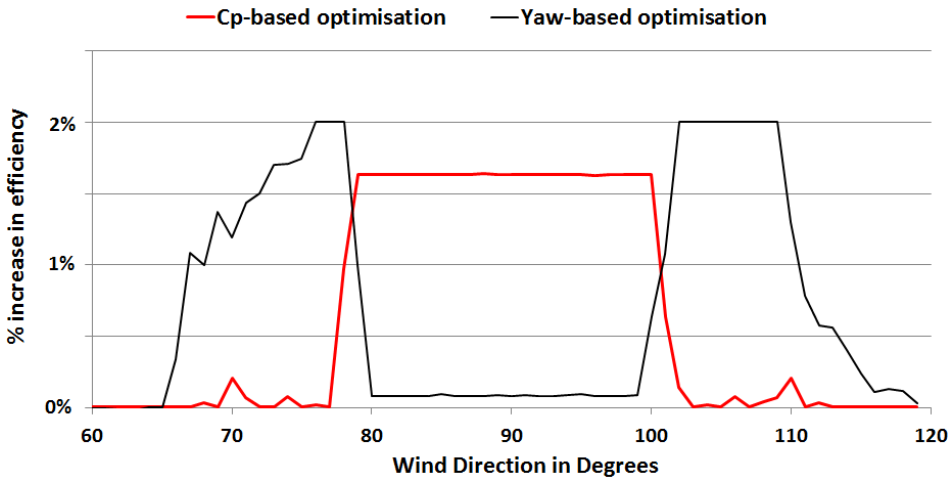

Figure 5.12 Percentage increase in Brazos efficiency with coordinated control strategies relative to the efficiency obtained with greedy control using TI-JM

result in a maximum of 7% increase in farm production [29]. A single simulation for optimisation always took less than 15 seconds in this case.

The contour plots in Figure 5.13 also show the increase in wake-width as the wind flows through the wind farm representing the impact of wake added turbulence intensity.

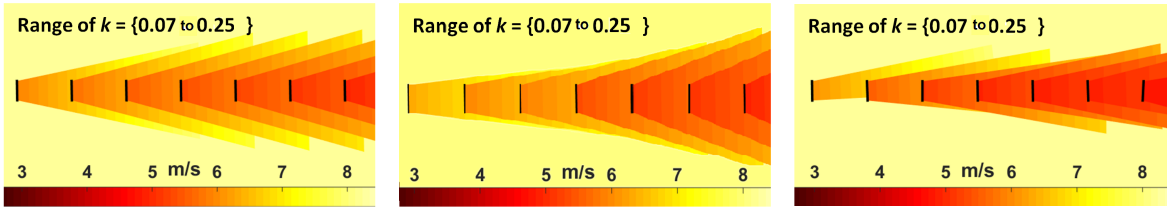

(a) Greedy Control **(b)** C_P-based Control **(c)** Yaw-based control

Figure 5.13 Comparison of Greedy, C_P-based and yaw-based control for the Brazos wind farm at 8m/s in full wake conditions

5.5.2 Le Sole de Moulin Vieux (SMV)

Average efficiency (in wind direction from the south) for the SMV farm is shown in Figure 5.14. The direction sector of $160° - 220°$ represents full or near-full wake conditions. The shifted efficiency shows that efficiency can be as low as 78% in full wake conditions. WindPRO predicts that losses can be as high as 30% resulting in decreased efficiency of 70%. The standard value of $k_{Jensen} = 0.07$ for onshore wind farms is used

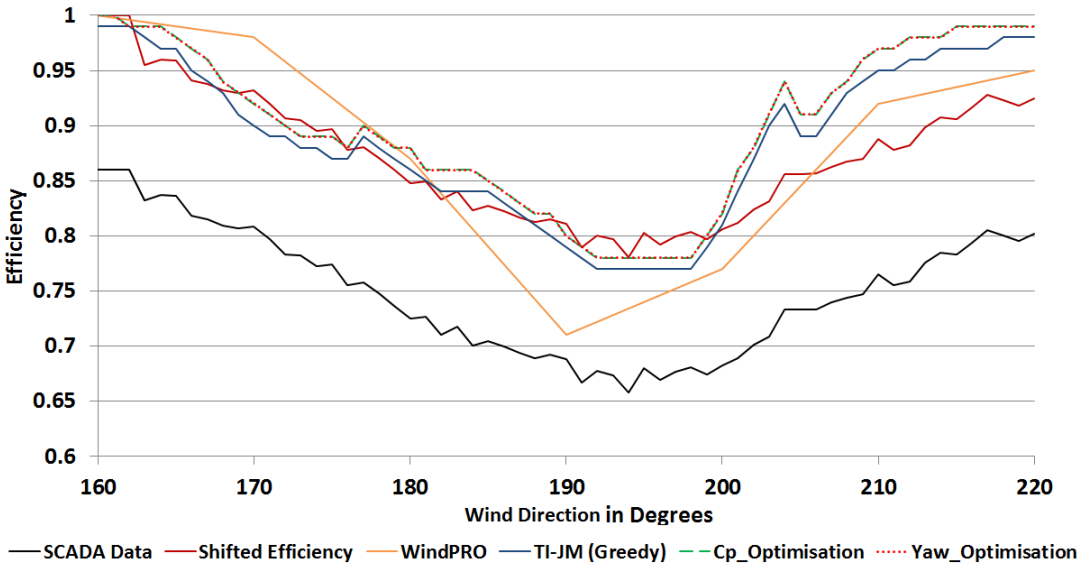

Figure 5.14 SMV Efficiency in Full and near-full wake conditions

in WindPRO. Details of how these efficiencies were obtained were provided in section 5.4.2.

The TI-JM estimates that efficiency can be as low as 76% in the worst case. TI-JM estimates value of k_{Jensen} up to 0.20 for better wake prediction inside the wind farm. Efficiency obtained with TI-JM (greedy control) fits well with the shifted efficiency from $160° - 200°$. However, WindPRO estimates better in the sector $200° - 220°$. TI-JM captures the shape of the efficiency curve but the difference in predicted efficiency is high for the direction sector of $200° - 220°$ as wake losses are under-estimated. This shows that even a higher value of k_{Jensen} cannot capture the wake accurately. This can be attributed to the highly unstable surface layer conditions on site [138, 174, 175] as discussed in section 5.1.2.

With coordinated control strategies, average efficiency can be increased by up to 4% as can be seen in Figures 5.14 and 5.15. C_P-based and yaw-based control strategies perform equally well (on average) in this case over all wind directions. This is because of the layout of the farm as discussed in section 5.1.2. As turbines are not installed completely in-line, the wake effects (conditions) for different wind turbines are different. For example, SMV1 to SMV4 are under full or near-full wake effects produced by SMV5 in the $180° \pm 10°$ sector, however SMV6 is under minimal partial effect of SMV7 in this sector. Similarly SMV6 is under full wake effects of SMV7 in the $200° \pm 10°$ but all other turbines are under partial wake effects of their corresponding upstream

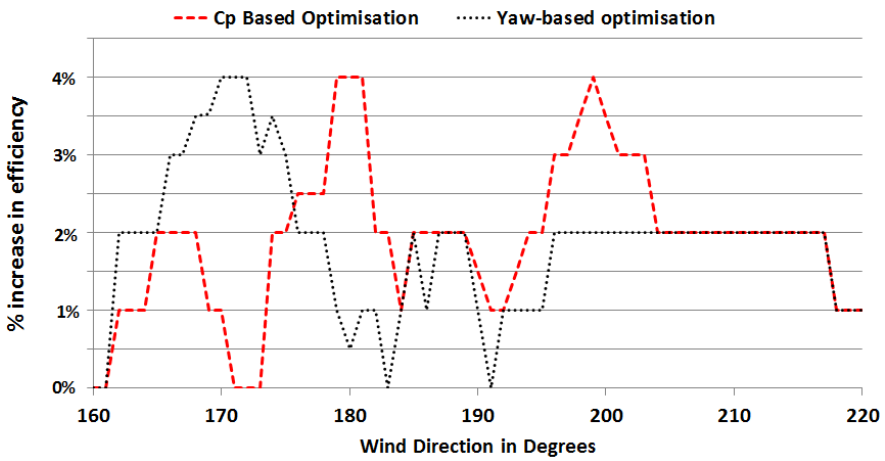

Figure 5.15 Percentage increase in SMV efficiency with coordinated control strategies relative to the efficiency obtained with greedy control using TI-JM

turbines. Hence no specific pattern of increase in efficiency was observed as can be seen in Figure 5.15.

Contours in Figure 5.16 present a comparison of greedy, C_P-based and yaw-based optimisation strategies for the farm. It was observed while estimating the efficiency that a maximum increase of up to 8% in power production is possible for this farm with both C_P-based and yaw-based optimised control [29]. A single simulation for optimising farm power production always took less than 15 seconds in this case.

5.5.3 Lillgrund

The efficiency of this two-dimensional offshore wind farm can be as low as 40% in full wake conditions ($45° \pm 10°, 135° \pm 10°, 225° \pm 10°, 315° \pm 10°$) [9] as shown in Figure 5.17. Average efficiency in below rated wind conditions is 67% resulting in 33% wake losses [9]. The methodology for estimating efficiency of this wind farm was presented in section 5.4.3.

It is estimated (with simulations) that the values of k_{Jensen} given in Equation 5.4 shall be used with the TI-JM for free-stream conditions. These values fit well with the

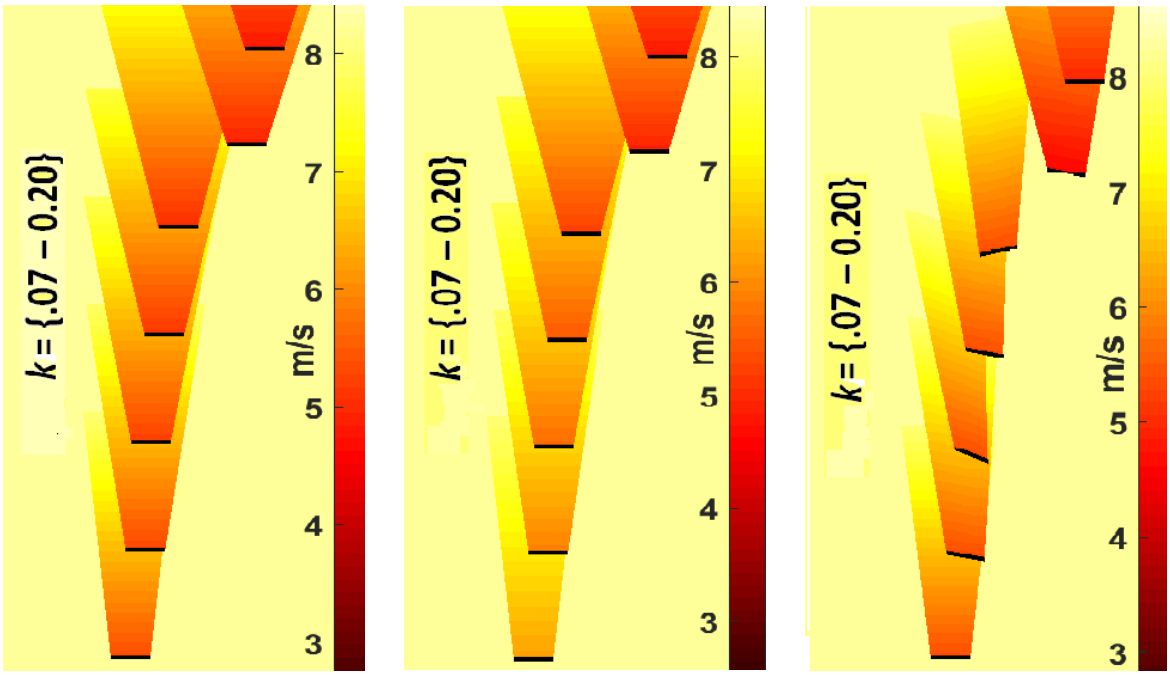

(a) Greedy Control **(b)** C_P-based Control **(c)** Yaw-based control

Figure 5.16 Comparison of Greedy, C_P-based and yaw-based control for the SMV wind farm at 8m/s in full wake conditions

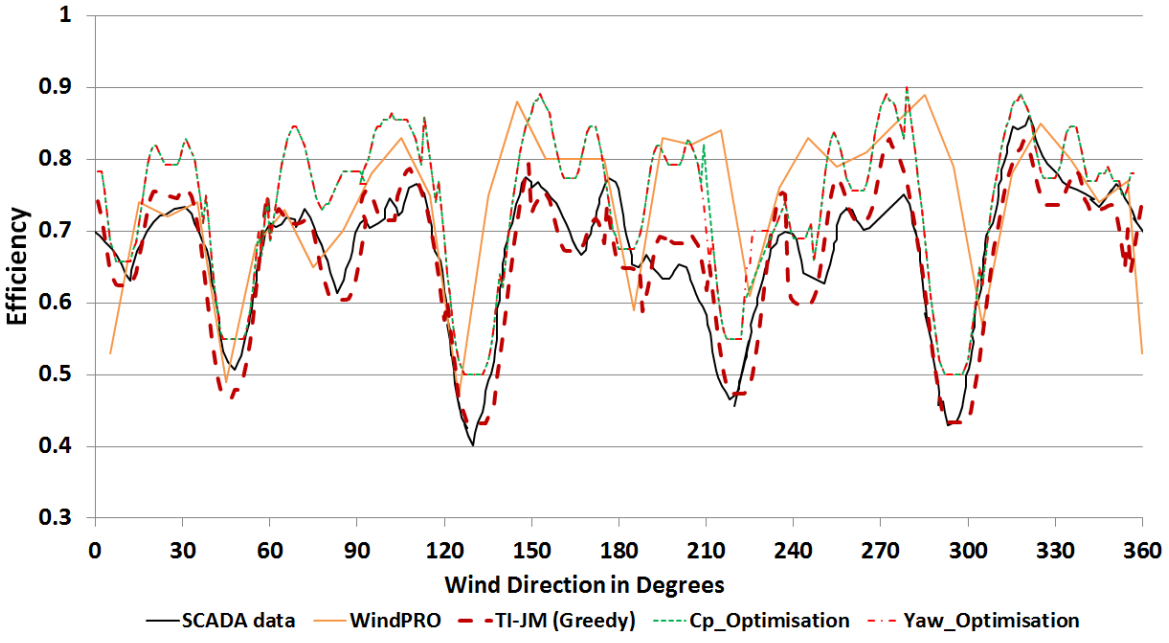

Figure 5.17 Lillgrund 360° average efficiency in below rated wind conditions

farm efficiency curve given in [9].

$$k_{Jensen} = 0.04 \qquad when \quad u_0 \leq 7.0\,m/s$$
$$k_{Jensen} = 0.08 \qquad when \quad 7.0\,m/s < u_0 \leq 12.0\,m/s$$

Above rated wind conditions are not considered in simulations, as suggested in [9] (5.4)

It can be seen in Figure 5.17 that efficiency based on greedy control using TI-JM fits well with the efficiency based on SCADA data (obtained from [9]). With the limited available information, it can be concluded that TI-JM is in good agreement with the efficiency obtained from real time data. The standard $k_{Jensen} = 0.04$ for offshore wind farms is used in WindPRO for estimating the efficiency. WindPRO captures the shape of average efficiency curve but results are inaccurate for most of the wind directions. This shows that WindPRO identifies wind conditions where wakes have higher impact on farm production but the wake prediction is incorrect.

Coordinated control can bring significant improvement in efficiency of such dense farms. C_P-based and yaw-based optimised farm control can improve the efficiency by up to 6% relative to the greedy control based on TI-JM. Efficiency can be increased in almost all wind directions due to the dense layout. C_P-based control performs better in full wake conditions ($45° \pm 10°, 135° \pm 10°, 225° \pm 10°, 315° \pm 10°$) than the yaw-based control as was discussed in section 5.5.1. Yaw-based control generally performs better than C_P-based control in partial wakes (all other directions than the full-wakes) as can be seen in Figures 5.17 and 5.18 and section 5.5.1.

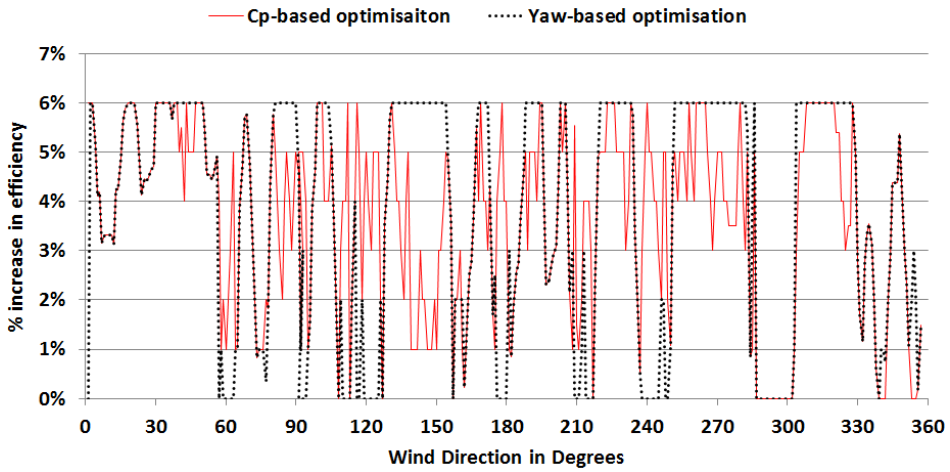

Figure 5.18 Percentage increase in Lillgrund efficiency with coordinated control strategies relative to the efficiency obtained with greedy control using TI-JM

The contour plots in Figure 5.19 compare conventional, C_P-based and yaw-based control of Lillgrund wind farm. It was observed with simulations with innovative control strategies result in production increase of up to 8% for Lillgrund under full wake conditions (below rated power) as compared to the greedy operations. In reality, over all wind directions and all wind speeds, the total potential increase will be rather

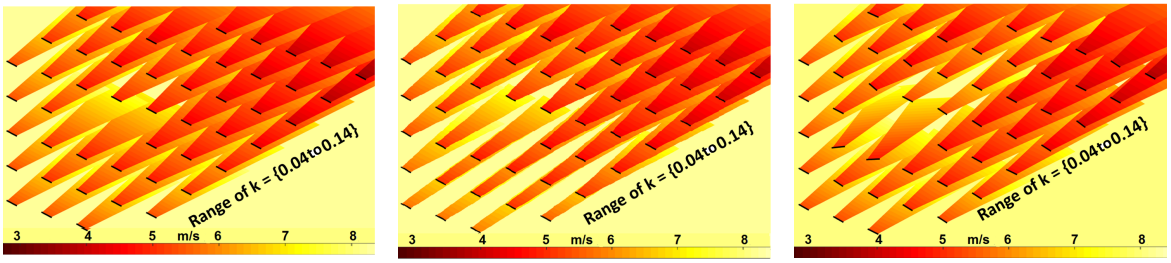

(a) Greedy Control **(b)** C_P-based Control **(c)** Yaw-based control

Figure 5.19 Comparison of Greedy, C_P-based and yaw-based control for the Lillgrund wind farm at 8m/s in full wake conditions

smaller. A single simulation for optimising farm power production took less than 50 seconds in this case.

5.6 Conclusion

This chapter presented main experimental results, based on simulations. Data from two onshore (Brazos and SMV) and one offshore (Lillgrund) wind farms was used in the simulations. First the wind deficit model (TI-JM) developed in section 4.3 was validated using SCADA data from the SMV wind farm. This validation confirmed that the TI-JM accurately predicts the wind speed deficit inside the wind farm in most of the cases with high processing speed as was discussed in section 5.2.

The assessment methodology developed in section 4.4 was applied on the SMV wind farm visualising and analysing wake effects in the wind farm. It was observed that wakes can severely affect turbines' productions in the direction sectors of $0° \pm 40°$ and $180° \pm 40°$. These sectors were divided into $\pm 5°$ direction bins and a wind speed bin of ± 0.5m/s. Analysis using relative efficiency with respect to the turbine producing maximum power shows that relative efficiency can be as low as 40% for some of the turbines.

Coordinated control strategies were evaluated using wind farm efficiencies. Efficiencies based on SCADA data and WindPRO were used as benchmarks. The TI-JM accurately predicted efficiencies of the wind farms case studies in most of the cases. It was concluded that generally C_P-based optimisation strategies perform better in full wake conditions while yaw-based optimisation strategies perform better in partial wake conditions. This answered RQ-5 which is about performance comparison of different control strategies in different wind conditions.

In full wakes conditions, even larger yaw-offset (greater than 15°) cannot skew the wake away from downstream turbines and this larger yaw offset also reduces power of upstream turbine significantly. A partial wake can be converted into a no-wake situation with an optimised yaw-offset applied on the upstream turbine increasing overall farm production.

Average efficiency in below rated wind speeds is increased by up to 2% for Brazos-row, 4% for SMV and 6% for Lillgrund wind farm as can be seen in Figures 5.12, 5.15 and 5.18. The increase in efficiency is relative to the greedy control when simulated using TI-JM. Simulations confirmed that production increase of up to 8% is possible with these innovative control strategies in full-wake conditions and below rated wind conditions. In reality, over all wind directions and all wind speeds, the total potential increase will be rather smaller. The percentage increase in production was estimated while calculating the efficiency as was discussed in section 5.5. Optimisation process for Brazos-row and SMV is completed in a maximum of 15 seconds and a maximum of 50 seconds for Lillgrund. This high speed and accuracy make the controller suitable for real time on-line field implementation.

Chapter 6

Field Implementation

This chapter is mainly based on the collaborative work with Maïa Eolis (now Engie Green) detailing the filed implementation of coordinated control strategies in the SMV wind farm as a part of the French Government SmartEOLE project [181]. The work in this chapter answers the final RQ-6 explaining the approach adopted, for implementing coordinated control strategies in the SMV wind farm, given the operational limitations. A part of this work is present in [**191**][1]. To the best knowledge of the author, this is the first practical implementation of Light Detection And Ranging (LiDAR) based coordinated control strategies in an operating wind farm.

Two 2MW turbines in the SMV wind farm are investigated for this purpose. State of the art LiDAR were installed in the wind farm for accurately measuring the wind characteristics up to a frequency of 1Hz. Simulations are performed using WindPRO and the TI-JM for designing the practical experiments and predicting the impact of coordinated control strategies on farm production.

Analyses on real time field data are performed and results are compared with simulations. Results based on simulations are mostly in good agreement (within a range of 1.5%) with field results. It is shown that a gain of up to 11.5% is possible in downstream turbine production, using a hard curtailment strategy, by reducing power of the upstream turbine (using C_P) by about 17%. Overall combined production is decreased with the hard curtailment strategy, indicating that the upstream turbine must be optimally curtailed for avoiding any production loss. The yaw-based coordinated control strategies are also implemented in the field but the data cannot be collected due to technical problems and malfunctioning of one of the LiDAR.

[1] Self-citations by the author are presented in bold

The experimental setup for this field implementation is given in section 6.1. This is followed by the methodology adopted for designing the field experiments and the field implementation of coordinated control strategies in section 6.2. Details of the data and data-filtering are given in section 6.3. Simulated and field results of the C_P-based curtailment experiment are presented in section 6.4 while simulated results of the yaw-based experiment are presented in section 6.5. Conclusion of this chapter is provided in section 6.6. The structure of this chapter is presented in Figure 6.1.

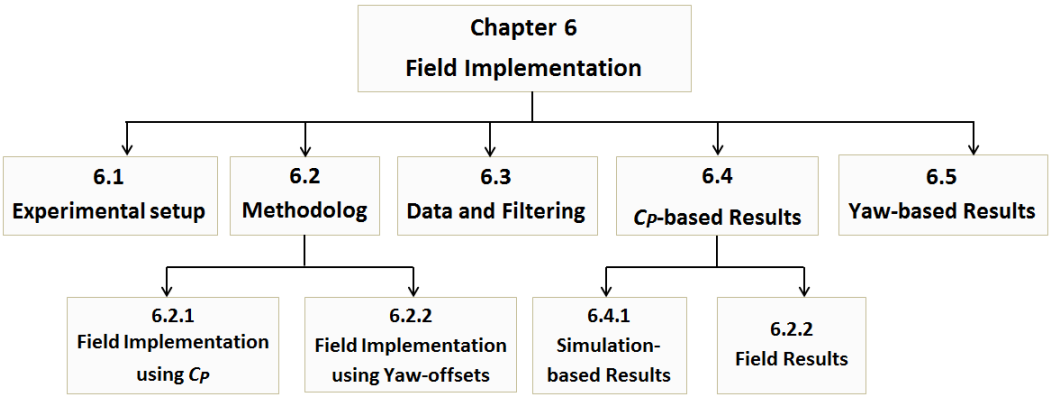

Figure 6.1 Structure of chapter 6

6.1 Experimental Setup

The aim of the SmartEOLE project is to propose and implement innovative wind farm control strategies for improving farm efficiency [181]. One major part of the SmartEOLE project is to develop and implement centralised farm control strategies analysing wake interactions using LiDAR. LiDAR can greatly help in removing the uncertainty in wind characteristics, making it possible to investigate coordinated control strategies in wind farms [11, 122]. LiDAR can provide information about wind conditions before it reaches the turbines. This information can be used for optimising combined output of the wind farm.

The control strategies are implemented in the SMV wind farm. Details of this wind farm were presented in section 5.1.2. The wind-rose in Figure 5.3b shows that the prevailing wind direction is from south and south-west, mainly in the direction from SMV6 to SMV5. Hence these two turbines were chosen for the field experiment. Figure 6.2 shows the wind conditions during the C_P-based curtailment experiment confirming the prevailing wind direction (south-west) and justifying the selection of

the two turbines. SMV6 is upstream and acts as the wake producing turbine, hence curtailment is applied on this turbine.

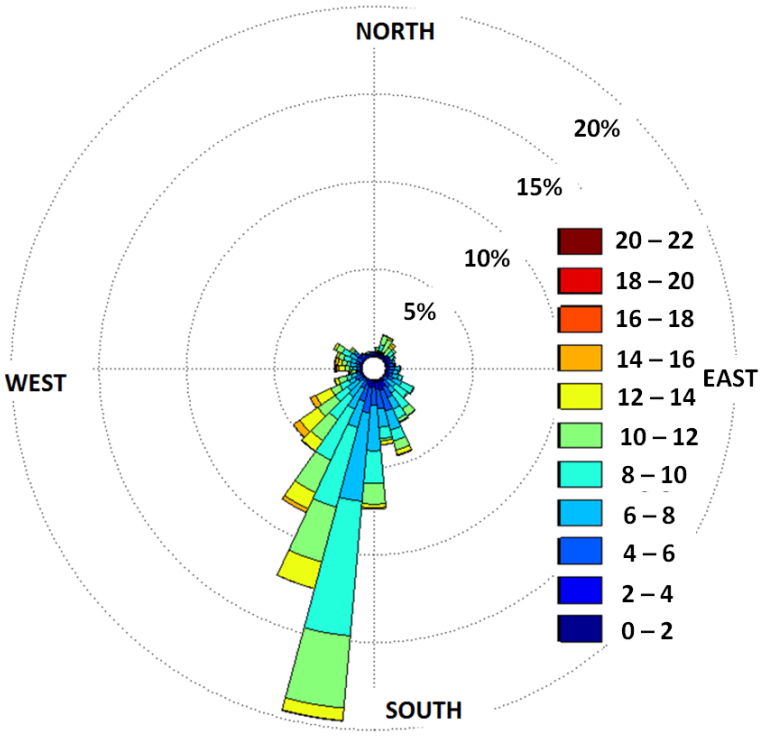

Figure 6.2 Wind conditions during the C_P-based curtailment experiment

SMV6 is equipped with nacelle mounted Orion 5-beam LiDAR [181] facing the free-stream wind as shown in Figure 6.4. A Wind iris LiDAR [181] is mounted on top of SMV5. A ground based LiDAR, Windcube V1 type [181] has been installed between turbines SMV2 and SMV3 as shown in Figure 6.3. This LiDAR measures the wind speed at heights between 40m and 200m with 1Hz frequency. A scanning LiDAR [181] is also installed at 1.2km to the east of the wind farm as shown in Figure 6.5. The scanning LiDAR is programmed to carry out three horizontal and one vertical scan. This allows measurement of wind characteristics at hub height of SMV6 in wake situations for SMV5. These LiDAR provide valuable and accurate information about the wake flow and wind characteristics at a frequency of up to 1Hz.

6.2 Methodology

This section explains the methodology for designing the experiments based on C_P and yaw offsets. It was concluded in Chapter 5 that the power production of SMV

Figure 6.3 SMV layout and surrounding with positions of met mast and LiDAR [187]

Figure 6.4 Leosphere 5 beam LiDAR mounted on top of SMV6

Figure 6.5 Scanning LiDAR 1.2km east of SMV for horizontal and vertical scans

wind farm is significantly affected by wake effects when the wind flows in $0° \pm 40°$ and $180° \pm 40°$ sectors. The direction sector $180° \pm 40°$ was further analysed with the assessment methodology given in section 4.4.

It was observed that SMV5 is under wake effects of SMV6 in the sector $200° \pm 20°$ as shown in Figure 6.6. WindPRO predicted 26% losses in SMV5 production caused by SMV6 wakes, in this directional sector using yearly data from 2015 and 2016. Figure 6.7 presents power production of SMV5 and SMV6 in two steps in normal operations, showing the impact of SMV6 wake on SMV5 production. It can be observed in Figure 6.7 that SMV5 production is significantly affected by the SMV6 wake in the $200° \pm 20$ sector. Different production settings of SMV5 and SMV6 were evaluated for developing a curtailment strategy. The two steps (settings) presented in Figure 6.7 was found to be the most suitable for implementations due to the limitations on turbine curtailment. This will be discussed in detail in section 6.2.1. Wind also flows predominantly in this direction, hence this is the chosen direction sector for this experiment.

Simulations were performed in the chosen wind direction sector using WindPRO and the TI-JM. Optimal settings for curtailment based on C_P were obtained with the optimised coordinated control strategies as will be discussed in section 6.4.1.

WindPRO does not have any mechanism for estimating impact of yaw-offsets on wake produced. Hence the yaw-based simulations are performed using the TI-JM only. For refined analysis, the direction bin is halved making it $\pm 2.5°$. Tables were created for each direction bin of $5°$ with a speed bin of ± 0.5m/s showing the optimum yaw-offset on SMV6 as will be discussed in section 6.5.

The C_P-based and yaw-based field experiments are detailed in the following sections 6.2.1 and 6.2.2 respectively.

6.2.1 Field Implementation using C_P

This C_P-based experiment lasted for six months. The aim of this experiment is to analyse the impact of SMV6 curtailment on SMV5 production. The optimised control strategies cannot be implemented due to operational limitations. Some changes were made in the turbine's control software by the turbine manufacturer, which did not allow to change the turbine's power production settings for each wind speed and direction bin as required for the optimised control. Due to these changes, the curtailment has to be applied manually on SMV6. That is why a two-step curtailment strategy was adopted, which can be easily implemented on SMV6. The strategy is aimed at curtailing SMV6

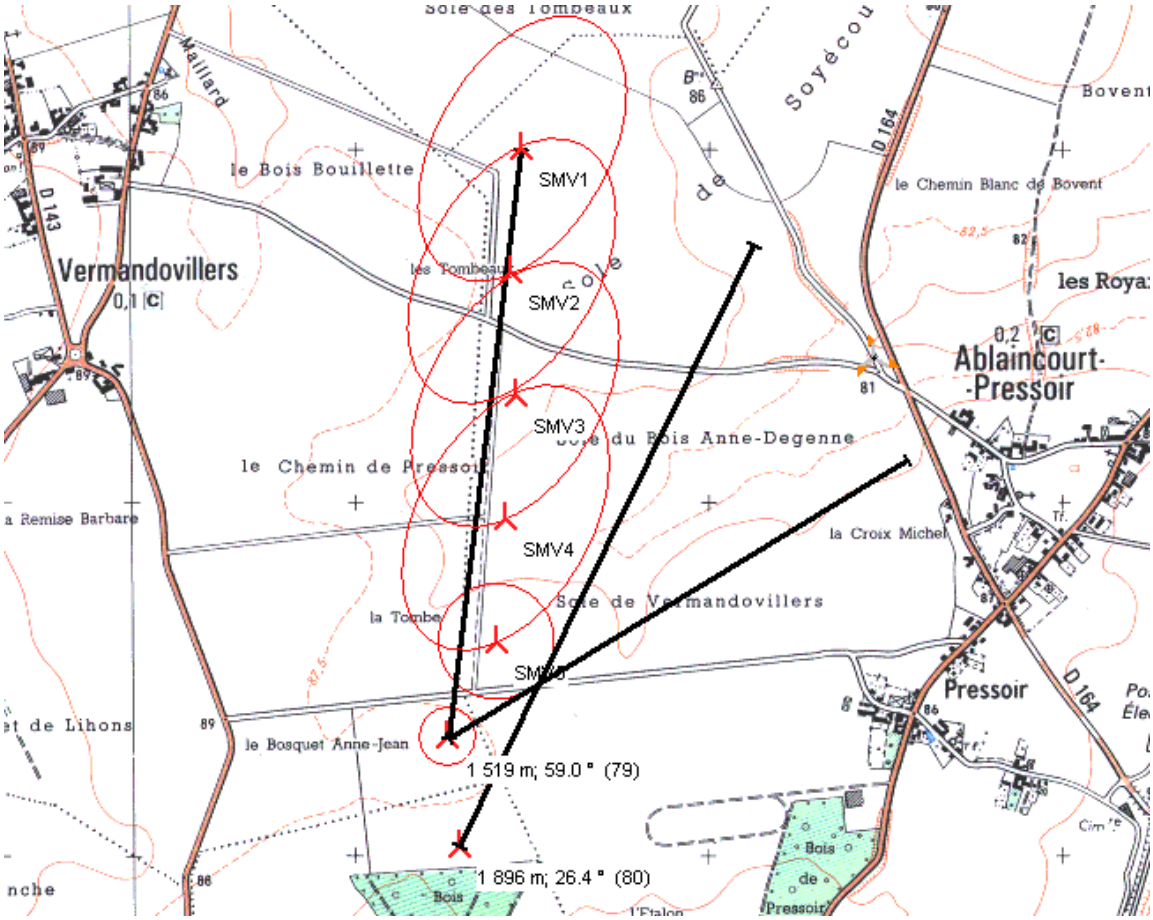

Figure 6.6 Predicting wake effects in the wind direction sector $200° \pm 20$ using WindPRO

power to a maximum of 20% in two steps in the selected direction sector according to the criteria given in Table 6.1.

SMV7 power production is used as the reference, as it is unaffected by wakes when the wind flows in the chosen sector. In the first step, when the power of SMV7 is between 1200kW and 1500kW and SMV6 power is above 1200kW, SMV6 is curtailed to 1200kW. In the second step if SMV7 power is between 1600kW and 1900kW and SMV6 power production is above 1600kW then SMV6 is curtailed to 1600kW. This means that a maximum of 20% curtailment is allowed on SMV6 power production. This curtailment approach is named as hard curtailment strategy due to the hard curtailment limits. The region between 1500kW and 1600kW is not considered for curtailment due to operational limitations on the turbines.

The curtailment ranges given in Table 6.1 were identified using a series of surveys, discussions and simulations, considering the operational limitations (changes in turbine's

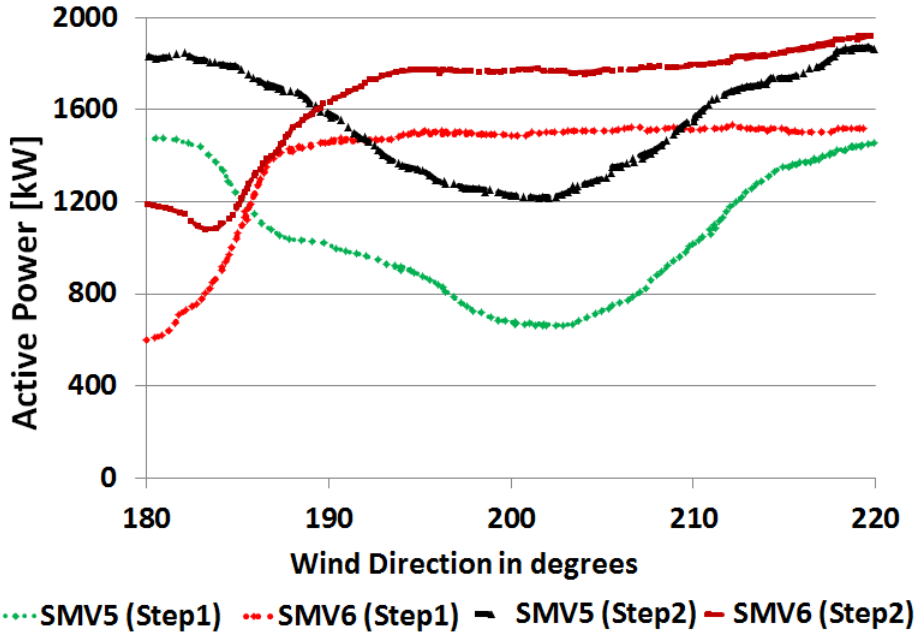

Figure 6.7 SMV5 and SMV6 power production in $180° - 220°$ in normal operations

control software). These settings were found to be the most suitable for implementations due to the limitations on turbine curtailment.

The optimised control requires a different C_P or turbine's production settings for each wind speed and direction bin. It was not possible to change the production of SMV6 for each wind speed and direction bin, due to restrictions in the turbine's control software. Therefore, different possible curtailment settings were evaluated by simulating production of the two experiment turbines (SMV6 and SMV5) and the whole wind farm with real time data. The curtailment settings given in Table 6.1 were found to be most suitable for field implementation. The curtailment settings given in Table 6.1 were the closest to the the optimum settings, implementable in the field [181]. It should be noted that these settings do not completely reflect the optimum settings, but provides a broader idea of how SMV6 wake affects SMV5 production.

The curtailment strategy in Table 6.1 was implemented in the selected wind directional sector i.e. $200° \pm 20°$. Each time when wind conditions were favourable for the hard-curtailment, an engineer manually curtailed SMV6 accordingly. The wind-rose in Figure 6.8 shows the wind conditions when SMV6 was actually hard curtailed in the field as per the criteria given in Table 6.1. The power curve based on this hard curtailment strategy is shown in Figure 6.9. It can be observed with the hard curtailed power curve in Figure 6.9 that SMV6 was curtailed only when the wind speed was

Table 6.1 Two steps of the hard curtailment strategy

if 180° ≤ Wind Direction ≤ 220°		
Step1:	if	1200kW < SMV7 ≤ 1500kW
	then	curtail SMV6 to 1200kW
Step2:	if	1600kW < SMV7 ≤ 1900kW
	then	curtail SMV6 to 1600kW

above 10m/s. The curtailed power curve is the same as standard power curve below 10m/s and above 14m/s as can be seen in Figure 6.9.

Senvion MM82 2050 are variable speed turbines and their power can be curtailed as desired, by controlling the C_P using blade pitch angle or rotational speed [16]. The turbine controller is configured to follow the manufacturer standard power curve by default i.e. the greedy control. This standard power curve is given in Figure 6.9. These power curves in Figure 6.9 show how SMV6 should operate with different control settings. Figures 5.11, 5.14 and 5.17 showed the efficiency of Brazos, SMV and Lillgrund wind farms when the turbines productions were simulated using the standard and optimised power curves. Power productions is plotted against wind speed rather than efficiency against wind direction in this chapter due to the limited availability of field data as will be explained in section 6.4.2. Furthermore, the aim is to analyse the impact on coordinated control strategies in each wind speed and direction bin, hence plotting power production against wind speed for a given direction bin is a better option.

For optimised control, the turbine must follow an optimised power curve for each direction bin communicated by the farm controller. This requires fast processing and efficient on-line control strategies, to formulate the power curve according to the wind conditions, as discussed in Chapter 5. Due to operational constraints, it was not possible to use the optimised power curve during the field implementation as explained earlier.

Efficiency was plotted against wind direction in Figures 5.11, 5.14 and 5.17 where more data was available as compared to the data obtained from the field implementation in this chapter. The aim was to show the overall percentage increase farms' productions in below rated wind conditions with coordinated control strategies. The aim in this

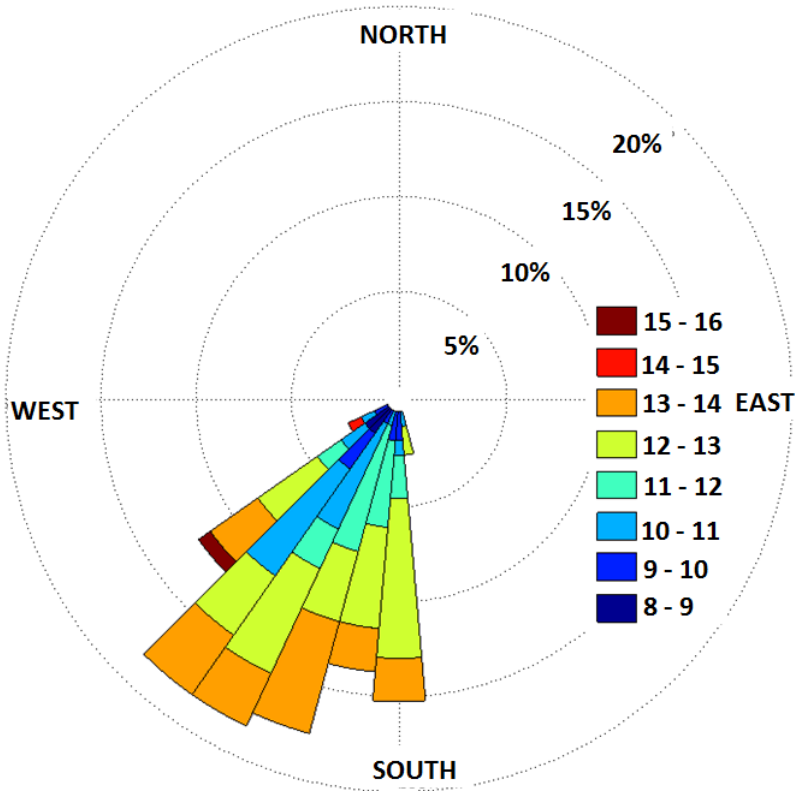

Figure 6.8 Wind-rose for the periods when SMV6 was curtailed with the hard strategy

chapter is to analyse the impact of coordinate control (hard-curtailed) strategies on net production in each direction and speed bin. A turbine's power curve show the power production of the turbine in each bin as shown in Figure 6.9, hence power curves are used in this chapter, instead of efficiency for depicting impact of curtailment of power production.

The field implementation is based on SMV6 and SMV5, with the wind flowing from south and south-east. This takes SMV7 production out of the analysis as SMV7 power production is unaffected when SMV6 is curtailed. Hence from this point onwards the farm means turbines SMV1 - SMV6.

6.2.2 Field Implementation using Yaw-offsets

The yaw-based optimisation strategy for SMV6 and SMV5 predicts that the optimal yaw-offset range is $-10°$ to $15°$, as will be discussed in section 6.5. However, the operational limitations allow a maximum yaw-offset range of $-12°$ to $8°$.

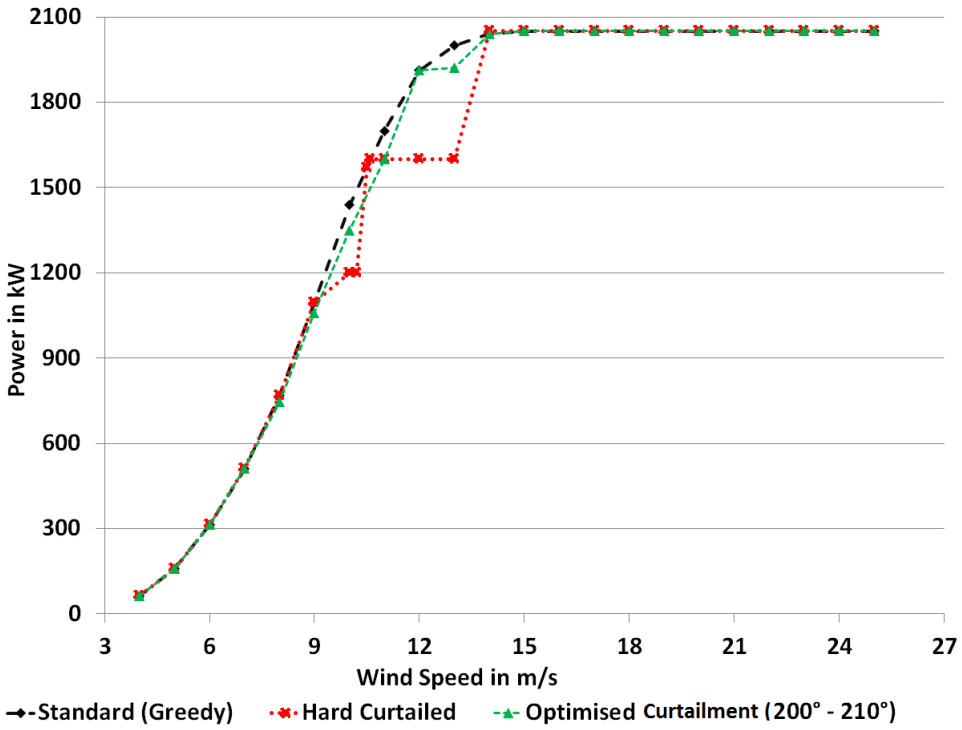

Figure 6.9 Comparison of SMV6 standard, hard-curtailed and optimised power curve

This yaw-based coordinated control strategy was implemented in two steps. In the first step: SMV6 was operated with a yaw-offset of $-12°$ for ten days. In the second step: the yaw-offset on SMV6 was increased to $8°$. SMV6 operated for four weeks with this $8°$ offset. The analysis will be performed in the $200° \pm 20°$ sector: SMV5 is under wake effects of SMV6 in this direction sector as discussed in section 6.2. It was observed during normal operations that turbines are not always completely in-line with the wind direction. Hence there is always some unwanted yaw-error in normal (greedy) operations.

The aim here is to choose a dynamic yaw-offset by adding the intentional yaw-offset ($-12°$ or $8°$) and the actual yaw-error (unwanted). The actual yaw-error is obtained from the network management systems of Maïa Eolis (now Engine Green). This results in a larger yaw-offset range as the effective yaw-offset may be beyond the $-12°$ to $8°$ range.

The yaw-offset decreases SMV6 production but at the same time skews the wake away from SMV5, increasing its production. The optimum yaw-offsets result in increase in net production. The full data set could not be collected from the 5-beam LiDAR due to some technical problems. First, the communication cable was cut mistakenly

by road workers during the execution of the experiment. Second, further problems occurred during data retrieval from the LiDAR storage system after the experiment. The field implementation is complete and analysis is left for future work as will be discussed in section 7.2.1.

6.3 Data and Filtering

It was discussed in section 6.2.2 that the data for yaw-based experiment is not available due to equipment malfunctioning. All the devices were fully functional during the C_P-based curtailment experiment and data was collected from these devices for further analysis. This section presents details of the data collected through different sources and the filtering process to make the data noise free.

As discussed in section 6.2.1, the C_P-based experiment lasted for six months. During this period, data from different sources (met-mast, SCADA, LiDAR and MERRA [183]) was recorded. Availability of data from these sources is shown in Figure 6.10. The curtailment periods are also given in Figure 6.10 which is 19 hours, corresponding to more than 200 data points. Filtering criteria is to have at least 10 valid points in a given directional and speed bin. Wind conditions with less than 10 points are not considered for analysis.

Figure 6.10 also shows atmospheric stability in the wind farm. It can be seen that atmosphere is mostly unstable as discussed in section 5.1.2. The atmospheric stability given in Figure 6.10 is displayed as Monin Obukhov length (MOL) sampled in 10 classes, starting from very unstable moving to strongly stable conditions as given in Table 6.2 [138, 181]. The MOL is calculated using MERRA 2 reanalysis data [183]. Detailed description of how the MOL is calculated is given in [138]. The Obukhov length ($L(m)$) is a surface layer scaling parameter that is a function of surface heat and momentum fluxes [138, 174]. The atmospheric stability is not used in calculations in this work. The purpose of depicting it in Figure 6.10 is to show that atmosphere is mostly unstable in the SMV wind farm.

Another important issue was the difference in wind directions reported by different sources. Instantaneous wind directions can differ from a measuring device placement to another because of wind turbulence. Nevertheless, offsets are mostly due to calibration errors.

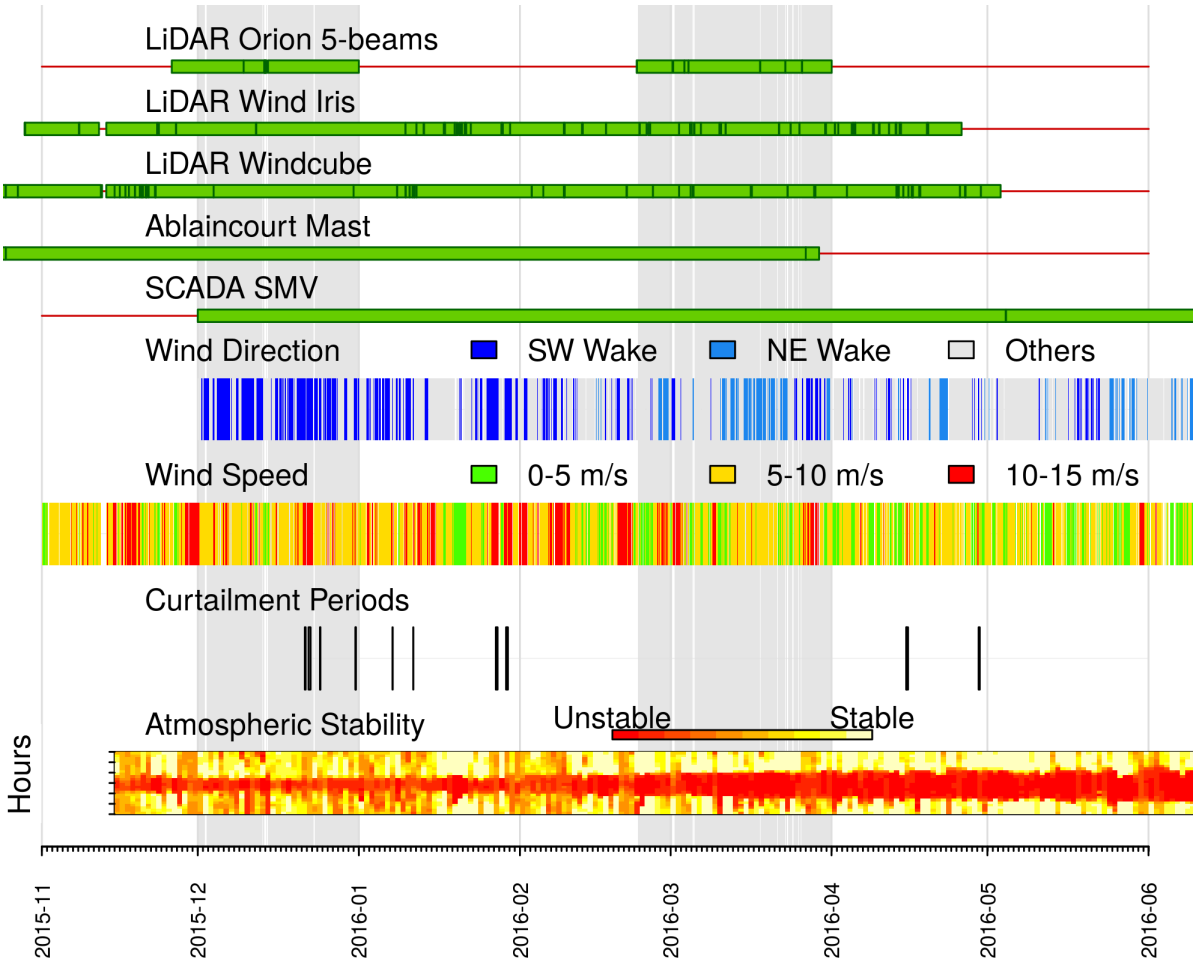

Figure 6.10 Data Availability for the C_P-based experiment from different sources

To avoid any directional discrepancy in analyses, LiDAR Windcube data at a height of 80m were corrected by analysing directions of wakes and then used as a reference. Unlike nacelle mounted instruments, this LiDAR's wind direction is independent of nacelle position and wake effects do not interfere in the directions of interest. Indeed, the measurement of LiDAR wind direction is heavily perturbed in situation of inhomogeneous wind flow (complex terrain and wake conditions). Finally, directional offsets using this reference were applied to all the devices i.e. LiDAR, turbines and met mast.

Table 6.2 Monin Obukhov Length classification [138]

$L(m)$	**WT Classes**	**Stability**
$-140 < L < 0$	0	Very unstable
$-1000 < L < -140$	1	Unstable
$L < -1000 or L > 2500$	2	Neutral
$1000 < L < 2500$	3	Slightly stable
$600 < L < 1000$	4	Stable
$380 < L < 600$	5	Stable
$240 < L < 380$	6	Stable
$160 < L < 240$	7	Very stable
$80 < L < 160$	8	Very stable
L <80	9	Strongly stable

6.4 C_P-based Results

This section presents results from the C_P-based curtailment experiment. Results based on simulations are presented in section 6.4.1 followed by results based on real time data (collected during the field implementation) in section 6.4.2.

6.4.1 Simulation-based Results

WindPRO and the TI-JM are used in the simulations discussed in this section. The standard Jensen model [75] is used for wake prediction with WindPRO. It shall be noted that for a two turbines case, the TI-JM behaves exactly the same as the standard Jensen model (WindPRO). The standard $k_{Jensen} = 0.07$ given in Table 4.1 for onshore wind farms, is used in both WindPRO and TI-JM. Hence there is no difference between WindPRO and TI-JM in this case as both produce the same results for a two turbines study using the standard Jensen model. The percentage increase or decrease in production was determined by simulating the available wind data with the standard, hard-curtailed and optimised power curve and then finding the difference in production accordingly.

6.4.1.1 Simulations with all the Collected Data

WindPRO predicted an average increase of almost 3% in SMV5 power production in the $(200^\circ \pm 20^\circ)$ directional sector with the hard curtailment strategy as compared to normal operations. This increase in each 10° bin is shown in Figure 6.11. The highest increase 1.15% is achieved in the $190^\circ - 200^\circ$ bin. This was the prevailing wind direction bin in the farm during the field implementation as can be seen in Figure 6.2. SMV5 is almost completely shadowed by the wake produced by SMV6 in the $190^\circ - 200^\circ$ bin. Hence WindPRO predicts a higher gain for this bin. The lowest increase is in the bin $200^\circ - 210^\circ$ where SMV5 is under full wake effects of SMV6. As compared to other three bins, wind blew less frequently in this bin as can be seen in Figure 6.2. Production gain in the other two bins (partial wake conditions) is almost the same.

If equal weight (for wind direction and speeds) is given to all the bins then the gain in SMV5 production increases as the wake moves from partial to full wake conditions. WindPRO simulation of SMV6 normal operation (greedy control) with all the collected data predicts losses of up to 26% in SMV5 production due to SMV6 wake. This also provides more space for improvement with coordinated control. It was assumed in this simulation that SMV6 is under free flow wind conditions and wake produced by SMV7 was ignored, hence SMV5 is solely under the wake effects of SMV6. These WindPRO simulations in Figure 6.11 show that curtailment of SMV6 can produce more increase in SMV5 power production in full or near-full wake conditions.

WindPRO predicted a loss in combined production of SMV6 and SMV5 when SMV6 is hard curtailed as shown in Figure 6.11. This is expected with the hard curtailment strategy as SMV6 can be curtailed as high as 20%. The aim is to analyse the impact of this curtailment on SMV5 production and not to increase the combined production. The loss in net production shows that the loss in SMV6 power production due to curtailment is not compensated by gain in SMV5 power production. The highest loss in combined production is predicted in the $180^\circ - 190^\circ$ bin, as SMV5 is under minimal wake effect of SMV6 as compared to other three bins. Loss in combined production decreases as the wake moves from partial to full wake conditions. The smallest loss is in full wake conditions in the $200^\circ - 210^\circ$ bin.

Figure 6.11 also shows the optimised increase in SMV5 production in all the four bins predicted by the C_P-based farm control strategy developed in this thesis. The farm controller predicted that no net increase can be achieved by curtailing SMV6 in the $180^\circ - 190^\circ$ bin, as wake impact on SMV5 is minimal. Therefore, SMV6 shall follow

its standard power curve resulting in maximum combined production. When the wake moves to near-full wake conditions in $190° - 200°$ bin, SMV5 can benefit more from curtailment of SMV6. Highest possible gain in combined production is 0.4% in this bin $190° - 200°$ as wind conditions are favourable for implementation of coordinated control and wind blew more frequently in this bin (Figure 6.11). Optimised gain in SMV5 production in full wake conditions is 0.35%.

As discussed earlier if it is assumed that wind flow is same in all the four bins then the highest optimised gain is possible in full wake conditions. Analyses of these results show no clear trend with respect to wind speeds. This is in confirmation with the findings in [99].

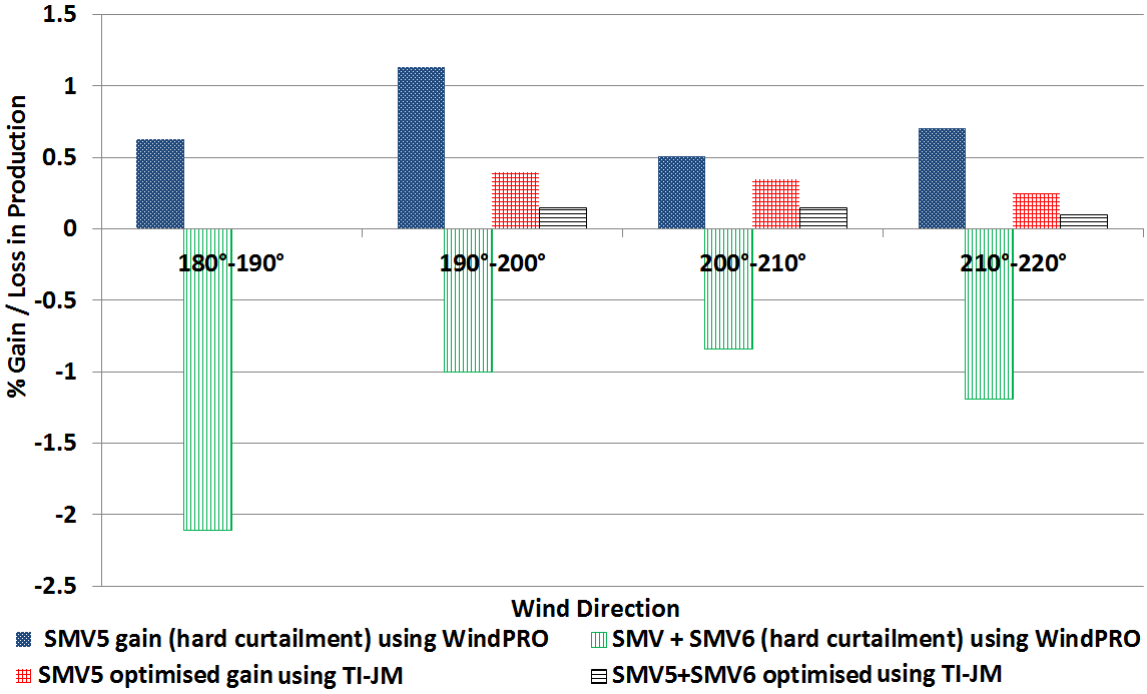

Figure 6.11 Simulated percentage increase/decrease in SMV5 and net production (SMV5+SMV6) when SMV6 is curtailed, weighted according to wind frequency

The farm controller (optimised operations) makes sure that there is no loss in combined production. The controller curtails SMV6 only when the loss in production can be compensated by the gain in SMV5 production. If no net gain is possible by curtailing SMV6, the farm controller instructs SMV6 to operate greedily resulting in maximum combined production. The optimised control could not be implemented in the field due to the operational constraints as discussed in section 6.2.1. However simulations with the optimised strategies are performed to analyse the impact on

production of the optimised control as shown in Figure 6.11. This also provides information for comparing the hard and optimised control strategies.

It was discussed in Chapter 2 that the gain in production depends upon many parameters including number of turbines in the farm that can be curtailed and number of downstream turbines that can benefit from this curtailment, wind conditions and surface roughness on the site. The number of turbines in this case is only two. Turbulence intensity and roughness on the site is very high allowing the wake to diffuse quickly [138]. Hence the optimised increase in SMV5 production and net gain is low. If all seven turbines in the farm are optimally controlled, a gain of up to 7% is possible in farm production in full or near-full wake conditions [**29**].

These simulations predict that SMV5 production can be increased by curtailing SMV6. Simulations also predicted decrease in net production with the hard curtailment strategy relative to normal operations. Optimised control of SMV6 can assure that there is no decrease in net production and can also result in increased net production in favourable wind conditions.

6.4.1.2 Simulations with Filtered Data

This section presents simulated results with the filtered data. The filtered data is obtained after applying the filtering criteria given in section 6.3 on all the collected data. It was found that there are not enough valid data points available for the first step of curtailment strategy i.e. when $1200kW < SMV6 \leq 1500kW$. Filtering criteria (minimum of 10 points in each bin) given in section 6.3 are not met for this part of curtailment strategy. Hence results, only for the second step of curtailment strategy are presented. Valid speed bins range from 11m/s to 13m/s as data in only these speeds met the filtering criteria.

The real time filtered data was simulated with the TI-JM using the hard curtailment strategy given in Table 6.1 and results are presented in Figure 6.12. The simulated results in Figure 6.12 can be compared with results given in Table 6.3 as same set of data is used for obtaining these results. Simulations show an increase of 12.5% in SMV5 production in full wakes in the $200° - 210°$ bin as can be observed in Figure 6.12 while the actual increase based on analysis of field data is 11.5% in the same bin as shown in Table 6.3. Simulations resulted in 6% decrease in combined production of SMV5 and SMV6 in the $200° - 210°$ bin, while the actual decrease is 6.4% in the same bin. The overall farm production is decreased by 2.5% in the $200° - 210°$ bin as per

the simulations while the actual decrease is 1.9% in the same bin. Similar patterns can be observed for other wind turbines in different directional bins by comparing the simulation based results in Figure 6.12 and results based on field data given in Table 6.3. This comparison shows that these simulations are in good agreement with the results based on field data.

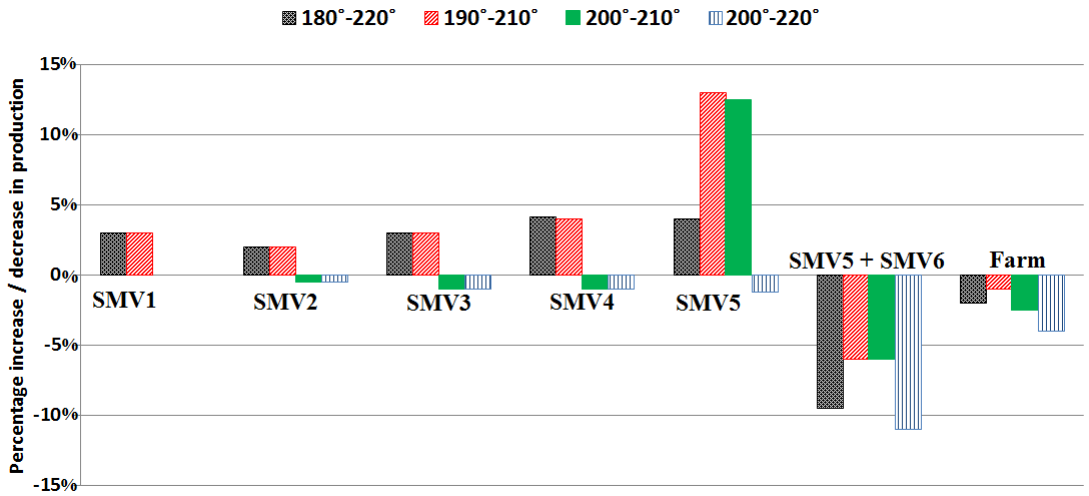

Figure 6.12 Results based on simulating the filtered data with TI-JM

6.4.2 Field Results

Results in this section are based on field data collected in the C_P-based curtailment experiment, filtered as per the criteria defined in section 6.3 as discussed in section 6.4.1.2. These results are plotted with 80% confidence interval represented by the bar on figures in this section. All the analyses in this section are based on the results give in Table 6.3. The SMV6 power curve during the curtailment periods, compared to the normal operations is shown in Figure 6.13.

Impact of the curtailment strategy on downstream turbines and farm power production in each valid data bin is given in Table 6.3. The directional bins $180° - 190°, 190° - 200°$ and $210° - 220°$ are ignored as the number of data points in these bins is not significant (less than 10 points in each bin). When the bin size is increased to $\pm 10°$, number of valid data points are increased meeting the filtering criteria. This results in some overlapped bins as can be seen in Table 6.3, but provides more data for analyses.

SMV6 curtailment in the whole sector ($200° \pm 20°$) on average is 17.5% and in full wakes it is 18.6% as shown in Table 6.3. Average gain, during the experiment,

Table 6.3 Impact of SMV6 hard curtailment on SMV wind farm (% increase/decrease compared to normal operations)

Turbine(s)	$180° - 220°$	$190° - 210°$	$200° - 210°$	$200° - 220°$
SMV6	-17.5	-17.1	-18.6	-19
SMV5	4.5	11.5	11.5	-0.7
SMV4	3.5	4.9	-0.9	-1.5
SMV3	2.0	2.3	-0.3	-0.5
SMV2	1.6	1.9	0.2	0.2
SMV1	2.6	2.7	0.5	0.6
SMV5+SMV6	-8.1	-5.6	-6.4	-10.9
Farm	-0.7	0.4	-1.9	-3.4

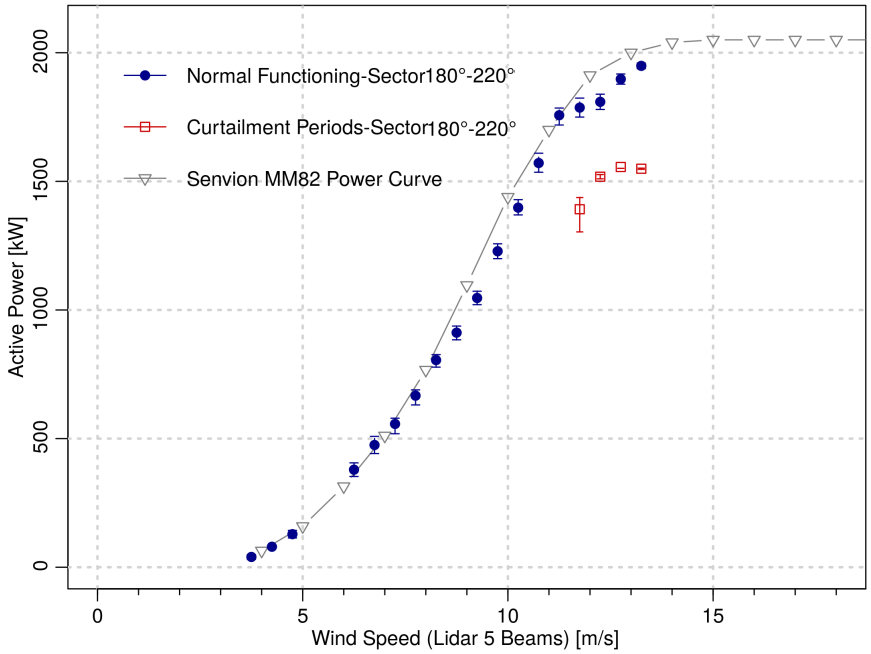

Figure 6.13 SMV6 power curve obtained from field data with 80% confidence interval

in SMV5 production is 4.5%. The highest gain is observed in full wake conditions ($200° - 210°$), which is 11.5%. Power curve of SMV5 during the curtailment period in full wake conditions compared to normal operations is presented in Figure 6.14. The increase in SMV5 production in the valid speed bins confirms positive impact of the hard curtailment strategy. This increase is propagated through the wind farm and increase in production is observed for all the downstream turbines SMV4 - SMV1 as given in Table 6.3.

Combined production of SMV5 and SMV6 during the curtailment experiment is also given in Table 6.3. It should be noted that the combined production of SMV5 and SMV6 is different than simply adding the production of SMV5 and SMV6 given in Table 6.3. The combined production is actually taken from the data, when production of the two turbines (SMV5 and SMV6) is analysed, the number of data points is increased, fulfilling the filtering criteria. When individual production of SMV5 or SMV6 is considered, number of data points is reduced and for some wind speed and direction bins, the filtering criteria was not met as explained earlier. This is the reason that the sum of the values in "SMV5" and "SMV6" is not the same as the value "SMV5 + SMV6" in Table 6.3. Overall, the combined production is decreased by almost 5%. This means that the loss in SMV6 production is not compensated by gain in SMV5 production with the hard curtailment strategy. The lowest decrease in combined production is in full wake conditions ($200° - 210°$) as given in Table 6.3 and Figure 6.15. By definition, SMV6 wake has highest impact on SMV5 production in full-wake conditions. Hence, the benefit of curtailment is also high in this bin. In partial wake conditions, impact of SMV6 is relatively low, hence gain in production is also low.

This loss in combined production is the reason to opt for optimised control strategies. When fully implemented, the optimised control strategies never produce losses in combined production. If the loss in upstream turbine's production is not compensated by gain in downstream turbine's production, the optimised control strategies operate with the standard power curve, moving back to greedy control, avoiding any power loss as discussed in section 6.4.1.

Overall farm production (SMV1 - SMV6) is also reduced by an average of 0.7%, as a result of SMV6 curtailment as given in Table 6.3. The average loss is less than 1% showing that the five downstream turbines (SMV1 - SMV5) have benefited from the 17.5% curtailment of SMV6. The farm power curve in the $200° \pm 20°$ is presented in Figure 6.16 showing the small loss in production, during the curtailment period. This

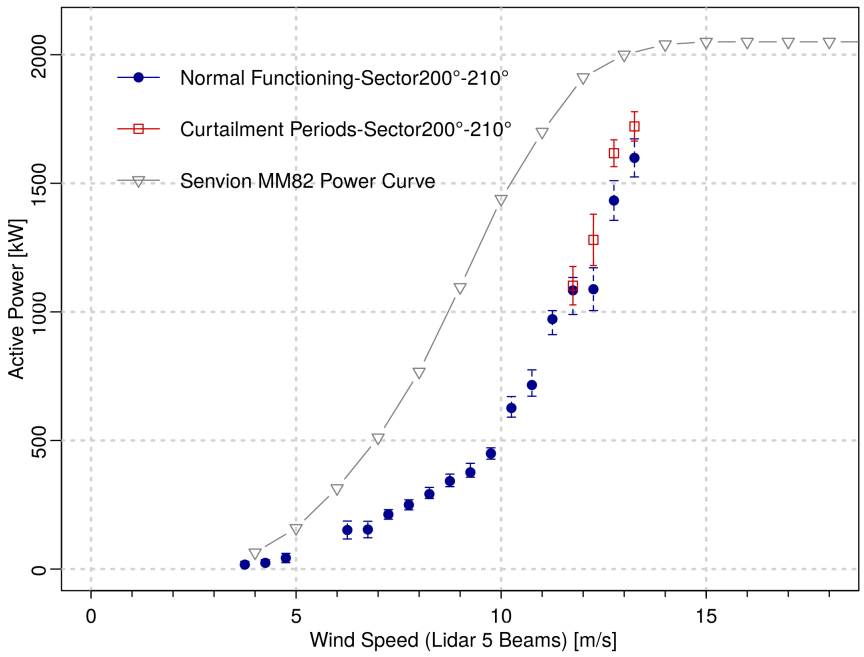

Figure 6.14 Impact of the hard curtailment strategy on SMV5 in full wake conditions (80% confidence interval)

small decrease in overall farm production relative to normal operations suggests that if turbines are curtailed optimally, then overall farm production can be increased.

6.5 Yaw-offsets based Results

This section is based on the results obtained from simulations for designing the yaw-offset based field experiment as given in Table 6.4. Real-time field data is not available due to equipment malfunctioning as discussed in section 6.2.2. The simulations in this section are based on the TI-JM, as WindPRO does not have any mechanism for calculating impact of yaw-offsets on wake-effects [48].

The optimised yaw-offsets with maximum percentage increase in net production for each wind speed bin and 5° direction bin are given in Table 6.4. It is observed that generally higher wind speeds (in below-rated conditions) result in more increase in net production with yaw-based coordinated control. PSO estimated higher yaw-offsets for higher wind speeds as can be observed in Table 6.4 for the $190° - 195°$ bin to $215° - 220°$ bins. In higher wind speeds, a yaw-offset on SMV6 does not affect its production by much but the wake is skewed away considerably with a higher angle from SMV5 increasing its production significantly, hence net production is increased. For example

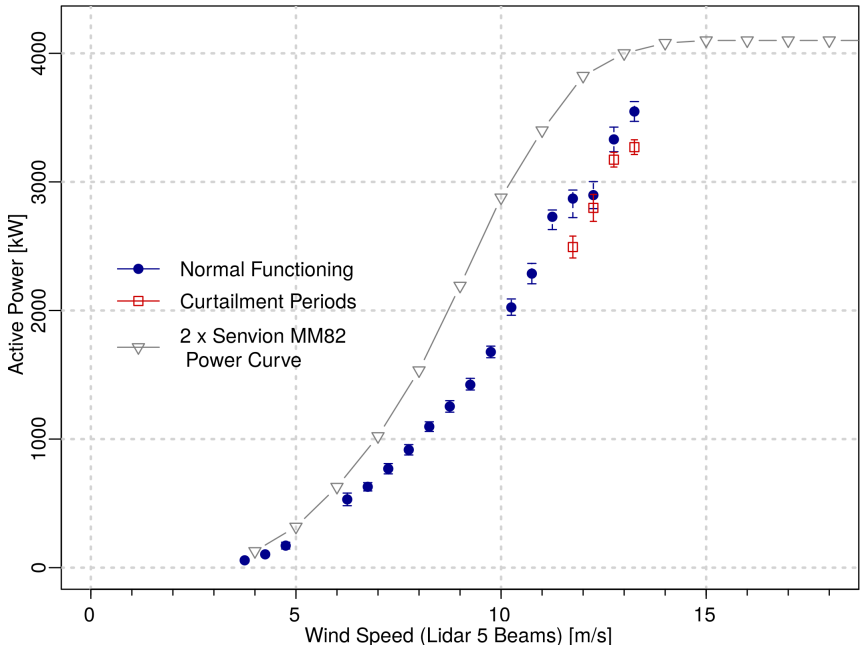

Figure 6.15 Impact of hard curtailment strategy on combined production (SMV5 + SMV6) in full wake conditions (80% confidence interval)

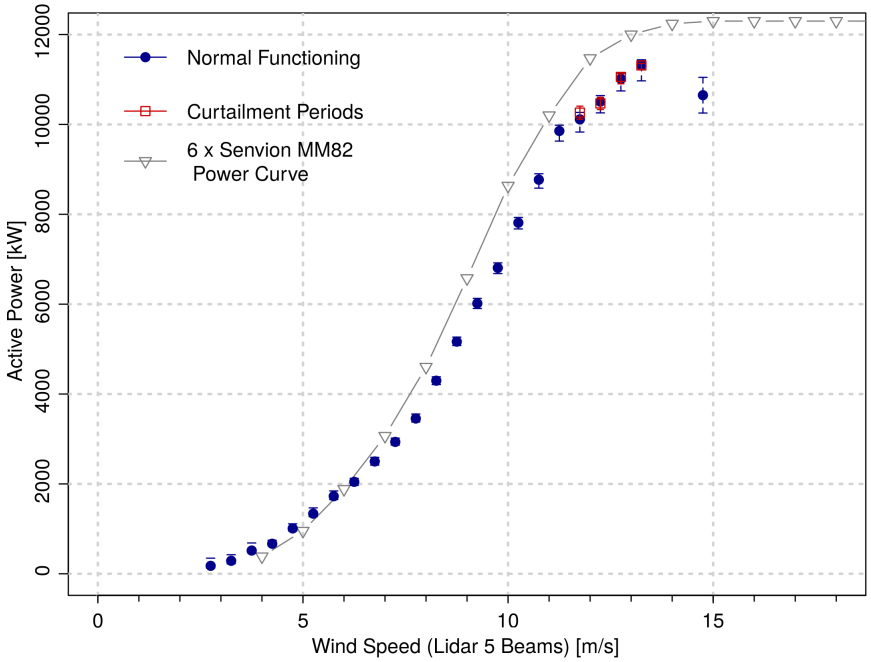

Figure 6.16 Impact of the hard curtailment strategy on overall farm production (SMV1-SMV6) in $200° \pm 20°$ bin (80% confidence interval)

with a yaw-offset of 12° (the maximum in Table 6.4), production of the yawed turbine will be decreased by 0.95 times ($\cos^2(12)$) as was discussed in section 3.1.4. Different powers of "$\cos^2\alpha$" (within a range of 1 to 5) were evaluated as researchers have used different powers for the term "$\cos^2\alpha$" [119] as was discussed in section 3.1.3. It was found that the power of "2" models the field data (SCADA data) more accurately as compared to other powers. Hence, the term "$\cos^2\alpha$" is used in this work for predicting impact of yaw-offsets on power production of a turbine.

It is also observed that as the wind flow moves from partial to full-wake conditions, higher yaw-offsets (up to 12°) are required for skewing the wake away from SMV5. Impact of SMV6 wake is not significant on SMV5 production in partial wake conditions. The decrease in production depends upon how much swept area of SMV5 is affected by SMV6 wake. The impact on production increase as more and more swept area is affected by the wake as wind speed deficit on SMV5 increases. The specific decrease in SMV5 production due to SMV6 wake is dependent upon this wind speed deficit. A smaller yaw-offset (within a range of 1° to 6°, as per Table 6.4) can move the wake away from SMV5 swept area. This smaller yaw-offset does not impact SMV6 production significantly but the partial wake situation for SMV5 is converted into a no-wake or much reduced wake situation. Wake effects are minimal in the $180° - 185°$, SMV5 swept area is not affected by SMV6 wake as the two turbines are not completely in-line in this direction as can be seen in Figure 6.3, hence PSO estimates that the standard operations with greedy control is the best option keeping yaw-offset closer to 0°. The impact of SMV6 on SMV5 production (in standard greedy control) was shown in Figure 6.7 where it can be observed that SMV5 production decrease as the wind direction moves from 180° to 205° and then increases from 206° to 220°. The specific wake losses in production depend upon wind conditions, hence it is difficult to quantify these wake effects. However, as a linear wind deficit model (TI-JM) was used in simulations, it was observed that a maximum of 8% swept area of SMV5 can be affected by SMV6 wake in the $180° - 185°$ bin.

In full wake conditions i.e. $200° - 205°$ and $205° - 210°$, SMV6 wake has significant impact on SMV5 production. A yaw-offset on SMV6 within a range of $[-10°, 15°]$, though reduces its production but also reduces wake effect on SMV5 increasing its production, hence net gain in production is observed. The decrease in SMV5 production depends upon the actual yaw-offset applied, for example a yaw-offset of 15° reduces the production of the yawed turbine by 0.93 times. The impact on SMV5 production depends upon specific wind conditions and parameters such as frequency of wind speed in a specific direction.

It was discussed in section 6.2.2 that the yaw-offset range implemented in field is $[-12°, 8°]$. That is why dynamic (effective) yaw-offsets shall be used as this increases range of the yaw-offsets. This dynamic yaw-offsets can be estimated by adding the yaw-error (unwanted yaw-offset) to the intentional yaw-offset applied on SMV6.

Table 6.4 Estimated optimised yaw offsets in degrees with % increase relative to greedy control in ±2.5° direction bin and ±0.5m/s speed bin

Wind Speed (m/s)	180° – 185°		185° – 190°		190° – 195°		195° – 200°		200° – 205°		205° – 210°		210° – 215°		215° – 220°	
	Yaw offset	% increase	Yaw offset	% increase	Yaw offset	% increase	Yaw offset	% increase	Yaw offset	% increase	Yaw offset	% increase	Yaw offset	% increase	Yaw offset	% increase
5	0	0	-3	1	-6	2.1	***-7***	***5***	-8	1.5	8	2.3	***6***	***5.1***	5	2.1
6	0	0	-3	1	-6	2.7	**-8**	**5**	-9	2.4	10	2	***7***	***5.3***	5	3.3
7	0	0	-3	1	-6	3.7	***-8***	***6.5***	-10	2.1	15	2.5	***7***	***6.4***	5	3
8	0	0	-3	1	-6	3.4	***-8***	***6.5***	-10	1	15	3.1	***11***	***6.4***	5	2.9
9	-1	0.1	-3	1	-6	3.7	***-8***	***6.5***	-10	1	15	3.2	***11***	***6.7***	7	3.1
10	-1	0.2	-3	1	-6	3.5	***-9***	***6.1***	-10	2.3	15	3.3	***11***	***6.7***	7	2.5
11	-1	0.9	-3	1	-8	4	***-9***	***6.6***	-10	4.6	15	5.6	***11***	***6.6***	9	3.6
12	-5	1	-3	1.8	-8	4	**-9**	**6.5**	-10	5.7	15	6	***12***	***6.6***	9	3.8

It is concluded with these simulations that for a two-turbine (SMV6 and SMV5) case, coordinated control based on yaw optimisation results in higher production gain relative to C_P-based coordinated control and greedy control. According to equation

(3.1), the yaw-offset reduces power of SMV6 but as the turbine still operates at its maximum capacity according to the effective wind conditions, turbine's production is only reduced by a factor of $\cos^2\alpha$, where α is the yaw-offset applied.

A yaw-offset in the range of 15° does not have a significant impact on turbine's production but as the skew-angle is greater than the yaw-offset, the wake is skewed away from SMV5. This was discussed in detail in section 3.1.4. The skew angle for 15° yaw-offset is around 18° (equation (3.9)), which means that a partial wake situation can be converted into no-wake situation and a full-wake situation can be converted to a partial-wake situation with optimum yaw-offsets. This produces a positive impact on net production.

6.6 Conclusion

This chapter detailed the field implementation of coordinated control strategies answering RQ-6 by presenting an approach for implementation of coordinated control strategies in an operating wind farm, constraint to the operational limitation. Two turbines (SMV6 and SMV5) in the onshore SMV wind farm were chosen for real-time implementation. The farm and turbines were equipped with modern LiDAR. These LiDAR provided high frequency accurate data about the wind characteristics in the farm.

SMV7 power production was used as a reference for defining a two-step hard curtailment strategy in the directional sector $200° \pm 20°$. The curtailment strategy reduced SMV6 production (using C_P) by a maximum of 20% analysing the wake effect produced on SMV5 and the overall production.

WindPRO predicted 3% increase in SMV5 production with the given hard curtailment strategy in the chosen directional sector. A decrease in combined production of SMV5 and SMV6 is predicted as the loss in SMV6 production is not compensated by gain in SMV5 production. The optimised control strategies were used to estimate optimised power settings of SMV6. Simulations with the farm controller predicted an optimised increase of up to 0.4% in SMV5 production. The farm controller assures no losses in net production.

Data from different sources namely LiDAR, met-mast, SCADA and MERRA database was analysed during the curtailment period. An increase of up to 11.5% was observed on SMV5 production with real time field data. It was observed that increase

in SMV5 production becomes more significant as the partial wake moves towards full wake conditions. The gain in SMV5 production was propagated through the farm as downstream turbines benefited from reduced wake effects. No particular trend was observed with respect to the variations in wind speed.

A decrease in net production of SMV5 and SMV6 and overall farm (SMV1 - SMV6) production was observed with the hard curtailment strategy. This confirms the importance of optimised control strategies. Simulations confirm that if SMV6 power is curtailed with an optimised strategy, the loss in SMV6 production is always compensated by gain in SMV5 production. Off-line optimisation can be a solution. But as observed in the SMV wind farm, atmospheric instability and abrupt changes in wind characteristics requires on-line farm control and optimisation. This can only be achieved with fast and computationally efficient optimised strategies.

The difference between simulations (with filtered data) and field results is within a range of 1.5%. It can be concluded that the simulation (WindPRO and TI-JM) were in good agreement with field results for the bins where field data was available.

The yaw-based coordinated control strategies were also implemented in the SMV wind farm using SMV6 and SMV5. Data cannot be collected due to some technical problems and equipment malfunctioning. WindPRO does not have any mechanism for predicting the impact of yaw-offsets on wake effects. Hence only the TI-JM was used in yaw-offset based simulations. A refined direction bin with a resolution of 5° was used for in-depth analysis. Simulations for each directional and speed bin were performed for obtaining an optimised yaw-offset for SMV6 and results were reported.

The optimum yaw-offsets fall in a range of $[-10°, 15°]$. However the operational limitations only allowed a yaw-offset range of $[-12°, 8°]$. SMV6 was first operated with $-12°$ yaw-offset for almost two weeks and then with 8° yaw-offset for four weeks.

Simulations, using optimum yaw-offsets, concluded that net gain in production increases as wind speed increases (below-rated wind conditions). It was also concluded that higher yaw-offsets are required for increasing net production in full wake conditions.

It is concluded that for a two-turbine case (SMV6 and SMV5); the yaw-based coordinated control can be more beneficial for farm production relative to C_P-based coordinated control and the standard greedy control, in wake affected conditions. According to simulations, if SMV6 is operated with the optimum yaw-offsets according to the wind conditions, net production (SMV6 + SMV5) can be increased by up to 6.7%.

Chapter 7

Conclusions

The main objective of this thesis was to develop intelligent, fast processing and accurate wind farm control strategies, which are easily implementable in the field. A set of six research questions was generated in Chapter 1 showing the aims, for achieving the objective. Each chapter in this thesis answered one or more of these research questions.

This chapter provides the overall conclusion of this thesis in section 7.1. Some future exploration areas are detailed in section 7.2.

7.1 Conclusions

In this thesis, innovative coordinated control strategies for wind farm production maximisation, have been presented. A review of previous research regarding wind farm coordinated control in section 2.4 concluded that the main challenge in the field implementation of coordinated control is the inverse relationship between accuracy and computational efficiency of control strategies based on this concept. The innovative control strategies developed in this work specially emphasises on computational efficiency without compromising accuracy. This has been achieved by answering the research questions given in section 1.3 as follows.

7.1.1 Coordinated Control Concept

RQ-1: What is the state of the art in coordinated control of wind farms? What are the requirements for developing on-line coordinated control strategies?

It was discussed in section 2.4 that optimised curtailment of upstream turbines can be beneficial for overall farm production as downstream turbines have more wind to produce with.

7.1.1.1 Contribution

The literature review in section 2.4 concluded that a farm controller based on the coordinated control concept has a wind deficit model and an optimiser as two integral parts. It was also concluded in section 2.4 that the controller must be computationally efficient and accurate if on-line coordinated control is required.

7.1.2 PSO: The most suitable Optimiser for Coordinated Control

RQ-2: What are the key properties of the optimisation technique that enables on-line coordinate control? Which optimisation technique is the most appropriate for optimising wind farm power production with on-line coordinated control?

It was concluded in section 2.4 that iterative techniques with intrinsic intelligence shall be used for solving the complex problem of coordinated control. It was discussed in section 3.1.1 that researchers have used heuristic optimisation techniques for solving complex non-linear problems.

7.1.2.1 Contribution

Four heuristic optimisation techniques (GA, SA, ACO, PSO) were selected for performance evaluation in section 3.1.1 as a conclusion of a detailed literature review of performance comparison of different optimisation techniques in section 3.1.1. These optimisers are intelligent and solve real time complex problems iteratively exhibiting high processing speed, fulfilling the criteria developed in section 2.4.2. The BF technique was used as a benchmark.

Performance evaluation of the selected optimisers was performed in section 3.8 using an artificial wind farm detailed in section 3.1.2. The evaluation criteria were based upon the processing speed, number of iterations used for solving the problem, the number of overheads used, success rate and accuracy as discussed in section 2.4.2. It was concluded in section 3.8 that PSO outperformed other optimisers in

terms of processing speed, number of iterations and overheads used. A comparison of different PSO neighbourhood topologies in section 3.9.10 confirmed that PSO with the global-best topology (all particles are connected) is the most suitable for wind farm coordinated control. Hence, PSO with global-best topology was used for developing the coordinated control strategies in this work.

7.1.3 Combining Accuracy of CFD Wake Models With Engineering Wake Models

RQ-3: What is the most appropriate wind deficit model for on-line coordinated control which can achieve the required level of accuracy without compromising computational efficiency? How the accuracy of CFD models and computationally efficiency of engineering models can be combined for developing hybrid wind deficit models having positive characteristics of both the models?

It was concluded in section 2.3.1 that the accuracy of CFD wake models shall be combined with the speed of engineering wake models. It was concluded in section 2.5 that the Jensen model is most suitable for wind farm coordinated control because of its processing speed but the parameters must be tuned for accurate wind deficit prediction.

7.1.3.1 Contribution

A wind deficit model (TI-JM) was developed in section 4.3 which uses free-stream and wake added turbulence intensities for estimating the effective value of wake decay coefficient (k_{Jensen}). This information was combined with the standard Jensen model for predicting wind speed deficit inside the wind farm, taking deep array effect and wake added turbulence intensity into account, resulting in fast and accurate wind deficit modelling.

The TI-JM was validated using real-time data from two onshore wind farms (Brazos and SMV) in section 5.2.The TI-JM was also validated by estimating efficiencies of the wind farms case studies using conventional greedy control in section 5.5. It was observed that the efficiencies estimated with TI-JM match well with the efficiencies based on SCADA data. It was concluded in section 5.5 that higher values of wake decay coefficient (k_{Jensen}) must be used inside the wind farm for accurate estimation of wind speed deficit, hence power production.

7.1.4 Evaluating Performance of Wind Farms using Wake Assessment Methodology

RQ-4: What is the most appropriate methodology / strategy for assessing impacts of wakes on farm production and identifying wind conditions where coordinated control can be beneficial for increasing farm production? How can SCADA data from wind farms be used effectively for visualising and analysing wake effects on production?

An assessment methodology for performance evaluation of a wind farm in different wind conditions (using SCADA data) was presented in section 4.4.

7.1.4.1 Contribution

The assessment methodology first calculates production in 360° for a given wind speed or averaging production in all wind speeds. This visualises the impact of wakes on farm production as shown in section 5.3. Wind conditions with severe wake effects were further analysed by calculating relative efficiency comparing performance of different wind turbines in the farm as given in section 5.3.

Data from the Brazos and SMV wind farms was used for comparing performance of turbines installed in a similar layout in section 5.3. This methodology was also applied on two turbines in the SMV wind farm for designing C_P-based and yaw-based coordinated control field experiments in section 6.2.

7.1.5 Implementing Control Strategies according to Wake Conditions

RQ-5: How different control strategies (Conventional greedy, C_P-based or yaw-based) behave in different wind conditions? Which strategy is better for maximising farm production considering full, partial and no-wake conditions?

Efficiencies based on SCADA data from three wind farms case studies (Brazos, SMV, Lillgrund) and WindPRO were used as benchmarks for evaluating the performance of coordinated control strategies (developed in this work) in different wind conditions in section 5.5.

7.1.5.1 Contribution

The coordinated control strategies can improve efficiencies by up to 6% for the wind farms case studies, as discussed in section 5.5. The control process for Lillgrund wind farm consisting of 48 wind turbines took a maximum of 50 seconds indicating the computational efficiency of the farm controller as discussed in section 5.5.3. Wind farm production was increased by up to 8% with the innovative coordinated control strategies as detailed in section 5.5.

It was concluded in section 5.6 that C_P-based control performs better than the yaw-based and greedy control in full or near-full wake conditions. Yaw-based control performs better in partial wake conditions while greedy control is the obvious choice in no-wake conditions.

7.1.6 Implementing the C_P-based control in the SMV Wind Farm

RQ-6: What is the best approach for practical implementation of coordinated control?

The coordinated control strategies were implemented in the SMV wind farm using two turbines setup equipped with modern LiDARs as discussed in Chapter 6. The optimised control strategies cannot be implemented in field due to operational limitations on the turbines as detailed in section 6.2. Therefore other strategies (hard-curtailment) were adopted for field implementation as given in section 6.2. To the best knowledge of the author, this is the first practical implementation of LiDARs based coordinated control strategies in an operating wind farm.

7.1.6.1 Contribution

The C_P-based control strategy was implemented in the SMV wind farm as presented in section 6.2.1. A curtailment of maximum 20% was applied on the upstream turbine (SMV6), in a two-step hard curtailment strategy and the impact on downstream turbine's (SMV5) production and net production was analysed. The aim in this case was not to increase the net production but to analyse the impact on downstream turbine's production.

It was observed in section 6.4.2 with real time field data that a reduction of almost 17% in upstream turbine's production can increase the downstream turbine's production

by almost 11%. The analysis in section 6.4.2 concluded that there is little decrease (less than 2%) in overall farm (SMV1-SMV6) production as a result of the hard curtailment strategy showing that the loss in upstream turbine's production is compensated by increase in downstream turbines' productions. There is significant decrease in the net production of the two experiment turbines (SMV5, SMV6) concluding that upstream turbine must be optimally curtailed for increasing net production as discussed in section 6.6.

7.1.7 Implementing the Yaw-based Control in the SMV Wind Farm

The yaw-based field experiments were also implemented in two steps in August/September 2016 as discussed in section 6.2.2.

7.1.7.1 Contribution

The upstream turbine (SMV6) was operated with a yaw-offset of $-12°$ and $8°$ during the experiment as discussed in section 6.2.2. The optimised yaw-offsets fall mainly in this range as estimated by the yaw-based optimisation strategy as given in Table 6.4.

Simulations in section 6.5 predicted a net increase of up to 7% in net production with the optimised yaw offsets relative to the standard greedy operations as can be seen in Table 6.4.

7.1.8 Thesis Conclusion

To summarise, this research work developed computationally efficient and accurate optimised control strategies for increasing wind farm production. A fast processing and accurate wind deficit model (TI-JM) was developed. PSO with global best neighbourhood topology was chosen as the most suitable optimiser for on-line coordinated control. PSO and the TI-JM were combined for developing C_P-based and yaw-based on-line coordinated control strategies bringing an improvement of up to 6% in wind farm efficiency relative to the standard greedy operations, as was discussed in section 5.5.3.

Coordinated control strategies were implemented in an operating wind farm for the first time using modern LiDARs in the history of wind energy. The analysis on field

data showed decrease in net production with the hard curtailment strategy confirming that fast processing, intelligent and accurate on-line coordinated control strategies must be used for increasing wind farm production. This makes sure that if no net gain can be achieved, then the turbines should operate greedily, resulting in zero production loss.

7.2 Future Work

In the course of this PhD work many new techniques and methodologies have been presented. These can be further developed and extended for achieving other objectives and exploring new research areas. Some of the possible extensions of this research work are presented as follows.

7.2.1 Analysis of Data Obtained from Yaw-based field Implementation

The 5-beam LiDAR contains important information such as the free-stream wind direction and speed as was discussed in section 6.2.2. As soon as the device is operational, data will be collected and analyses will be performed. The theoretical background and methodology for analyses is already completed as was discussed in section 6.5.

The results in Table 6.4 will be validated once the 5-beam LiDAR is operational. The dynamic yaw-offsets will be used for analysing the impact on SMV6, SMV5 and their combined production. This will be used for identifying optimum yaw-offsets using real-time field data suggesting an innovative way to operate a wind farm for increasing net production. This will result in another publication as a result of this PhD work.

7.2.2 Optimising Farm Power Production and Fatigue Loads

The emphasis in this work was on increasing farm production using the available resources efficiently. However, there are cases when the grid-requirement is less than the maximum available farm production, hence some of the turbines must be curtailed to meet the grid requirements. This provides an opportunity for multi-objective optimisation of farm power production and fatigue loads on the turbines. This will

require an objective function where grid-required farm production is used as a constraint while DEL or fatigue loads on different parts such as tower bending moment and blade bending moment are optimised. Reducing DEL or fatigue loads will reduce O&M costs.

7.2.3 Providing Ancillary Services

The control strategies can be extended to manage power flows in the network so maximum and efficient utilisation of wind assets is achieved, indirectly incentivised higher levels of wind integration. The control algorithms can have more than one objective and constraints e.g. fatigue loading in the wind farm and / or voltage, line flow limits and economics constraints of using the network paving the way for active network management. These complex control strategies can help streamline better integration of wind resources into existing networks without the need for grid reinforcement.

7.2.4 Evaluating other Optimisers and Different Coding Environments

Performance of GA, SA, ACO and PSO was evaluated with BF as a benchmark using Matlab®. There are many other optimisation techniques available such as TS, BFO and ABC as discussed in Chapter 3. Performance of these optimisers shall be evaluated for any potential improvement in computational efficiency and accuracy. The impact of coding environment shall be analysed by using environments other than Matlab®.

7.2.5 Data Driven Techniques for Wake Modelling

A generic analytical expression for estimating wake added turbulence intensity was used in Chapter 4 for developing TI-JM. However, performance and accuracy of the TI-JM can be improved using farm-specific expressions obtained with data-driven techniques. If high frequency and accurate data is available (such as data obtained from LiDARs in Chapter 6), it can be used for developing analytical expressions for developing wind deficit models.

7.2.6 Sensitivity analysis of TI-JM

A sensitivity study to the TI-JM model results to varying k_{Jensen} through the wind farm will provide further details and impact of increasing k_{Jensen} inside the wind farm. The sensitivity analysis can be performed using a CFD model such as SOWFA as a benchmark or the wind farm data can also be used for this purpose. Other expressions for determining I_+ shall be used. When a cup anemometer is used, sensitivity analysis shall be performing by assuming I_0 equals to I_u.

References

[1] Steve Sawyer, Klause Rave, and Fatih Birol. Global Wind Report: Annual Market Update. Online, Global Wind Energy Council (GWEC), 2015. Available at: http://www.gwec.net/wp-content/uploads/vip/GWEC-Global-Wind-2015-Report_April-2016_22_04.pdf.

[2] David Griggs, Mark Stafford-Smith, Owen Gaffney, Johan Rockström, Marcus C Öhman, Priya Shyamsundar, Will Steffen, Gisbert Glaser, Norichika Kanie, and Ian Noble. Policy: Sustainable development goals for people and planet. *Nature*, 495(7441):305–307, 2013.

[3] O. Edenhofer, R. Pichs-Madruga, Y. Sokona, E. Farahani, S. Kadner, K. Seyboth, A. Adler, I. Baum, S. Brunner, P. Eickemeier, B. Kriemann, J. Savolainen, S. Schlimer, C. von Stechow, T. Zwickel, and J.C. Minx (eds.). Climate Change 2014: Mitigation of Climate Change, Contribution of Working Group III to the fifth Assessment Report of the Intergovermental Panel on Climate Change. Online 3^{rd} part of the 5^{th} Assessment Report, Intergovernmental Panel on Climate Change (IPCC), Cambridge University Press, Cambridge, United Kingdom and New York, NY, USA, 2014. Available at: https://www.ipcc.ch/report/ar5/wg3/.

[4] G Keith, S Jackson, A Napoleon, T Comings, and J Ramey. The hidden costs of electricity: Comparing the hidden costs of power generation fuels. *Synapse Energy Economics*, 2012.

[5] Graphical flip-chart of nuclear & energy related topics 2014. Online, The Federation of Electric Power Companies of Japan, Keidanren-kaikan, 1-3-2, Otemachi, Chiyoda-ku, Tokyo 100-8118, Japan, 2014. Available at: https://www.fepc.or.jp/english/library/graphical_flip-chart/___icsFiles/afieldfile/2014/07/07/all_english_2014.pdf.

[6] Conti et.al John. International Energy Outlook 2016. Online DOE/EIA-0484(2016), U.S. Energy Information Administration (EIA), Forrestal Building, Washington, DC 20585, May 2016. Available at: https://www.eia.gov/outlooks/ieo/pdf/0484(2016).pdf.

[7] Paul Arwas, David Charlesworth, Duncan Clark, Richard Clay, Gareth Craft, Ian Donaldson, Andy Dunlop, Adrian Fox, Richard Howard, Chris Lloyd, Clare Lovett, Alan Marshall, and Fay Wiles. Offshore wind cost reduction/ pathways study. Online, May 2012. https://www.thecrownestate.co.uk/media/5493/ei-offshore-wind-cost-reduction-pathways-study.pdf.

[8] Ryan Wiser, Joachim Seel, and Bentham Paulos. Cost reductions for offshore wind: Signs of progress, expectations for more. Online (Renewable Energy World), October 2016. Available at: http://www.renewableenergyworld.com/articles/2016/10/cost-reductions-for-offshore-wind-signs-of-progress-expectations-for-more.html.

[9] James A. Dahlberg. Assessment of the Lillgrund windfarm: Power performance. Technical Report 21858-1, Vatenfall, Vindkraft AB, September 2009.

[10] Eilyan Bitar and Pete Seiler. Coordinated control of a wind turbine array for power maximization. In *American Control Conference (ACC)*, pages 2898–2904, 136, 2013. IEEE.

[11] Lucy Y. Pao and Kathryn E. Johnson. A tutorial on the dynamics and control of wind turbines and wind farms. In *American Control Conference, ACC'09*, pages 2076–2089, 172, 2009. IEEE.

[12] Kathryn E. Johnson and Naveen Thomas. Wind farm control: addressing the aerodynamic interaction among wind turbines. In *American Control Conference, ACC'09*, pages 2104–2109, 155, 2009. IEEE.

[13] Maryam Soleimanzadeh, Rafael Wisniewski, and Kathryn Johnson. A distributed optimization framework for wind farms. *Journal of Wind Engineering and Industrial Aerodynamics*, 123:88–98, 2013.

[14] L.E.M. Lignarolo, D. Ragni, C. Krishnaswami, Q. Chen, C.J. Simão Ferreira, and G.J.W. van Bussel. Experimental analysis of the wake of a horizontal-axis wind-turbine model. *Renewable Energy*, 2014.

[15] Charlotte Bay Hasager, Leif Rasmussen, Alfredo Peña, Leo E Jensen, and Pierre-Elouan Réthoré. Wind farm wake: The horns rev photo case. *Energies*, 6(2):696–716, 2013.

[16] Senvion wind energy solutions, Senvion GmbH, Hamburg Germany. *Senvion MM82 [50 Hz/2050 kW] Product Description*. www.senvion.com/global/en/wind-energy-solutions/wind-turbines/mm/mm82/.

[17] Patrick Moriarty, Javier Sanz Rodrigo, Pawel Gancarski, Matthew Chuchfield, Jonathan W Naughton, Kurt S Hansen, Ewan Machefaux, Eoghan Maguire, Francesco Castellani, Ludovico Terzi, et al. IEA-Task 31 WAKEBENCH: Towards a protocol for wind farm flow model evaluation. Part 2: Wind farm wake models. In *Journal of Physics: Conference Series*, volume 524, page 012185. IOP Publishing, 2014.

[18] Natalia Moskalenko, Krzysztof Rudion, and Antje Orths. Study of wake effects for offshore wind farm planning. In *Modern Electric Power Systems (MEPS), Proceedings of the International Symposium*, pages 1–7, 170, 2010. IEEE.

[19] Akshay Ambekar, Venkatarao Ryali, and Awadesh Kumar Tiwari. Methods and systems for optimizing farm-level metrics in a wind farm, December 1 2015. US Patent 9,201,410.

[20] Christian Schram and Parag Vyas. Windpark turbine control system and method for wind condition estimation and performance optimization, November 29 2005. US Patent App. 11/288,081.

[21] Andrew Kusiak and Zhe Song. Design of wind farm layout for maximum wind energy capture. *Renewable Energy*, 35(3):685–694, 2010.

[22] J Serrano González, ÁG González Rodríguez, J Castro Mora, M Burgos Payán, and J Riquelme Santos. Overall design optimization of wind farms. *Renewable Energy*, 36(7):1973–1982, 2011.

[23] Souma Chowdhury, Jie Zhang, Achille Messac, and Luciano Castillo. Unrestricted wind farm layout optimization (UWFLO): Investigating key factors influencing the maximum power generation. *Renewable Energy*, 38(1):16–30, 2012.

[24] Christopher N. Elkinton, James F. Manwell, and Jon G. McGowan. Algorithms for offshore wind farm layout optimization. *Wind Engineering*, 32(1):67–84, 2008.

[25] M.S. Adaramola and P.A Krogstad. Experimental investigation of wake effects on wind turbine performance. *Renewable Energy*, 36(8):2078–2086, 2011.

[26] Barthelmie R., J. and Jensen L., E. Evaluation of wind farm efficiency and wind turbine wakes at the nysted offshore wind farm. *Wind Energy*, 13:573–586, June 2010.

[27] Rebecca Jane Barthelmie, Sten Tronæs Frandsen, Ole Rathmann, Kurt Schaldemose Hansen, E. Politis, J. Prospathopoulos, J.G. Schepers, K. Rados, D. Cabezón, W. Schlez, et al. *Flow and wakes in large wind farms: Final report for UpWind WP8*. Danmarks Tekniske Universitet, Risø Nationallaboratoriet for Bæredygtig Energi, 2011.

[28] B. Sanderse. Aerodynamics of wind turbine wakes. *Energy Research Center of the Netherlands (ECN), ECN-E–09-016, Petten, The Netherlands, Tech. Rep*, 2009.

[29] Tanvir Ahmad, Nicolas Girard, Behzad Kazemtabrizi, and Peter Matthews. Analysis of two onshore wind farms with a dynamic farm controller. In *EWEA, Paris France*, November 2015.

[30] Keith Walker, Neil Adams, Brian Gribben, Breanne Gellatly, Nicolai Gayle Nygaard, Andrew Henderson, Miriam Marchante Jimémez, Sarah Ruth Schmidt, Javier Rodriguez Ruiz, Daniel Paredes, et al. An evaluation of the predictive accuracy of wake effects models for offshore wind farms. *Wind Energy*, 2015.

[31] M. Magnusson and A.S. Smedman. Air flow behind wind turbines. *Journal of Wind Engineering and Industrial Aerodynamics*, 80(1):169–189, 1999.

[32] Maryam Soleimanzadeh. *Wind Farms: Modeling and Control*. PhD thesis, Department of Electronic Systems, Aalborg University, Denmark, 2012.

[33] J. Shu, B.H. Zhang, and Z.Q. Bo. A wind farm coordinated controller for power optimization. In *Power and Energy Society General Meeting, IEEE*, pages 1–8, 184, 2011. IEEE.

[34] J.G. Schepers and S.P. Van der Pijl. Improved modelling of wake aerodynamics and assessment of new farm control strategies. In *Journal of Physics: Conference Series*, volume 75. IOP Publishing, 2007.

[35] Jennifer Annoni, Pieter M.O. Gebraad, Andrew K. Scholbrock, Paul A. Fleming, and Jan-Willem Van Wingerden. Analysis of axial-induction-based wind plant control using an engineering and a high-order wind plant model. *Wind Energy*, 19:1135–1150, 2015.

[36] Sanghyeon Jeon, Bumsuk Kim, and Jongchul Huh. Comparison and verification of wake models in an onshore wind farm considering single wake condition of the 2 MW wind turbine. *Energy*, 93:1769–1777, 2015.

[37] Silvio Marcacci. Clean technica. Online, August 2013. Available at: https://cleantechnica.com/2013/08/05/wind-energy-research-facility-launched-to-boost-wind-farm-output/.

[38] Rebecca Jane Barthelmie, Ole Rathmann, Sten Tronæs Frandsen, K.S. Hansen, E. Politis, J. Prospathopoulos, K. Rados, D. Cabezón, W. Schlez, J. Phillips, et al. Modelling and measurements of wakes in large wind farms. In *Journal of Physics: Conference Series*, volume 75, page 012049. IOP Publishing, 2007.

[39] R.J. Barthelmie, G.C. Larsen, S.T. Frandsen, L. Folkerts, K. Rados, S.C. Pryor, B. Lange, and G. Schepers. Comparison of Wake Model Simulations with Offshore Wind Turbine Wake Profiles Measured by Sodar. *Journal of atmospheric and oceanic technology*, 23(7):888–901, 2006.

[40] M. Gaumond, Pierre-Elouan Réthoré, Andreas Bechmann, Søren Ott, Gunner Chr Larsen, A Peña, and Kurt Schaldemose Hansen. Benchmarking of wind turbine wake models in large offshore wind farms. In *Proceedings of the Science of Making Torque from Wind Conference*, 2012.

[41] Douwe J. Renkema. Validation of wind turbine wake models. Master's thesis, Faculty of Aerospace Engineering, TU Delft, June 2007.

[42] Jungchul Choi and Martin Shan. Advancement of Jensen (Park) wake model. In *Proceedings of the European Wind Energy Conference and Exhibition*, pages 1–8, 2013.

[43] Ola Eriksson, Karl Nilsson, Simon-Philippe Breton, and Stefan Ivanell. Analysis of long distance wakes behind a row of turbines–a parameter study. In *Journal of Physics: Conference Series*, volume 524, page 012152. IOP Publishing, 2014.

[44] A.J. Brand, E.T.G. Bot, and H. Ozdemir. Accurate wind farm development and operation advanced wake modelling. *Presented at: EWEA Offshore*, 19:21, 2013.

[45] Muhammad Ali and J.V. Milanovic. Probabilistic assessment of wind farm energy yield considering wake turbulence and variable turbine availabilities. *17 Power Systems Computation Conference (PSCC'11)*, 2011.

[46] Wind Energy The Facts Growth of Wind TEnergy . online. Available at https://www.wind-energy-the-facts.org/growth-of-wind-turbine-size.html "accessed Monday 6$^{\text{th}}$ November, 2017".

[47] Matthew J. Churchfield, Patrick J. Moriarty, Yujia Hao, Matthew A. Lackner, Rebecca Barthelmie, Julie K. Lundquist, and Gregory S. Oxley. A comparison of the dynamic wake meandering model, large-eddy simulation, and field data at the Egmond aan Zee Offshore wind plant. In *AIAA Science and Technology Forum and Exposition (SciTech 2015)*, 2015.

[48] Nielsen Per, Villadsen Jens, Kobberup Jon, Madsen Per, Jacobsen Thomas, Thørgersen Morten, L., Sørensen Mads, V., Sørensen Thomas, Svenningsen Lasse, Motta Mauricio, and Bredelle Karina. *WindPRO 2.7 User Guide*. EMD International A/S, Aalborg, Denmark, 3rd edition, October 2010.

[49] L.J. Vermeer, Jens Nørkær Sørensen, and A. Crespo. Wind turbine wake aerodynamics. *Progress in aerospace sciences*, 39(6):467–510, 2003.

[50] John F. Ainslie. Calculating the flowfield in the wake of wind turbines. *Journal of Wind Engineering and Industrial Aerodynamics*, 27(1):213–224, 1988.

[51] V.M.M.G. Costa Gomes, José M.L.M. Palma, and A. Silva Lopes. Improving actuator disk wake model. In *Journal of Physics: Conference Series*, volume 524, page 012170. IOP Publishing, 2014.

[52] Maryam Soleimanzadeh, Rafael Wisniewski, and S. Mojtaba Shakeri. Wind deficit model in a wind farm using finite volume method. In *American Control Conference (ACC), 2010*, pages 4343–4348, 189. IEEE.

[53] F. González-Longatt, P. Wall, and V. Terzija. Wake effect in wind farm performance: Steady-state and dynamic behavior. *Renewable Energy*, 39(1):329–338, 2012.

[54] F. Koch, M. Gresch, F. Shewarega, I. Erlich, and U. Bachmann. Consideration of wind farm wake effect in power system dynamic simulation. In *Power Tech, 2005 IEEE Russia*, pages 1–7, 167. IEEE.

[55] Lars Landberg. Wind resources and wakes. Elforsk survey report, 2012.

[56] Jennifer Annoni, Patrick Seiler, Kenneth Johnson, Paul Fleming, and Pieter Gebraad. Evaluating wake models for wind farm control. In *American Control Conference (ACC), 2014*, pages 2517–2523. IEEE, 2014.

[57] Konstantinos Rados, G. Larsen, R. Barthelmie, W. Schlez, B. Lange, G. Schepers, T. Hegberg, and M. Magnisson. Comparison of wake models with data for offshore windfarms. *Wind Engineering*, 25(5):271–280, 2001.

[58] Paulo E Arratia. Viewpoint: Complex fluids at work. *Physics*, 4:9, 2011.

[59] B. Sanderse, S.P. Pijl, and B. Koren. Review of Computational Fluid Dynamics for wind turbine wake aerodynamics. *Wind Energy*, 14(7):799–819, 2011.

[60] Andre Bakker. Introduction to CFD - Applied Computational Fluid Dynamics, 2002. Available at www.bakker.org/dartmouth06/engs150/01-intro.pdf.

[61] D. Kuzmin. Introduction to Computational Fluid Dynamics. *University of Dortmund, Dortmund*, 2003. Available at http://www.mathematik.uni-dortmund.de/ kuzmin/cfdintro/lecture2.pdf.

[62] J. Franke, C. Hirsch, A.G. Jensen, H.W. Krüs, M. Schatzmann, P.S. Westbury, S.D. Miles, J.A. Wisse, and N.G. Wright. Recommendations on the use of CFD in wind engineering. In *Cost action C*, volume 14, page C1, 2004.

[63] Xabier Pedruelo Tapia. Modelling of wind flow over complex terrain using OpenFoam. Master's thesis, Department of Technology and Built Environment, University of Gävle, June 2009.

[64] F. Harms, B. Leitl, M. Schatzmann, and G. Patnaik. Validating LES-based flow and dispersion models. *Journal of Wind Engineering and Industrial Aerodynamics*, 99(4):289–295, 2011.

[65] E Cheng and J Shang. Kinematic flow model based extreme wind simulation. *Journal of Wind Engineering and Industrial Aerodynamics*, 77:1–11, 1998.

[66] Bengtsson Jimmy. Turbulence Wind Flow Modeling in Complex Terrain - A Comparison Between na Linear Model, a CFD Model and a NWP Model. Online, Department of Applied Mechancis, Chalmers University of Technology, 2015. Available at: http://publications.lib.chalmers.se/records/fulltext/219399/219399.pdf.

[67] Philippe Beaucage, N. Robinson, M. Brower, and Chuck Alonge. Overview of six commercial and research wake models for large offshore wind farms. In *Proceedings of the European Wind Energy Association Conference*, pages 95–99, 2012.

[68] Mathias Hoelzer, Michael Hölling, Gerrit Wolken-Möhlmann, Pascal Knebel, Julia Gottschall, Edgar Anahua, Stephan Barth, and Joachim Peinke. Annual Report 2007 - Research Projects (RP). Technical report, ForWind - Center for Wind Energy Research of the Universities of Oldenburg and Hannover, Marie-Curie-StraBe 1, 26129 Oldenburg, Germany, 2007.

[69] Garrad Hassan. *WindFarmer 5.3: Theory Manual*. Garrad Hassan & Partners Ltd. DNV GL - Energy, Bristol, England, April 2014.

[70] M. Avila, A. Folch, Guillaume Houzeaux, Beatriz Eguzkitza, L. Prieto, and D. Cabezón. A Parallel CFD Model for Wind Farms. *Procedia Computer Science*, 18:2157–2166, 2013.

[71] Gretar Tryggvason. Classical turbulence modelling. Online, 2011. Computational Fluid Dynamics Course - University of Notre Dame.

[72] Paul Fleming, Pieter Gebraad, Matt Churchfield, Sang Lee, Kathryn Johnson, John Michalakes, Jan-Willem van Wingerden, and Patrick Moriarty. SOWFA + super controller user's manual. *National Renewable Energy Laboratory, Golden, CO*, 2013.

[73] Paul Fleming, Pieter M.O. Gebraad, Sang Lee, Jan-Willem Wingerden, Kathryn Johnson, Matt Churchfield, John Michalakes, Philippe Spalart, and Patrick Moriarty. Simulation comparison of wake mitigation control strategies for a two-turbine case. *Wind Energy*, 18(12):2135–2143, 2015.

[74] M.J. Churchfield. Review of wind turbine wake models and future directions (presentation). Technical Report NREL/PR-5000-60208, National Renewable Energy Laboratory (NREL), Golden, CO., 2013.

[75] Niels Otto Jensen. A note on wind generator interaction. Technical Report Risø -M-2411, Risø National Laboratory, Roskilde, Denmark, November 1983.

[76] I. Katic, J. Højstrup, and Niels Otto Jensen. A simple model for cluster efficiency. In *European Wind Energy Association Conference and Exhibition*, pages 407–410, 1986.

[77] Gunner Chr Larsen, H. Aagaard, Madsen, and Niels N. Sørensen. Mean wake deficit in the near field. In *European Wind Energy Conference and Exhibition*. European Wind Energy Association (EWEA), 2003.

[78] Sten Frandsen, Rebecca Barthelmie, Sara Pryor, Ole Rathmann, Søren Larsen, Jørgen Højstrup, and Morten Thøgersen. Analytical modelling of wind speed deficit in large offshore wind farms. *Wind energy*, 9(1-2):39–53, 2006.

[79] Tanvir Ahmad, Peter Matthews, and Behzad Kazemtabrizi. PSO based wind farm controller. In *The 11th edition of the International Conference on Evolutionary and Deterministic Methods for Design, Optimization and Control with Applications to Industrial and Societal Problems, EUROGEN-2015 Glasgow, UK*, pages 277–283, September 2015.

[80] Demetrios Zigras and Kai Moennich. Farm efficiencies in large wind farms. In *German Wind Energy Conference*, 2006.

[81] Rabia Shakoor, Mohammad Yusri Hassan, Abdur Raheem, and Yuan-Kang Wu. Wake effect modeling: A review of wind farm layout optimization using Jensen model. *Renewable and Sustainable Energy Reviews*, 58:1048–1059, 2016.

[82] Gunner Chr Larsen. A simple stationary semi-analytical wake model. Technical report, Risø National Laboratory for Sustainable Energy, Technical University of Denmark, 2009.

[83] Gunner Chr Larsen. A simple wake calculation procedure. Technical Report Risø - M - 2760, Department of Meterology and Wind Energy, Risø, Denmark, Risø National Laboratory, DK-4000 Roskilde, Denmark, December 1988.

[84] David Ryan VanLuvanee. Investigation of observed and modeled wake effects at Horns Rev using WindPRO. *Technical University of Denmark Department of Mechanical Engineering*, 2006.

[85] A. Arbaoui N. Charhouni and M. Sallaou. Qualification of three analytical wake models. *S12 Fiabilité et robustesse des systèmes mécaniques*, 2015.

[86] A. J. (Jeroen) Janssen, J. Development of a wind farm power forecast model. Master's thesis, Wind Energy Research Group, Delft University of Technology, March 2012.

[87] R.J. Barthelmie, S.T. Frandsen, K. Hansen, J.G. Schepers, K. Rados, W. Schlez, A. Neubert, L.E. Jensen, and S. Neckelmann. Modelling the impact of wakes on power output at Nysted and Horns Rev. In *European Wind Energy Conference*, 2009.

[88] Wolfgang Schlez and Anja Neubert. New developments in large wind farm modelling. In *Proceedings of the European Wind Energy Association Conference*, 2009.

[89] Søren Juhl Andersen, Jens Nørkær Sørensen, Stefan Ivanell, and Robert Flemming Mikkelsen. Comparison of engineering wake models with CFD simulations. In *Journal of physics: Conference series*, volume 524, page 012161. IOP Publishing, 2014.

[90] Luis M Fernandez, José Ramón Saenz, and Francisco Jurado. Dynamic models of wind farms with fixed speed wind turbines. *Renewable Energy*, 31(8):1203–1230, 2006.

[91] James F Manwell, Jon G McGowan, and Anthony L Rogers. *Wind energy explained: theory, design and application*. John Wiley & Sons, 2010.

[92] Nicholas Sidewell, Tanvir Ahmad, and Peter C. Matthews. Onshore Wind Farm Fast Wake Estimation Method: Critical Analysis of the Jensen Model. In *EWEA, Paris, France*, 2015.

[93] Klaus Vogstad, Vaibhav Bhutoria, John Amund Lund, and Stefan Ivanell. Instant wind model reduction for fast CFD computations. Technical Report 12:72, Elforsk, November 2012.

[94] Maarten Steinbuch, W.W de Boer, O.H. Bosgra, S.A.W.M. Peters, and Jeroen Ploeg. Optimal control of wind power plants. *Journal of Wind Engineering and Industrial Aerodynamics*, 27(1):237–246, 1988.

[95] Christopher John Spruce. *Simulation and control of windfarms*. PhD thesis, University of Oxford, 1993.

[96] G.P. Corten, P Schaak, and E.T.G. Bot. More power and less loads in wind farms: Heat and Flux. In *European Wind Energy Conference & Exhibition, London, UK*, 2004.

[97] L.A.H. Machielse, S Barth, E.T.G. Bot, H.B. Hendriks, and G.J. Schepers. Evaluation of (Heat and Flux) farm control. Technical Report ECN-E–07-105, ECN, Petten, The Netherlands, 2007.

[98] K. Boorsma. Heat and flux. analysis of field measurements. Technical Report ECN-E–12-048, ECN, Petten, The Netherlands, November 2012.

[99] S.K. Kanev and F.J. Savenije. Active Wake Control: loads trends. Technical Report ECN-E–15-004, ECN, Petten, The Netherlands, January 2015.

[100] J.W. Wagenaar, L.A.H. Machielse, and J.G. Schepers. Controlling wind in ECN scaled wind farm. *Proc. Europe Premier Wind Energy Event*, pages 685–694, April 2012.

[101] K. Boorsma. Power and loads for wind turbines in yawed conditions. Technical report, ECN-E-12-047, ECN, Petten, The Netherlands, 2012.

[102] Dogukan Kucuksahin and E.T.G. Bot. Heat and flux configurations on offshore wind farms. In *Journal of Physics: Conference Series*, volume 555, page 012061. IOP Publishing, 2014.

[103] Maryam Soleimanzadeh, Arno J. Brand, and Rafael Wisniewski. A wind farm controller for load and power optimization in a farm. In *Computer-Aided Control System Design (CACSD), 2011 IEEE International Symposium on*, pages 1202–1207, 186. IEEE.

[104] Maryam Soleimanzadeh and Rafael Wisniewski. Controller design for a wind farm, considering both power and load aspects. *Mechatronics*, 21(4):720–727, 2011.

[105] Maryam Soleimanzadeh, Rafael Wisniewski, and Stoyan Kanev. An optimization framework for load and power distribution in wind farms. *Journal of Wind Engineering and Industrial Aerodynamics*, 107:256–262, 2012.

[106] Peter Fogh Odgaard, M. Baekgaard, and Brian Astrup. Model based control of wind parks. In *EWEC Conference*, 2010.

[107] Vedrana Spudic, M Jelavic, M Baotic, and Nedjeljko Peric. Hierarchical wind farm control for power/load optimization. *The Science of making Torque from Wind (Torque2010)*, 2010.

[108] Vedrana Spudic, Mato Baotic, and Nedjeljko Peric. Wind farm load reduction via parametric programming based controller design. In *Proceedings of the 18th IFAC World Congress*, 2011.

[109] Vedrana Spudić, Mate Jelavić, and Mato Baotić. Wind turbine power references in coordinated control of wind farms. *Automatika–Journal for Control, Measurement, Electronics, Computing and Communications*, 52(2), 2011.

[110] Kathryn Johnson and Geraldine Fritsch. Assessment of extremum seeking control for wind farm energy production. *Wind Engineering*, 36(6):701–716, 2012.

[111] Jason R. Marden, Shalom D. Ruben, and Lucy Y. Pao. A model-free approach to wind farm control using game theoretic methods. *IEEE Transactions on Control Systems Technology*, 21(4):1207–1214, 2013.

[112] Jason R. Marden, Shalom D. Ruben, and Lucy Y. Pao. Surveying game theoretic approaches for wind farm optimization. In *Proceedings of the AIAA aerospace sciences meeting*, pages 1–10, 2012.

[113] Jinkyoo Park, Soonduck Kwon, and Kincho H. Law. Wind farm power maximization based on a cooperative static game approach. In *SPIE Smart Structures and Materials+ Nondestructive Evaluation and Health Monitoring*, pages 86880R–86880R. International Society for Optics and Photonics, 2013.

[114] P. Fleming, P. Gebraad, S. Lee, J.W. van Wingerden, K. Johnson, M. Churchfield, J. Michalakes, P. Spalart, and P. Moriarty. High-fidelity simulation comparison of wake mitigation control strategies for a two-turbine case. In *Proceedings of ICOWES Conference*, 2013.

[115] Paul A. Fleming, Pieter M.O. Gebraad, Sang Lee, Jan-Willem van Wingerden, Kathryn Johnson, Matt Churchfield, John Michalakes, Philippe Spalart, and Patrick Moriarty. Evaluating techniques for redirecting turbine wakes using SOWFA. *Renewable Energy*, 70:211–218, 2014.

[116] P.M.O. Gebraad, F.W. Teeuwisse, J.W. Wingerden, P.A. Fleming, S.D. Ruben, J.R. Marden, and L.Y. Pao. Wind plant power optimization through yaw control using a parametric model for wake effects: a CFD simulation study. *Wind Energy*, 19(1):95–114, 2016.

[117] Javier Serrano González, Manuel Burgos Payán, Jesús Riquelme Santos, and Ángel Gaspar González Rodríguez. Maximizing the overall production of wind farms by setting the individual operating point of wind turbines. *Renewable Energy*, 80:219–229, 2015.

[118] Flavio Heer, Peyman Mohajerin Esfahani, Maryam Kamgarpour, and John Lygeros. Model based power optimisation of wind farms. In *Control Conference (ECC), 2014 European*, pages 1145–1150. IEEE, 2014.

[119] Torben Knudsen, Thomas Bak, and Mikael Svenstrup. Survey of wind farm control power and fatigue optimization. *Wind Energy*, 2014.

[120] P.M.O. Gebraad and J.W. Wingerden. Maximum power-point tracking control for wind farms. *Wind Energy*, 18(3):429–447, 2015.

[121] Tomislav Horvat, Vedrana Spudić, and Mato Baotić. Quasi-stationary optimal control for wind farm with closely spaced turbines. In *MIPRO, 2012 Proceedings of the 35th International Convention*, pages 829–834. IEEE, 2012.

[122] Félix Avia Aranda. Wind farm control methods, IEA R&D wind task 11 - topical expert meeting. Technical report, International Energy Agency, November 2012.

[123] Rebecca Jane Barthelmie, SC Pryor, Sten Frandsen, and Søren Ejling Larsen. Analytical modelling of large wind farm clusters. In *Proceedings special topic conference: The science of making torque from Wind, Delft (NL)*, pages 292–303, 2004.

[124] Mathworks. Matlab global optimization toolbox user's guide (r2015b). User's guide, Mathworks, The MathWorks, Inc. 3 Apple Hill Drive, Natick, MA 01760-2098, 2015. Available at http://www.mathworks.com/help/pdf_doc/gads/gads_tb.pdf.

[125] Emad Elbeltagi, Tarek Hegazy, and Donald Grierson. Comparison among five evolutionary-based optimization algorithms. *Advanced engineering informatics*, 19(1):43–53, 2005.

[126] Dutta Chowdhury Debirupa Hore. Review: An analysis of different population based optimization techniques used for optimum allocation and sizing of distributed generations in distributed network. *International Journal of Advanced Research in Electrical, Electronics and Instrumentation Engineering*, 2(5):12, 2013.

[127] Jong-Bae Park, Ki-Song Lee, Joong-Rin Shin, and Kwang Y Lee. A particle swarm optimization for economic dispatch with nonsmooth cost functions. *Power Systems, IEEE Transactions on*, 20(1):34–42, 2005.

[128] Voratas Kachitvichyanukul. Comparison of Three Evolutionary Algorithms: GA, PSO, and DE. *Industrial Engineering and Management Systems*, 11:215–223, 2012.

[129] S.A. Ethni, B. Zahawi, D. Giaouris, and P.P. Acarnley. Comparison of particle swarm and simulated annealing algorithms for induction motor fault identification. In *Industrial Informatics, 2009. INDIN 2009. 7th IEEE International Conference on*, pages 470–474, 148. IEEE.

[130] C. Alabas, F. Altiparmak, and Berna Dengiz. A comparison of the performance of artificial intelligence techniques for optimizing the number of kanbans. *Journal of the Operational Research Society*, 53(8):907–914, 2002.

[131] James Kennedy and William M. Spears. Matching algorithms to problems: an experimental test of the particle swarm and some genetic algorithms on the multimodal problem generator. In *Proceedings of the IEEE international conference on evolutionary computation*, pages 78–83. Citeseer, 1998.

[132] David B. Fogel. The Advantages of Evolutionary Computation. In *BCEC*, pages 1–11. Citeseer, 1997.

[133] Arora Toolika and Gigras Yogita. A survey of comparison between various meta-heuristic techniques for path planning problem. *International Journal of Computer Engineering & Science*, 3(2):62–66, November 2013.

[134] Meenakshi. Comparative analysis of ant colony optimization problem with tabu search. *International Journal of Enhanced Research in Science, Technology & Engineering*, 5(1):127–132, January 2016.

[135] Boussaïd Ilhem, Lepagnot Julien, and Siarry Patrick. A survey on optimization metaheuristics. *Information Sciences*, 237:82–117, July 2013.

[136] Peter J. Fleming and R.C. Purshouse. Genetic algorithms in control systems engineering. Research Report 789, Department of Automatic Control and Systems Engineering, University of Sheffield, Sheffield, S1 3JD, UK, May 2001. Available at http://eprints.whiterose.ac.uk/83979/.

[137] Jason Mark Jonkman, Sandy Butterfield, Walter Musial, and George Scott. *Definition of a 5-MW reference wind turbine for offshore system development*. National Renewable Energy Laboratory Golden, CO, 2009.

[138] Olivier Coupiac. Four vertical extrapolation methods. *WindTech International*, 12(2):5–8, March 2016.

[139] Walid Husien, Wedad El-Osta, and Elhadi Dekam. Effect of the wake behind wind rotor on optimum energy output of wind farms. *Renewable Energy*, 49:128–132, 2013.

[140] G.P. Corten and P. Schaak. Heat and flux: Increase of wind farm production by reduction of the axial induction. In *Proceedings of the European Wind Energy Conference*, 2003.

[141] Whei-Min Lin and Chih-Ming Hong. Intelligent approach to maximum power point tracking control strategy for variable-speed wind turbine generation system. *Energy*, 35(6):2440–2447, 2010.

[142] Ueda Yoshinori, Itaka Hidehiko, and Inoue Kosuke. *Mitsubishi new wind turbines, MWT-1000 A and MWT-S 2000*. Mitsubishi Heavy Industries, Ltd., vol. 40 No. 4 edition, August 2003.

[143] J. Bueno Gayo. Reliawind project final report. Technical Report Project Nr 212966, Gamesa Innovation and Technology, 2011.

[144] J Sanz Rodrigo and P Gankarski. WAKEBENCH: Benchmarking of Flow Models for Wind Applications. online, 2014. Summary available at https://www.ieawind.org/summary_page_31.html.

[145] Scott M. Thede. An introduction to genetic algorithms. *Journal of Computing Sciences in Colleges*, 20(1):115–123, 2004.

[146] Melanie Mitchell. *An introduction to genetic algorithms*. MIT press, 1998. Available at https://svn-d1.mpi-inf.mpg.de/AG1/MultiCoreLab/papers/ebook-fuzzy-mitchell-99.pdf.

[147] A.J. Chipperfield and P.J. Fleming. The matlab genetic algorithm toolbox. In *Applied control techniques using MATLAB, IEE Colloquium on*, pages 10–1. IET, 1995.

[148] Abdullah Konak, David W. Coit, and Alice E. Smith. Multi-objective optimization using genetic algorithms: A tutorial. *Reliability Engineering & System Safety*, 91(9):992–1007, 2006.

[149] Scott Kirkpatrick. Optimization by simulated annealing: Quantitative studies. *Journal of statistical physics*, 34(5-6):975–986, 1984.

[150] Stephen P. Brooks and Byron J.T. Morgan. Optimization using simulated annealing. *The Statistician*, pages 241–257, 1995.

[151] Darrall Henderson, Sheldon H. Jacobson, and Alan W. Johnson. The theory and practice of simulated annealing. In *Handbook of metaheuristics*, pages 287–319. Springer, 2003.

[152] Marco Dorigo. *Optimization, learning and natural algorithms*. PhD thesis, Politecnico di Milano, 1992.

[153] Marco Dorigo and Luca Maria Gambardella. Ant colony system: a cooperative learning approach to the traveling salesman problem. *Evolutionary Computation, IEEE Transactions on*, 1(1):53–66, 1997.

[154] Marco Dorigo and Thomas Stützle. *Ant colony optimization: overview and recent advances*, pages 227–263. Springer, 2010.

[155] Christian Blum. Ant colony optimization: Introduction and recent trends. *Physics of Life reviews*, 2(4):353–373, 2005.

[156] M Duran Toksari. A hybrid algorithm of Ant Colony Optimization (ACO) and Iterated Local Search (ILS) for estimating electricity domestic consumption: Case of Turkey. *International Journal of Electrical Power & Energy Systems*, 78:776–782, 2016.

[157] Daniel Merkle and Martin Middendorf. *Swarm intelligence*, pages 401–435. Springer, 2005.

[158] . Tavares Neto R, .F and Filho M., Godinho. Literature reviewregardingantcolonyoptimizationappliedtoscheduling problems: Guidelinesforimplementationanddirectionsforfutureresearch. *Engineering ApplicationsofArtificialIntelligence*, 26:150–161, 2013.

[159] James Kennedy and Russell Eberhart. Particle swarm optimization. In *Proceedings of IEEE international conference on neural networks*, volume 4, pages 1942–1948, 162, 1995. Perth, Australia.

[160] Russell C Eberhart and Yuhui Shi. Particle swarm optimization: developments, applications and resources. In *evolutionary computation, 2001. Proceedings of the 2001 Congress on*, volume 1, pages 81–86. IEEE, 2001.

[161] Yuhui Shi. Particle swarm optimization. *IEEE Connections*, 2(1):8–13, 2004.

[162] Riccardo Poli, James Kennedy, and Tim Blackwell. Particle swarm optimization. *Swarm intelligence*, 1(1):33–57, 2007.

[163] Qinghai Bai. Analysis of particle swarm optimization algorithm. *Computer & Information Science*, 3(1), 2010.

[164] Yuhui Shi and Russell C Eberhart. Empirical study of particle swarm optimization. In *Evolutionary Computation, 1999. CEC 99. Proceedings of the 1999 Congress on*, volume 3, 183. IEEE.

[165] Yamille Del Valle, Ganesh K Venayagamoorthy, Salman Mohagheghi, J-C Hernandez, and Ronald G Harley. Particle swarm optimization: basic concepts, variants and applications in power systems. *Evolutionary Computation, IEEE Transactions on*, 12(2):171–195, 2008.

[166] Dian Palupi Rini, Siti Mariyam Shamsuddin, and Siti Sophiyati Yuhaniz. Particle swarm optimization: technique, system and challenges. *International Journal of Computer Applications*, 14(1):19–26, 2011.

[167] Margarita Reyes-Sierra and C.A. Coello Coello. Multi-objective particle swarm optimizers: A survey of the state-of-the-art. *International journal of computational intelligence research*, 2(3):287–308, 2006.

[168] Jin S. Heo, Kwang Y. Lee, and Raul Garduno-Ramirez. Multiobjective control of power plants using particle swarm optimization techniques. *Energy Conversion, IEEE Transactions on*, 21(2):552–561, 2006.

[169] James Kennedy. Small worlds and mega-minds: effects of neighborhood topology on particle swarm performance. In *Evolutionary Computation, 1999. CEC 99. Proceedings of the 1999 Congress on*, volume 3, 161. IEEE.

[170] James Kennedy and Rui Mendes. Population structure and particle swarm performance. *Evolutionary Computation (IEEE)*, May 2002. Available at http://repositorium.sdum.uminho.pt/bitstream/1822/2291/1/wcci2002.pdf.

[171] Reyes Medina Angelina, Jane, Pulido Gregorio, Toscano, and Rai'rez Torres Jose', Gabriel. A comparative study of neighborhood topologies for particle swarm optimizers. In *IJCCI - International Joint Conference on Computational Intelligence*, pages 152 – 159, 2009.

[172] Tanvir Ahmad. Coordinated control of wind turbines in a wind farm, July 2014. 1st Year PhD Progress Report.

[173] M.L. Thørgersen, T. Sørensen, P. Nielsen, A. Grötzner, and S. Chun. *WindPRO/PARK: Introduction to wind turbine wake modelling and wake generated turbulence*. EMD International A/S, Niels Jernesvej 10, 9220 Aalborg, 2005. Available at: http://www.emd.dk/files/windpro/manuals/for_print/Appendices-all_UK.pdf.

[174] Sonia Wharton and Julie K Lundquist. Assessing atmospheric stability and its impacts on rotor-disk wind characteristics at an onshore wind farm. *Wind Energy*, 15(4):525–546, 2012.

[175] Olivier Texier, Tristan CLARENC, Céline BEZAULT, Nicolas GIRARD, and Johan DEGELDER. Integration of atmospheric stability in wind power assessment through cfd modeling. *Proc. EWEC 2010 (Warsaw, Poland, 20-23 April 2010)*, 2010.

[176] Jennifer F Newman and Petra M Klein. The impacts of atmospheric stability on the accuracy of wind speed extrapolation methods. *Resources*, 3(1):81–105, 2014.

[177] Tanvir Ahmad, Peter Matthews, and Behzad Kazemtabrizi. Wake flow model for wind farm control. In *10th PhD Seminar on Wind Energy in Europe*, October 2014.

[178] Tony Burton, David Sharpe, Nick Jenkins, and Ervin Bossanyi. *Wind energy handbook*. John Wiley & Sons, 2001.

[179] Angel G. Gonzalez-Rodriguez, Manuel Burgos-Payan, Jesus Riquelme-Santos, and Javier Serrano-Gonzalez. Reducing computational effort in the calculation of annual energy produced in wind farms. *Renewable and Sustainable Energy Reviews*, 43:656–665, 2015.

[180] Tanvir Ahmad, Peter C. Matthews, Behzad Kazemtabrizi, and Olivier Coupiac. Intelligent and fast proprocess wind farm controller for production maximisation. *Journal of Renewable Energy*, 2016. under review.

[181] S. Aubrun, D. Averbuch, S. Baleriola, C. Braud, M. Boquet, O. Coupiac, N. Girard P. Devinant, F. Guillemin, E. Guilmineau, A. Leroy, D. Nelson-Grüel, D. Peaucelle, and A. Petit. SMARTEOLE Deliverable D1-1: Installation Protocol and test plans for field test 1 and wind tunnel test 1 and 2. Technical Report ANR Project no 14-CE05-0034, Maïa Eolis, Univ. Orléans, INSA-CVL, PRISME EA4229, IFPEN, LEOSPHERE, École Centrale de Nantes, LHEEA UMR CNRS 6598, LAAS-CNRS, September 2016. Confidential.

[182] Joakim Jeppsson, Poul Erik Larsen, and Å. Larsson. Technical description Lillgrund wind power plant. Technical Report 21858-1, Vattenfall, Vindkraft AB, September 2008.

[183] Michele M Rienecker, Max J Suarez, Ronald Gelaro, Ricardo Todling, Julio Bacmeister, Emily Liu, Michael G Bosilovich, Siegfried D Schubert, Lawrence Takacs, Gi-Kong Kim, et al. MERRA: NASA's modern-era retrospective analysis for research and applications. *Journal of Climate*, 24(14):3624–3648, 2011.

[184] M. Gaumond, Pierre-Elouan Réthoré, Andreas Bechmann, Søren Ott, Gunner Chr Larsen, Alfredo Pena Diaz, and K.S. Kurt. D1. 3 benchmark report on wake models at the wind farm scale. Technical report, EERA DTOC, 2013.

[185] EUROGEOSURVEYS - (EGS). online. http://www.eurogeosurveys.org/about-us/mission-and-vision/ "accessed Monday 6$^{\text{th}}$ November, 2017".

[186] U.S. Geological Survey. online. https://www.usgs.gov/ "accessed Monday 6$^{\text{th}}$ November, 2017".

[187] Google earth. http://www.google.com/earth/ accessed Monday 6$^{\text{th}}$ November, 2017.

[188] Ankit Rohatgi. Webplotdigitizer. online. http://arohatgi.info/WebPlotDigitizer/ Accessed Monday 6$^{\text{th}}$ November, 2017.

[189] Andrew Karl Scholbrock. *Optimizing wind farm control strategies to minimize wake loss effects*. PhD thesis, UNIVERSITY OF COLORADO AT BOULDER, 2011.

[190] J.G. Schepers, T.S. Obdam, and J. Prospathopoulos. Analysis of wake measurements from the ECN wind turbine Test Site Wieringermeer, EWTW. *Wind Energy*, 15(4):575–591, 2012.

[191] Tanvir Ahmad, Olivier Coupiac, Arthur Petit, Sophie Guignard, Nicolas Girard, Behzad Kazemtabrizi, and Peter C. Matthews. Field Implementation and Investigation of Coordinated Control of Wind Farms. *IEEE Transactions on Sustainable Energy*, 2016. under review.

Appendix A

The environmental impact and hidden costs of energy generating sources

This appendix presents a detailed description of Table 1.1 showing the environmental impact and hidden costs of different energy sources. This appendix is mainly based on the details given in [4]. The planning and cost risks are presented in section A.1. This is followed by climate change impact in section A.2. Details of energy sources on air pollution are give in section A.3. The land, water and visual and noise impacts are presented in sections A.4, A.5 and A.6 respectively.

A.1 Planning and Cost Risks

This section presents the planning and cost risks of generating power from different energy sources. The owner's costs are used as a proxy for up-front costs. These costs include: development costs; preliminary feasibility and engineering studies; environmental studies and permitting; legal fees; project management; interconnection costs; owner's contingency; and insurance and taxes during construction.

The overall planning and cost risks of biomass are moderate. The lead time for new units is typically 3 to 4 years. Up-front costs are in the range of $650 per kW, putting significant money at risk in the event of project cancellation. Fuel cost risk is

usually significant; this risk is sometimes shifted to customers via a fuel adjustment mechanism.

The overall planning and cost risks of coal projects are high. The lead time for new projects is 5 to 8 years. This increases planning risks relative to the plants that can be developed more rapidly. Cost overruns of 50% to 100% have been common in recent years. Up-front costs are in the range of $430 to $530. Utilities are often allowed to begin charging customers for new units before the units are completed, increasing the cost of energy for consumers.

The overall planning and cost risks for nuclear are high. New projects have 6 to 10+ years lead time, creating very high planning risk. Up-front costs are around $960 per kW, prompting significant losses in the event of project cancellation. Cost overruns are often passed on to ratepayers, and utilities are allowed to begin charging customers for new units before the units are completed.

The overall planning and cost risks for natural gas projects are moderate. The lead time of 3 to 4 years for new projects reduces the planning risk. Up-front costs are round $160 per kW. The primary risk of gas-fired units is the risk of rising gas prices.

The overall planning and cost risks for solar are low. The lead time for commercial projects is around 3 to 4 years while for residential projects it is well under a year. There are no fuel cost risk. Estimated upfront costs range from $470 to $650. Most solar projects are being developed by non-utility companies, reducing ratepayer risk.

The overall planning and cost risks for wind are low. The lead time for large projects is typically 3 to 4 years, smaller projects can be developed more rapidly. Up-front costs of onshore projects are very low – roughly $140 per kW – reducing losses in the event of a cancelled project. Up-front costs for offshore projects are high, due to the costs of working at sea. Wind projects impose no fuel cost risk. Most onshore and offshore projects are developed by non-utility companies, reducing ratepayer risk.

A.2 Climate Change Impacts

The climate change impact of biomass is moderate. The direct CO_2 emissions from operation are in the range of 1250 g/kWh. There are additional carbon emissions from fuel harvesting and transportation. It takes between 15 and 40 years for biomass carbon emissions to be equivalent to coal-fired emissions, depending on the biomass fuel type. It takes longer to reach carbon payback relative to gas-fired generation.

The climate change impacts for power generation with coal is high. Analysis found that life-cycle emissions estimates for existing projects range from 880 to 1270 g CO_2-eq/kWh with a mean of 1010 g CO_2-eq/kWh. These emissions depend upon the coal type used for power generation and plant efficiency. For new projects, the life-cycle estimates fall between 730 nd 1010 g CO_2-eq/kWh with a mean of 790 g CO_2-eq/kWh.

The impacts of power generation through nuclear power plants on climate is low. Direct emissions from nuclear plan operation are low. Major sources of life-cycle emissions are uranium mining, enrichment and transportation, plant construction and decommissioning. It is found with analysis that estimates of life-cycle GHG range from 3.7 to 110 g CO_2-eq/kWh, with a mean of 18 g CO_2-eq/kWh.

The climate change impacts of plants running on natural gas are high. Direct emissions from these plants range between 350 and 400 g/kWh depending on the efficiency of the plant. There are additional GHG emissions from gas drilling, processing and pipeline leakages. The life-cycle GHG emissions are not given.

The impacts of solar projects on climate are low. Direct emissions from plant operations are negligible. Major sources of life-cycle emissions are: extracting and refining resources; and manufacturing PV panels and "balance of system" components. It is estimated that GHG emissions range between 26 and 183 g CO_2-eq/MWh, with a mean of 52 g CO_2-eq/kWh. Life-cycle emissions range between 9 to 55 g CO_2-eq/kWh, with a mean of 23 g CO_2-eq/kWh.

Wind energy projects have low impacts on climate. Direct emissions from wind turbines are negligible. Major sources of life-cycle emissions are: extracting and refining resources; production of steel, concrete and composites; construction of supply factories. The life-cycle GHG emissions range between 3.0 to 45 g CO_2-eq/kWh, with a mean of 15 g CO_2-eq/kWh.

A.3 Air Pollution Impacts

The impacts of biomass on ir pollution are moderate. Biomass power plants emit significant quantities of sulphur and air toxics. There are additional emissions from fuel harvest and transport. These emissions per unit of biomass fuel cannot be quantified with the available data in [4].

Coal has high impacts on air pollution. Coal plants are the largest sources of SO_2, mercury, arsenic, acidic gases and other toxics. Direct emission rates (g/kWh) are in the following ranges:

- SO_2: 0.5 - 14
- Mercury: 1.5×10^{-6} to 3.0×10^{-5}
- HCl: 0.2
- HF: 0.03

Estimated annual damages from the US coal fleet (not including climate change) range from $70 to $190 billion. Coal mining is also associated with serious health problems because of emission of CO and other air toxics.

Nuclear plants have low impacts on air pollution. Direct emissions from operations are low. Major sources of life-cycle emissions are: uranium mining, enrichment and transportation, plant construction and decommissioning. Life-cycle emission rates (g/kWh) are in the following ranges:

- SO_2: 0.03 to 0.04
- HCl: 1.7×10^{-4} to 1.8×10^{-4}
- HF: 4.8×10^{-5} to 5.2×10^{-5}
- Low level emissions of other air pollutants are also reported.

The impact of power generation through gas plants is moderate. These plants emit significant amounts of toxic gases and air pollutants. There are additional emissions from drilling (fugitive emissions from wells and exhaust from diesel equipment) and emissions from gas processing and pipeline operation. Upstream emissions have not been quantified well enough to estimate life-cycle emissions from gas-fired generation.

The impact of solar power plants on air pollution is low. Direct emissions are negligible. The life-cycle air emissions of SO_2 is in the range of 0.05 to 0.2 g/kWh. Quantification of other air pollutants, acidic and toxic gases is not provided.

Wind energy projects have negligible impacts on air pollution. Direct operational emissions are negligible. Major sources of life-cycle emissions are: production of steel, concrete and composites; construction of supply factories. An analysis of wind energy

projects in Europe, including both onshore and offshore projects, produced the following life-cycle emission rates (g/kWh):

- SO_2: 0.03
- HCl: 4.5×10^{-4}
- HF: $2.9 \times 10{-}4$

A.4 Land Impacts

Biomass has moderate impacts on land. The acidic gas emissions contribute to soil acidification. Increased harvest of woody biomass affects soil quality. Biomass combustion produces large amounts of ash. Some ash can be used as a soil amendment; other ash must be landfilled.

Coal has high impacts on land. SO_2 emissions from coal plants are a major source of soil acidification. Impacts from underground mining include land subsidence, underground fires and safety risks at abandoned mines.

Nuclear power plants have high impacts on land. A typical power plant produces between 4.4×10^{-8} and $7.9 \times 10{-}8$ m^3/kWh of radioactive waste, not including spent fuel. Life-cycle production of hazardous waste is between 0.07 and 0.10 g/kWh and other solid waste is 43 g/kWh. High-level waste must be stored securely for thousands of years. Land use and property values are affected around long-term waste storage sites.

The impacts natural gas on land is moderate. Natural gas combustion contribute to soil acidification. Land cleared for drilling reduces and fragments wildlife habitat. Up to 5 acres (20,000 m2) are cleared per well pad, and waste ponds and roads add to occupied land. Drilling adversely impacts other land uses such as farming, ranching, horse breeding and hunting. In some cases domesticated animals have been killed by exposure to toxins.

Solar projects have moderate land impacts. The estimated life-cycle solar projects land use ranges from 0.4 m^2/MWh for roof integrated to 5.5 m^2/MWh for ground-mounted. There is concern about impacts on some threatened species' habitat due to large desert solar projects. Developers have been required to relocate animals.

Wind projects have moderate impacts on land. Wind projects encompass large areas, but most of the land can continue to be used for its prior purpose, typically farming, ranching or wilderness. The life-cycle land use is in the range of 0.002 m^2/MWh. Estimated average bird mortality is between 0.2 and 2 deaths per GWh. At remote sites, roads and towers could affect species sensitive to habitat disruption.

A.5 Water Impacts

Biomass has moderate impacts on water. These plants typically withdraw 500 to 600 gal/MWh and lose most of this to evaporation. Forest biomass does not require irrigation, but its harvest can affect stream water quality.

Coal plants have high impacts on water. The cooling systems withdraw between 20000 and 50000 gal/MWh and lose roughly 300 gal/MWh of this via evaporation. Coal mining degrades surface water quality in many ways; acid mine drainage is the largest source of water pollution. Air emissions from coal plants contribute to the eutrophication of lakes and bays. Liquid effluent from power plants degrades river water quality. Coal waste impoundments pose risks to ground and surface water, and large-scale accidents pose safety and environmental risks.

Nuclear have high impacts on water. The nuclear plants draw between 20000 and 60000 gal/MWh and lose 400 gal/MWh of this via evaporation. Estimated life-cycle water use ranges between 2600 to 6900 gal/MWh. Waste-water production ranges from 6.3 to 7.4 gal/MWh. The major life-cycle water impacts are from uranium mining; groundwater contamination has been documented at a number of old uranium mines, and current mining techniques can leave elevated levels of contaminants in ground water.

Water impacts of natural gas projects are high. Plants withdraw water at a rate of roughly 230 gal/MWh and lose about 180 gal/MWh. Water impacts in the gas fuel cycle are significant but difficult to quantify.

The water impacts of solar projects are negligible. It is estimated that life-cycle water withdrawals of solar projects is between 225 and 520 gal/MWh.

The water impacts of wind energy projects are negligible. Estimates of the life-cycle water withdrawals from wind projects, including both onshore and offshore projects, range from 55 to 85 gal/MWh. Construction of offshore wind projects adversely affects marine life; however the majority of these impacts cease with the end of construction.

A.6 Noise and Visual Impacts

The noise and visual impacts of biomass are moderate. These impacts are commonly cited as problems by groups opposing new projects. Currently these impacts cannot be quantified with the available data. Truck delivery of biomass fuel impacts the surrounding community and may affect property values near a plant.

Coal projects have moderate noise and visual impacts. These impacts are cited as problems by groups opposing new projects. These impacts cannot be quantified with the available data. Coal trains up to two miles long disrupt traffic and deposit coal dust in the communities through which they pass.

Noise and visual and other impacts of nuclear are high. The opposing groups cite new projects as problems in terms of noise and visual impacts. Production of enriched uranium presents nuclear weapons proliferation risk. There is evidence of adverse health effects from depleted uranium used in conventional munitions.

Noise and visual impacts are commonly cited as problems by groups opposing new units. However no quantification can be provided with the available data. These risks can be termed moderate as compared to other energy sources. Unconventional drilling increases heavy truck traffic significantly.

Solar projects have low noise and visual impacts. Solar plants are not often opposed on the basis of these impacts.

Noise and visual impacts of wind energy projects are moderate. These impacts are commonly cited as problems by groups opposing new and existing projects. These impacts cannot be quantified with the available data. Visual impacts are likely to be more significant for onshore wind projects than for offshore, because turbines are tall, usually spread over a large area and cannot often be hidden behind trees. As more and more projects are moving offshore, visual impacts are reducing. With the use of latest technology, noise impacts are also reducing.

Appendix B

Literature Review

This appendix summarises the literature review of performance comparison of different wake models (section 2.3), coordinated control of wind farms (section 2.4) and performance comparison of different optimisation techniques for solving complex problems (section 3.1.1).

Studies regarding performance comparison of different wake models are given in Table B.1. Previous studies regarding coordinated control are presented in Table B.2 discussing the optimisation technique and wind deficit model used for developing the control strategy and conclusion of each study. Studies regarding performance comparison of different optimisation techniques for solving complex problems are presented in Table B.3 discussing the optimiser used for comparison and conclusion of each study.

B.1 Comparison of Wake Models

This section summarises previous studies comparing performances of different wake models in different wind conditions as discussed in section 2.3. The following Table B.1 presents a discussion about the models used for comparison in each study along with the conclusion and corresponding reference(s). A conclusion drawn from these studies is to use engineering models in combination with CFD models for achieving high computational efficiency and accuracy.

Table B.1 Literature review of comparison of different wake models

Wake Models	**Discussion and Conclusion**	**Ref**
CFD models and software discussed in this table: DWM, SOWFA, Wakefarm, Robert Gordon University (RGU)CFD, Fuga, WindFarmer-CFD, Fluent, National Technical University of Athens (NUTA) CFD, Risoe Linearised Flow, Flow, Ainslie, Deep-Array Wake Model (DAWM), WindModeller, ARPS, Risoe CFD and semi-analytical models, Uppsala University analytical mode, RGU $k-\varepsilon$ model, FarmFlow, Eddy viscosity, LES, CRES-Farm, CENER, Actuator Disk using CFD		
Engineering models and software discussed in this table: Jensen, Larsen, Frandsen, Risoe Engineering, WAsP Engineering, WindFarmer-Jensen, FLaP-Jensen, WAsP-Jensen		
Jensen, CFD (general)	Even the most sophisticated CFD models cannot predict the wind deficit accurately. The Jensen model is a better option for wind farm control	[12]
Jensen, Larsen, Frandsen, Eddy viscosity	The Jensen model outperforms other models for single wake conditions. Larsen and eddy viscosity models accurately captures width of the wake	[36]

WAsP, CRES-Farm, WindFarmer, WakeFarm, CENER, NTUA CFD	Engineering models need to be tuned for better results. CFD models generally over-predict wake losses.	[38]
Risoe Engineering, WAsP and analytical model, FLaP, Wakefarm, RGU CFD model	Engineering models can perform as good as CFD models. However the wake decay coefficient in WAsP has to be tuned according to the wind and wake conditions	[39]
Jensen, Larsen, Fuga	All the models predict wake losses accurately within an error margin of 1.5%. Parameters in the Jensen model are tuned to get better results.	[40]
Jensen, Ainslie, FarmFlow	Both Ainslie and FarmFlow (CFD) models have the same reliability higher than the Jensen model	[44]
DWM, LES	Both the models under-predict power losses and over-predict fatigue loads	[47]
Jensen, DWM, Actuator Disk, SOWFA	The Jensen model is the simplest, fastest and most suitable for feedback wind farm control. DWM is not suitable for farm control. Actuator Disk model can be an option but the complexity is high. SOWFA can be used for testing farm control strategies but the computational requirements are extremely high	[56]
Park Jensen, Ainslie, DAWM, Fuga, WindModeller, ARPS	CFD models performs better than the Jensen model. Parameters in the Jensen model have to be tuned for better results.	[67]
Jensen, Ainslie, Larsen	If wake decay coefficient in the Jensen model is tuned, it can perform better than the other two models	[80]

Wakefarm, WindFarmer, WAsP Engineering, NTUA CFD model	Engineering models under-predict wake losses while CFD based models over-predict wake losses	[27]
WAsP, WindFarmer, Risoe Linearised Flow, Wakefarm, Fluent, Flow, NTUA	All the models predicted the efficiency accurately in most of the cases	[87]
Risoe CFD and semi-analytical models, Uppsala University analytical model, WindFarmer, RGU $k-\varepsilon$ model, FLaP, Wakefarm	None of the models predicted wake losses accurately. Further research is necessary for developing better wake models.	[57].
CFD models are relatively accurate but computationally very expensive. Parameters in Engineering models have to be tuned in order to get better and accurate results		[29, 35, 90, 92]
Engineering models can be highly effective if used properly with the right values for parameters. High fidelity and computationally expensive models shall be used to inform and reduce other models.		[74]

B.2 Coordinated Control Strategies

This section summarises previous studies regarding the concept, benefits, and requirements of coordinated control discussed in section 2.4. Table B.2 presents the wind deficit model(s) and optimisation technique(s) used in these studies and a short discussion with conclusion of each study.

The conclusion drawn from these studies is that coordinated control can be beneficial for increasing overall farm production and reducing fatigue loads on the turbines in the farm. Ideally, this type of control shall be performed on-line. This on-line coordinated control requires a fast processing and accurate wind deficit model which provides mean wind deficit in the vicinity of each turbine in the farm and a fast processing, accurate and computationally efficient optimiser. These studies also suggest that the controller shall be designed with intrinsic intelligence and iterative intelligent optimisation techniques shall be used for optimising farm production and/or loads.

Table B.2 Literature Review of Wind Farm Control Strategies

Wind Deficit Model / Method	**Optimisation Technique**	**Discussion and Conclusion**	**Reference**
Park Jensen model	Numerical analysis	Coordinated control of wind farms is better than conventional greedy control in terms of power production	[10]
Model based on discrete time non-linear equations	Numerical Optimisation	The controller should be developed with intelligence or adaptive learning	[12]
CFD models (offline)	Iterative numerical optimisation scheme	Calculations and optimisation shall be done off-line as CFD models are computationally expensive	[19]
Modified version of the Jensen model	PSO	An increase of up to 10% can be achieved in a dense wind farm in certain wind conditions. The controller has high computing efficiency and accuracy	**[29]**

Mosaic-tiles wake model	Non-linear Model Predictive Control (NLMPC)	Coordinated controller can increases energy capture	[33]
FLORIS and SOWFA	Numerical Optimisation	Benefits of cooperative control depends upon wind conditions and farm layout. Engineering models have to be adjusted for coordinated control	[35]
Navier-Stokes equation	Numerical Optimisation	The controller is computationally expensive	[13]
Jensen, DWM, Actuator disk, SOWFA	Not discussed	Tuning parameters in Jensen model can make it most suitable for farm control	[56]
Jensen Park model	PSO, GA, SA, Brute Force	PSO outperforms other optimisers in terms of processing speed and number of trials. An increase of up to 3% is achieved in farm output for the given artificial wind farm	[79]
Axial induction factor	Numerical optimisation	Compensation of aerodynamic interactions is beneficial for farm output maximisation and fatigue loads minimisation	[94]
Jensen model and analytical expressions	Genetic algorithm	Coordinated control can significantly reduce fatigue damage and increasing farm output	[95]
WAKEFARM and axial induction factor	Numerical optimisation	A gain of maximum 2% can be achieved with cooperative control with measurements on the EWTW test wind farm. Yaw-offsets can be used for increasing in farm power production as wake skew angle is larger than the yaw offset angle	[34, 96–102]

Analytical wind speed deficit model	Numerical optimisation	Coordinated control can be beneficial for wind farms but the given control strategy is computationally expensive	[103]
Model based on Navier-Stokes equation	Numerical optimisation	Reduction of structural and dynamic loads can be achieved with the proposed controller	[104, 105]
Park Model	Numerical optimisation	Simulations show a clear potential for improving the wind park generation	[106]
AEOLUS SimWindFarm	Optimisation problem is divided into sub-problems	The controller can reduce structural loads	[107, 108]
Discrete state space model	Numerical optimisation	DELs were reduced up to 8% on the second with turbine in a two turbines array	[109]
Standard and modified Park models	Extremum seeking control	Coordinated control can increase energy capture in low turbulence intensity conditions, but not in high turbulence conditions	[110]
Model free control based on axial induction factor	Game theory	25% increase in efficiency on the simulated wind farms. Some of the assumptions are unrealistic	[111]
Park model	Game theoretic control with multi-agent systems	Coordinated control can increase energy production by up to 10%	[112]
Park wake model and empirical expression	Cooperative static game approach, Steepest descent method	Yaw offset angles using cooperative control strategy can increase farm output	[113]

SOWFA	-	Properly curtailing or yawing the upstream turbine will significantly increase power production of downstream turbine	[114, 115]
FLORIS and SOWFA	Game theoretic approach	CFD simulations show that the increase in farm output and reduction in loads is possible through yaw control	[116]
Park model	Genetic Algorithms	Results are promising for increasing production for below rated wind speeds	[117]
AEOLUS SimWindFarm	Heuristic algorithm (used off-line)	The possible energy gain depends on the wake model and can go up to 7%	[118]
Jensen model	Gradient-based optimisation	Coordinated control can achieve increase in farm output as wake interactions are taken into account	[120]
Empirical models based on experimental results	Numerical optimisation	A gain of up to 2.85% is possible with coordinated control for the given wind farm. High loads on certain turbines are evaded	[121]
Sensors on the wind turbines can be combined with wind deficit models for reducing fatigue loading on the turbines using coordinated control			[20]
Wind tunnel experiments of a two turbine wind farm shows that the power of the downstream turbines can be substantially increased by adjusting the power of the upstream turbines using C_P or yaw			[25]
Survey of wind farm control literature is presented. This work concludes that there is no solid result that shows a reduced fatigue load while following a power reference below the available power			[119]
Some of the important open problems in wind farm control are faster optimisation and wake modelling tools, broad knowledge about turbulence intensity, use of LiDARs, Intelligent farm control and using yaw offsets for farm power maximisation			[122]

B.3 Performance Comparison of Optimisation Techniques

This section summarises previous studies about performance comparison of different optimisation techniques for solving complex problems discussed in 3.1.1. A brief discussion about these studies is presented in Table B.3. This literature review was used for selecting a set of optimisers (BF, GA, SA, ACO and PSO) for evaluation using coordinated control.

Table B.3 Literature review of comparison of different optimisation techniques

Optimisers	**Optimisation Problem**	**Conclusion**	**Ref**
GA, PSO, ACO, MA, SFL	Discrete and continuous complex problems	PSO outperformed other techniques in terms of solution quality, success rate and processing speed for continuous problems. For discrete problems all techniques performed equally well.	[125]
GA, PSO, ABC, CSA, BFO, ACO and Firefly	Optimum power flow and economic dispatch	PSO and BFO performed better than others in terms of speed and solution quality	[126]
GA, TS, MPSO, ANN, numerical methods and evolutionary programming approaches	Economic dispatch	MPSO success rate and speed make it the first choice for solving such complex problems	[127]
GA, PSO and DE	Different discrete and continuous problems	GA are more suitable for discrete problems. PSO and DE are better options for continuous problems.	[128]
PSO and SA	Condition monitoring of induction motors	PSO is suitable for real-time complex problems because of it's success rate and high processing speed.	[129]
GA, SA, ANN and TS	Optimum number of kanbans in JIT	Solution quality is the same for all optimisers. Speed ranking is TS, SA, GA and ANN respectively.	[130]
Modified PSO and several kinds of GA	Binary problems	Modified PSO outperformed GA in solving complex problems	[131]

Appendix C

Implementation of Optimisers in Matlab

This appendix discusses implementation of different optimisers (GA, SA, ACO) and tuning of parameters of these optimisers for achieving best possible results. Details of GA implementation are given in section C.1 which is followed by SA implementation details in section C.2 while details of ACO implementation are given in section C.3.

Different parameters values and functions were evaluated for minimising the value of $f(P_{max}, C_{P(max)}, \alpha_{max})$. This evaluation is performed on a hit and trial basis where each function or value is compared to every other available option for a given parameter. The first priority was to achieve the highest solution quality even at the expense of computational efficiency. If different functions / values of a parameter resulted in the same solution quality, then the option with highest computational efficiency is chosen. If there is no difference in solution quality and computational efficiency for different values of a parameter, the default available in Matlab is used.

C.1 GA Implementation in Matlab Global Optimisation Toolbox

This section provides details of GA implementation in Matlab global optimisation toolbox and that how different functions and parameters were tuned for achieving the best possible results as per the criteria in section 2.4.2. This section is mainly based

on the details provided in [124]. It is mentioned in [124] that the default parameters for each optimiser are the most optimum value for solving complex problems.

Details of all the available functions and parameters along with the evaluation process are presented. Justification for selecting a specific function or parameter's value is provided as a result of this evaluation. These results are summarised in Table C.1.

C.1.1 Population

Size: Population size specifies the number of individuals there are in each generation. Different population sizes were used and evaluated. The default population size for five or fewer variables is 50. The number of variables for optimisation (number of turbines) in the wind farm case study (3.1.2) is six. Different sizes of population ranging between 20 and 100 were evaluated (with a step size of 10). It was found that the population size of 50 performed well in this case as per the criteria in section 2.4.2. A greater population size increases the optimisation time while a lower population size increased the number of iterations and overheads required for optimisation, resulting in increased processing time. Solution quality remained the same for all population sizes.

Initial Scores: This specifies scores for the initial population for GA. Different initial scores were used in order to avoid the local optima, however each time the same results in terms of processing speed and solution quality were achieved. When no initial scores were defined, the GA algorithm (in Matlab) by default computes the scores using the given objective function ($f(P_{max}, C_{P(max)}, \alpha_{max})$ in this case). No initial scores were provided in this case.

Initial Range: This range specifies lower and upper bounds for the population. The range of C_T [0.20 to 0.52] were used which corresponds to the C_P values of [0.189 to 0.45]. These values correspond to the the minimum and maximum C_P for the assumed wind speed (10m/s) as discussed in section 3.1.2.

C.1.2 Selection

The selection function chooses parents for the next generation based on their values. The following options are available and each one was tested for solving the coordinated control problem.

Table C.1 Evaluating the parameters in GA implementation as per the criteria in section 2.4.2

Parameter	**Values / Functions evaluated**	**Selected value / function**	**Reason for selection**
Population	20 to 100 in a step of 10	50	Achieved optimum result with lower overheads with higher processing speed
Selection	Stochastic uniform, Tournament and Roulette functions	Roulette	Solution quality is relatively better
Elite count	1 to 50 in a step of 1	3	Achieves optimum result with highest computational efficiency
Crossover fraction	0 to 1 in an interval of 0.05	0.80	Relatively high processing speed
Mutation	Uniform, Adaptive feasible, Gaussian	Gaussian	In case of no constraints, this function is used.
Crossover	Single point, Two points, Heuristic, Arithmetic, Scattered	Scattered	Scattered is used in case of no constraints.

Stochastic uniform: This function lays out a line in which each parent corresponds to a section of the length of the line proportional to its expectation. The algorithm moves along the line in steps of equal size, one step for each parent. At each step, the algorithm allocates a parent from the section it lands on. The first step is a uniform random number less than the step size.

Tournament Function: This function selects each parent by randomly choosing individuals, the number of which is specified by the tournament size. The best individual is then chosen to be a parent.

Roulette Function: This function selects the area of each segment from a simulated roulette wheel proportional to its expectation. A section is selected randomly with a probability equal to its area. It was found that this function produced better solutions as compared to stochastic uniform and tournament functions and hence was used in this work.

C.1.3 Reproduction

Reproduction determines how the GA creates children at each new generation. The following parameters were tuned for coordinated control of wind farms.

Elite Count: This specifies the guaranteed number of individuals to survive to the next generation. The elite count can be any positive integer less than or equal to the population size. Different values (1 to 50 in a step of 1) of elite count were used; the simulations resulted in the same value of the objective function, however processing speeds were different. The default value available in Matlab for a population size of 50, which is 3, was found to be computationally more efficient and was used in this thesis.

Crossover Fraction: This is a fraction between 0 and 1. This fraction specifies the next generation that crossover produces while the remaining individuals are produced by mutation. Different fractions from 0 to 1 with an interval of 0.05 were evaluated for solving the coordinated control problem. It was found that the default value of 0.80 produced better results (high processing speed for the most optimum (achieved) result) as compared to other values.

C.1.4 Mutation

Small random changes are made in the individuals in the population through mutation functions. Different functions are available for mutation in Matlab and each one was evaluated for maximising farm production. A suitable mutation function ensures that feasible parents give rise to feasible children, where feasibility is with respect to the bounds.

Uniform: Uniform mutation is based on two steps. First, the algorithm selects a fraction of the vector entries of an individual for mutation, where each entry has the same probability as the mutation rate of being mutated. The mutation rate was varied and it was noted that the default rate of 0.01 produces better results in terms of solution quality and processing speed. In the second step, the algorithm replaces each selected entry by a random number selected uniformly from the range for that entry.

Adaptive Feasible: Random directions for mutation are generated adaptive with respect to the last successful or unsuccessful generation. The step length is then chosen along each direction based on the bounds specified.

Gaussian: This mutation function adds a random number to each individual taken from a Gaussian distribution cantered on zero. If there are no constraints then Gaussian mutation shall be used, hence Gaussian was used in this work as there are not constraints. The Scale and Shrink parameters control the standard deviation of this distribution. Standard deviation in the first generation is determined by the Scale parameter while Shrink controls how the standard deviation shrinks as the generation goes by. If Shrink is 0, the standard deviation remains constant. If Shrink is 1, the standard deviation shrinks to 0 linearly as the last generation is reached. A bar given in the toolbox adjusts the Shrink and standard deviation values accordingly. Only the Shrink value needs to be defined and the standard deviation value is adjusted accordingly. A Shrink value of 1 has been used in this study as this produced better solution quality as compared to other Shrink values.

C.1.5 Crossover

Crossover combines two individuals (parents), to form a new individual (child) for the next generation. Different crossover functions available in Matlab were evaluated in this work for solving the coordinated control problem. A brief description of these functions is given as following:

Single Point: The function first selects a random number between 1 and number of variables (six in this case). Then the genes (entries) numbered less than or equal to the randomly selected number are selected from the first parent, while rest of the genes are selected from the second parent. The two resultant vectors are concatenated to form a child.

Two Points: This function selects two random number between 1 and number of variables (six in this case). Genes between the first number and the second number are selected from the second parent and rest of the genes are selected from the first parent. The resultant genes are concatenated to form a single gene (child).

Heuristic: This function creates new individuals (genes) randomly from the line containing the two parents, a small distance away from the parent with the better fitness, in the direction away from the parent with worst fitness value.

Arithmetic This crossover function creates new individuals that are a random arithmetic mean of two parents, uniformly on the line between parents.

Scattered This function creates a random binary vector, which then selects genes from the first parent where the vector is 1, otherwise genes from the second parent are selected. This way, genes are combined to form a child. It is suggested that the Scattered crossover shall be used when there are no constraints. This ensures that feasible parents give rise to feasible children where feasibility is with respect to bounds. As there are no constraints for the coordinated control problem, this function is used in this work. The results achieved were better in terms of solution quality relative to the other crossover functions.

C.2 SA Implementation in Matlab Global Optimisation Toolbox

This section provides details of SA implementation in Matlab global optimisation toolbox and that how different functions and parameters were tuned for achieving the best possible results as per the criteria described in section 2.4.2. This section is mainly based on the details provided in [124]. Tuning of these parameters is summarised in Table C.2.

C.2.1 Annealing Function

Annealing is used for generating new points (solutions) for the next iteration. Different options for annealing are available in Matlab. All of them were evaluated for solving the coordinated control problem.

Boltzmann annealing: This function takes random steps where size of each step is proportional to the square root of the temperature.

Fast annealing: This function takes random steps and size of each step is proportional to the temperature. Results obtained with this function are relatively better in terms of processing speed as compared to the Boltzmann annealing, hence this function was used in this thesis. Solution quality is same for both of these functions.

C.2.2 Reannealing Interval

The reannealing interval shows the number of points to be accepted before reannealing. Different number of points was used for reannealing starting from 50 up to 200 with

Table C.2 Evaluating the parameters in SA implementation as per the criteria in section 2.4.2

Parameter	**Values / Functions evaluated**	**Selected value / function**	**Reason for selection**
Annealing	Boltzmann, Fast	Fast	Achieves the optimal solution with higher computational efficiency
Reannealing interval	50 to 200 in a step of 10	100	Processing speed is relatively high
Temperature update	Logarithmic, Linear, Exponential	Exponential ($0.95^{iteration}$)	Solution quality and processing speed is relatively better
Initial temperature	50 to 150 in a step of 10	100	Processing speed is relatively higher

a step size of 10 and it was found that the default value of 100 performs better as compared to other values in terms of processing speed. The same quality of solution was achieved with all the values of reannealing interval.

C.2.3 Temperature Update Function

Logarithmic: Temperature decreases as 1/log(iteration).

Linear: Temperature is decreased as 1/iteration.

Exponential: Temperature is decreased as $0.95^{iteration}$. This function performed better relative to logarithmic and linear functions in terms of processing speed and solution quality and is used in this work.

C.2.4 Initial Temperature

This is the temperature at the beginning of the run. A temperature from 50 to 150 with a step of 10 was evaluated in this study and it was observed that the default temperature (100) performed better in terms of processing speed. Solution quality remained the same for all the temperatures. Hence the default temperature(100) was used in this thesis.

C.3 ACO implementation in Matlab

This section presents implementation and tuning of ACO variables in Matlab for achieving the optimum result with high processing speed. A construction graph was developed and ACO was implemented in Matlab as ACO is not a part of Matlab's global optimisation toolbox. The C_T upper and lower bounds are same as for other optimisers. The variables in the algorithm were tuned by evaluating different values for solving coordinated control problem as per the criteria described in section 2.4.2. Results are briefly discussed in section 3.6.1. The parameters tuning is summarised in Table C.3.

C.3.1 Population size

Different populations of ants within a range of 20 to 100 in a step of 10 were evaluated. A population size of 50 was found to be the most optimum for coordinated control problem as the optimum solution was achieved with highest computational efficiency relative to other population sizes.

Table C.3 Evaluating the parameters in ACO as per the criteria in section 2.4.2

Parameter	**Values / Functions evaluated**	**Selected value / function**	**Reason for selection**
Population	20 to 100 in a step of 10	50	Achieves optimum solution with highest computational efficiency
Pheromone level	1 to 25 in a step of 5	10	Better solution quality
Pheromone exponential weight for favourable paths	0 to 0.60 in a step of 0.03	0.30	Processing speed is the highest for achieving optimum solution
Pheromone exponential weight for less favourable paths	0.05 to 0.25	0.1	Better solution quality

C.3.2 Initial Pheromone Level

The initial pheromone level is used for identifying different paths in the construction graph. The pheromone level was initialised with different values from 1 up to 25 in a step of 5. It was observed that a value of 10 is suitable for coordinated control of wind farms as the optimum solution is achieved with the highest processing speed. All the paths are initialised with the same value (10 in this case) at the start of the algorithm.

C.3.3 Pheromone Exponential Weight

The pheromone exponential weight was kept at 0.3 after evaluating different values (0.0 to 0.60 in a step of 0.03). This exponential weight is used for increasing the probability of ants moving through the most optimum path. Pheromone evaporation rate for less attractive or long paths was kept at 0.1. Different values were evaluated starting from 0.05 up to 0.25 with a step of .05. The evaporation rate of 0.1 was found to be suitable for farm production maximisation problem in terms of both solution quality and processing speed. It should be noted that the exponential weight of favourable paths (0.30) is greater than for less favourable paths (0.1). This is to replicate the increase of pheromone on attractive paths and decrease the pheromone level on less attractive paths.

Appendix D

Turbines' Characteristics in the Wind Farms Case-Studies

This appendix contains information about the turbines installed in the case study wind farms detailed in Chapter 5. Only the information required for simulations in this work is provided. Characteristics of the turbines installed in the Brazos wind farm are given in Table D.1 and the standard power curve along with C_P and C_T is shown in Figure D.1. Characteristics of the turbines in the SMV wind farm are given in Table D.2 and Figure D.2 shows the standard power curve along with C_P and C_T of the turbines. Characteristics of turbines installed in the Lillgrund wind farm are given in Table D.3 while the standard power curve along with C_P and C_T are shown in Figure D.3.

Table D.1 Mitsubishi MWT-1000 turbine characteristics (Brazos) [142, 143]

Rated output (kW)	1000
Rotor diameter (m)	57
Hub height (m)	60
Max C_P	0.406
Rated wind speed (m/s)	13.5
Cut-in wind speed (m/s)	3.5
Cut-off wind speed (m/s)	24

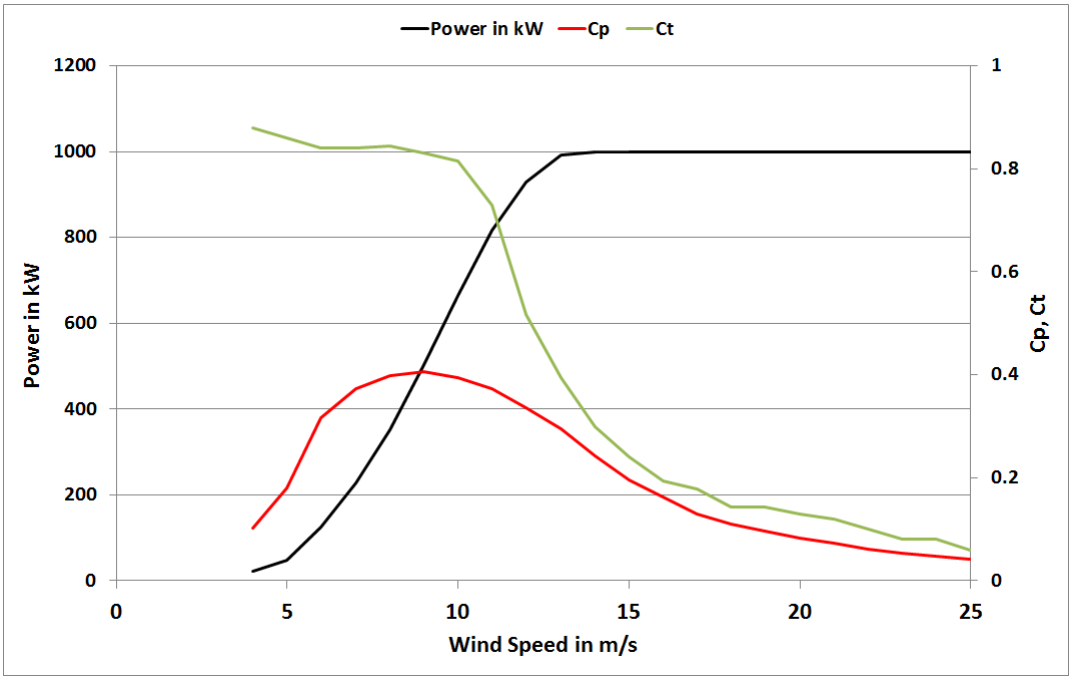

Figure D.1 Mitsubishi MWT-1000 turbine (Brazos) standard power curve with C_P and C_T [142, 143]

Table D.2 Senvion MM82-2050 kW turbine characteristics (SMV) [16]

Rated output (kW)	2050
Rotor diameter (m)	82
Hub height (m)	80
Max C_P	0.465
Rated wind speed (m/s)	12.5
Cut-in wind speed (m/s)	3.5
Cut-off wind speed (m/s)	25

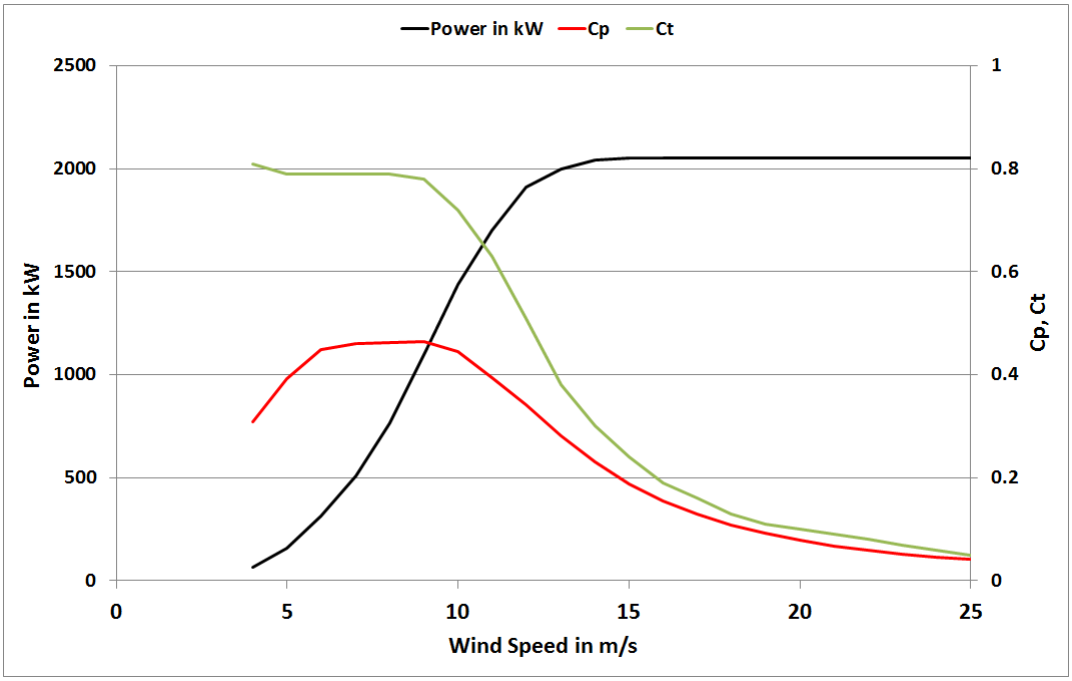

Figure D.2 Senvion MM82-2050 kW turbine (SMV) standard power curve with C_P and C_T [16]

Table D.3 Siemens SWT-2.3-93 turbine characteristics (Lillgrund) [17]

Rated output (kW)	2300
Rotor diameter (m)	93
Hub height (m)	80
Max C_P	0.466
Rated wind speed (m/s)	10.9
Cut-in wind speed (m/s)	3.0
Cut-off wind speed (m/s)	25

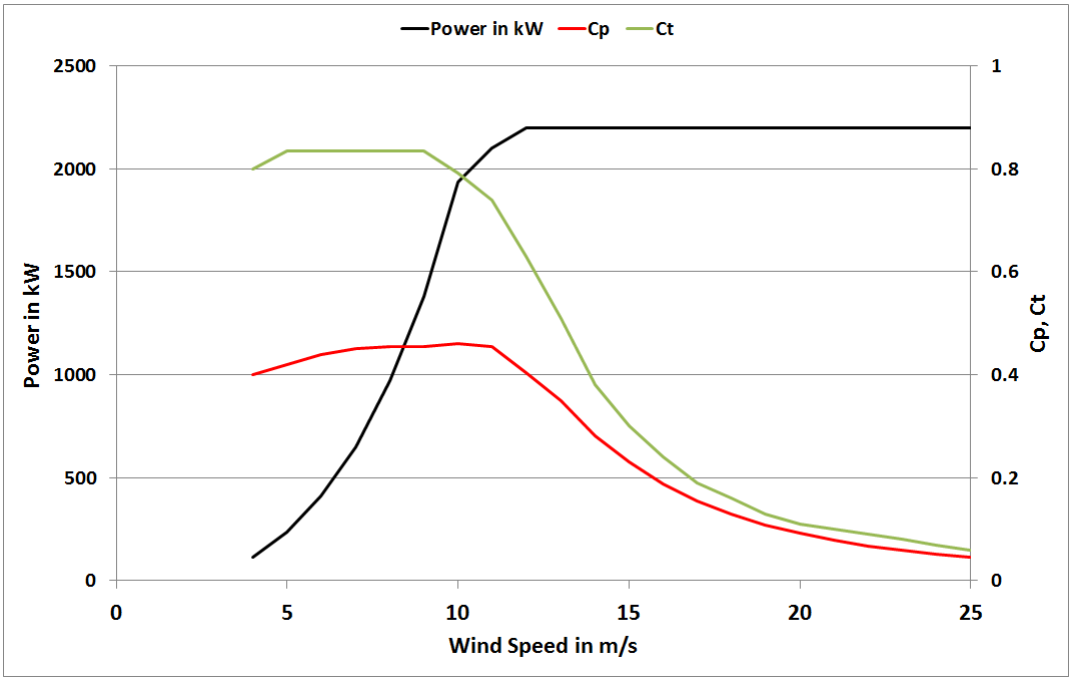

Figure D.3 Siemens SWT-2.3-93 turbine characteristics (Lillgrund) standard power curve with C_P and C_T [17]

Appendix E

Journal Publications

The two journal publications resulting from this work are presented in this appendix.

FIELD IMPLEMENTATION and TRIAL of COORDINATED CONTROL of WIND FARMS

Tanvir Ahmad, Olivier Coupiac, Arthur Petit, Sophie Guignard, Nicolas Girard, Behzad Kazemtabrizi and Peter Matthews

***Abstract*—This paper demonstrates, with live field experiment, the potential of increasing wind farm production through minimising wake effects by curtailing upstream wind turbines. Two 2MW turbines from the SMV (Le Sole de Moulin Vieux) wind farm are used for this purpose. The farm is equipped with state of the art LiDARs (Light Detection And Ranging) for measuring wind characteristics, up to a frequency of 1Hz. Simulations are performed using WindPRO for wake effects prediction. Optimised curtailment strategies are simulated for finding optimum curtailment settings of the upstream turbine. Results based on real time data are compared with simulated results. It is found that simulations are mostly in good agreement with field results, with a maximum difference of 1.5%. Analysis shows that a gain of up to 11.5% is possible in downstream turbine production, using a hard curtailment strategy by reducing power of the upstream turbine by about 17%. In this experiment, the combined production of the two turbines decreased with the hard curtailment strategy, indicating that the upstream turbine must be optimally curtailed for avoiding any production loss. To the best knowledge of the authors, this is the first practical implementation of LiDAR based coordinated control strategies in an operating wind farm.**

***Index Terms*—Coordinated control of wind farms, wind farm power production maximisation, wind farm control and optimisation, wake mitigation, LiDAR based wind farm control**

I. Introduction

Wind turbines are installed together in wind farms mainly to get advantages of economies of scale. Wind farms reduce civil engineering, grid connection and operation & maintenance costs. Other than economies of scale, factors such as navigational constraints also lead to closely spaced wind turbine in wind farms, such as the Lillgrund wind farm [1]. Though creating wind farms has major benefits, installing turbines in clusters creates aerodynamic interactions, namely wake effects, producing negative impact on farm production. Wake losses can reach as high as 60% in wind farms [1]. Wake effects also increase fatigue loading inside the wind farm. Hence, it is always desirable to mitigate and control wake effects.

This paper presents innovative wind farm coordinated control strategies that reduce wake effects inside the farm. Curtailing upstream turbines by using coefficient of power (C_P) or deflecting the wakes away from downstream turbines using yaw-offsets, can produce a positive impact on downstream turbines' production. The current state of the art control is based on greedy approach, as each turbine only maximises its own production neglecting the wake impact on downstream turbines. Using a coordinated control, the turbine optimises its contribution to the whole farm production along with minimising the wake impact on downstream turbines. This wake minimisation enables the downstream turbine to have a greater production.

Coordinated control of wind farms has recently been an active area of research. A detailed literature review of coordinated control studies is presented in section II. All of the previous studies regarding coordinated control are based either on simulations or scaled wind farms in wind tunnel experiments. There is a lack of field testing for evaluating coordinated control strategies. One major reason for this is the stochastic nature of the wind. There can be great variations in wind speed and direction over a short span of time. This stochastic nature of wind makes it hard to validate the experimental results with the field results. Uncertainties and errors in SCADA data, introduced by nacelle anemometer; especially in wake situations and met mast, adds to the problem.

With the introduction of modern LiDARs, it is now possible to determine the actual wind characteristics in a wind farm [2], [3]. LiDARs can provide information about wind conditions before it reaches the turbines. This information can be used for optimising farm production. In addition to the stochastic nature of the wind, major barriers to the implementation of wind farm coordinated control are the lack of sufficiently fast real-time optimisation and wake modelling methods, and the effective use of LiDAR systems [3]. This paper addresses all these issues by detailing implementation and investigations of C_P-based coordinated control strategies using LiDARs.

A setup of two operating wind turbines in the SMV is used for evaluating the benefits of C_P based coordinated control. The wind farm and turbines are equipped with state of the art LiDARs. The wake assessment methodology detailed in [4] is used for developing a two-step hard curtailment strategy. This hard strategy can curtail the upstream turbine by a maximum of 20% in full or near-full wake conditions on the downstream turbines, in certain wind speeds. Simulations are performed using WindPRO [5] for hard curtailment strategy while optimised control strategy is simulated using TI-JM (Turbulence Intensity based Jensen Model) [4].

The aim of this experiment is to assess the impact of curtailment of an upstream on the downstream turbine and not increasing the combined power production. Hence, a decrease in combined production was expected because of the high curtailment.

This paper is organised as follows. First previous studies of wind farm control are reviewed in section II. Details of the

Tanvir Ahmad is a PhD student and is supervised by Peter Matthews and Behzad Kazemtabrizi at Durham University, UK

Olivier Coupiac, Arthur Petit, Sophie Guignard and Nicolas Girard are from Maïa Eolis (now Engie Green), France

experimental setup are provided in section III. This is followed by the methodology and details of the hard curtailment strategy in section IV. Filtering and availability of data from different sources is detailed in section V. A brief overview of the optimised control strategy and TI-JM is provided in section VI. A short introduction of WindPRO is given in section VII. Analysis based on simulated results are presented in section VIII. The real-time results and analysis are presented in section IX, with conclusions in section X.

II. Literature Review

Wind farm coordinated control and optimisation has been an ongoing research area for the last three decades, as it can improve farm efficiency without any additional material costs. This section reviews previous wind farm coordinated control studies.

Works in [2], [6], [7] use simulations based on artificial wind farms for exploiting benefits of global control of wind farms. The patents [8]–[10] discuss different methods for improving efficiency of wind farms using coordinated control strategies. A complex wake flow model SOWFA (Simulator for Offshore Wind Farm Analysis) is used in [11]–[13] for analysing different curtailment strategies. Simulations with field data using a CFD (Computational Fluid Dynamics) based wind deficit model in [14] optimise wind farm production and loads. Wind tunnel experiments in [8], [15] use axial induction factor for evaluating different control strategies. Wind tunnel experiments and simulations based on data obtained from ECN (Energy Research Centre of the Netherlands) test wind farm in [16]–[21] confirm that if properly implemented, wind farm coordinated control can increase wind farm efficiency and can also decrease fatigue loading on the turbines.

The research presented in [4] has extended the standard Jensen wake model to include turbulence aspects in the TI-JM. By using heuristic optimisation techniques, the TI-JM is able to be used to identify optimal coordinated control strategies based on data from one offshore and two onshore wind farms in [4], [22]. These studies [4], [22] conclude that coordinated control can be beneficial for wind farms in certain wind conditions.

These previous studies are helpful in understanding the impact of curtailment strategies on downstream turbines. What lacks is the implementation and analyses of coordinated control strategies in live operating conditions. This paper fills this gap by applying curtailment strategies in an operating wind farm using LiDARs as discussed in the next section.

III. Experimental Setup

The purpose of this experiment is to implement and analyse C_P-based coordinated control strategies. This experiment started in November 2015 and ended in April 2016 at the SMV wind farm. Details of this field experiment are provided as follows.

A. Le Sole de Moulin Vieux (SMV) wind farm

The SMV wind farm is owned by Maïa Eolis (now Engie Green) and is located in the north of France. The farm consists seven Senvion REpower MM82 2050kW wind turbines [23], installed in a one-dimensional array. Turbines are labelled as SMV1 - SMV7 from north to south as shown in Figure 1. An 80 meters-high lattice met mast with ultrasonic anemometers at 80, 60, 40 and 20m height, is located 1km east of SMV2 and 1.6km north-east of SMV6 as shown in Figure 1. This met mast provides free-stream wind information.

The spacing between the turbines varies between $3.7D$ and $4.3D$. Prevailing wind direction is from south and south-west. The terrain is rough with grass or vegetation. There are woods to the south of the farm as can be seen in Figure 1. The trees are about 15m high and are located at a distance of 100m (less than $1.5D$) from the wind farm. This influences atmospheric stability and results in high turbulence intensity in the wind farm. The farm also suffers from diurnal and seasonal variations in wind conditions [24].

WindPRO suggests free-stream turbulence intensity of 15% for this wind farm clearly exhibiting the roughness on site [5]. This high surface roughness and turbulence intensity result in quick wake recovery. The surrounding wind flow quickly diffuses the momentum loss created by the wakes, resulting in an increased turbulence intensity. This wake added turbulence intensity changes wind characteristics abruptly in the farm.

The experiment focuses on two turbines: SMV5 and SMV6. These two turbines are chosen because of the close spacing ($3.7D$) and prevailing wind direction in the farm. SMV6 is upstream and acts as the wake producing turbine hence curtailment is applied on this turbine. SMV6 is equipped with nacelle mounted Orion 5-beam LiDAR, facing the free-stream wind. A Wind Iris LiDAR is mounted on top of SMV5. A ground based LiDAR, Windcube V1 type has been installed between turbines SMV2 and SMV3. This LiDAR measures wind speed at heights between 40m and 200m with 1Hz frequency. A scanning LiDAR is also installed at 1.2km to the east of the wind farm, as shown in Figure 1. The scanning LiDAR is programmed to carry out three horizontal scans and one vertical scan. This allows hub height measurements of SMV6 in wake situations for SMV5. Full details of the field setup are given in [25].

IV. Methodology

SMV is a one-dimensional array of turbines. When the free-stream wind flows from the east or west, there are no wake effects. However, when the wind flows from the south or north, then the farm production is affected by wake effects. SCADA data from 2011–2014 was used in assessing wake effects in this wind farm in [4]. It was observed that wakes can significantly impact farm production in the direction sector $180^\circ \pm 40^\circ$ and $0^\circ \pm 40^\circ$. Details of this wake assessment methodology and data filtering can be found in [4].

The experiment in this paper used SMV6 and SMV5. Historical wake assessment shows that the wakes from SMV6 can incur significant effects on SMV5 production in the direction sector $200^\circ \pm 20^\circ$ as shown in Figure 2. WindPRO predicts 26% wake losses annually in SMV5 production, caused by SMV6 wakes (normal uncurtailed operation), in this wind direction sector. Hence, this is the chosen direction sector

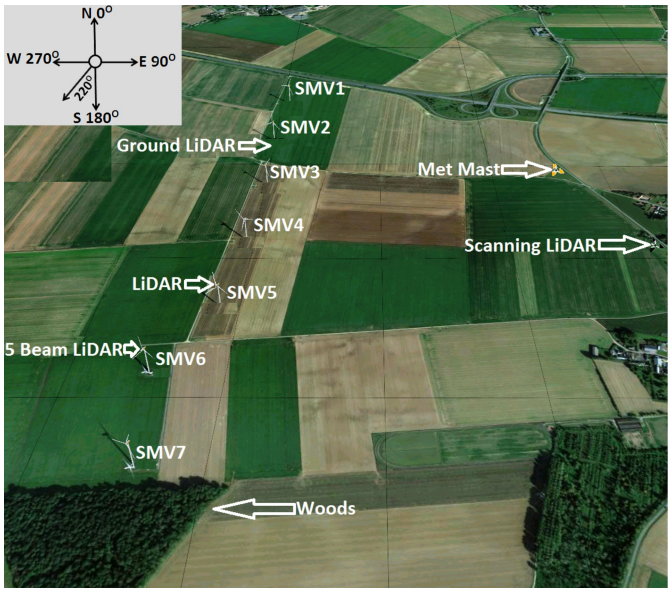

Fig. 1: SMV layout and surrounding with positions of met mast and LiDARs [26]

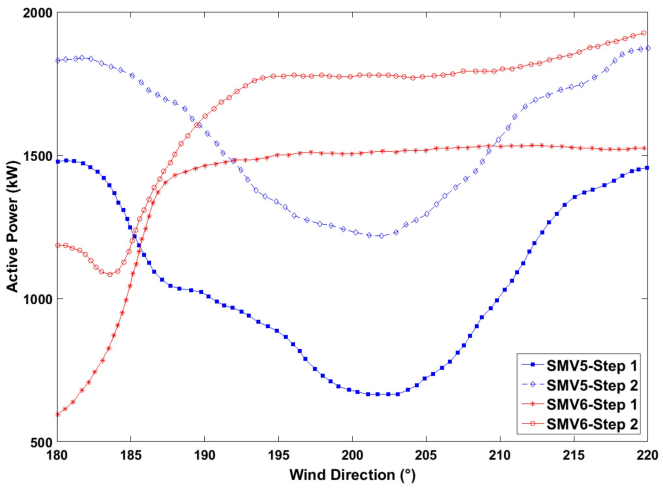

Fig. 2: Wake effects on SMV5 and SMV6 production in $180° - 220°$ during uncurtailed operation.

for this experiment. Figure 2 illustrates the adverse impact the SMV6 wake has on SMV5 production during normal operation. Using the power production of SMV7 as a reference for available wind resource, the production of SMV5 and SMV6 are shown in two different steps. Step 1 represents the lower wind resource availability (SMV7 producing less than 1500kW) and Step 2 represents the higher wind resource availability (SMV7 producing more than 1600kW). From Figure 2, the impact of SMV6 wake on SMV5 can be clearly seen: SMV5 production dips as the wind direction moves the wake from SMV6 fully on to SMV5, with maximal effect at 202°. Similarly, the impact of SMV7 can also be seen on SMV6 production in the region 180°–185°.

A. Hard Curtailment Strategy

A two step C_P-based curtailment strategy, easily implementable on SMV6, was adopted. The strategy is aimed at curtailing SMV6 power to a maximum of 20% in two steps in the selected direction sector as given in Table I. SMV7 production is used as the reference as it is unaffected by wakes when wind flows in the chosen sector. In the first step when SMV7 power is between 1200kW and 1500kW and SMV6 power is above 1200kW then SMV6 is curtailed to 1200kW. In the second step if SMV7 power is between 1600kW and 1900kW and SMV6 power is above 1600kW then SMV6 is curtailed to 1600kW. This curtailment strategy is referred to as hard curtailment strategy due to the hard curtailment limits applied by the wind turbine controller.

TABLE I: Two steps hard curtailment strategy

if 180° ≤ Wind Direction ≤ 220°		
Step 1:	if	1200kW < SMV7 ≤ 1500kW
	then	curtail SMV6 to 1200kW
Step 2:	if	1600kW < SMV7 ≤ 1900kW
	then	curtail SMV6 to 1600kW

When appropriate wind conditions occurred (wind direction and speed), a technician manually curtailed SMV6 accordingly. The wind-rose in Figure 3 shows the wind conditions when SMV6 was actually curtailed as per Table I. The power curve based on this hard curtailment strategy is presented in Figure 4. It can be seen in Figure 4 that SMV6 is curtailed only when the wind speed is above 10m/s.

The Senvion MM82 2050 controller is configured to follow the manufacturer standard power curve by default i.e. the greedy control [23]. This standard power curve is presented in Figure 4. For optimised control, the turbine must follow an optimised power curve for each direction bin. This requires fast processing and efficient control strategies as will be discussed in section VI. It was not possible to implement the optimised power curve during this experiment due to technical limitations [25]. Hence the optimised strategy was only used in simulations for identifying the optimal curtailment settings.

The experiment in this paper is based on curtailment of SMV6 with the wind coming from south and south-west. This takes SMV7 out of analyses as SMV7 is unaffected when SMV6 is curtailed. Hence from this point onwards the wind farm means turbines SMV1 to SMV6.

V. Data and Filtering

During this experiment, data from different sources (metmast, SCADA, LiDAR, and MERRA [27]) were recorded. The availability of data from these sources is shown in Figure 5. The curtailment periods are also given in Figure 5, which represents a total of 19 hours, corresponding to more than 200 data points. To ensure reasonable statistical analysis, it was found that for this data should be placed in bin sizes (resolutions) of 1m/s for wind speed and $\pm 5°$ (i.e. 10° resolution) for wind direction. Wake effects can be assumed to remain the same in these bins, hence averages of the variables under observation are taken in the designated bins. The filtering criteria was set to have at least 10 valid data

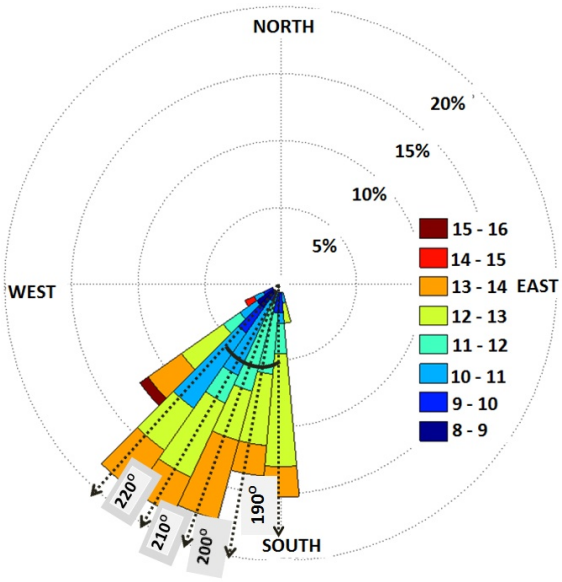

Fig. 3: Wind-rose for the periods when SMV6 was curtailed with the hard strategy

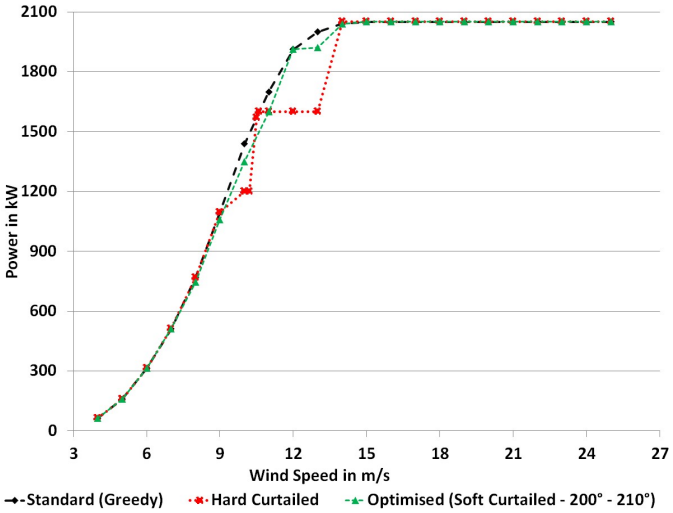

Fig. 4: Comparison of SMV6 standard, hard-curtailed and optimised power curve

points in a given directional and speed bin. Wind conditions with less than 10 data points per bin were not considered for analysis.

Figure 5 also shows atmospheric stability in the wind farm. It can be seen that atmosphere is mostly unstable as discussed in section III-A. This affects the wind conditions inside the wakes and brings abrupt changes in wind direction and speed as discussed in section III-A.

Another important issue was the difference in wind directions, reported by different sources. Instantaneous wind directions can differ from a measuring device placement to another because of wind turbulence. Nevertheless, offsets are mostly due to calibration errors. To avoid any directional discrepancy in analyses, LiDAR Windcube data at a height of 80m was corrected by analysing directions of wakes and

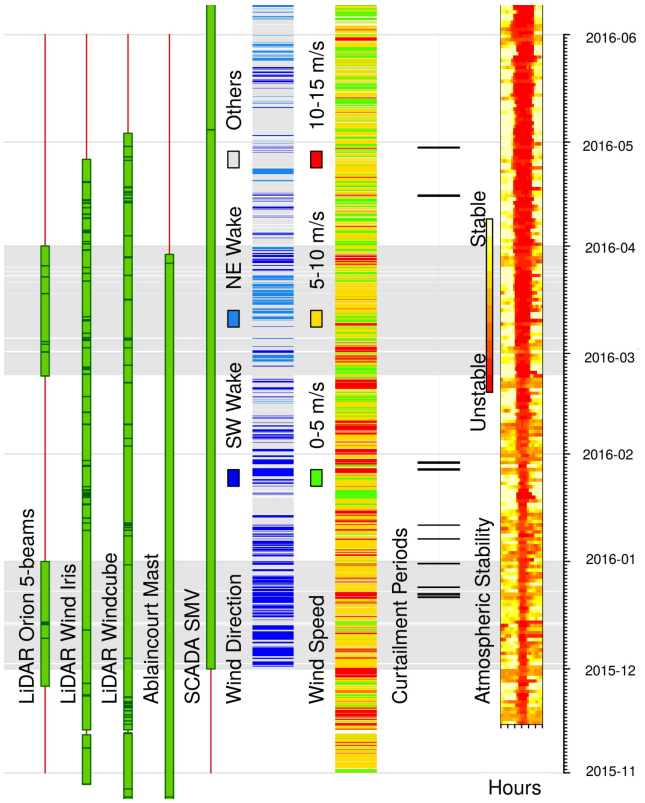

Fig. 5: Data Availability for the experiment from different sources

then used as a reference. Unlike nacelle mounted instruments, this LiDAR's wind direction is independent of nacelle position and wake effects do not interfere in directions of interest. Indeed, the measurement of LiDAR wind direction is heavily perturbed in under inhomogeneous wind flow (complex terrain and wake conditions). Finally, directional offsets using this reference were applied to all the devices i.e. LiDARs, turbines and met mast.

VI. Optimised Control

A computationally efficient and optimised control strategy for real-time on-line coordinated control is presented in [4], [22]. The optimised strategy uses the TI-JM for mean production estimation in the farm. The TI-JM estimates wind deficit inside the farm considering deep array effect and wake added turbulence intensity. PSO (Particle Swarm Optimisation) is used for optimising the farm production using C_P-based coordinated control strategies [4], [22].

The optimised strategy curtails SMV6 in such a way that the loss in production is always compensated by gain in SMV5 production. If no level of curtailment results in any increase in the combined (SMV5 + SMV6) production, then the SMV6 follows the standard power curve. The optimised power curve for full wake conditions in the wind direction 200°–210° is presented in Figure 4. This power curve suggests a very small change in the standard power curve from 8–14 m/s. The maximum reduction in SMV6 power is only 4% as compared to the 20% reduction in the hard curtailment

strategy. The optimised curtailment requires the power to be controlled precisely depending on wind speed and direction. This means that each directional bin has its own optimised power curve.

A. Turbulence Intensity based Jensen Model (TI-JM)

The TI-JM is based on the Jensen model [28]. Wind speed (u_x) on a wake affected downstream turbine with radius (r_0) at distance (x) can be found with equation (1) using the Jensen model. Coefficient of thrust of the wake producing turbine is given by (C_T). The standard Jensen model and TI-JM require a pre-determined initial (standard) value of wake decay coefficient (k) for free-stream conditions. The value of k depends upon hub heigh (z) and surface roughness length (z_0) as given in equation (2). In the standard Jensen model, k remains constant as ideal wind conditions are assumed [28]. In reality, wind flow inside the farm is affected by deep array effect and wake-added turbulence intensity, which also affect k [5].

The TI-JM takes wake-added turbulence intensity into account while estimating wind speed deficit. The value of k varies inside the farm as per the wake-added turbulence intensity as given in equation (3) [4], where (I_u) is the longitudinal component of turbulence intensity. For a two turbines case, the TI-JM performs exactly the same as the standard Jensen model as only the standard value ($k = 0.07$) [5] is used for wake estimation. For the whole wind farm, values of k up to 0.20 were used for wake estimation inside the wind farm as suggested in [4].

$$u_x = u_0 \left(1 - \left(\frac{1 - \sqrt{1 - C_T}}{\left(1 + \frac{kx}{r_0}\right)^2} \right) \right) \tag{1}$$

$$k = \frac{1}{2 \ln\left(\frac{z}{z_0}\right)} \tag{2}$$

$$I_u = \frac{1}{\ln\left(z/z_0\right)} \qquad k = \frac{I_u}{2} \tag{3}$$

VII. WindPRO

WindPRO is one of the most widely used and industry standard software for design, development and assessment of wind energy projects [5]. WindPRO calculations in this study are based on the WAsP (Wind Atlas Program) method. The standard Jensen model available in WindPRO and given in equation (1) is used for predicting wake losses. The standard value of $k = 0.07$ for onshore wind farms [5] is used in simulations. This value of k is same as in the TI-JM for two turbines case as discussed in section VI-A. Hence there is no difference between WindPRO and the TI-JM in case of two turbines as both use the standard Jensen model.

VIII. Simulation based Results and Analysis

This section presents results and analysis based on simulations. Hard control simulations using all the collected data, when SMV6 was curtailed, are presented in section VIII-A. Simulation results based on optimised control are presented in section VIII-B. While simulations based on hard control with filtered data are presented in VIII-C.

A. Hard Control Simulations based on All Collected Data

All the collected data (unfiltered) during the experiment (when SMV6 was hard-curtailed) was used to execute a WindPRO based simulation. The simulation predicted an average production increase of almost 3% in SMV5 in the $200^\circ \pm 20^\circ$ sector, as compared to normal operation. The weighted increase in each 10° bin is shown in Figure 6. The greatest increase (1.15%) is achieved in the $190^\circ - 200^\circ$ bin. This was the prevailing wind direction during this experiment as evident from Figure 3. SMV5 is almost completely shadowed by SMV6 wake in the $190^\circ - 200^\circ$ bin. Hence WindPRO predicted a higher gain for this bin. The smallest increase is in the bin $200^\circ - 210^\circ$ where SMV5 is under full wake affects of SMV6. The wind blew less frequently in this bin, in comparison to the other three bins (see Figure 3). The production gain in the other two bins (partial wake conditions) is almost the same.

If equal weight (for wind direction and speeds) is given to all the bins then the gain in production increases as the wake moves from partial to full wake conditions. These WindPRO simulations show that curtailment of SMV6 can produce a greater increase in SMV5 power production in full or near-full wake conditions.

WindPRO predicted a loss in the combined production of SMV6 and SMV5 when SMV6 is hard curtailed as shown in Figure 6. The loss in the combined production shows that the loss in SMV6 production due to curtailment is not compensated by gain in SMV5 production. The greatest loss in combined production is predicted in the $180^\circ - 190^\circ$ bin as SMV5 is under minimal wake effect of SMV6, as compared to the other three bins. The loss in combined production decreases as the wake moves from partial to full wake conditions. The lowest loss is in full wake conditions, in the $200^\circ - 210^\circ$ bin.

B. Optimised Control Simulations

This section presents the simulations based on optimised control strategy using all the collected data (unfiltered, when SMV6 was curtailed) during the experiment. Figure 6 shows the optimised increase in SMV5 production in all the four bins. Simulations predicted that no combined increase can be achieved by curtailing SMV6 in the $180^\circ - 190^\circ$ bin, as wake impact on SMV5 is minimal. SMV6 follows its standard power curve (operating greedily) in this $180^\circ - 190^\circ$ bin, resulting in maximum combined production. When the wake moves to near-full wake conditions in $190^\circ - 200^\circ$ bin, SMV5 benefits more from curtailment of SMV6. The maximum possible gain in combined production is 0.4% in

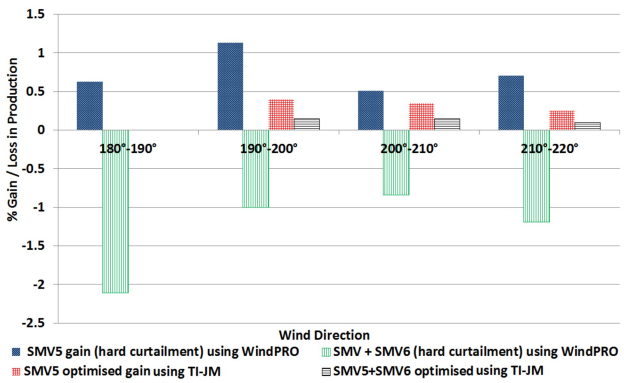

Fig. 6: Simulated % increase/decrease in SMV5 and combined production of SMV5+SMV6, using all the collected data

this bin $190^\circ - 200^\circ$, as wind conditions are favourable for implementation of coordinated control and wind blew more frequently in this bin.

The gain in production depends upon many parameters including number of turbines in the farm that can be curtailed and number of downstream turbines that can benefit from this curtailment, wind conditions and surface roughness on the site. The number of turbines that can be curtailed is only one. Turbulence intensity and roughness on the site is very high allowing the wake to diffuse quickly. Hence the optimised increase in SMV5 production and net gain is low. If all seven turbines in the farm are optimally controlled, a gain of up to 7% is possible in farm production in full or near-full wake conditions [4].

C. Hard Control Simulations based on Filtered Data

This section presents simulated results using the filtered data with the hard control strategy. These simulations are performed using the TI-JM and are presented in Table II. The impact of the curtailment strategy on downstream turbines and farm production in each valid data bin is analysed. The directional bins $180^\circ - 190^\circ, 190^\circ - 200^\circ$ and $210^\circ - 220^\circ$ are ignored as the number of data points in these bins are not significant. When the bin size is increased to $\pm 10^\circ$, the number of valid data points are increased, fulfilling the filtering criteria. This results in some overlapping bins. Unfortunately, there are not enough valid data points available for Step 1 of the hard curtailment strategy. Filtering criteria given in section V is not met for Step 1. Hence results are only presented for Step 2. Valid speed bins range from 11m/s to 13m/s as data in only these speed bins fulfilled the filtering criteria.

SMV6 curtailment in the whole sector ($200^\circ \pm 20^\circ$) on average is 17.5% and in full wakes it is 18.6%. These simulations predict a decrease of up to 11% in combined production of SMV5 and SMV6, however an increase of up to 13% is predicted in SMV5 production. This indicates that SMV5 has benefited from the curtailment of SMV6. Impact of SMV6 hard curtailment on other turbines' and farm production is also shown in Table II. It should be noted that the combined production of SMV5 and SMV6 is different than simply adding the production of SMV5 and SMV6 given in Tables II and III. When combined production of the two turbines (SMV5 and SMV6) is analysed, the number of data points is increased, fulfilling the filtering criteria. When individual production of SMV5 or SMV6 is considered, number of data points is reduced and for some wind speed and direction bins, the filtering criteria was not met as explained earlier.

TABLE II: Simulated impact of SMV6 curtailment on SMV wind farm (% increase/decrease) using filtered data

Turbine(s)	$180^\circ - 220^\circ$	$190^\circ - 210^\circ$	$200^\circ - 210^\circ$	$200^\circ - 220^\circ$
SMV6	-17.5	-17.1	-18.6	-19
SMV5	4.0	13	12.5	-1.2
SMV4	4.2	4.0	-1.0	-1.0
SMV3	3.0	3.0	-1.0	-1.0
SMV2	2.0	2.0	-0.5	-0.5
SMV1	3.0	3.0	0	0
SMV5+SMV6	-9.5	-6.0	-6.0	-11
Farm	-2	-1.0	-2.5	-4.0

TABLE III: Actual impact of SMV6 curtailment on SMV wind farm (% increase/decrease) using filtered data

Turbine(s)	$180^\circ - 220^\circ$	$190^\circ - 210^\circ$	$200^\circ - 210^\circ$	$200^\circ - 220^\circ$
SMV6	-17.5	-17.1	-18.6	-19
SMV5	4.5	11.5	11.5	-0.7
SMV4	3.5	4.9	-0.9	-1.5
SMV3	2.0	2.3	-0.3	-0.5
SMV2	1.6	1.9	0.2	0.2
SMV1	2.6	2.7	0.5	0.6
SMV5+SMV6	-8.1	-5.6	-6.4	-10.9
Farm	-0.7	0.4	-1.9	-3.4

IX. Hard Control Field Results

Results in this section are based on filtered data obtained in this experiment, presented in Table III. These results are plotted with 80% confidence interval represented by the bar on the figures in this section. This confidence interval is chosen due to the limited data volume.

SMV6 power curve during the curtailment periods compared to the normal operations is shown in Figure 7. Average gain in SMV5 production is 4.5%. The highest gain in SMV5 production is observed in full wake conditions i.e. $200^\circ - 210^\circ$, which is 11.5%. The increase in SMV5 production confirms the positive impact of the hard curtailment strategy. The reduced wakes are propagated through the wind farm and increase in production is observed for all the downstream turbines SMV4–SMV1.

The combined production of SMV5 and SMV6 is decreased by almost 8.1% in the chosen directional sector. This means that the loss in SMV6 production is not compensated by gain in SMV5 production with the hard curtailment strategy.

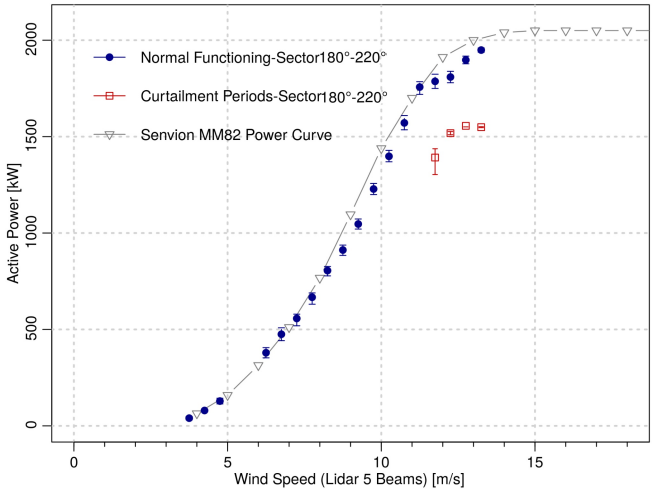

Fig. 7: SMV6 power curve obtained from data with 80% confidence interval

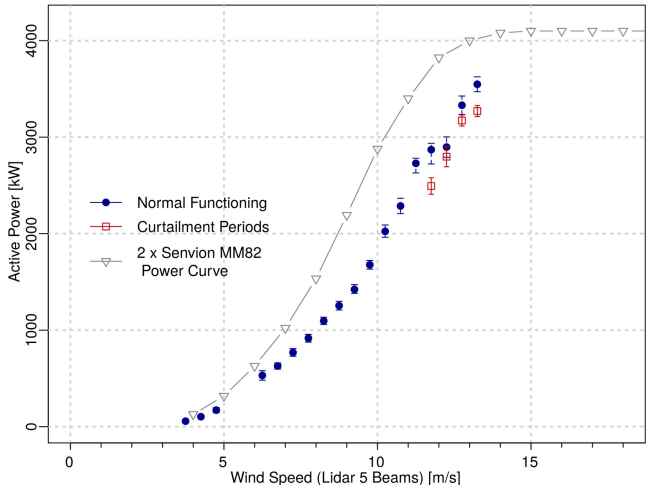

Fig. 8: Combined production of SMV5 + SMV6 in full wake ($200^\circ - 210^\circ$) conditions (80% confidence interval)

The lowest decrease in combined production is in full wake conditions as shown in Figure 8. By definition SMV6 wake has highest impact on SMV5 production in full-wake conditions. Hence, the benefits of curtailment are also greater in this bin. In partial wake conditions, impact of SMV6 is relatively low, hence gain in production due to curtailment, is also low.

This loss in combined production is the reason to opt for soft optimised control strategies. Simulations in section VIII-B suggest that when properly implemented, the optimised strategy never produces losses in combined production.

The farm production is reduced by an average of 0.7% as a result of SMV6 curtailment. The average farm production loss is less than 1%, indicating that the five downstream turbines have benefited from the 17.5% curtailment applied on SMV6. The farm power curve in the $200^\circ \pm 20^\circ$ is presented in Figure 9 showing the small loss in production during the curtailment period. This small decrease in overall farm production relative to normal operations suggests that if turbines are curtailed optimally then overall farm production can be increased.

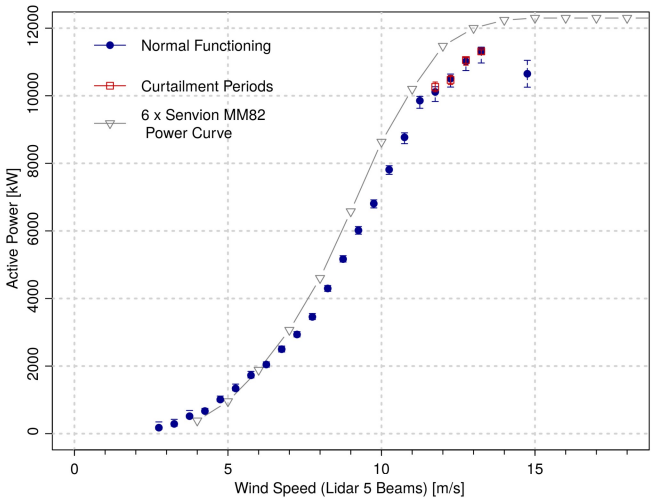

Fig. 9: Impact of the hard curtailment strategy on overall farm production in $200^\circ \pm 20^\circ$ bin (80% confidence interval)

Results in Table II can be compared with results in Table III. Simulations in section VIII-C predicted an overall increase of 4% in SMV5 production with the hard curtailment strategy (with filtered data) while an increase of 4.5% was observed in the actual experiment. Simulations predicted a decrease of 9.5% in combined production of SMV5 and SMV6, while the actual decrease is 8.1%. The overall decrease in farm production predicted with simulations is 2% while the actual decrease is 0.7%. A maximum difference of 1.5% is observed between simulated and real-time results. This shows that simulations are in good agreement with the field results.

X. Conclusion

Preliminary results of the C_P-based curtailment experiment from the SmartEOLE project are presented. The potential of coordinated control of wind farms, for increasing farm production, is investigated using live experiments. Two turbines in the SMV wind farm (SMV5 and SMV6) were chosen as the experiment turbines. The farm and turbines were equipped with modern LiDARs. SMV7 production was used as a reference for defining a two step hard curtailment strategy in the directional sector $200^\circ \pm 20^\circ$. The curtailment strategy reduced SMV6 production (using C_P) by a maximum of 20% for analysing the wake effect produced on SMV5 and the overall farm production.

Data from different sources was analysed during the curtailment period. WindPRO predicted 3% increase in SMV5 production with the given hard curtailment strategy in the chosen directional sector when all the collected data was simulated. A decrease in combined production of SMV5 and SMV6 was predicted as the loss in SMV6 production cannot be compensated by gain in SMV5 production. Optimised control strategy was simulated to predict the optimal power settings of SMV6. Simulations with the optimised strategy predicted an increase of up to 0.4% in SMV5 production.

A production increase of up to 11.5% was observed for the downstream turbine SMV5 with the field data. It was observed that the increase in SMV5 production becomes more

significant as the turbine moves from experiencing partial wake to full wake conditions. The gain in SMV5 production was propagated through the farm as the downstream turbines benefited from the reduced wake effects. Simulations performed with the TI-JM (using filtered data) has a difference of a maximum of 1.5% with the real time results, showing that simulations are in good agreement with field results.

A decrease in combined production of SMV5 and SMV6 and overall farm production (SMV1–SMV6) was observed with the hard curtailment strategy. This confirmed the importance of optimised control strategies. The simulations based on optimised strategy show that if SMV6 power is curtailed optimally, the loss in SMV6 power is always compensated by gain in SMV5 production. It should be noted that the only change required for implementing the optimised strategy is the control algorithm (greedy to optimised) and no additional hardware is required. The experimental setup given in section III-A was used only to obtain high frequency wind data. Offline optimisation can be a solution. But as observed in the SMV wind farm, atmospheric instability and abrupt changes in the wind characteristics require faster and computationally efficient on-line optimised control strategies.

It can be concluded that coordinated control of wind farms is beneficial for overall gain and production maximisation of downstream turbines. Wake affected turbine(s) can benefit from the curtailment of upstream turbine(s). Though a net increase in combined production was not observed in this experiment, the gain in SMV5 production proves that there is potential for coordinated control for maximising overall farm production. If turbines are curtailed optimally, this can increase the combined power production and hence the efficiency of a wind farm in certain wind conditions. The impact of coordinated control can be more significant in stable wind conditions such as offshore and dense wind farms as wakes travel for longer distances. If turbines are densely designed, more downstream turbines will be shadowed by upstream turbines' wakes, reducing farm production. If these wakes are controlled with an optimised strategy, a positive impact on overall farm production can be achieved.

ACKNOWLEDGEMENT

The authors would like to thank the French National Project SMARTEOLE (ANR-14-CE05-0034) and the Commonwealth Scholarships Commission UK.

REFERENCES

[1] J. A. Dahlberg, "Assessment of the Lillgrund windfarm: Power performance," Vatenfall, Vindkraft AB, Tech. Rep. 21858-1, September 2009.

[2] L. Y. Pao and K. E. Johnson, "A tutorial on the dynamics and control of wind turbines and wind farms," in *American Control Conference, ACC'09*. 172: IEEE, 2009, Conference Proceedings, pp. 2076–2089.

[3] F. A. Aranda, "Wind farm control methods, IEA R&D wind task 11 - topical expert meeting," International Energy Agency, Tech. Rep., November 2012.

[4] T. Ahmad, N. Girard, B. Kazemtabrizi, and P. Matthews, "Analysis of two onshore wind farms with a dynamic farm controller," in *EWEA, Paris France*, November 2015.

[5] N. Per, V. Jens, K. Jon, M. Per, J. Thomas, T. Morten, L., S. Mads, V., S. Thomas, S. Lasse, M. Mauricio, and B. Karina, *WindPRO 2.7 User Guide*, 3rd ed., EMD International A/S, Aalborg, Denmark, October 2010.

[6] E. Bitar and P. Seiler, "Coordinated control of a wind turbine array for power maximization," in *American Control Conference (ACC)*. 136: IEEE, 2013, Conference Proceedings, pp. 2898–2904.

[7] K. E. Johnson and N. Thomas, "Wind farm control: addressing the aerodynamic interaction among wind turbines," in *American Control Conference, ACC'09*. 155: IEEE, 2009, Conference Proceedings, pp. 2104–2109.

[8] G. Corten and P. Schaak, "Heat and flux: Increase of wind farm production by reduction of the axial induction," in *Proceedings of the European Wind Energy Conference*, 2003.

[9] C. Schram and P. Vyas, "Windpark turbine control system and method for wind condition estimation and performance optimization," Nov. 29 2005, US Patent App. 11/288,081.

[10] A. Ambekar, V. Ryali, and A. K. Tiwari, "Methods and systems for optimizing farm-level metrics in a wind farm," Dec. 1 2015, US Patent 9,201,410.

[11] J. Annoni, P. M. Gebraad, A. K. Scholbrock, P. A. Fleming, and J.-W. V. Wingerden, "Analysis of axial-induction-based wind plant control using an engineering and a high-order wind plant model," *Wind Energy*, vol. 19, pp. 1135–1150, 2015.

[12] P. Fleming, P. M. Gebraad, S. Lee, J.-W. Wingerden, K. Johnson, M. Churchfield, J. Michalakes, P. Spalart, and P. Moriarty, "Simulation comparison of wake mitigation control strategies for a two-turbine case," *Wind Energy*, vol. 18, no. 12, pp. 2135–2143, 2015.

[13] P. A. Fleming, P. M. Gebraad, S. Lee, J.-W. van Wingerden, K. Johnson, M. Churchfield, J. Michalakes, P. Spalart, and P. Moriarty, "Evaluating techniques for redirecting turbine wakes using SOWFA," *Renewable Energy*, vol. 70, pp. 211–218, 2014.

[14] M. Soleimanzadeh, R. Wisniewski, and S. Kanev, "An optimization framework for load and power distribution in wind farms," *Journal of Wind Engineering and Industrial Aerodynamics*, vol. 107, pp. 256–262, 2012.

[15] G. Corten, P. Schaak, and E. Bot, "More power and less loads in wind farms: Heat and Flux," in *European Wind Energy Conference & Exhibition, London, UK*, 2004.

[16] J. Schepers and S. Van der Pijl, "Improved modelling of wake aerodynamics and assessment of new farm control strategies," in *Journal of Physics: Conference Series*, vol. 75, no. 1. IOP Publishing, 2007.

[17] L. Machielse, S. Barth, E. Bot, H. Hendriks, and G. Schepers, "Evaluation of (Heat and Flux) farm control," ECN, Petten, The Netherlands, Tech. Rep. ECN-E–07-105, 2007.

[18] K. Boorsma, "Heat and flux. analysis of field measurements," ECN, Petten, The Netherlands, Tech. Rep. ECN-E–12-048, November 2012.

[19] S. Kanev and F. Savenije, "Active Wake Control: loads trends," ECN, Petten, The Netherlands, Tech. Rep. ECN-E–15-004, January 2015.

[20] J. Wagenaar, L. Machielse, and J. Schepers, "Controlling wind in ECN scaled wind farm," *Proc. Europe Premier Wind Energy Event*, pp. 685–694, April 2012.

[21] K. Boorsma, "Power and loads for wind turbines in yawed conditions," ECN-E-12-047, ECN, Petten, The Netherlands, Tech. Rep., 2012.

[22] T. Ahmad, P. Matthews, and B. Kazemtabrizi, "PSO based wind farm controller," in *The 11th edition of the International Conference on Evolutionary and Deterministic Methods for Design, Optimization and Control with Applications to Industrial and Societal Problems, EUROGEN-2015 Glasgow, UK*, September 2015, pp. 277–283.

[23] *Senvion MM82 [50 Hz/2050 kW] Product Description*, Senvion wind energy solutions, Senvion GmbH, Hamburg Germany, www.senvion.com/global/en/wind-energy-solutions/wind-turbines/mm/mm82/.

[24] O. Coupiac, "Four vertical extrapolation methods," *WindTech International*, vol. 12, no. 2, pp. 5–8, March 2016.

[25] S. Aubrun, D. Averbuch, S. Baleriola, C. Braud, M. Boquet, O. Coupiac, N. G. P. Devinant, F. Guillemin, E. Guilmineau, A. Leroy, D. Nelson-Grüel, D. Peaucelle, and A. Petit, "SMARTEOLE Deliverable D1-1: Installation Protocol and test plans for field test 1 and wind tunnel test 1 and 2," Maïa Eolis, Univ. Orléans, INSA-CVL, PRISME EA4229, IFPEN, LEOSPHERE, École Centrale de Nantes, LHEEA UMR CNRS 6598, LAAS-CNRS, Tech. Rep. ANR Project no 14-CE05-0034, September 2016, confidential.

[26] "Google earth," http://www.google.com/earth/ accessed August 8, 2017.

[27] M. M. Rienecker, M. J. Suarez, R. Gelaro, R. Todling, J. Bacmeister, E. Liu, M. G. Bosilovich, S. D. Schubert, L. Takacs, G.-K. Kim *et al.*, "MERRA: NASA's modern-era retrospective analysis for research and applications," *Journal of Climate*, vol. 24, no. 14, pp. 3624–3648, 2011.

[28] N. O. Jensen, "A note on wind generator interaction," Risø National Laboratory, Roskilde, Denmark, Tech. Rep. Risø -M-2411, November 1983.

Fast processing intelligent wind farm controller for production maximisation

Tanvir Ahmad[1,1], Peter C. Matthews[1], Behzad Kazemtabrizi[1], Olivier Coupiac[2]

Abstract

A realistic wind farm controller for production maximisation based on coordinated control is presented. The farm controller emphasises computational efficiency without compromising accuracy. The controller combines Particle Swarm Optimisation (PSO) with a turbulence intensity based Jensen wake model (TI-JM) for exploiting the benefits of either curtailing upstream turbines using coefficient of power (C_P) or deflecting wakes by applying yaw-offsets for maximising overall farm production. The wind deficit model takes free-stream and wake added turbulence intensities into account for estimating effective values of wake decay coefficients inside the wind farm on turbine by turbine basis. The wind deficit model is validated using WindPRO and SCADA data from three wind farms (Brazos, Le Sole de Moulin Vieux (SMV) and Lillgrund) as benchmarks. PSO is used for optimisation because of its high processing speed and computational efficiency. The innovative control strategies can optimise a medium size wind farm, Lillgrund consisting of 48 wind turbines, in less than 50 seconds increasing farm production by a maximum of 8% in full wake conditions.

Keywords: **wind farm production maximisation, coordinated control, C_P-based optimisation, yaw-based optimisation, Jensen model, particle swarm optimisation**

*Corresponding author
Email address: tanvir.ahmad@durham.ac.uk (Tanvir Ahmad)
[1]School of Engineering & Computing Science, Durham University, UK
[2]Maïa Eolis (now ENGIE Green), France

Nomenclature

α	Yaw offset	γ	Wake skew angle
η	Brazos / SMV farm efficiency	η_{Lill}	Lillgrund efficiency
ρ	Wind density	A	Turbine swept area
$C_{P(max)}$	Maximum coefficient of power	C_P	Coefficient of power
C_T	Coefficient of thrust	D	Turbine diameter
I_0	Free-stream turbulence intensity	I_+	Wake-added turbulence intensity
I_u	Longitudinal component of turbulence intensity	I_{wake}	Turbulence intensity inside wake
i	Turbine under consideration	j	Turbines used for normalising Lillgrund efficiency
k	Wake decay coefficient	N	Number of turbines in the wind farm
P_{Actual}	Actual farm production	P_{max}	Maximum farm production in no-wake conditions
P_{Wakes}	Wake affected wind farm production	r_0	Blade length
P_{Turb}	Power production of a turbine	u	Predicted wind speed
u_0	Free-stream wind speed	x	Distance at which wind deficit is calculated
x_n	Length of the near wake region	z	Hub height
z_0	Surface roughness length	CFD	Computational Fluid Dynamics
EU	European Union	FLORIS	FLOw Redirection and Induction in Steady-state
GA	Genetic Algorithm	LCoE	Levelised Cost of Energy
MWh	Mega Watt hour	PSO	Particle Swarm Optimisation
SCADA	Supervisory Control And Data Acquisition	SMV	Le Sole de Moulin Vieux
SOWFA	Simulator fOr Wind Farm Applications	TI-JM	Turbulence Intensity based Jensen Model

1. Introduction

Wind energy is a very good alternative to the traditional sources of energy. Hydro-carbon based fuels are the primary sources of global warming and are responsible for more than 70% of greenhouse gas emissions [1]. In comparison, wind energy is green and renewable. One major hindrance in implementation of wind energy is the higher Levelised Cost of Energy (LCoE), currently stabilised at around £140/MWh for offshore wind farms [2]. LCoE has to be reduced to less than £100/MWh in order to become a competitive alternate; to ensure the EU renewable energy targets for 2020 and beyond [2].

Wind farms take advantages of economies of scale for reducing LCoE by clustering turbines together. However, the aerodynamic interactions, namely wake effects, created by the upstream turbines in these farms can greatly decrease the total production compared to the same number of turbines under free flow conditions [3, 4, 5]. A turbine is in the wake of an upstream turbine when the wake produced intersects the swept area of the downstream turbine [6]. Wakes result in lower wind speed and increased turbulence intensity for the shadowed turbines. This results in lower production and increased fatigue loading [3, 4, 7, 8]. It is always desired to reduce wake effects in a wind farm.

Wake effects decrease with increasing downstream distance. Therefore a possible way of reducing wake effects is to install the turbines as far as possible from one another with an optimised layout. But due to space and economic constraints, it is impossible to completely diminish these interactions [9]. As a compromise, industry best practice tends to bias the farm layout on prevailing wind directions by installing turbines with increased spacing between them, termed as downwind [4]. For non-prevailing wind directions spacing between the turbines is low, termed as crosswind [4]. For example, the downwind spacing between wind turbines in the Brazos wind farm is $7D+$ but the crosswind spacing is only $2D - 3D$ [10]. Due to this close spacing, wake losses in the non-prevailing wind directions can be as high as 50% [10]. Lillgrund, an offshore wind farm has a downwind spacing of $4.4D$ and a crosswind spacing of $3.3D$,

reducing the farm efficiency to as low as 40% [11, 12].

Another way of reducing wake effects is global optimisation of the whole wind farm using coordinated control. With the most common approach, every turbine maximises its own production, neglecting the wake effects on shadowed turbines [4]. Wake effects can be reduced with coordinated control of the whole wind farm. Coordinated control based on global optimisation of the whole wind farm instead of local optimisation of individual turbines can result in increased annual energy production. Curtailing the upstream turbines reduces the wake effects produced, hence leaving more wind for the downstream turbines. If this curtailment is undertaken in such as way that decrease in upstream turbines' production is less than increase in downstream turbines' production then the net production will increase. Coordinated control and optimisation cannot only increase overall farm production but also decrease average and fatigue loading on the turbines with no additional cost [7, 10, 13]. The only change required in the existing control system will be the coordinated control algorithm, specifically a change in the software. As real time on-line optimisation is required because of the stochastic nature of wind, the controller must be very fast and accurate. Specifically, control updates need to be made in seconds.

Development of such on-line, accurate and computationally efficient coordinated control strategies is the aim of this paper. Particle Swarm Optimisation (PSO) is combined with a fast processing wind deficit model for developing a realistic and practical on-line wind farm controller. The wind deficit model developed in this work is a modified version of the Jensen model [14] and is referred to as the Turbulence Intensity based Jensen Model (TI-JM). The effective value of wake decay coefficient is estimated using the wake added turbulence intensity as the wake moves inside the farm. The TI-JM is validated using WindPRO (a commercial software widely used for wind energy research and projects in the industry) [15] and SCADA data from the three wind farms (Brazos, SMV and Lillgrund). The controller can optimise the Lillgrund wind farm consisting of 48 wind turbines in seconds, producing accurate results using a basic PC (4 cores, 3.50GHz processor and 16GB RAM), increasing the production by up to 8%.

This paper is organised as follows. Section 2 presents a detailed literature review of coordinated control strategies. The TI-JM is detailed in section 3. A brief review of optimisation techniques, used for coordinated control is given in section 4. This is followed by the control problem and objective function formulation in section 5. Information about the three wind farms - Brazos, SMV and Lillgrund is provided in sections 6.1, 6.2 and 6.3 respectively. The methodologies for obtaining efficiencies of the farms case studies are discussed in section 7. Results and analyses are presented in section 8. Conclusion of this work is given in section 9.

2. Coordinated control background

Coordinated control of a wind farm can be achieved by curtailing power of the upstream turbines optimally by varying their C_P or yaw offsets (α). The concept of coordinated control was first presented almost three decades ago in [16]. Simulations in [16, 17] demonstrated that compensation of aerodynamic interactions between wind turbines in a wind farm can maximise farm production and reduce fatigue loading on the turbines. Wind tunnel experiments in [18] suggested that wind farm production can be increased by reducing axial induction factor of the upstream turbines. The Heat & Flux and Active Wake Control (Controlling Wind) techniques perform numerical optimisation with WAKEFARM software using axial induction factor and yaw offsets, achieving a gain of maximum 2% with simulations on real time data [13, 19, 20, 21, 22, 23, 24].

The work in [7] concluded that coordinated control can increase wind farm production and off-line lookup tables should be used for minimising computational efforts. However turbines' properties in a wind farm vary frequently, such as switching them off due to O&M issues. Therefore going completely off-line is not always possible or desired. Curtailment strategies in different operating conditions are discussed in [8] stating that coordinated control can be of significant importance for reducing loads in a wind farm.

The farm controllers developed in [25, 26] used Computational Fluid Dynam-

ics (CFD) based wind deficit models for exploiting the benefits of coordinated control. These controller are computationally expensive making them unsuitable for real time on-line operations [25, 26].

Numerical analyses in [3] demonstrated an increase in net production of a three turbine wind farm. Simulations of artificial wind farms consisting of two and three wind turbines in [5] resulted in increased combined output with coordinated control. This study [5] suggested that the farm controller must be developed with some intelligence or adaptive learning.

Cooperating static game approach using yaw offset angles was used for maximising efficiency of a wind farm using numerical simulations [27]. Game theory has been used in [28] for coordinated control of a simple three turbine wind farm. This study shows an increase of up to 25% in farm production as compared to the conventional greedy control. However, it is discussed that most of the assumptions about the wind conditions are unrealistic [28].

Studies in [29, 30, 31, 32] used the high-order wind farm model Simulator fOr Wind Farm Applications (SOWFA) and an engineering model FLOw Redirection and Induction in Steady-state (FLORIS), for coordinated control of an artificial wind farm. These studies concluded that an adaptive optimisation strategy is beneficial for coordinated control, as this reduces computational efforts [29].

The farm control problem is distributed into sub-problems for analysing the impact on structural loads of wind turbines in the farm in [33, 34, 35]. Simulations are performed using the SimWindFarm wind deficit model and numerical optimisation. This control approach [33, 34, 35] concluded that structural load reduction is possible using coordinated control of wind turbines in a wind farm. The simulations in [35] concluded that damage equivalent load can be reduced by up to 8% on the downstream turbine in a two-turbine example array.

The works in [10, 36] used a modified version of the Park-Jensen model and heuristic techniques for maximising farm production using coordinated control. The research in [37] used the Jensen-Park model and GA for optimising farm power production. Heuristic algorithms were used (off-line) for maximising farm

output using the AEOLUS SimWindFarm model in [38]. The work in [38] concluded that the possible energy gain depends upon the wake model used and can reach up to 7%. The work done in [39] presented a survey of wind farm control and optimisation literature.

These studies concluded that the possible benefits of coordinated control depend upon the following factors:

1. **Terrain characteristics** - Wakes can travel for longer distances in terrains with low roughness, such as offshore.
2. **Wind conditions** - This includes turbulence intensity, wind direction and speed. In certain wind directions downstream turbines can be under full wake effects producing the worst impact on farm production. There are no or minimal wake effects in above rated wind conditions. Wake diffuses quickly in high turbulent wind conditions.
3. **Layout of the wind farm** - Farms with low spacing between the turbines (denser farms) are affected more by wakes.
4. **Number of turbines under consideration** - Number of turbines in a wind farm which can benefit from curtailing upstream turbine(s) and number of upstream turbines which can be curtailed.

The literature review [4, 5, 7, 10, 28, 36, 40] also suggested that the farm controller requires two integral parts, a wind deficit model and an optimiser. The wind deficit model is used by the optimiser for evaluating different combinations of productions of the turbines in the wind farm, for achieving the optimum power production.

An important question, which arises here is that if the concept of coordinated control was presented back in 1988 [16]and if it is beneficial for wind farms, then why is it not implemented yet? The answer is the inverse relationship between accuracy and computational efficiency of the farm controller. According to [40] some of the main open areas of research in coordinated control are faster control systems and tools for optimisation and wake modelling.

This paper addresses all these issues by developing computationally effi-

cient, accurate and practical coordinated control strategies for maximising farm production. A fast processing and accurate wind deficit model (TI-JM) is developed. The optimiser (PSO) uses minimum combinations of productions using the wind deficit model for maximising overall farm production, resulting in high processing speed. The aim of this work is to emphasise computational efficiency without compromising accuracy for increasing wind farm production.

3. Turbulence Intensity based Jensen Model (TI-JM)

This section presents development of the wind deficit model, used for designing coordinated control strategies. The standard Jensen model [14, 41] is modified using an analytical expression for turbulence intensity obtained from [42]. The TI-JM has all the characteristics of the standard Jensen model [14, 41] except for the constant wake decay coefficient (k) which is a function of surface roughness length and hub height as shown in equation (2).

The Jensen model has widely been used for developing farm control strategies due to its processing efficiency [4, 10, 17, 27, 36, 37, 43, 44, 45] and is also part of many industry standard software such as WindFarmer [46] and WindPRO [15]. The Jensen model is a practical tool as long as the aim is to predict wind deficit inside the wind farm for estimating mean production [41]. The model cannot provide detailed wake flow information. Simple assumptions such as the ideal wind flow, constant k and linear wake expansion make the Jensen model computationally very efficient. However, keeping k constant means ignoring the farm-added roughness and wake-added turbulence intensity, making the model less accurate [10, 31, 47].

Turbines under wake effects experience more turbulent wind because of wake added turbulence [31]. This affects atmospheric stability and k inside the wind farm. The farm acts as a roughness generator itself [15]. This increased turbulence intensity must be considered for predicting wind speed deficit inside a wind farm. Different approaches have been used for adjusting the value of k for improved wake prediction inside the wind farm. The works in

[10, 15, 31, 42, 46, 48, 49, 50, 51, 52, 53, 54, 55] suggest to tune k according to wind conditions and terrain characteristic.

The work in [42] uses two different values of k, one for the free-stream and the other one for wake affected wind conditions. A correction factor for k is used in WindFarmer for improved prediction considering the deep array effects inside the farm [46]. The modified version of the Jensen model in WindPRO combines turbulence models with the Jensen model [15, 56]. It is recommended in [15] to increase the value of k inside the wind farm as the farm itself changes the roughness, hence the free-stream wind may not follow the assumptions of the Jensen model. Linear regression is used for estimating k using SOWFA as a benchmark in [31]. Discrete bins of turbulence intensity are used in [57] for estimating k using WindPRO as the benchmark. The work in [54] estimates k using SCADA data under different wind conditions.

The TI-JM estimates effective value of k using an analytical expression given in equation (3) [42] for predicting wake added turbulence intensity. The added roughness created by the wind farm is also considered while estimating speed deficits in the wind farm. The aim of this model is to predict the effective wind speed deficit and not to model the detailed wind flow.

Wind deficit on any turbine is predicted using the following steps, illustrated by using the 4×4 wind farm in Figure 1. The farm in Figure 1 consists of 16 equidistant turbines with a spacing of $3D$ between them.

1. Input parameters required: Coordinates (easting, northing) of the turbines, number or rows, number of turbines in each row, total number of turbines (N), free-steam wind speed (u_0) and free-stream turbulence intensity (I_0), wind direction and an initial value of k for free-steam conditions which can be obtained from SCADA data or literature [58], and is based on terrain characteristics.
2. It is assumed that wakes can affect downstream turbines up to $10D$ as suggested in [56, 59].
3. If a downstream turbine, at distance (x) from an upstream turbine, is

shadowed by the wake produced, the wind speed at the wake affected downstream turbine (u_x) is estimated using the standard Jensen model [14] according to equation (1), also shown in Figure 1a.

$$u_x = u_0 \left(1 - \left(\frac{1 - \sqrt{1 - C_T}}{\left(1 + \frac{kx}{r_0}\right)^2} \right) \right) \tag{1}$$

According to [14, 41], k depends upon hub height (z) and surface roughness length (z_0) and can be determined using equation (2) [14, 41].

$$k = \frac{1}{2 \ln\left(\frac{z}{z_0}\right)} \tag{2}$$

4. Wake added turbulence (I_+), at hub height can now be estimated using equation (3) [42].

$$I_+ = 5.7 \times C_T^{0.7} \times I_0^{0.68} \times (x/x_n)^{-0.96} \tag{3}$$

If I_0 is given then the only unknown is length of the near wake (x_n) which can be found as given in [42].

5. The effective turbulence intensity inside wakes (I_{wake}) is estimated using equation (4).

$$I_{wake} = \sqrt{I_+^2 + I_0^2} \tag{4}$$

6. This information is combined with the standard Jensen model [14] for predicting the effective wind speed deficit inside the wind farm. According to [42], the longitudinal component of turbulence intensity (I_u) can be specified by equation (5).

$$I_u = \frac{1}{\ln\left(z/z_0\right)} = 2k \tag{5}$$

If isotropic conditions are assumed then the three components of turbulence intensity (lateral, vertical and longitudinal) are equal. Therefore I_u is one third of I_{wake} as given in equation (6). The new value of k from equation (5) is replaced in equation (1) for predicting the effective wind speed deficit.

$$I_u = \frac{I_{wake}}{3} \tag{6}$$

7. If a turbine is affected by multiple wakes then these are superimposed assuming that wind speed in the wake ($u_{x(i)}$) is same as the linear sum of wind deficits for each wake as given in equation (7) [41]. This is shown in Figure 1b.

$$u_{x(i)} = u_0 \left[1 - \sqrt{\sum_{n=1}^{i-1} \left(1 - \frac{u_{n,i}}{u_0} \right)^2} \right] \tag{7}$$

where ($u_{x(i)}$) is the wind speed at i^{th} wind turbine at distance (x) and ($u_{n,i}$) is the wind speed at i^{the} wind turbine as a result of wake of n^{th} wind turbine.

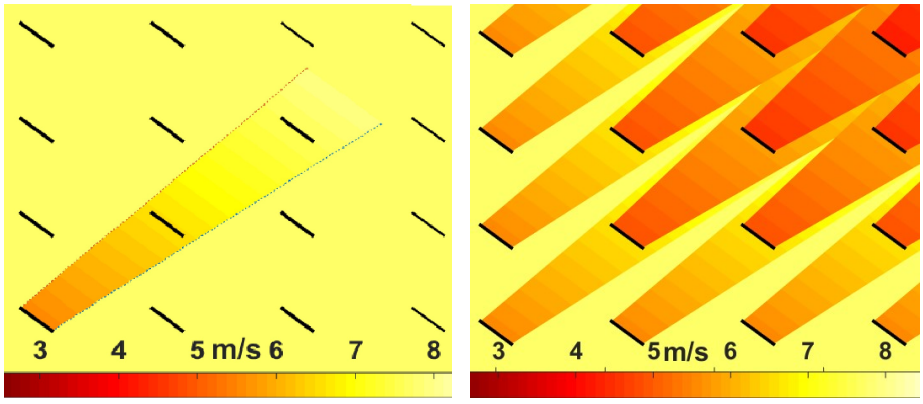

(a) Wind deficit calculation as the wake expands up to $10D$

(b) Superimposing multiple wakes

Figure 1: **Illustration of the TI-JM using an artificial 4×4 wind farm when the wind flows at 225° (north-west) and wind speed of 8 m/s**

The value of k varies on turbine by turbine basis inside the farm according to I_+. Wake expands more inside the farm as a result of the increased k as shown in 1b. This increased expansion brings two consequences. First, more downstream turbines will be in wakes. Second, the wake diffuses quickly because of I_+, as wind from the surroundings flows quickly to diffuse the momentum loss.

The TI-JM can be used for any wind direction, speed and layout of the farm.

The TI-JM was validated using data from two one-dimensional onshore wind farms in [10]. The TI-JM provides speedy and accurate results as input to the optimiser.

4. Optimisation

In order to use the controller on-line, an acceptable solution has to be achieve in the order of seconds so that the C_P or yaw-offset of each turbine can be calculated before the wind reaches it. Better and faster control systems are required to help optimise the wind farm control [40]. The farm controller requires an accurate, fast processing and computationally efficient optimiser. Intelligent farm control aimed at maximising net present value will replace turbine power curve as the main performance characteristic [40].

Numerical optimisation [3, 16, 18, 25, 35], game theory approach [27, 32, 43], hill climbing algorithm [45] and GA [17, 37] are some of the optimisation techniques that have been used by researchers for wind farm coordinated. It is suggested in [5, 7] that iterative learning control algorithms can improve performance of farm controllers. Therefore, performances of different optimisation techniques (Brute Force, GA, Simulated Annealing and PSO) were evaluated for wind farm control in [36] concluding that PSO is the most suitable technique for wind farm control because of its high processing speed and computational efficiency.

5. Control Problem

The farm controller is aimed at maximising the overall farm production. PSO uses the TI-JM for producing different combinations of power productions, moving towards the best combination (solution) by evaluating them according to the given objective function specifically for increasing total farm production.

The total wind farm power production is the sum of individual wind turbine's

production as given in equation (8) [4].

$$P_{Wakes} = \sum_{i=1}^{N} P_{Turbine(i)} = \sum_{i=1}^{N} \frac{1}{2}\rho A u(i)^3 C_P(i) \cos^2 \alpha_i \tag{8}$$

where (P_{Wakes}) is the actual farm production, (N) is the total number of turbines in the wind farm, ($P_{Turbine}$) is production of a turbine, (i) is the turbine under consideration, (ρ) is the air density, (A) is turbine swept area and (α) represents the yaw offset.

Usually all the turbines in a wind farm have the same configurations and characteristics i.e. hub height, blade length, power curve and hence maximum C_P ($C_{P(max)}$). If it is assumed that ρ remains constant inside the wind farm then the term ($\frac{1}{2}\rho A$) is constant. If this constant is ignored then the control problem or objective function is to maximise the expression $\sum_{i=1}^{N} u(i)^3 C_P(i) \cos^2 \alpha_i$ in equation (8).

If all the turbines are under no wake effects then all of them experience the same wind speed u_0 and there is no need to yaw, $\alpha = 0°$. As the objective is to maximise the farm production, all the turbines operate with $C_{P(max)}$. The control objective is to minimise the difference between power production in no-wake conditions and power production affected by wakes (actual production) as shown in equation (9). If the constant ($\frac{1}{2}\rho A$) is ignored then the objective function is formulated as equation (9).

$$Objective\ Function = min\left(\sum_{i=1}^{N} u_0^3 C_{P(max)} - \sum_{i=1}^{N} u(i)^3 C_P(i) \cos^2 \alpha\right) \tag{9}$$

The controller minimises the value in equation (9) by optimally varying C_P or α. C_P in equation (9) is related to C_T in equation (1) through the axial induction factor which is a measure of the slowing of the wind speed between the free stream and the rotor plane [4, 13].

When yaw offset is applied at an upstream turbine, the wake produced deflects away from the downstream turbine's swept area. This wake deflection is more than the offset applied [23]. Hence an optimum combination of yaw offsets can deflect the wake away from downstream turbines increasing the net produc-

tion. The analytical relationship between α and wake skew angle (γ) given in equation (10) [23] is used in this study.

$$\gamma = 1.20 \times \alpha \tag{10}$$

The objective function in equation (9) can be used for C_P and yaw based optimisation. For simplicity, with C_P optimisation, α is kept constant and vice versa.

6. Case Study Wind Farms

Two onshore wind farms: Brazos and SMV, and one offshore wind farm: Lillgrund, are used as case studies. Brazos is a medium sized wind farm where turbines are placed in a non-grid pattern. SMV is a small wind farm consisting of seven wind turbines installed approximately as a one-dimensional array. Lillgrund is a medium sized wind farm with a grid-like layout. A brief overview of these wind farms case studies is presented in the following sections.

6.1. Brazos

The Brazos wind farm is located in Texas, USA and is owned by Shell Wind Energy/Mitsui. The farm is divided into two sister wind farms: Brazos-A and Brazos-B. A wind farm with a non-grid shape and high downwind spacing such as Brazos can be considered made up of several smaller sub-farms (each row or group of turbines is a sub-farm) as shown in Figure 2a. This makes the control process fast and efficient as each sub-farm is optimised individually.

The case study in this work is based on the encircled row from Brazos-A, shown in Figure 2a. The selected row consists of seven Mitsubishi MWT 1000 turbines [60] with $3D$ spacing between them. The $3D$ spacing represents industry standards more accurately as compared to the $2D$ spacing between turbines in some other rows.

When the wind flows from the east, the wind speed experienced by turbines in the selected row is free-stream wind speed, as no turbines are installed to

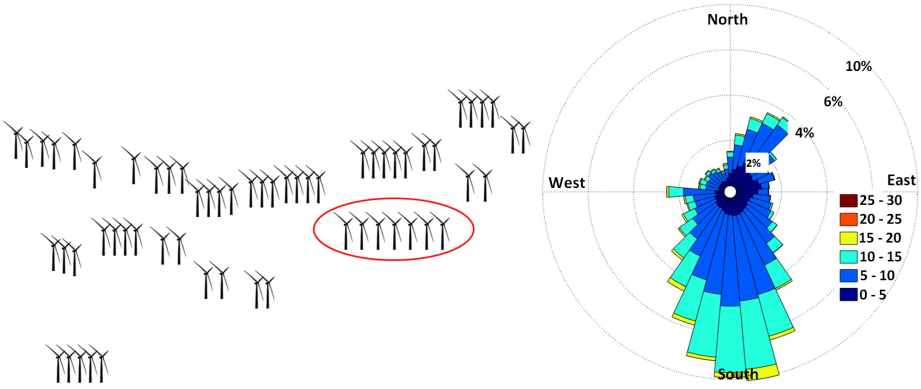

(a) Brazos A Layout with selected row encircled

(b) WindRose obtained from SCADA data from 2004 - 2006

Figure 2: Brazos A layout (rows under consideration encircled) and wind-rose

the east of this row. The nearest turbine to the west is installed at a distance of more than $20D$, hence it can be assumed that the wind flowing from west is also free-stream. The row of turbines in the north-west of the selected row can affect wind characteristics when the wind flows from north-west. The terrain is flat and open with low grass [54]. The wind-rose can be seen in Figure 2b showing the prevailing wind direction and frequency of wind speeds.

6.2. Le Sole de Moulin Vieux (SMV)

SMV is an onshore one-dimensional wind farm located in the northern France and is owned by Maïa Eolis (now Engie Green). The farm consists of seven Senvion MM82 2050 kW wind turbines [61]. Spacing between the turbines varies from $3.3D - 4.3D$. The farm approximately as a one-dimensional array as shown in Figure 3a. The terrain is rough with fresh grass or vegetation. There are woods to the south at a distance of almost 100m (less than $1.5D$) from the wind farm, affecting atmospheric stability in the farm [62]. Prevailing wind direction and frequency of the wind speeds can be found in the wind-rose in Figure 3b.

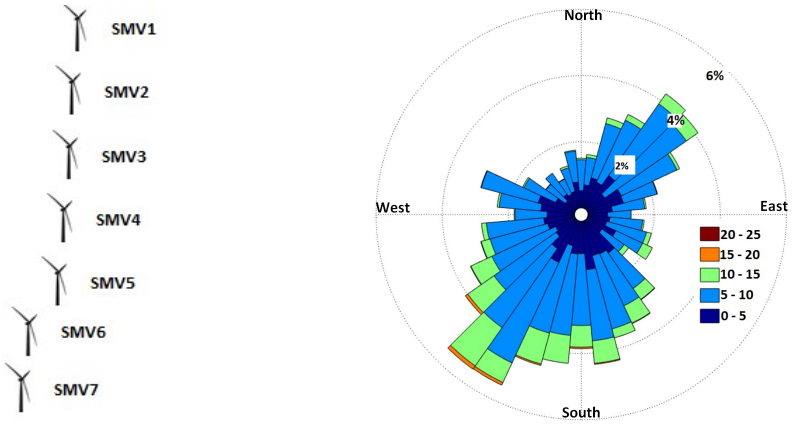

(a) SMV layout

(b) WindRose obtained from SCADA data from 2011 - 2014

Figure 3: SMV layout and wind-rose

6.3. Lillgrund

Third wind farm case study is the two-dimensional offshore wind farm: Lillgrund, which is located between Sweden and Denmark in the Öresund and is owned by Vattenfall. The farm consists of 48 Siemens SWT-2.3-93 wind turbines [63] installed in 8 rows. Spacing between the turbines within a row is $4.5D$ and spacing between the rows is $3.5D$ [11, 63]. The farm has a grid-like layout as can be seen in Figure 4a. The prevailing wind direction is from south and south-west and the mean wind speed is 8.5m/s [11] as shown in Figure 4b. Wind data from 2000 - 2015 at 50m height accessed from [64] was used to create the wind-rose in Figure 4b. Turbines inside the farm are almost always under wake effects as the layout is very dense.

7. Methodology for Calculating Efficiency

This section explains the methodology adopted in this study for analysing the impact of coordinated control strategies on the farms' performances. Details and data from the wind farms case studies are used for validating and evaluating the TI-JM and optimised coordinated control strategies. Efficiencies obtained

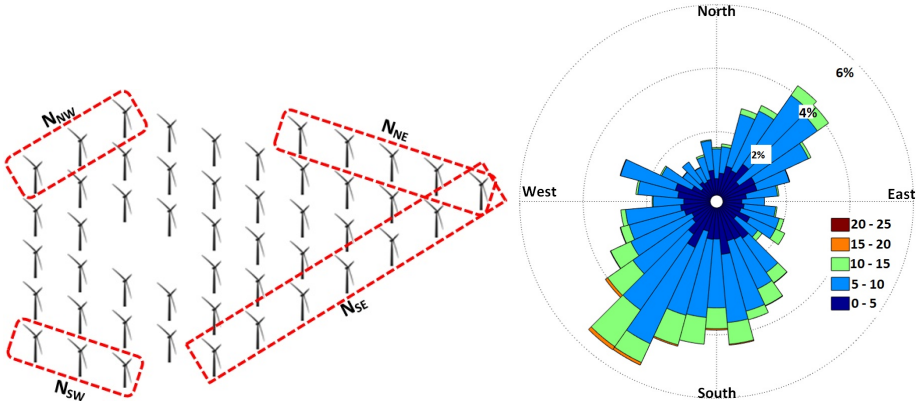

(a) Layout and highlighted rows (turbines) used for normalisation

(b) Lillgrund WindRose

Figure 4: Lillgrund layout and wind characteristics on the site

from SCADA data and WindPRO are used as benchmarks for evaluating the TI-JM. There are no or minimal wake effects in the above rated conditions, hence only below rated wind speeds are considered in the simulations [12]. From this point onwards average efficiency explicitly means average efficiency in below rated wind conditions.

Standard values of k (for onshore and offshore wind farms) available in the literature [58] are used in WindPRO in a 10° direction bin (finest possible). Initial value of k in the TI-JM is tuned using the SCADA data (Brazos and SMV) for matching the efficiency based on SCADA data using the greedy control. The C_P-based and yaw-based optimised control strategies are simulated for the three farms case studies using TI-JM. Efficiencies based on the optimised strategies are compared with the standard greedy control. Direction resolution is kept at 1° for efficiencies obtained with SCADA data and TI-JM. PSO is used for optimisation as discussed in section 4.

Contour plots of the three wind farms case studies in full-wake conditions are used for depicting a comparison of conventional and coordinated control strategies.

7.1. Brazos and SMV

Efficiency of the selected Brazos-A row is calculated using the SCADA data from 2004 - 2006, available on the ReliaWind database server in Durham University, UK [65]. SCADA data of the SMV wind farm from 2011 - 2014 is provided by Maïa Eolis (now Engie Green). Full or near-full wake conditions are assumed in the simulations. It was made sure by data filtering only that data is used in analyses where a turbine is operational. Details of the data filtering can be found in [10]. Equation (11) [4] is used for estimating efficiencies (η) of Brazos and SMV. The actual power produced by the wind farm is denoted by (P_{actual}) while the maximum possible power assuming no-wake effects is given by (P_{max}).

$$\eta = \frac{P_{actual}}{P_{max}} \tag{11}$$

Efficiency based on the SCADA data is maximum of 82% and 86% for Brazos and SMV respectively even in no-wake conditions. However, efficiency should be almost 100% in no-wake conditions. The discrepancies may be caused by anomalies in SCADA data or other unknown operational issues. WindPRO and the TI-JM only take wake effects into account for estimating farm production, ignoring any other issues or anomalies. Therefore, maximum efficiency is shifted to 1 i.e. 100% by adding the difference $(1 - \max(\mathrm{Eff}(0 - 360)))$ to the whole efficiency curve. This does not change shape of the efficiency curve but makes it possible to compare it with WindPRO and TI-JM by ignoring all other issues with the farm and data.

7.2. Lillgrund

SCADA data for the wind farm could not be accessed. However, important information such as turbine characteristics, 360° farm efficiency and layout is given in [11, 12, 63, 66]. Access to details of the surface roughness length, turbulence intensity and average efficiency was provided by [63]. The average 360° efficiency based on SCADA data for below-rated wind conditions is reproduced from [12, 63] digitising data with [67]. Equation (12) [63] is used for estimating

Table 1: Turbines used for normalisation for estimating Lillgrund efficiency [63]

Wind Direction	Figure 4a	N_j	j
North-east	N_{NE}	5	First turbine of row 1 to row 5
South-east	N_{SE}	7	Seven turbines of row 1
South-west	N_{SW}	3	Last turbine of row 2 to row 4
North-west	N_{NW}	3	Three turbines of row 8

efficiency of this wind farm (η_{Lill}).

$$\eta_{Lill} = \frac{N_j}{48} \frac{\sum_{i=1}^{48} P_i}{\sum_{j} P_j} \tag{12}$$

Where (i) is the turbine under consideration, (P_i) is average power of a turbine, (j) denotes the number of turbines and is a set containing only the turbines used for normalisation as given in Table 1 and shown in Figure 4a. The set j depends upon free stream wind direction and contains wind turbines facing the free-stream wind. Total number of turbines in the farm is 48, number of turbines in set j is denoted by (N_j), as given in Table 1 and specified in Figure 4a. According to [63], the average free-stream turbulence intensity (I_0) in Lillgrund is 0.06, and that k can be tuned as per the wind deficit model.

8. Results and Analysis

Efficiencies obtained through different sources and methods for Brazos, SMV and Lillgrund are presented in Figures 5, 6 and 7 respectively. Detailed analyses of these results are presented in the following sections.

8.1. Brazos

Turbines in the case study row in the Brazos wind farm are installed in a straight line as can be seen in Figure 2a. Average efficiency for $90° \pm 30°$ is shown

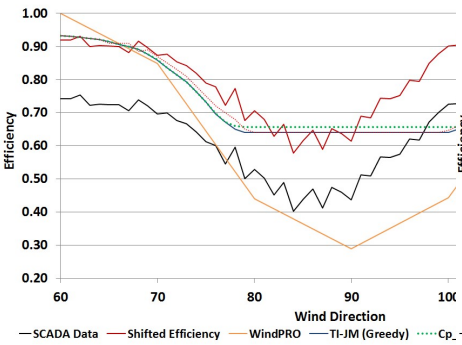

Figure 5: Brazos Efficiency in Full wakes

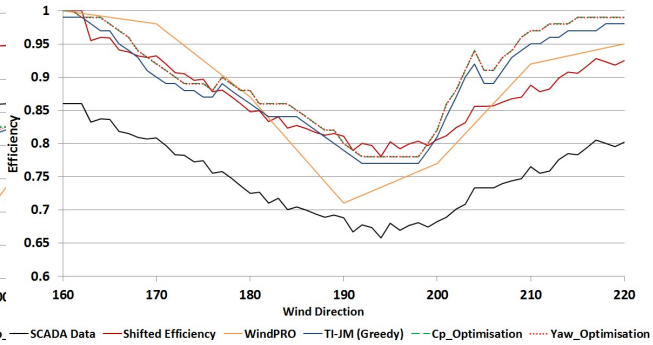

Figure 6: SMV Efficiency in Full wakes

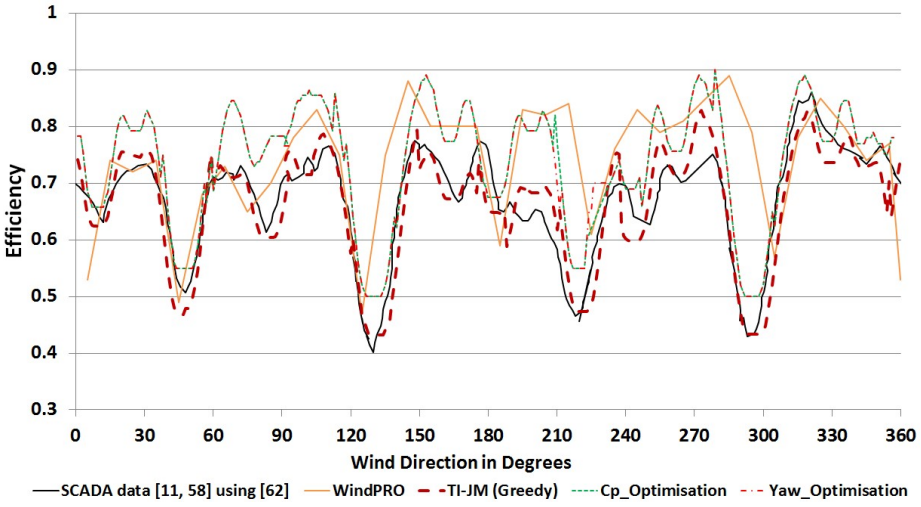

Figure 7: Lillgrund 360° average efficiency in below rated wind conditions

in Figure 5. It can be seen that shifted efficiency can be as low as 58% showing how adversely wakes can impact the farm production. WindPRO predicts that efficiency can be as low as 30% in the worst cases (full wakes) with such layout.

The TI-JM predicts a minimum average efficiency of 62% in full wake conditions. Higher values of wake decay coefficient (up to $k = 0.25$) are used as estimated by the TI-JM for predicting effective wind speeds deep inside the farm as shown in Figure 8. This shows that standard value of k for onshore wind farms ($k = 0.07$) must be tuned according to the conditions (inside the farm) as concluded in section 2. The data driven initial value of k keeps the efficiency constant and closer to the efficiency curve based on the SCADA data in the $80° - 100°$ region as shown in Figure 5.

With the standard constant k, efficiency based on the TI-JM follows efficiency obtained with WindPRO. The average efficiency predicted by the TI-JM follows the shifted efficiency much closer as compared to WindPRO specially from $60° - 90°$. WindPRO and TI-JM produce symmetrical results around $90°$, as it is a straight line one-dimensional array of turbines. However the shifted efficiency based on SCADA data is not symmetrical. Unknown operational issues, problems with the SCADA data and wakes produced by the Brazos-B wind farm and turbines in other rows of Brazos-A are potential reasons for this loss in production. WindPRO and the TI-JM ignore the impact of the nearby farms, assuming free-stream conditions.

It can also be seen in Figure 5 that the C_P and yaw-based control strategies can improve the average efficiency by up to 2%. The C_P-based control performs better in full wakes while the yaw-based control performs better in partial wakes.

The contour plots in Figure 8 compare the wind flow using conventional, C_P-based and yaw-based control. It can be seen that the upstream turbines produce lower wind speed deficit with the C_P-based control, as compared to the conventional control, as their production has been curtailed. Yaw-based control on the other hand skews the wake away from the downstream turbines by yawing the upstream turbine. The C_P-based optimisation strategy can increase the farm production by up to 5% while yaw-based optimised control can result in

a maximum of 7% increase in the farm production. The contour plots also show the increase in wake-width, representing the impact of wake added turbulence intensity. A single simulation for optimisation took less than 15 seconds in this case.

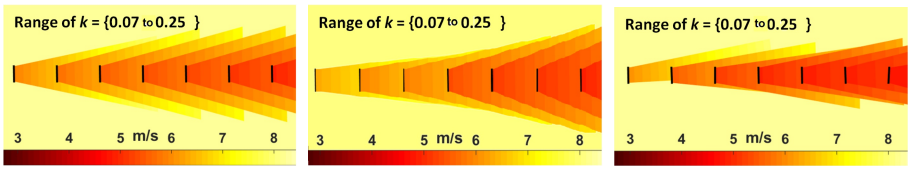

(a) Greedy Control (b) C_P-based Control (c) Yaw-based control

Figure 8: **Comparison of the greedy, C_P-based and yaw-based control of Brazos wind farm at 8m/s in full wake conditions. Range of k varies from 0.07 (free-stream conditions) to 0.025 (deep inside the farm)**

395

8.2. Le Sole de Moulin Vieux (SMV)

The average efficiency from the south $160° - 220°$ is shown in Figure 6 representing the full or near-full wake conditions. The shifted efficiency shows that efficiency can be as low as 78% in full wake conditions. WindPRO predicts
400 that the losses can be as high as 30% resulting in a decreased efficiency of 70%. The standard constant value of $k = 0.07$ [58] is used in WindPRO. The TI-JM estimates that efficiency can be as low as 76% in the worst case predicting k up to 0.20 for better wake estimation inside the wind farm.

Efficiency obtained with the TI-JM (greedy control) fits well with the shifted
405 efficiency from $160° - 200°$. However, WindPRO performs better in the sector $200° - 220°$. The TI-JM captures the shape of the efficiency curve but the difference in predicted efficiency is high in $200° - 220°$, as wake losses are underestimated. This shows that even a higher value of k cannot capture the wake accurately. This can be attributed to the highly unstable wind conditions on
410 site as discussed in section 6.2.

With the optimised farm control strategies, average efficiency can be increased by up to 4% as can be seen in Figure 6. The C_P-based and yaw-based

control strategies performs equally well in this case in all wind conditions. This is because of the layout of the farm as discussed in section 6.2.

Contour plots in Figure 9 presents a comparison of the greedy, C_P-based and yaw-based optimisation strategies for the farm. A maximum increase of up to 8% in power production is achieved in simulations of this farm, with both the C_P-based and yaw-based optimised control. A single simulation for optimisation always took less than 15 seconds in this case.

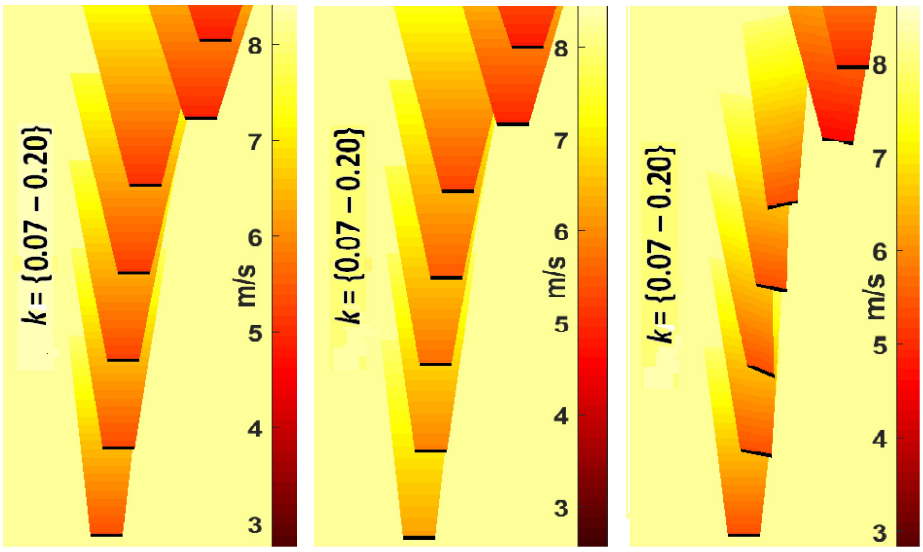

(a) Greedy Control (b) C_P-based Control (c) Yaw-based control

Figure 9: **Comparison of the greedy, C_P-based and yaw-based control of SMV wind farm at 8m/s in full wake conditions. Value of k ranges from 0.07 (free-stream conditions) to 0.20 (deep inside the farms)**

8.3. Lillgrund

The efficiency of this two-dimensional offshore wind farm can be as low as 40% in full wake conditions as shown in Figure 7 [12]. Average efficiency in below rated wind conditions is 67% resulting in 33% wake losses [12]. It is found with simulations that the values of k given in equation (13) shall be used with the TI-JM for free-stream wind conditions. These values fit well with the

farm efficiency given in [12].

$$\begin{aligned} k &= 0.04 \qquad when \quad u_0 \leq 7.0\,m/s \\ k &= 0.08 \qquad when \quad 7.0\,m/s < u_0 \leq 12.0\,m/s \end{aligned} \tag{13}$$

$$wind\ speeds > 12\ not\ considered\ as\ suggested\ in\ [12]$$

It can be seen in Figure 7 that efficiency based on the TI-JM, using greedy control fits well with the efficiency obtained from [12]. With the limited available information, it is concluded that efficiency based on the TI-JM is in good agreement with the efficiency based on the SCADA data. The standard constant k for offshore wind farm $k = 0.04$ [58] is used in WindPRO for estimating the efficiency. WindPRO captures the shape of average efficiency curve but results are inaccurate for most of the wind directions.

Coordinated control can bring great improvement in efficiency of such dense wind farms. The C_P-based and yaw-based optimised farm control can improve the efficiency by up to 6%. Efficiency can be increased in almost all of the wind directions due to the dense layout. The C_P-based control performs better in full wake conditions than the yaw-based control. The yaw-based control generally performs better than the C_P-based control in partial wakes as can be seen in Figure 7.

The contour plot in Figure 10 compares the conventional, C_P-based and yaw-based control of Lillgrund wind farm. Simulations with the innovative control strategies result in a maximum production increase of up to 8%. A single simulation for optimisation farm the production always took less than 50 seconds in this case.

9. Conclusion

Wake losses can be as high as 60% in wind farms [12]. Coordinated control can improve wind farm efficiency by up to 6% in suitable wind conditions. Previous research suggests that the farm controller shall be built with adaptive intelligence and shall be computationally efficient [4, 7]. The wind deficit model used by the controller shall be fast processing and accurate [7, 40].

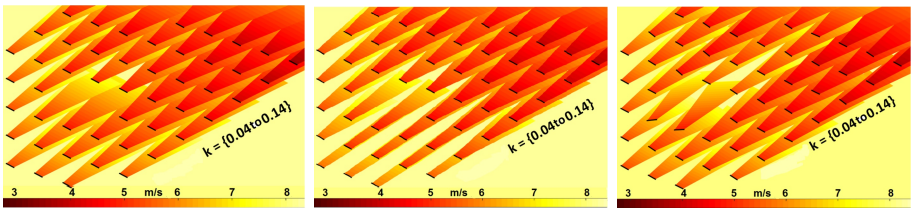

(a) Greedy Control (b) C_P-based Control (c) Yaw-based control

Figure 10: **Comparison of the greedy, C_P-based and yaw-based control of Lillgrund wind farm at 8m/s in full wake conditions. Value of k ranges from 0.04 (free-stream conditions) to 0.14 (deep inside the farm)**

The wind deficit model developed in this work (TI-JM) is a modified version of the Jensen model. The TI-JM takes deep array effect into consideration using free-stream and wake added turbulence intensities and can accurately predict the wind speed deficit and hence farm efficiency in most of the cases for the wind farms case studies. The value of k must be tuned for accurate estimation inside the wind farms. Both the C_P-based and yaw-based curtailment strategies increase wind farm efficiency as compared to the conventional greedy control.

It is concluded that generally the C_P-based optimisation strategies perform better in full wake conditions while the yaw-based optimisation strategies perform better in partial wake conditions. In full wakes, even larger yaw-offset cannot skew the wake away from downstream turbines and the larger yaw offset also reduces production of the upstream turbine significantly. A partial wake can be converted into a no-wake situation with the optimised yaw-offset of the upstream turbine increasing the overall farm power.

Average efficiency in below rated wind speeds is increased by up to 2% for the selected Brazos-A row, 4% for SMV and 6% for Lillgrund wind farm. Simulations confirm that a maximum production increase of up to 8% is possible with these innovative control strategies. Optimisation process for the Brazos-A row and SMV takes a maximum of 15 seconds while the process is completed in a maximum of 50 seconds for the Lillgrund wind farm. This high speed and accuracy makes the controller suitable for real time on-line field implementation.

References

[1] O. Edenhofer, R. Pichs-Madruga, Y. Sokona, E. Farahani, S. Kadner, K. Seyboth, A. Adler, I. Baum, S. Brunner, P. Eickemeier, B. Kriemann, J. Savolainen, S. Schlimer, C. von Stechow, T. Zwickel, J. M. (eds.), Climate Change 2014: Mitigation of Climate Change, Contribution of Working Group III to the fifth Assessment Report of the Intergovermental Panel on Climate Change, Online 3^{rd} part of the 5^{th} Assessment Report, Intergovernmental Panel on Climate Change (IPCC), Cambridge University Press, Cambridge, United Kingdom and New York, NY, USA, available at: https://www.ipcc.ch/report/ar5/wg3/ (2014).

[2] P. Arwas, D. Charlesworth, D. Clark, R. Clay, G. Craft, I. Donaldson, A. Dunlop, A. Fox, R. Howard, C. Lloyd, C. Lovett, A. Marshall, F. Wiles, Offshore wind cost reduction/ pathways study, Online, https://www.thecrownestate.co.uk/media/5493/ei-offshore-wind-cost-reduction-pathways-study.pdf (May 2012).

[3] E. Bitar, P. Seiler, Coordinated control of a wind turbine array for power maximization, in: American Control Conference (ACC), IEEE, 136, 2013, pp. 2898–2904.

[4] L. Y. Pao, K. E. Johnson, A tutorial on the dynamics and control of wind turbines and wind farms, in: American Control Conference, ACC'09, IEEE, 172, 2009, pp. 2076–2089.

[5] K. E. Johnson, N. Thomas, Wind farm control: addressing the aerodynamic interaction among wind turbines, in: American Control Conference, ACC'09, IEEE, 155, 2009, pp. 2104–2109.

[6] F. Gonzlez-Longatt, P. Wall, V. Terzija, Wake effect in wind farm performance: Steady-state and dynamic behavior, Renewable Energy 39 (1) (2012) 329–338.

[7] A. Ambekar, V. Ryali, A. K. Tiwari, Methods and systems for optimizing farm-level metrics in a wind farm, US Patent 9,201,410 (Dec. 1 2015).

[8] C. Schram, P. Vyas, Windpark turbine control system and method for wind condition estimation and performance optimization, US Patent App. 11/288,081 (Nov. 29 2005).

[9] M. Adaramola, P. Krogstad, Experimental investigation of wake effects on wind turbine performance, Renewable Energy 36 (8) (2011) 2078–2086.

[10] T. Ahmad, N. Girard, B. Kazemtabrizi, P. Matthews, Analysis of two onshore wind farms with a dynamic farm controller, in: EWEA, Paris France, 2015.

[11] J. Jeppsson, P. E. Larsen, Å. Larsson, Technical description Lillgrund wind power plant, Tech. Rep. 21858-1, Vattenfall, Vindkraft AB (September 2008).

[12] J. A. Dahlberg, Assessment of the Lillgrund windfarm: Power performance, Tech. Rep. 21858-1, Vatenfall, Vindkraft AB (September 2009).

[13] G. Corten, P. Schaak, Heat and flux: Increase of wind farm production by reduction of the axial induction, in: Proceedings of the European Wind Energy Conference, 2003.

[14] N. O. Jensen, A note on wind generator interaction, Tech. Rep. Risø -M-2411, Risø National Laboratory, Roskilde, Denmark (November 1983).

[15] N. Per, V. Jens, K. Jon, M. Per, J. Thomas, T. Morten, L., S. Mads, V., S. Thomas, S. Lasse, M. Mauricio, B. Karina, WindPRO 2.7 User Guide, EMD International A/S, Aalborg, Denmark, 3rd Edition (October 2010).

[16] M. Steinbuch, W. de Boer, O. Bosgra, S. Peters, J. Ploeg, Optimal control of wind power plants, Journal of Wind Engineering and Industrial Aerodynamics 27 (1) (1988) 237–246.

[17] C. J. Spruce, Simulation and control of windfarms, Ph.D. thesis, University of Oxford (1993).

[18] G. Corten, P. Schaak, E. Bot, More power and less loads in wind farms: Heat and Flux, in: European Wind Energy Conference & Exhibition, London, UK, 2004.

[19] J. Schepers, S. Van der Pijl, Improved modelling of wake aerodynamics and assessment of new farm control strategies, in: Journal of Physics: Conference Series, Vol. 75, IOP Publishing, 2007.

[20] L. Machielse, S. Barth, E. Bot, H. Hendriks, G. Schepers, Evaluation of (Heat and Flux) farm control, Tech. Rep. ECN-E–07-105, ECN, Petten, The Netherlands (2007).

[21] K. Boorsma, Heat and flux. analysis of field measurements, Tech. Rep. ECN-E–12-048, ECN, Petten, The Netherlands (November 2012).

[22] S. Kanev, F. Savenije, Active Wake Control: loads trends, Tech. Rep. ECN-E–15-004, ECN, Petten, The Netherlands (January 2015).

[23] J. Wagenaar, L. Machielse, J. Schepers, Controlling wind in ECN scaled wind farm, Proc. Europe Premier Wind Energy Event (2012) 685–694.

[24] K. Boorsma, Power and loads for wind turbines in yawed conditions, Tech. rep., ECN-E-12-047, ECN, Petten, The Netherlands (2012).

[25] M. Soleimanzadeh, A. J. Brand, R. Wisniewski, A wind farm controller for load and power optimization in a farm, in: Computer-Aided Control System Design (CACSD), 2011 IEEE International Symposium on, IEEE, 186, pp. 1202–1207.

[26] M. Soleimanzadeh, R. Wisniewski, Controller design for a wind farm, considering both power and load aspects, Mechatronics 21 (4) (2011) 720–727.

[27] J. Park, S. Kwon, K. H. Law, Wind farm power maximization based on a cooperative static game approach, in: SPIE Smart Structures and Materials+ Nondestructive Evaluation and Health Monitoring, International Society for Optics and Photonics, 2013, pp. 86880R–86880R.

[28] J. R. Marden, S. D. Ruben, L. Y. Pao, A model-free approach to wind farm control using game theoretic methods, IEEE Transactions on Control Systems Technology 21 (4) (2013) 1207–1214.

[29] P. Fleming, P. Gebraad, S. Lee, J. van Wingerden, K. Johnson, M. Churchfield, J. Michalakes, P. Spalart, P. Moriarty, High-fidelity simulation comparison of wake mitigation control strategies for a two-turbine case, in: Proceedings of ICOWES Conference, 2013.

[30] P. A. Fleming, P. M. Gebraad, S. Lee, J.-W. van Wingerden, K. Johnson, M. Churchfield, J. Michalakes, P. Spalart, P. Moriarty, Evaluating techniques for redirecting turbine wakes using SOWFA, Renewable Energy 70 (2014) 211–218.

[31] J. Annoni, P. M. Gebraad, A. K. Scholbrock, P. A. Fleming, J.-W. V. Wingerden, Analysis of axial-induction-based wind plant control using an engineering and a high-order wind plant model, Wind Energy 19 (2015) 1135–1150.

[32] P. Gebraad, F. Teeuwisse, J. Wingerden, P. Fleming, S. Ruben, J. Marden, L. Pao, Wind plant power optimization through yaw control using a parametric model for wake effects: a CFD simulation study, Wind Energy 19 (1) (2016) 95–114.

[33] V. Spudic, M. Jelavic, M. Baotic, N. Peric, Hierarchical wind farm control for power/load optimization, The Science of making Torque from Wind (Torque2010).

[34] V. Spudic, M. Baotic, N. Peric, Wind farm load reduction via parametric

programming based controller design, in: Proceedings of the 18th IFAC World Congress, 2011.

[35] V. Spudić, M. Jelavić, M. Baotić, Wind turbine power references in coordinated control of wind farms, Automatika–Journal for Control, Measurement, Electronics, Computing and Communications 52 (2).

[36] T. Ahmad, P. Matthews, B. Kazemtabrizi, PSO based wind farm controller, in: The 11th edition of the International Conference on Evolutionary and Deterministic Methods for Design, Optimization and Control with Applications to Industrial and Societal Problems, EUROGEN-2015 Glasgow, UK, 2015, pp. 277–283.

[37] J. S. González, M. B. Payán, J. R. Santos, Á. G. G. Rodríguez, Maximizing the overall production of wind farms by setting the individual operating point of wind turbines, Renewable Energy 80 (2015) 219–229.

[38] F. Heer, P. M. Esfahani, M. Kamgarpour, J. Lygeros, Model based power optimisation of wind farms, in: Control Conference (ECC), 2014 European, IEEE, 2014, pp. 1145–1150.

[39] T. Knudsen, T. Bak, M. Svenstrup, Survey of wind farm control power and fatigue optimization, Wind Energy.

[40] F. A. Aranda, Wind farm control methods, IEA R&D wind task 11 - topical expert meeting, Tech. rep., International Energy Agency (November 2012).

[41] I. Katic, J. Højstrup, N. O. Jensen, A simple model for cluster efficiency, in: European Wind Energy Association Conference and Exhibition, 1986, pp. 407–410.

[42] J. F. Manwell, J. G. McGowan, A. L. Rogers, Wind energy explained: theory, design and application, John Wiley & Sons, 2010.

[43] J. R. Marden, S. D. Ruben, L. Y. Pao, Surveying game theoretic approaches for wind farm optimization, in: Proceedings of the AIAA aerospace sciences meeting, 2012, pp. 1–10.

[44] K. Johnson, G. Fritsch, Assessment of extremum seeking control for wind farm energy production, Wind Engineering 36 (6) (2012) 701–716.

[45] P. Gebraad, J. Wingerden, Maximum power-point tracking control for wind farms, Wind Energy 18 (3) (2015) 429–447.

[46] G. Hassan, WindFarmer 5.3: Theory Manual, Garrad Hassan & Partners Ltd. DNV GL - Energy, Bristol, England (April 2014).

[47] J. Choi, M. Shan, Advancement of Jensen (Park) wake model, in: Proceedings of the European Wind Energy Conference and Exhibition, 2013, pp. 1–8.

[48] R. Barthelmie, G. Larsen, S. Frandsen, L. Folkerts, K. Rados, S. Pryor, B. Lange, G. Schepers, Comparison of Wake Model Simulations with Offshore Wind Turbine Wake Profiles Measured by Sodar, Journal of atmospheric and oceanic technology 23 (7) (2006) 888–901.

[49] M. Gaumond, P.-E. Réthoré, A. Bechmann, S. Ott, G. C. Larsen, A. Peña, K. S. Hansen, Benchmarking of wind turbine wake models in large offshore wind farms, in: Proceedings of the Science of Making Torque from Wind Conference, 2012.

[50] D. Zigras, K. Moennich, Farm efficiencies in large wind farms, in: German Wind Energy Conference, 2006.

[51] P. Beaucage, N. Robinson, M. Brower, C. Alonge, Overview of six commercial and research wake models for large offshore wind farms, in: Proceedings of the European Wind Energy Association Conference, 2012, pp. 95–99.

[52] R. J. Barthelmie, O. Rathmann, S. T. Frandsen, K. Hansen, E. Politis, J. Prospathopoulos, K. Rados, D. Cabezón, W. Schlez, J. Phillips, et al., Modelling and measurements of wakes in large wind farms, in: Journal of Physics: Conference Series, Vol. 75, IOP Publishing, 2007, p. 012049.

[53] M. Churchfield, Review of wind turbine wake models and future directions (presentation), Tech. Rep. NREL/PR-5000-60208, National Renewable Energy Laboratory (NREL), Golden, CO. (2013).

[54] N. Sidewell, T. Ahmad, P. C. Matthews, Onshore Wind Farm Fast Wake Estimation Method: Critical Analysis of the Jensen Model, in: EWEA, Paris, France, 2015.

[55] K. Vogstad, V. Bhutoria, J. A. Lund, S. Ivanell, Instant wind model reduction for fast CFD computations, Tech. Rep. 12:72, Elforsk (November 2012).

[56] D. J. Renkema, Validation of wind turbine wake models, Master's thesis, Faculty of Aerospace Engineering, TU Delft (June 2007).

[57] T. Ahmad, P. Matthews, B. Kazemtabrizi, Wake flow model for wind farm control, in: 10th PhD Seminar on Wind Energy in Europe, 2014.

[58] M. Thørgersen, T. Sørensen, P. Nielsen, A. Grötzner, S. Chun, WindPRO/PARK: Introduction to wind turbine wake modelling and wake generated turbulence, EMD International A/S, Niels Jernesvej 10, 9220 Aalborg, available at: http://www.emd.dk/files/windpro/manuals/for_print/Appendices-all_UK.pdf (2005).

[59] A. G. Gonzalez-Rodriguez, M. Burgos-Payan, J. Riquelme-Santos, J. Serrano-Gonzalez, Reducing computational effort in the calculation of annual energy produced in wind farms, Renewable and Sustainable Energy Reviews 43 (2015) 656–665.

[60] U. Yoshinori, I. Hidehiko, I. Kosuke, Mitsubishi new wind turbines, MWT-1000 A and MWT-S 2000, Mitsubishi Heavy Industries, Ltd., vol. 40 No. 4 Edition (August 2003).

[61] Senvion wind energy solutions, Senvion GmbH, Hamburg Germany, Senvion MM82 [50 Hz/2050 kW] Product Descrip-

tion, www.senvion.com/global/en/wind-energy-solutions/wind-turbines/mm/mm82/.

[62] O. Coupiac, Four vertical extrapolation methods, WindTech International 12 (2) (2016) 5–8.

[63] P. Moriarty, J. S. Rodrigo, P. Gancarski, M. Chuchfield, J. W. Naughton, K. S. Hansen, E. Machefaux, E. Maguire, F. Castellani, L. Terzi, et al., IEA-Task 31 WAKEBENCH: Towards a protocol for wind farm flow model evaluation. Part 2: Wind farm wake models, in: Journal of Physics: Conference Series, Vol. 524, IOP Publishing, 2014, p. 012185.

[64] M. M. Rienecker, M. J. Suarez, R. Gelaro, R. Todling, J. Bacmeister, E. Liu, M. G. Bosilovich, S. D. Schubert, L. Takacs, G.-K. Kim, et al., MERRA: NASA's modern-era retrospective analysis for research and applications, Journal of Climate 24 (14) (2011) 3624–3648.

[65] J. Bueno Gayo, Reliawind project final report, Tech. Rep. Project Nr 212966, Gamesa Innovation and Technology (2011).

[66] M. Gaumond, P.-E. Réthoré, A. Bechmann, S. Ott, G. C. Larsen, A. Pena Diaz, K. Kurt, D1. 3 benchmark report on wake models at the wind farm scale, Tech. rep., EERA DTOC (2013).

[67] A. Rohatgi, Webplotdigitizer, online, http://arohatgi.info/WebPlotDigitizer/ Accessed August 22, 2017.